ÇUKUROVA UNIVERSITY
INSTITUTE OF NATURAL AND APPLIED SCIENCES

PhD THESIS

Çağrı UZAY

DEVELOPING AND TESTING OF POLYMER FOAM CORE SANDWICH STRUCTURES WITH HYBRID CARBON FIBER/WIRE MESH SHEET FACINGS

DEPARTMENT OF MECHANICAL ENGINEERING

ADANA, 2020

ABSTRACT

PhD THESIS

DEVELOPING AND TESTING OF POLYMER FOAM CORE SANDWICH STRUCTURES WITH HYBRID CARBON FIBER/WIRE MESH SHEET FACINGS

Çağrı UZAY

ÇUKUROVA UNIVERSITY
INSTITUTE OF NATURAL AND APPLIED SCIENCES
DEPARTMENT OF MECHANICAL ENGINEERING

Supervisor: Prof. Dr. Necdet GEREN
Year: 2020, Page: 209
Jury : Prof. Dr. Necdet GEREN
: Prof. Dr. Melih BAYRAMOĞLU
: Prof. Dr. Uğur EŞME
: Assoc. Prof. Dr. Kerimcan ÇELEBİ
: Assoc. Prof. Dr. Erinç ULUDAMAR

In this study, flexural characteristics of sandwich structures consist of carbon fiber/epoxy facings hybridized with fine wire mesh sheets and extremely low-density PVC foam core were investigated. A comprehensive work was conducted considering the following parameters: core thickness, wire mesh size, stacking sequences of wire mesh sheets, and support span length in flexural tests. During the evaluation of bending properties, both analytical and experimental approaches were utilized. To test the effect of design parameters on experimental results, two-way ANOVA was also applied. Failure mode analysis was made based on analytical collapse force mechanisms and primary failure modes were addressed. Significant improvements in flexural characteristics of sandwich structures were obtained. Besides improving bending behavior and the increased load-carrying capacity even at the same deflection values, the sandwiches with wire mesh sheets also prevented catastrophic sudden failure. The developed sandwiches can be good candidates in applications where both high stiffness-to-weight ratio and resistance to sudden failure are desired.

Keywords: Sandwich Structures, Flexural Stiffness, Bending Characteristics, Tensile Properties, Failure Mode, Wire Mesh Sheets, ANOVA

ÖZ

DOKTORA TEZİ

KARBON ELYAF/ TEL ÖRGÜ LEVHALAR İLE HİBRİTLENMİŞ YÜZEY TABAKALI POLİMER KÖPÜK ÇEKİRDEKLİ SANDVİÇ YAPILARIN GELİŞTİRİLMESİ VE TEST EDİLMESİ

Çağrı UZAY

ÇUKUROVA ÜNİVERSİTESİ
FEN BİLİMLERİ ENSTİTÜSÜ
MAKİNA MÜHENDİSLİĞİ ANABİLİM DALI

Danışman : Prof. Dr. Necdet GEREN
Yıl: 2020, Sayfa: 209
Jüri : Prof. Dr. Necdet GEREN
: Prof. Dr. Melih BAYRAMOĞLU
: Prof. Dr. Uğur EŞME
: Doç. Dr. Kerimcan ÇELEBİ
: Doç. Dr. Erinç ULUDAMAR

Bu çalışmada, çok ince elek tel levhalarla hibritlenen karbon elyaf/epoksi yüzeyler ve oldukça düşük yoğunluklu PVC köpük çekirdek malzemelerden oluşan sandviç yapıların eğilme karakteristikleri araştırılmıştır. Çekirdek kalınlığı, elek tel boyutu, elek tellerin laminasyon sırası, eğilme testlerindeki mesnet açıklığı gibi parametrelerin dikkate alınması ile kapsamlı bir çalışma yürütülmüştür. Eğilme karakteristiklerinin hesaplanmasında hem analitik hem de deneysel standartlarından yararlanılmıştır. Tasarım parametrelerinin deneysel sonuçlara etkisini test etmek için de iki yönlü ANOVA uygulandı. Hasar modu analizi, analitik çökme kuvveti mekanizmalarına dayanarak yapılmış ve başlıca hasar tipleri belirlenmiştir. Karbon elyaf/epoksi yüzeylerin elek tel levhalarla hibritleştirilmesi ile sandviç yapıların eğilme karakteristiklerinde dikkate değer iyileşmeler elde edilmiştir. Elek tel levhalı sandviçler aynı çökme değerlerinde bile çok daha fazla eğilme kuvveti taşımalarının yanı sıra, elek tel içermeyen sandviçlerde hasar anında katastrofik bir şekilde meydana gelen ani kuvvet düşüşünü de engellemektedir. Geliştirilen sandviçler düşük ağırlıklarına karşı rijitliği yüksek ve ani hasarlanmaya karşı dirençli yapıların istendiği uygulamalar için uygundur.

Anahtar Kelimeler: Sandviç Yapılar, Eğilme Rijitliği, Eğilme Karakteristikleri, Çekme Özellikleri, Hasar Modu, Elek Tel Levhalar, ANOVA

EXTENDED ABSTRACT

Engineering materials are commonly classified into six main categories. These are metals, ceramics, glasses, elastomers, polymers, and hybrids. The hybrids can be composed of the other five material families in various shapes, dimensions, and amounts. They play an important role to combine the best features of the constituent materials by eliminating their drawbacks and have a wider range to obtain desired mechanical properties that cannot be achieved from a single composite. Sandwich composites, belong to the class of hybrid materials, have emerged as a structural member for most of the engineering fields such as aviation, aerospace, automotive, transportation, marine applications, etc. Due to their very high flexural stiffness to weight ratio, resistance to impact and environmental conditions, and better insulation to both noise and heat, they are good candidates for replacing with conventional engineering materials. They have two face sheets separated by a core and are constructed with a suitable binder. While very thin metal alloys and fiber-reinforced composites are used as face sheets, relatively thick and low-density industrial polymer and metal foams, balsa wood, honeycombs, corrugated, and truss materials are used as core. Thermoset and thermoplastic resins are available for the construction of sandwiches. Besides common advantages, multi-functionality can also be achieved by assembling the best combinations of constituents.

In this study, carbon fiber facings with inner wire mesh sheets were sandwiched with polyvinylchloride (PVC) foam core by using the epoxy resin matrix. Carbon fiber fabrics are woven plain, 200 g/m^2 in areal density. PVC foam core is linear cross-linked, closed-cell, rigid, and has an extremely low density of 48 kg/m^3 when compared to the existing literature. Three different core thicknesses were used as 10 mm, 20 mm, and 30 mm. Carbon/epoxy composite facings were hybridized with very thin AISI 304 stainless steel wire mesh sheets. Two different wire mesh sheets having 100-mesh and 200-mesh sizes were used. Wire mesh

steels, in a porous form, are available from very fine to coarse sizes at various wire thickness. In the literature, the use of wire mesh sheets has recently been encountered in civil and mechanical engineering applications, but they were in very coarse sizes. One of the main intentions of this thesis work is to investigate the effect of wire mesh sheets on bending characteristics of the carbon fiber sandwich panels and to develop multi-functional structural members by designing it with extremely low-density polymer foam core and very fine size wire mesh sheets. Because the major disadvantage of CFRP facings is their brittleness during failure. Although CFRP/PVC foam core sandwich panels can carry a larger amount of bending loads, failure of the structure occurs catastrophically with a sudden drop in force. The preliminary conducted experiments indicated that sudden drops can be prevented with the hybridization of CFRP and wire mesh sheets. The second main purpose of the study is to produce lightweight, stiff, and strong sandwich composite panels that will fill the holes in the material universe. Therefore, the results obtained from the sandwich panels developed in this work are going to contribute to both the literature and the material universe.

The sandwich panels were fabricated with a vacuum bagging method. The process is more suitable for small batch production such as research applications made in a laboratory, due to its simplicity and cost-effectiveness, but the quality of the output depends upon the labor skill. The manufacturing is performed on an open mold. Before starting the production, the weight ratios of the constituents were determined carefully to provide sufficient impregnation of the matrix to each layer. The amount of matrix was sufficiently prepared considering the total weight of fabrics, wire mesh sheets, and foam core materials. And the weight ratio of the epoxy resin to its hardener was set to 100:25. During fabrication, all layers including fiber fabrics, core material, and wire mesh sheets sequentially stacked by hand lay-up resin impregnation. After stacking all the layers, a perforated release film was placed over the sandwich. It excludes air bubbles from the product, allows to release the excessive resin throughout the perforations, and to ease of handling

after curing. Over the perforated release film, a breather cloth was placed to transmit gases, and collect the excessive resin properly. Lastly, the sandwich panel was enclosed by a sealed tape and kept inside a vacuum bag. The sandwich curing process was carried out under a 0,01 mbar vacuum atmosphere at room temperature for 24 hours. The sandwich layers were co-cured instead of separate bonding of face sheets to core.

Stacking sequences, wire mesh size, and its locations for laminating the sandwich facings, core thickness, and support span length determined the configurations of sandwich panels. The fiber facings of the sandwich composites are stacked as symmetrical to the neutral axis of the sandwich, but wire mesh sheets were placed either under the first fiber fabric of top facing denoted as *M1* or at top facing-core interface denoted as *M2* or combination of both of two cases denoted as *M3*. As mentioned before three different core thicknesses were used, and the tests were carried out under two different support span lengths (150 mm and 200 mm). For this reason, a systematic production process was specified and a sandwich code system was identified for each sample. The code of "XXXMP.TC.SL" identifies the sandwich panel. The first term, three digits (XXX) defines mesh size and the following letters (M) and (P) represent its location, the second term specifies core thickness and the last one specifies span length. For instance, a sandwich panel coded as 100M2.T20.S15 has a 20 mm thick (T) core, includes 100-mesh (M) size wire sheet at the top facing-core interface and the specimens are going to be subjected to flexural tests under 150 mm span (S) length. To find out the effect of wire mesh sheets, the reference panels were also produced and called WM.T20.S15 which means *"without wire mesh (WM)"*, has 20 mm core thickness and subjected to flexural tests under 150 mm span length.

The sandwich specimens were subjected to three-point bending tests with a crosshead speed of 2 mm/min according to ASTM C393, D7249 standards. The flexural characteristics were evaluated in terms of load-carrying capacity, maximum bending moment, flexural stiffness, core shear stress, facing stress,

transverse shear rigidity, and core shear modulus. These are obtained by calculations according to the equations presented by both classical sandwich beam theory and ASTM D7250 standards. In addition, tensile tests of the specimens were performed based on ASTM D3039 Standard for facing materials to obtain tensile strength and modulus data which are required for the evaluation of flexural characteristics.

The existence of wire mesh sheets in facings allowed carrying more tensile load (N). Especially, 100M1 configuration improved the tensile load capacity (N) by 10,76% and yielded higher tensile modulus than others. 200M1 and 200M2 gave similar modulus results to WM one whereas 100M2, 100M3, and 200M3 exhibited lower modulus data.

According to the load-deflection curves of the sandwich panels, the existence of wire mesh sheets provided to carry a larger amount of bending loads (N) compared to WM ones. Moreover, WM specimens were failed suddenly after the maximum force was reached due to brittleness of CFRP facings. However, sandwiches with hybrid facings carried bending loads with a larger plateau for 10 mm thick core specimens and failed with a decreasing slope after the point of maximum force is reached. A similar failure behavior was also observed for both 20 mm and 30 mm thick foam core sandwich panels. Therefore, when WM sandwiches were failed suddenly the hybrid facings sandwiches continued to carry a larger amount of bending loads. For instance, when the sudden drop was seen for WM sandwiches at a certain deflection, 200M1.T10.S15 sandwich panel carried 85,75% higher bending load than WM.T10.S15 at the same deflection value. In another example, when the WM.T30.S15 sandwich lost 25,37% of the load capacity during a sudden failure, 100M1.T30.S15 lost only 4,28%. On the other hand, long-span beam sandwiches carried lower bending loads than that of short-span specimens as expected. But, wire mesh sheets in long-span sandwich panels were not as effective as the short-span sandwiches particularly during the failure.

Core shear and facing stress (MPa) values were calculated and the results showed that they are decreasing with the increase of core thickness. However, testing under long-span, the facing stress of the sandwich panels increases whereas core shear stress reduces. Wire mesh sheets also favorably affected the results.

Flexural stiffness ($N.m^2$) of the structures was evaluated based on both analytical classical sandwich beam theory and experimental ASTM approach. Two times increase of the core thickness improved flexural stiffness 3,88 times (3,64 for ASTM approach) whereas three times increase of core thickness yielded 8,78 times (8,63 for ASTM approach) higher results. 100M1 sandwich configuration, which was the most efficient one among all configurations, improved the flexural stiffness of the structures by 14,24%, 13,32%, and 13,00% for 10 mm, 20 mm and 30 mm thick core sandwiches respectively when compared to WM sandwich panels based on the analytical approach. According to the experimental results, 100M1 sandwiches increased the results by 13,37% for 10 mm, 16,60% for 20 mm, and 13,37% for 30 mm, respectively.

Transverse shear rigidity force (N) increases almost linearly with core thickness whereas core shear modulus (MPa) decreases nonlinearly. But the wire mesh sheets did not contribute to the transverse shear rigidity and the core shear modulus as much as the flexural stiffness. Small improvements were obtained.

Failure behavior of the sandwich panels was examined and primary failure modes were addressed as core shear and indentation. While 10 mm (both short and long span) and long-span 20 mm thick core sandwiches were failed due to core shear, 30 mm thick core sandwiches (both short and long span) were failed due to indentation. The failure of short-span 20 mm thick core sandwiches was observed at a boundary of core shear and indentation according to analytical collapse mechanisms. Because of the indentation failure mode, the flexural characteristics were nonlinearly improved with core thicknesses. For instance, 20 mm thick core WM sandwiches have a 60,55% higher bending load capacity than that of 10 mm whereas 30 mm thick core WM sandwiches have 4,04% higher bending load

capacity than that of 20 mm. However, the latter value was increased to 7,61% with the aid of 100M1 configuration. Wire mesh sheets also improved the failure behavior of the sandwich structures by preventing the catastrophic sudden drop of the bending force.

Sandwich design parameters considered in this work were examined via two-way ANOVA using Response Surface Methodology (RSM). Based on the constructed models and individual effects of the parameters, the results are statistically significant in the 95% confidence interval. In addition, according to high values of correlation coefficients (R^2), the results of ANOVA and regression analysis confirmed that the constructed models strongly explain the significant changes of flexural characteristics based on the design parameters, and the flexural characteristics can be predicted with minimum error.

GENİŞLETİLMİŞ ÖZET

Mühendislik malzemeleri genel olarak altı ana kategoriye ayrılmaktadır. Bunlar, metaller, seramikler, camlar, elastomerler, polimerler ve hibritlerdir. Hibritler çeşitli şekil, boyut ve miktar bakımından diğer beş malzeme ailesinin birleşiminden oluşabilmektedir. Bileşen malzemelerin olumsuz yanlarını elimine ederek en iyi özelliklerini bir araya getirir ve tek bir kompozit malzemeden elde edilmesi mümkün olmayan istenilen mekanik özelliklerin elde edilmesinde önemli bir rol oynamaktadır. Hibrit malzeme sınıfına dahil olan sandviç kompozitler, havacılık, uzay, otomotiv, taşımacılık, gemi inşası gibi birçok mühendislik alanında yapısal malzeme olarak kullanılmaktadır. Çok yüksek eğilme rijitliğine karşın hafifliği, ani ve darbe yüklerine karşı direnci, çevresel faktörlere karşı direnci, ısı ve gürültüye karşı izolasyon sağlaması gibi özellikleri sayesinde konvansiyonel mühendislik malzemelerinin yerine geçmeye aday malzemelerdir. Sandviçler, iki yüzey tabakanın bir çekirdek malzeme ile ayrılıp onların uygun bir bağlayıcı matrisle yapısal malzeme haline getirilmesi ile üretilir. Oldukça ince metal alaşımlar ve elyaf takviyeli kompozitler yüzey tabaka olarak kullanılırken, yüzeye göre oldukça kalın ve düşük yoğunluğa sahip endüstriyel polimer ve metal köpükler, balsa ağacı, bal peteği, oluklu ve kafesli yapıya sahip malzemeler de çekirdek (core) olarak kullanılmaktadır. Sandviçlerin oluşturulmasında termoset ve termoplastik reçineler bulunmaktadır. Bilinen avantajlarının yanı sıra, en iyi özelliklere sahip bileşen malzemelerin bir araya getirilmesi ile çok fonksiyonlu sandviçler de elde etmek mümkündür.

Bu çalışmada, epoxy matrix kullanılarak karbon elyaf ve dokunmuş elek teller içeren yüzey tabakalar ve polyvinylchloride (PVC) köpük ile sandviç yapı oluşturulmuştur. Karbon elyaf kumaşlar düz dokuma ve 200 g/m^2 alansal yoğunluktadır. PVC köpük ise lineer çapraz bağlı, kapalı hücre, rijit ve literatürle kıyaslandığında 48 kg/m^3 gibi oldukça düşük yoğunluğa sahiptir. 10 mm, 20 mm and 30 mm olmak üzere üç farklı çekirdek kalınlığı kullanılmıştır. Karbon/epoksi

kompozit yüzeyler, çok ince AISI 304 paslanmaz çelik dokuma elek teller ile hibritlenmiştir.100-mesh (154 mikron, tel kalınlığı 0,1 mm) ve 200-mesh (77 mikron, tel kalınlığı 0,05 mm) ölçülü iki farklı elek tel (levhalar) kullanılmıştır. Çelik elek teller, delikli yapıda olup çok inceden oldukça kaba boyutlara kadar farklı tel çaplarında bulunmaktadır. Yakın zamanda literatürde, kalın çelik elek tellerin kullanımına inşaat ve makine mühendisliği uygulamalarında rastlanılmaktadır. Bu tez çalışmasının başlıca amaçlarından biri çelik elek tellerin karbon elyaf sandviç panellerin eğilme karakteristikleri üzerine etkisini araştırmak ve oldukça düşük yoğunluğa sahip köpük çekirdekler ve çok ince boyutlardaki çelik elek teller ile çok fonksiyonlu yapısal elemanlar geliştirmektir. Çünkü karbon elyaf takviyeli polimer (CFRP) yüzey tabakaların en büyük dezavantajı gevrek ve heterojen bir yapıda olmasıdır. CFRP/PVC köpük çekirdekli sandviçler yüksek eğilme yüklerini taşıyabilmelerine rağmen, yapının hasara uğraması kuvvetteki ani düşüş ile birlikte beklenmedik bir şekilde ani (katastrofik) olarak meydana gelmektedir. Yapılan öncü deneyler ve elde edilen sonuçlar, CFRP yüzey tabakalarının çelik elek teller ile hibritlendiğinde ani kuvvet düşüşlerini engelleyebileceğini göstermiştir. Çalışmanın ikinci ana amacı, hafif, rijit ve güçlü sandviç kompozitler üreterek malzeme evreninde yer almayan fakat gereksinim duyulan yeni hibrit malzemeler ile malzeme evrenindeki boşlukların doldurulmasına katkıda bulunmaktır. Böylece, bu çalışmada geliştirilen sandviç panellerden elde edilen sonuçlar hem literatüre hem de malzeme evrenine katkı sağlayacaktır.

Sandviç paneller vakum torbalama yöntemi ile üretilmiştir. Bu yöntem, kolay ve maliyet etkin olması bakımından laboratuvar araştırmaları gibi az parçalı üretimlerde daha uygundur. Ancak ürün kalitesi operatörün uygulama becerisine bağlıdır. Üretim, alt tarafı cam yüzey ve üst tarafı açık bir şekilde gerçekleştirilir. Üretime başlamadan önce her bir katmana yeterli matrisin sağlanabilmesi için bileşen malzemelerin ağırlıkça oranları belirlenmelidir. Matris miktarı, elyaf kumaşların, elek tellerin ve çekirdek malzemelerin ağırlıkları dikkate alınarak

hesaplanmıştır. Epoksi reçine ve uygun sertleştiricisinin ağırlıkça oranı 100:25'tir. Üretim esnasında tüm katmanlar elle reçine emdirilmesi yoluyla belirli sıralamada üst üste istiflenmiştir. Tüm katmanların istiflenmesinden sonra sandviç üzerinden hava kabarcıklarının çıkabilmesi, fazla reçinenin dışarı atılabilmesi ve kürlenmeden sonra kolayca ürünün çıkarılabilmesi için sandviç üzerine delikli bir ayırıcı film serilmiştir. Onun üzerine ise ürün üzerinden gazların geçişi ve fazla reçinenin toplanması için vakum battaniyesi serilmiştir. Son olarak, sandviç panel bir vakum torbası içinde sızdırmaz bant ile çevrelenmiştir. Kürlenme işlemi oda sıcaklığında 0,01 mbar vakum atmosferi altında 24 saat bekletilerek gerçekleştirilmiştir. Sandviç katmanları, yüzey tabakaların çekirdek malzemeye ayrıca yapıştırılması yerine eş zamanlı kürlenmiştir.

Sandviç katmanların dizimlimleri, elek tellerin boyutu ve katmanlar arasındaki yeri, çekirdek kalınlığı ve mesnet açıklığı gibi parametreler sandviç panel konfigürasyonlarını belirlemiştir. Elyaf yüzeyler sandviç kompozitin nötr eksenine göre simetrik olarak dizilmiştir ancak çelik elek levhalar (M) ya üst yüzey tabakanın ilk karbon elyaf katmanının altına gelecek şekilde (M1) ya üst yüzey tabaka ile çekirdek ara yüzüne gelecek şekilde (M2) ya da her iki durumun uygulandığı şekilde (M3) yerleştirilmiştir. 1, 2 ve 3 kodları metal levhanın sandviç yapı içerisindeki pozisyonunu veya konumunu tanımlamaktadır. Daha önce bahsedildiği gibi üç farklı çekirdek kalınlığı kullanılmıştır ve testler iki farklı mesnet açıklığında (150 mm ve 200 mm) yapılmıştır. Bu sebeple, bir sistematik üretim prosesi belirlenmiş ve her bir örneklem sandviç panel bir kod sistemi ile tanımlanmıştır. "XXXMP.TC.SL" kodu sandviçi tanımlamaktadır. Üç haneli ilk terim (XXX) elek teli mesh ölçüsünü devamındaki (M) ve P ise metal teli ve telin katmanlar arasındaki pozisyonunu (M2 gibi), ikinci terim (TC) çekirdek kalınlığını ve son terim (SL) ise mesnetler arası açıklığı tanımlamaktadır. Örneğin, 100M2.T20.S15 olarak kodlanmış bir sandviç panel, 20 mm çekirdek kalınlığına (T20) sahip olup 100-mesh boyutunda elek tel levhayı üst yüzey tabaka ile çekirdek ara yüzünde (M2) barındırmaktadır ve sandviç numuneler 150 mm mesnet

açıklığında (S15) eğilme testlerine tabi tutulacaktır. Elek tellerin etkisini ortaya çıkarabilmek için elek tel levha barındırmayan (without Mesh-WM) referans paneller de üretilmiştir ve kod sistemindeki ilk terim WM olarak tanımlanmaktadır. WM.T20.S15 gibi.

Sandviç numuneler, ASTM C393, D7249 standartlarına göre, 2 mm/dk hızla üç nokta eğilme testlerine tabi tutulmuşlardır. Eğilme karakteristik özellikleri; yük taşıma kapasitesi, maksimum eğilme momenti, eğilme rijitliği, çekirdek kayma gerilmeleri, yüzey tabaka gerilmeleri, enlemesine (transvers) kayma rijitliği ve çekirdek kayma modülü değerleri hesaplanmıştır. Bunlar, hem klasik sandviç kiriş teoremine göre hem de ASTM D7250 standardına göre hesaplanmıştır. Ayrıca, yüzey tabaka malzemeleri ASTM D3039 standardına göre çekme testlerine tabi tutulmuştur ve çekme dayanımı özellikleri elde edilmiştir. Bu veriler sandviç yapıların eğilme karakteristik özelliklerinin hesaplanmasında kullanılmıştır.

Yüzey tabakalarda elek tel levhaların varlığı numunelerin daha fazla çekme yükü taşımasını sağlamıştır. Özellikle, 100M1 konfigürasyonu çekme yükü kapasitesini %10,76 oranında iyileştirmiş ve diğer konfigürasyonlara göre çekme yükü altında daha yüksek elastisite (Young) modülü sağlamıştır. 200M1 ve 200M2 numuneler WM konfigürasyonuna göre benzer elastisite modül değerlerini verirken, 100M2, 100M3 ve 200M3 numuneler daha düşük modül değerleri vermiştir.

Sandviç panellerin yük-çökme eğrilerine bakıldığında elek tel levhalara sahip sandviçlerin daha fazla eğilme yükü taşıdığı görülmüştür. WM konfigürasyonlu sandviçler maksimum kuvvet taşıma noktasına ulaştıktan sonra CFRP yüzeyler nedeniyle ani gevrek kırılma şekliyle hasara uğramıştır. Ancak hibrit yüzeyli sandviçlerin hasara uğraması, yapının maksimum yüke ulaştıktan sonra kuvvette ani düşüş yerine yavaşlayarak gerçekleşmiştir. Özellikle 10 mm çekirdek malzemeye sahip sandviçlerde, yapı maksimum yüke ulaştıktan sonra uzun bir düzlük boyunca eğilme kuvvetinin taşınması sağlanmıştır. Böylece, WM sandviçler ani bir şekilde kırılırken hibrit yüzeyli sandviçler çok daha fazla eğilme

kuvvetini taşıyabilmektedir. Örneğin, WM sandviçlerin ani kırılarak hasara uğradığı çökme değerlerinde 200M1.T10.S15 sandviç yapı WM numuneden %85,75 daha fazla yük taşımaktadır. Farklı bir örnekte ise, WM.T30.S15 sandviç yapı hasara uğradığında maksimum eğilme kuvvetinin %25,37'sini kaybederken 100M1.T30.S15 sandviç yapı sadece % 4,28'ini kaybetmiştir. Beklendiği üzere uzun mesnet açıklığına sahip numuneler kısa mesnetli numunelere göre daha az yük taşımıştır. Ancak elek tel levhalar, uzun mesnetli sandviçlerde kısa mesnetli numunelerin hasar davranışında etkili olduğu kadar etkili olamamıştır.

Çekirdek kayma ve yüzey gerilme değerleri hesaplanmış ve sonuçların çekirdek kalınlığı ile ters orantılı olarak değiştiği görülmüştür. Ayrıca, mesnet uzunluğu ile sandviçin yüzey gerilmeleri artarken, çekirdek kayma gerilmeleri azalmıştır. Elek tel levhalar sonuçlara olumlu etki yapmıştır.

Yapıların eğilme rijitliği ($N.m^2$) hem analitik olarak klasik sandviç kiriş teoremine göre hem de deneysel olarak ASTM yaklaşımlarına göre hesaplanmıştır. Çekirdek kalınlığının iki kat artması eğilme rijitliğini 3,88 kat (ASTM yaklaşımında 3,64) iyileştirirken üç kat kalınlık artışı eğilme rijitliğini 8,78 kat (ASTM yaklaşımında 8,63) iyileştirmiştir. 100M1 sandviç konfigürasyonu tüm konfigürasyonlar içinde en etkili olup eğilme rijitliğini 10 mm, 20 mm ve 30 mm çekirdek kalınlığındaki sandviçler için analitik yaklaşıma göre sırasıyla %14,24, %13,32 ve %13 oranında iyileştirmiştir. Deneysel yaklaşıma göre ise artış 10 mm için %13,37, 20 mm için %16,60 ve 30 mm için %13,37 olarak elde edilmiştir.

Transvers kayma rijitliği çekirdek kalınlığı ile hemen hemen doğrusal bir artış göstermekte olup çekirdek kayma modülü ise doğrusal olmayan bir şekilde azalmaktadır. Ancak elek tellerin varlığı bu özelliklere eğilme rijitliğindeki gibi anlamlı bir katkı sağlamamıştır, sadece küçük iyileşmeler mevcuttur.

Sandviç yapıların hasar davranışları incelendiğinde başlıca hasar modlarının çekirdek kayması ve batma şeklinde olduğu görülmüştür. 10 mm kalınlığındaki çekirdekli sandviç yapı çekirdek kaymasına göre hasara uğrarken 30 mm çekirdekli sandviçlerde batma görülmüştür. 20 mm sandviçler ise çökme

prensiplerine göre her iki davranışın sınır bölgelerinde bulunmaktadır. Batmadan dolayı eğilme karakteristikleri çekirdek kalınlığı ile doğrusal olmayan bir şekilde iyileşme göstermiştir. Örneğin, 20 mm çekirdek kalınlığına sahip WM sandviçler 10 mm çekirdek kalınlığına sahip sandviçlere göre %60,55 daha fazla eğilme yükü taşırken 30 mm çekirdek kalınlığına sahip WM sandviçler 20 mm çekirdek kalınlıktaki sandviçlere göre %4,04 daha fazla eğilme yükü taşımaktadır. Ancak 100M1 konfigürasyonu bu değeri %7,61'e çıkarabilmiştir. Elek tel levhalar katastrofik ani kırılmaları engelleyerek sandviç yapıların hasar davranışlarını da iyileştirmiştir.

Bu çalışmada göz önünde bulundurulan sandviç tasarım parametreleri ANOVA ile Response Surface Metodu ile incelenmiştir. Oluşturulan modellere ve parametrelerin bağımsız etkilerine dayanarak, %95 güven aralığında, parametrelerin sonuçlar üzerindeki etkisi istatistiksel olarak anlamlı bulunmuştur. İlaveten, regresyon analizlerine ve elde edilen yüksek korelasyon katsayılarına (R^2) göre oluşturulan modeller, tasarım parametreleri ile eğilme karakteristiklerinin anlamlı değişimlerini güçlü bir şekilde açıklamaktadır ve ayrıca eğilme karakteristikleri minimum hata ile tahmin edilebilmektedir.

ACKNOWLEDGMENT

Foremost, I would like to express my sincere gratitude to my supervisor, Prof. Dr. Necdet GEREN, for his invaluable guidance, advice, encouragement to develop myself and my studies. Feeling his support, both personal and professional helped me a lot during the thesis work.

I would like to thank specially to Head of the Mechanical Engineering Department, Prof. Dr. Hüseyin AKILLI, for his continuous morale and encouraging advice. His office door was always open for me and he always made an effort to solve the problems that I faced. I am also thankful to my thesis committee members, Prof. Dr. Melih BAYRAMOĞLU and Assoc. Prof. Dr. Kerimcan ÇELEBİ, for their advice during my study. I would like to thank to other members of the jury, Prof. Dr. Uğur EŞME and Assoc. Prof. Dr. Erinç ULUDAMAR, for their evaluation of my thesis.

I am truly grateful to my colleagues, Mete Han BOZTEPE, Hulusi DELİBAŞ, Ahmet ÇETİN, Durmuş Can ACER for their continuous support, motivation, and invaluable friendship. I wish to thank Technician Sefa MERAL for his help in the preparation of the specimens required in experimental studies.

In addition, I would like to thank all the staff at Mech. Engineering. Dept., the Unit of Teaching Staff Training Program (ÖYP), the Unit of Scientific Research Projects department (BAP). With the aid of the financial supports of ÖYP and BAP units, I carried out all the purchasing processes, I attended several scientific conferences and congress to present our studies.

Lastly but most importantly, many thanks go to my parents, Halime UZAY and İrfan UZAY, and my wife Fatma İŞLEK UZAY. No words can state my deep gratitude to you for your understanding, confidence, patience, endless love, and prayers. And lastly, I would like to express my very special thanks to my unborn baby who strongly motivated me after came into my life.

CONTENT **PAGE**

ABSTRACT I
ÖZ II
EXTENDED ABSTRACT III
GENİŞLETİLMİŞ ÖZET IX
ACKNOWLEDGMENT XV
CONTENT XVI
LIST OF FIGURES XX
LIST OF TABLES XXX
SYMBOLS AND ABBREVIATIONS XXXIV
1. INTRODUCTION 1
1.1. Importance of Using Composite Materials 5
1.2. Manufacturing of Composite Materials 7
1.3. Design of Sandwich Structures 12
1.4. The constituent of Sandwich Structures 14
2. PREVIOUS STUDIES 17
2.1. Utilization of Aluminum (Al) Foam Core for Sandwich Structures 17
2.2. Utilization of Polymer Foam Core for Sandwich Structures 24
2.3. Utilization of Other Core Materials for Sandwich Structures 42
2.4. Numerical Analysis for Sandwich Structures 46
2.5. Current Developments for Sandwich Core Materials 48
2.6. Advanced Technologies for Composite Manufacturing 54
2.6.1. Advances in Lay-up Processes 54
2.6.2. Advances in Pultrusion Method 56
2.6.3. Advances in Stitching Machines 56
2.6.4. Advances in Hot Press Molding Method 57
2.6.5. Same Qualified Resin Transfer Molding (SQRTM) 58
2.7. Significance and Goal of the Study 60

3. MATERIAL AND METHOD 67
3.1. Materials Used for the Sandwich Panels 67
3.1.1. Carbon Fiber Fabrics 67
3.1.2. Core Material 68
3.1.3. Matrix Material 70
3.1.4. Stainless Steel Wire Mesh Sheets 70
3.2. Equipment and Pre-processes for Sandwich Manufacturing 72
3.2.1. Vacuum Pump 72
3.2.2. Chemical Treatment Solution 73
3.2.3. Preparation of Composite Materials and Consumables 74
3.3. Fabrication of Sandwich Composites 74
3.4. Determination of Fiber Volume Fraction (V_f %) 79
3.5. Design of Experiments 80
3.5.1. Core Thickness 81
3.5.2. Wire Mesh Size 81
3.5.3. Stacking Sequence of Wire Mesh Sheets 81
3.5.4. Span Length 82
3.6. Preparation of Test Specimens 83
3.7. Tensile Tests 86
3.8. Three-point Bending Tests 88
3.9. Analytical and Experimental Approaches for Bending Characteristics 88
3.9.1. Core shear ultimate stress (MPa) 89
3.9.2. Core shear yield stress (MPa) 89
3.9.3. Facing stress (MPa)* 90
3.9.4. Facing 1 and facing 2 ultimate stress (MPa) 90
3.9.5. Flexural stiffness ($N.mm^2$) 91
3.9.6. Transverse shear rigidity (N) 92
3.9.7. Core shear modulus (MPa) 93
3.9.8. Bending strength of the core 94

3.9.9. The maximum stress in the face sheets of sandwich panels..... 94
3.9.10. Core shear stress..... 94
3.9.11. Maximum bending stress of face sheet..... 95
3.10. Examination of the Failure Modes..... 96
4. RESULTS AND DISCUSSION..... 97
4.1. Fiber Volume Fractions of the Sandwich Panels..... 97
4.2. Thickness and Weight of the Sandwich Panels..... 98
4.3. Tensile Test Results..... 99
4.4. Three-point Bending Test Results of Short-span Sandwich Beams..... 109
4.4.1. Load-Deflection Curves of 10 mm Thick Core Sandwich Panels..... 109
4.4.2. Load-Deflection Curves of 20 mm Thick Core Sandwich Panels..... 116
4.4.3. Load-Deflection Curves of 30 mm Thick Core Sandwich Panels..... 122
4.4.4. Comparison of the Sandwich Panels Based on the Core Thickness..... 129
4.5. Three-point Bending Test Results of Long-span Sandwich Beams..... 134
4.6. Comparison of the Bending Test Results of Both Short and Long-span Sandwich Panels..... 142
4.7. Evaluation of Flexural Characteristics..... 145
4.7.1. Load Carrying Capacity of the Sandwich Panels..... 145
4.7.2. Core Shear Ultimate Stress and Face Sheet Ultimate Stress..... 148
4.7.3. Bending Strength of the Core and Maximum Stress in the Sandwich Facings Based on Analytical Approach..... 152
4.7.4. Evaluation of Flexural Stiffness, Transverse Shear Rigidity, and Core Shear Modulus based on ASTM D7250 Standard..... 157
4.8. Examination of Failure Behavior of the Sandwich Panels..... 165
4.9. Investigation of the Sandwich Parameters with ANOVA..... 175

5. CONCLUSION 189
REFERENCES 195
CURRICULUM VITAE 209

LIST OF FIGURES **PAGE**

Figure 1.1. Material families in engineering 2
Figure 1.2. Hybrid materials; a) composites, b) sandwiches, c) segmented structures, d) cellular structures 2
Figure 1.3. Schematic of hand lay-up method 7
Figure 1.4. Schematic view of the vacuum bag method 8
Figure 1.5. Schematic view of RTM process 9
Figure 1.6. Schematic view of the VARTM method 10
Figure 1.7. Representation of autoclave process 11
Figure 1.8. Filament winding method 11
Figure 1.9. The similarity between I-beam and sandwich composite 13
Figure 1.10. Sandwich panel failure modes under bending loading 14
Figure 2.1. Theoretical failure mode map under a) Static loading, b) Fatigue 18
Figure 2.2. Typical load-displacement curve plot for each core thickness 19
Figure 2.3. Failure modes in quasi-static three-point bending 20
Figure 2.4. Configurations based on inner plate location: a) Case 1, b) Case 2, c) Case 3, d) Case 4, e) Case 5, f) Case 6 22
Figure 2.5. Stacking sequence of the panels a) Group 1, b) Group 2 23
Figure 2.6. (a) Schematic representation and (b) Al sheet/GFPP/Al foam sandwich 24
Figure 2.7. 20 wt % PP-g-MA/80 wt % PP blends (a) as fine granules (b) as adhesive film after hot pressing (Baştürk and Tanoğlu, 2011) 24
Figure 2.8. Transverse impact results based on; a) face thickness with fixed core density (97 kg/m3), b) core density with fixed thickness (1,02 mm) (width of the bending specimens were 20 mm) 25
Figure 2.9. Failure modes of sandwiches under three-point bending 26
Figure 2.10. Crack growth scenarios in foam core sandwiches 29
Figure 2.11. Comparative representation of the load-displacement curves 30

Figure 2.12. Sandwich beam loading in three-point bending test 32
Figure 2.13. Experimental set up (ZWICK Z250/SN5A machine)..... 33
Figure 2.14. Macroscopic and microscopic images of fractured surfaces of the SMS [04] sandwich 34
Figure 2.15. Macroscopic and microscopic images of fractured surfaces of the SMS [0/902/0] Sandwich..... 34
Figure 2.16. Macroscopic and microscopic images of the crack growing during the fatigue test of the sandwich SMS [0/902/0] 35
Figure 2.17. Effect of; a) core thickness at density of 80 kg/m3(1: 25 mm, 2: 15 mm), b) core density (1: 60 kg/m3, 2: 80 kg/m3)..... 35
Figure 2.18. Sandwich panels configurations; a) 2 x 4 mm grooves, spaced 40 mm (2 x 4(40)); b) 2 x 2 mm grooves, spaced 20 mm (2 x 2(20)); c) resin distribution medium; d) continuous filament mat; and e) no infusion aid but excess 2,4-P inhibitor (2,4-P) (Truxel et 37
Figure 2.19. Preparation of the facing/core interface using different methods on the top surface of the foam (before infusion) 37
Figure 2.20. a) Geometry and loading of the TSD specimen, b) Sketch of the TSD test setup..... 38
Figure 2.21. Visual inspection and C-scan results of impact damage area based on impact energy values of three types of sandwiches..... 39
Figure 2.22. One-core, two-core, and three-core sandwich structures..... 41
Figure 2.23. Sandwich panels with; a) non-filled corrugated core, b) aluminum foam-filled corrugated foam..... 43
Figure 2.24. Comparison of both aluminum foam-filled and empty corrugated core sandwich panels..... 44
Figure 2.25. The shape of truss, conventional and re-entrant honeycombs 45
Figure 2.26. Comparison of load-displacement curves obtained by both experimentally and numerically 47

Figure 2.27. Comparison of the load-displacement curves obtained from experiments, theoretical and numerical solutions 48
Figure 2.28. Manufacturing process of carbon fiber lattice core sandwich panel 49
Figure 2.29. Carbon fiber lattice core sandwich products; a) panel, b) shell, c) cylinder, d) double-layer panel 49
Figure 2.30. Core materials; a) YmaCell, b) polypropylene honeycomb, c) Airex foam 50
Figure 2.31. a) Stitching of the perforated core, b) developed sandwich panel 50
Figure 2.32. Load-displacement curves of the sandwiches (R: plain foam core, P: perforated, S1: 600-tex stitched, S2: 1200 tex stitched, S3: 1800 tex stitched, S4: 2400 tex stitched) 51
Figure 2.33. Load-displacement curves of stitched and unstitched and foam core sandwiches 53
Figure 2.34. Sandwich panels with; a) no-corrugated, plain foam core, b) triangular corrugated core, c) rectangular corrugated core, d) trapezoidal corrugated core 54
Figure 2.35. Hand lay-up vs. spray-up manufacturing methods 55
Figure 2.36. a) AFP process, b) Image of the AFP 56
Figure 2.37. Pultrusion method 56
Figure 2.38. Image of Stitching machine 57
Figure 2.39. Manufacturing process with developed hot press molding; a) placing the prepared composite strut into corresponding position, b) lay-up of five layers of carbon/epoxy prepregs on the mold, c) dispersing end of the struts by penetrating them into prepreg 58
Figure 2.40. a) traditional production of composite parts, b) net shape, single part composite production 58
Figure 2.41. Schematic presentation of SQRTM process 59

Figure 2.42. Comparative demonstration of curing cycles both in SQRTM and autoclave 60
Figure 2.43. Young modulus vs. density chart of the material families..... 62
Figure 3.1. Woven fabrics; a) plain, b) twill, c) satin, d) image of plain weave woven fabric used in this study 68
Figure 3.2. Stainless steel wire mesh; a) 100 mesh, b) 200 mesh..... 71
Figure 3.3. The vacuum pump used for the fabrication of the sandwich panels..... 73
Figure 3.4. Caustic soda..... 74
Figure 3.5. A schematic view of the manufacturing process 76
Figure 3.6. The production steps of sandwich composite panel 77
Figure 3.7. Flowchart of the produced sandwich configurations..... 78
Figure 3.8. Core material thickness; a) 10 mm, b) 20 mm, c) 30 mm 81
Figure 3.9. Layer position of stainless steel wire mesh sheets; a) without wire mesh, b) 200 mesh at interface, c) 200 mesh under 1st ply, d) combination of b and c, e) 100 mesh under 1st ply, f) 100 mesh at interface, g) combination of e and f..... 82
Figure 3.10. Schematic views based on span length, a) 150 mm, b) 200 mm 83
Figure 3.11. Schematic representation of tensile test specimen and composite lamination dimensions..... 84
Figure 3.12. a) schematic view of the tensile test specimen (untabbed), b) the tab formation, c) produced test specimen 85
Figure 3.13. Schematic representation of sandwich specimens and their panel dimensions, a) short beam, b) long beam 85
Figure 3.14. Attaching the dial gauge indicator to the tensile testing machine for measuring of strain during the tensile loading 87
Figure 3.15 a) Sandwich panel schematic representation, b) Samples' code system (Note: sandwiches which do not include any wire mesh sheets are named as "WM.TC.SL")..... 87

Figure 3.16. Three-point bending test of a short beam sandwich specimen 88
Figure 3.17. Determination of nonlinearity offset 92
Figure 4.1. Load-extension curves of WM face sheets 99
Figure 4.2. Load-extension curves of 100M1 face sheets 100
Figure 4.3. Load-extension curves of 100M2 face sheets 100
Figure 4.4. Load-extension curves of 100M3 face sheets 100
Figure 4.5. Load-extension curves of 200M1 face sheets 101
Figure 4.6. Load-extension curves of 200M2 face sheets 101
Figure 4.7. Load-extension curves of 200M3 face sheets 101
Figure 4.8. Stress-strain curves of WM face sheets 103
Figure 4.9. Stress-strain curves of 100M1 face sheets 103
Figure 4.10. Stress-strain curves of 100M2 face sheets 104
Figure 4.11. Stress-strain curves of 100M3 face sheets 104
Figure 4.12. Stress-strain curves of 200M1 face sheets 104
Figure 4.13. Stress-strain curves of 200M2 face sheets 105
Figure 4.14. Stress-strain curves of 200M3 face sheets 105
Figure 4.15. a) Maximum tensile load of the facings b) Maximum tensile strength of the facings 108
Figure 4.16. Load – deflection curves WM.T10.S15 sandwich specimens 109
Figure 4.17. Load – deflection curves 100M1.T10.S15 sandwich specimens 110
Figure 4.18. Load – deflection curves 200M1.T10.S15 sandwich specimens 110
Figure 4.19. Load – deflection curves 100M2.T10.S15 sandwich specimens 110
Figure 4.20. Load – deflection curves 200M2.T10.S15 sandwich specimens 111
Figure 4.21. Load – deflection curves 100M3.T10.S15 sandwich specimens 111
Figure 4.22. Load – deflection curves 200M3.T10.S15 sandwich specimens 111
Figure 4.23. Comparison of the 10 mm thick foam core sandwiches with and without wire mesh; a) WM and 100-mesh, b) WM and 200-mesh . 114
Figure 4.24. Reduction in bending load between the maximum point and 10 mm MS deflection 116

Figure 4.25. Load – deflection curves WM.T20.S15 sandwich specimens 116
Figure 4.26. Load – deflection curves 100M1.T20.S15 sandwich specimens..... 117
Figure 4.27. Load – deflection curves 200M1.T20.S15 sandwich specimens..... 117
Figure 4.28. Load – deflection curves 100M2.T20.S15 sandwich specimens..... 117
Figure 4.29. Load – deflection curves 200M2.T20.S15 sandwich specimens..... 118
Figure 4.30. Load – deflection curves 100M3.T20.S15 sandwich specimens..... 118
Figure 4.31. Load – deflection curves 200M3.T20.S15 sandwich specimens..... 118
Figure 4.32. Comparison of the 20 thick foam core sandwich panels with and without mesh; a) WM and 100-mesh, b) WM and 200-mesh 120
Figure 4.33. Reduction in bending force between the maximum point and 6,29 mm MS deflection 122
Figure 4.34. Load-deflection curves WM.T30.S15 sandwich specimens..... 123
Figure 4.35. Load-deflection curves 100M1.T30.S15 sandwich specimens..... 123
Figure 4.36. Load-deflection curves 200M1.T30.S15 sandwich specimens..... 123
Figure 4.37. Load-deflection curves 100M2.T30.S15 sandwich specimens..... 124
Figure 4.38. Load-deflection curves 200M2.T30.S15 sandwich specimens..... 124
Figure 4.39. Load-deflection curves 100M3.T30.S15 sandwich specimens..... 124
Figure 4.40. Load-deflection curves of 200M3.T30.S15 sandwich specimens ... 125
Figure 4.41. Comparison of the 30 mm thick foam core sandwiches with and without mesh; a) WM and 100-mesh, b) WM and 200-mesh 126
Figure 4.42. Reduction in bending force between the maximum point and 5,59 mm MS deflection 129
Figure 4.43. Comparison of the sandwich panels based on the core thickness. (Configurations: a) WM, b) 100M1, c) 100M2, d) 100M3, e) 200M1, f) 200M2, g) 200M3) 131
Figure 4.44. Comparison of sandwich load-deflection curves based on both facing and core thickness..... 133
Figure 4.45. Load-deflection curves of WM.T10.S20 sandwich specimens 136
Figure 4 46. Load- deflection curves of 100M1.T10.S20 sandwich specimens .. 136

Figure 4.47. Load- deflection curves of 200M1.T10.S20 sandwich specimens .. 137
Figure 4.48. Load- deflection curves of WM.T20.S20 sandwich specimens 137
Figure 4.49. Load- deflection curves of 100M1.T20.S20 sandwich specimens .. 137
Figure 4.50. Load- deflection curves of WM.T30.S20 sandwich specimens 138
Figure 4.51. Load- deflection curves of 100M1.T30.S20 sandwich specimens .. 138
Figure 4.52. Load-deflection curves of 10 mm thick long-span sandwich beams 139
Figure 4.53. Load-deflection curves of 20 mm thick long-span sandwich beams 140
Figure 4.54. Load-deflection curves of 30 mm thick long-span sandwich beams 140
Figure 4.55. Comparison of the maximum load capacity and the load at where WM sandwiches underwent to failure for long-span sandwiches ... 141
Figure 4.56. Comparison of sandwich bending load capacities tested under 150 mm and 200 mm span length..... 142
Figure 4.57. Load-deflection curves of short and long-span sandwiches having 10 mm core thickness; a) WM, b) 100M1, c) 200M1 143
Figure 4.58 Load-deflection curves of short and long-span beam sandwiches having 20 mm core thickness; a) WM, b) 100M1 144
Figure 4.59. Load-deflection curves of short and long-span beam sandwiches having 30 mm core thickness; a) WM, b) 100M1 145
Figure 4.60. Load-carrying capacities of sandwiches based on different configurations, span length, and core thickness 146
Figure 4.61. Load-carrying capacities at initiation point of sudden failure for WM sandwiches based on different configurations, span length, and core thickness..... 147
Figure 4.62. The change of core shear and facing stresses with respect to (wrt) core thickness of WM sandwich panels..... 152
Figure 4.63. Maximum bending moment of the sandwiches wrt core thickness . 154

Figure 4.64. Maximum bending moment (analyt.) wrt span length of sandwich panels 155
Figure 4.65. The change of maximum bending moment, core bending strength and maximum sandwich facing stress (analyt.) of the short-span 100M1 sandwich panels wrt core thickness 157
Figure 4.66. Comparison of flexural stiffness and transverse shear rigidity based on core thickness according to ASTM approach 161
Figure 4.67. Comparison of flexural stiffness and core shear modulus based on core thickness (ASTM approach) 161
Figure 4.68. Comparison of transverse shear rigidity and core shear modulus based on core thickness (ASTM approach) 162
Figure 4.69. Flexural stiffness of the produced sandwich panel based on analytical approach 164
Figure 4.70. Differences of flexural stiffness values between analytical and experimental approaches 165
Figure 4.71. Failure mechanisms of core shear modes; a) Case I, b) Case II (Ashby et al., 2000) 167
Figure 4.72. Indentation failure mode (Ashby et al., 2000) 168
Figure 4.73. Progressive representation of bending behavior of WM.T10.S15 sandwich panel 169
Figure 4.74. Bending behavior of sandwich panel; a) WM.T10.S20, b) 100M1.T10.S20 170
Figure 4.75. Failure mechanism map of the sandwich beams (Ashby et al., 2000) (yellow: 10 mm thick core sandwiches, red: 20 mm thick core sandwiches, blue: 30 mm thick core sandwiches; right-hand lines short-span specimens, left-hand lines: long-span specimens). 172
Figure 4.76. Bending behavior of WM.T20.S15 173
Figure 4.77. Bending behavior of 100M1.T30.S15 sandwich panel 174

Figure 4.78. The change of sandwich panels' weight wrt core thickness and wire mesh size 182
Figure 4.79. Normal plot of residuals for; a) maximum load-carrying capacity, b) load capacity at which WM sandwiches underwent to sudden failure 183
Figure 4.80. Residual vs. run charts for; a) maximum load carrying capacity, b) load capacity at which WM sandwiches underwent to sudden failure 183
Figure 4.81. Effect of design parameters to; a) maximum load carrying capacity, b) load capacity at which WM sandwiches underwent to sudden failure 184
Figure 4.82. Effects of parameters on; a) core shear stress (MPa), b) facing stress (MPa), c) flexural stiffness ($N.m^2$) 185
Figure 4.83. Changes of transverse shear rigidity and core shear modulus wrt core thickness and wire mesh size 187
Figure 5.1. Flexural modulus vs density chart 189

LIST OF TABLES **PAGE**

Table 2.1. Three-point bending results of Al skin Al foam core sandwiches..... 21
Table 2.2. Failure modes in sandwich beams 28
Table 2.3. Compression strength and modulus results of the sandwiches based on two different processes 30
Table 2.4. The flexural strength and modulus results of the sandwiches based on two different processes 31
Table 2.5. Interface shear test results of the sandwich panels based on the processes 31
Table 2.6. Barcol hardness and flatwise compressive test results (M:mat; C:Cloth) 42
Table 2.7. Core shear ultimate and facing stresses 43
Table 2.8. Specifications of the sandwich composite specimens 52
Table 2.9. Shear properties of stitched and unstitched foam core sandwiches 53
Table 3.1. Physical and mechanical properties of woven plain continuous carbon fiber fabric 67
Table 3.2. Physical and mechanical properties of PVC foam core material 69
Table 3.3. Physical and Mechanical Properties of the epoxy resin and its hardener 70
Table 3.4. Chemical composition of wire mesh 71
Table 3.5. Physical and Mechanical Properties of the wire mesh film..... 72
Table 3.6. Technical specifications of the Vacuum Pump 73
Table 3.7. The parameters and their levels considered in this study 80
Table 4.1. Fiber and wire mesh volume fractions (V_F% and V_{WM}%) of the produced sandwich panels 97
Table 4.2. Average values of thickness (mm) and weight (g) measurements 98

Table 4.3. Maximum load-carrying capacities of face sheets with 100-mesh and without wire mesh sheet 102
Table 4.4. Maximum load-carrying capacities of face sheets with 200-mesh and without wire mesh sheet 102
Table 4.5. Tensile strength and tensile modulus of the facings with 100-mesh and without wire mesh sheet 107
Table 4.6. Tensile strength and modulus of the facings with 200-mesh and without wire mesh sheet 107
Table 4.7. Maximum load-carrying capacities and MS deflection of the sandwich panels 112
Table 4.8. Load-carrying capacities of sandwich panels after 10 mm thick core WM sandwiches underwent to sudden failure at MS deflection of ~10 mm 115
Table 4.9. Maximum load-carrying capacities and MS deflection of the 20 mm thick core sandwich panels 119
Table 4.10. Load-carrying capacities of sandwich panels after 20 mm thick core WM sandwiches underwent to sudden failure at MS deflection of ~6,29 mm 121
Table 4.11. Maximum load-carrying capacities and MS deflection of the sandwich panels for 30 mm thick foam core 125
Table 4.12. Load-carrying capacities of sandwich panels after 30 mm thick core WM sandwiches underwent to sudden failure at MS deflection of ~5,59 mm 127
Table 4.13. Maximum load-carrying capacities and MS deflections of the long-span sandwich panels 138
Table 4.14. Load carrying capacities of long-span sandwich panels after WM sandwiches underwent sudden failure 141
Table 4.15. Core shear and facings ultimate stress values of the sandwich panels based on both experimental and analytical approaches 151

Table 4.16. Maximum bending moment, core bending strength and maximum facing stress of the sandwich panels according to analytical calculations 156
Table 4.17. Flexural stiffness, transverse shear rigidity and core shear modulus of the sandwich panels based on ASTM approach 159
Table 4.18. The flexural stiffness of the sandwich beams based on the analytical approach 163
Table 4.19. Maximum bending load and collapse force by shear failure for 10 mm thick sandwich panels 171
Table 4.20. Maximum bending load and collapse force by shear and indentation failures for 20 mm thick sandwich panels 174
Table 4.21. Maximum bending load and collapse force by shear and indentation failures for 30 mm thick sandwich panels 175
Table 4.22. ANOVA results for sandwich weights 177
Table 4.23. ANOVA results for load carrying capacities 178
Table 4.24. ANOVA results for load capacities after WM sandwiches underwent sudden failure 178
Table 4.25. ANOVA results for core shear stress values 179
Table 4.26. ANOVA results for facing stress values 179
Table 4.27. ANOVA results for flexural stiffness 180
Table 4.28. Illustration of both adjusted and predicted correlation coefficients (R^2) 180
Table 4.29 The developed mathematical expressions to predict the responses (CT: core thickness, MS: wire mesh size) 181
Table 4.30. ANOVA results for transverse shear rigidity 186
Table 4.31. ANOVA results for core shear modulus 186

SYMBOLS AND ABBREVIATIONS

a	: Loading roller diameter	mm
b	: Sandwich width	mm
c	: Core thickness	mm
d	: Sandwich thickness	mm
d/s	: Ratio of fiber diameter to fiber spacing	-
m_m	: mass of matrix material	g
m_f	: mass of facing material	g
t, t_f	: Facing thickness	mm
AFP	: Automated fiber placement	-
$(AG)_{eq}$	: Equivalent shear rigidity	N
ASTM	: American society for testing and materials	-
CAD	: Computer aided design	-
CCD	: Central composite design	-
CT	: Core thickness	mm
$(EI)_b$, D	: Bending (Flexural) stiffness	$N.m^2$
E	: Modulus of elasticity	GPa
E_2	: Transverse modulus of facing material	GPa
E_c	: Modulus of core material	MPa
E_f	: Modulus of face sheet	GPa
E_m	: Modulus of matrix material	MPa
F	: Collapse load	N
F_1^u	: Facing 1 (top) ultimate stress	MPa
F_2^u	: Facing 2 (bottom) ultimate stress	MPa

FEA	: Finite element analysis	-
F_s^{ult}	: Core shear ultimate stress	MPa
FML	: Fiber metal laminate	-
FRPC	: Fiber reinforced polymer composite	-
G, G_c	: Core shear modulus	MPa
L, S	: Span length	mm
MS	: Wire mesh size	mesh
M_{max}	: Maximum bending moment	N.m
P_{max}	: Maximum bending load	N
PMI	: Polymethacrylimide	-
PU	: Polyurethane	-
PVC	: Polyvinylchloride	-
R^2	: Correlation coefficients	%
RSM	: Response surface methodology	-
RTM	: Resin transfer molding	-
SQRTM	: Same qualified resin transfer molding	
U	: Transverse shear rigidity	N
V_f	: Fiber volume fraction	%
V_{WM}	: Wire mesh volume fraction	%
VARTM	: Vacuum assisted resin transfer molding	-
δ, Δ	: Deflection	mm
ε_2^{ult}	: Transverse ultimate strain of the facing	mm/mm
ε_m^{ult}	: Ultimate strain of the matrix	mm/mm
ρ_m	: Density of matrix material	kg/m^3

ρ_f	: Density of facing material	kg/m^3
σ_{max}, σ_c	: Maximum bending stress in core	MPa
σ_2^f	: Transverse tensile strength of the facing material	MPa
σ_f	: Maximum stress in facing	MPa
σ_{yf}, σ^y_f	: Yield strength of facing material	MPa
τ_y^c	: Core shear yield strength	MPa

1. INTRODUCTION

Materials are the basic part of all-natural and man-made structures. In general, new materials are developed due to the necessity to enhance the structural efficiency and their performance beyond the available ones. In addition, new materials in turn certainly provide new opportunities to improve state-of-the-art structures and technology used in new developments. But these require additional efforts and bring many problems based on materials science. Fortunately, using composites is almost the best way to develop new materials, structures, and technology as well (Vasiliev and Morozov, 2007). The engineering materials are classified into six main categories. These are metals, glasses, ceramics, polymers, elastomers, and hybrids. Each category contains material families. As shown in Figure 1.1, it is possible to create hybrid materials by combining the other five material families in various shapes and dimensions. For instance, metals and ceramics have high durability and moduli whereas polymers are weaker. Therefore, hybrids play an important role to obtain multi-functionality and have a wider range to obtain desired properties that cannot be achieved from a single type of composite (Uzay et al., 2019).

Hybrid materials family includes fiber-reinforced composites, sandwich structures, foams, laminates, cables, lattice structures. In addition to these, natural materials such as wood, leaf, skin, and bone are the members of the hybrid family. Figure 1.2 shows the structural engineering hybrid materials as examples (Ashby, 2011).

In the scope of this thesis work, the composites, sandwiches, and cellular structures are going to be discussed in detail. But segmented structures are going to be mentioned briefly since it is irrelevant to the study. The segmented structures provide damage-tolerant by subdividing the materials into segments like a puzzle. Therefore, any crack or damage in one segment cannot spread to its neighbors and

remains locally (Ashby, 2011). Cellular structures are foams and lattices. Foams include a gap in a solid body and are defined by Ashby (2011) as bending dominated structures. The gaps may also be filled with structural additives to improve structural efficiency. On the other hand, Ashby (2011) defined the lattice structures as stretch dominated structures. Their structural efficiency is higher when compared to unmodified foams. Hinged frames, truss forms, or any different shapes for obtaining higher stiffness can be given as examples for lattice structures.

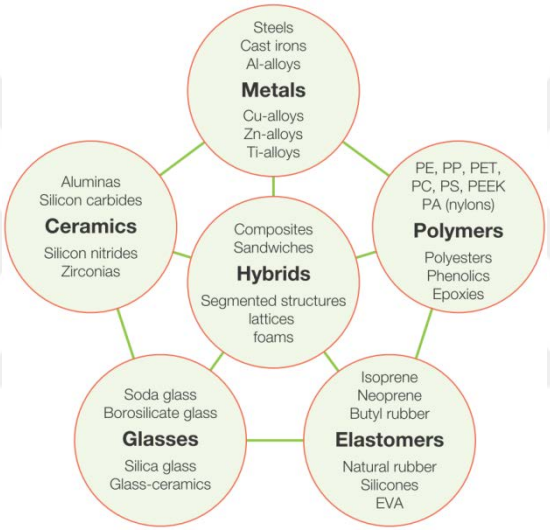
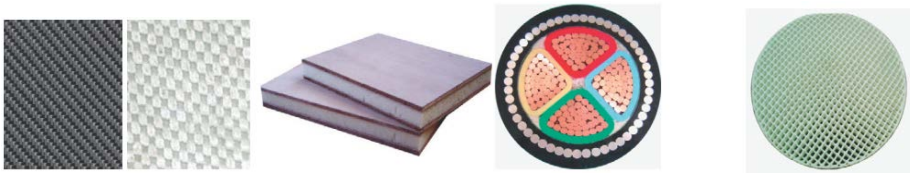


Figure 1.1. Material families in engineering (Ashby, 2011)



(a) (b) (c) (d)

Figure 1.2. Hybrid materials; a) composites, b) sandwiches, c) segmented structures, d) cellular structures (Ashby, 2011)

Composite materials are included as one of the classes of hybrid material family. They usually include at least two constituent materials to form a structural member and a large number of combinations can be obtained to develop composite

materials. Composites are used due to the attractive features that cannot be obtained with single constituent within them. The most well-known example to this is the fiber-reinforced composites immersed in a matrix material as a binder (Gibson, 2012). The mechanical loads are mainly carried by fibers, whereas the surrounding matrix firstly conserves the fibers in the desired orientation, then behaves as load transferring medium between fiber elements. In addition, the matrix prevents the fibers from the hazardous environment such as elevated temperatures and humidity. The strength and modulus values of most of the fiber-reinforced polymers (FRPs) are either better or more competitive than many conventionally used materials. They distinctively show superior properties over current metallic materials due to their low density, higher strength, and modulus to weight ratio, excellent fatigue damage tolerance. Therefore, FRPCs appear with a crucial role among the structural materials and they are currently used or considered to substitute with many conventional metals in most weight critical applications existed in sporting goods, automotive, marine, infrastructure, aerospace, etc. FRP composites have also usage area in electronics such as printed circuit boards, in power field such as transformer housing; biomedical applications such as bone plates for fracture fixation, prosthesis parts, implants; building construction such as wall and floors; furnishing such as chair springs, and in many industrial goods. As it is seen, FRPCs have many potential usage fields in the engineering industry. In order to reveal the composite materials into actual engineering use, a careful selection of individual materials, design considerations, and proper development of process techniques based on the realizing of their typical characteristics including physical, mechanical, and thermal is needed (Mallick, 2007).

Composites are classified according to reinforcement geometry or type of matrix material. While the geometry of reinforcement can be in the form of discontinuous or continuous fibers, flake, and particulate, but the matrix can be ceramic, polymer, and metal, etc. But particle and flake are not as effective as

fibers. In addition to these, structural composites are also available in the material universe called as hybrid and multilayered composites. One of the structural composites is sandwich materials. It is a special form of the laminated composites and typically consists of two very thin, stiff and strong face sheets such as lightweight metal alloys or FRP composites adhered to relatively lightweight and thicker material called as core such as corrugated panels, honeycomb, balsa wood, aluminum and/or polymer foams. In the near future, the sandwich structure is going to play a crucial role due to its lightweight and extremely high flexural stiffness and allows optimization for weight critical parts such as in marine, aviation, and automotive applications, satellites, turbine blades for wind power and sporting goods (Gibson, 2012; Carlsson and Kardomateas, 2011; Vinson, 1999). Multilayered composite laminates and sandwich beam structures are commonly available in many engineering practices. Composite laminates increase structural rigidity and strength with weight reduction over conventional metal alloys whereas sandwiches can contribute the mechanical performance of the structures beyond the composite laminates do without sacrificing rigidity and strength (Sayyad and Ghugal, 2017). Among these features other than lightweight and flexural rigidity, they provide heat and acoustic insulation, resistance to impact loading, improved fatigue life, resistance to corrosion and moisture, invisibility to radar waves, stable at very high speeds, getting aerodynamic surfaces. Due to the favorable features, most of the conventional metallic materials used in automotive, marine, aerospace, aviation, defense, energy, and civil industries with the growing technology will have replaced or augmented with the sandwich structures (Gibson, 2000; Baştürk and Tanoğlu, 2011; Liu et al., 2014; Tortoç, 2009; Peters, 1998; Kazak et al., 2016). The sandwich construction is the most attractive way for reducing the structural weight of a beam (or a panel). And it also allows improving its bending stiffness (Mallick, 2007).

1.1. Importance of Using Composite Materials

The need for lightweight structures significantly increases in many engineering industries. Because the decrease of oil reserves throughout the world and high demand for fossil fuels for energy leads to a higher price. Especially, it is known that the cost of transportation, carriage, and shipping fields mostly depends on fuel consumption. Consequently, the studies about the lightening of the structural body members are being developed rapidly. Producing the machines and their components from lightweight materials can help to improve load-carrying capacity with the same operational cost or in other words, it means the reduction of cost due to reduced fuel consumption or at the same payload, the transportation distance will be longer with less fuel consumption (Mileiko, 1997). At this point, sandwich composites will respond to the needs of industrial fields. For example, a polymer foam core sandwich structure provides 90% weight gain compared to the steel plate at the same deformation level. (Diab Group, 2012). Today, automotive manufacturers are in keen competition to reduce the emission rates in order to come across the requirements of EU legislation for newly manufactured vehicles. Therefore, the use of sandwich panels in the body of the vehicles does not only reduce the weight but also provides eco-friendly vehicles with reduced fuel consumption and CO_2 emissions (Elmarakbi, 2013).

In the early stages of composite structures, they were used in limited areas as secondary parts such as lightly loaded small parts. However, the recent applications show that the usage of composites is growing in primarily heavy loaded large structures such as fuselage and wings. For example, the Boeing 787 is the first commercial airliner uses composite fuselage and wings. Using of the composites on the primary body parts of the 787 is approximately 50% and based on carbon FRP. A similar development can be seen in Airbus A350 XWB. On the other hand, in the automotive industry, there has been an increasing interest to reduce structural weight of vehicles, and the use of composite parts is continuously growing. Glass FRP composites are highly available and dominate the automotive

market, but the interest to advanced high strength CFRP composites is increasing as the carbon fiber prices reduce. Weight gain on particular parts such as composite leaf spring can exceed 70% with higher fatigue resistance when compared to conventionally used steel springs. Chopped glass FRP composites have a wider application area and have commonly been used in body components since the appearance and structural rigidity are the basic design considerations. While the composites used in vehicles have mainly been applied to secondary structural members and appearance parts, the potential usage of composite materials on primary parts has been investigated. With the growing attention in electric vehicles, there is a strong need for composite usage to reduce the structural weight of vehicles to compensate for the heavily loaded batteries required for making more distances. Using composite materials in the body in white (BIW) parts provides a significant weight reduction. Because it was reported that approximately 90% of the energy consumption of urban concept automobiles is based on vehicle weight. When the components are made from carbon fibers, vehicles generally become 60% lighter than steel ones. Therefore, it can be possible to obtain longer distances with the same battery packages or to use fewer battery packages for the same distance. Moreover, providing electrical and thermal insulation, and resistance to corrosion are the additional benefits of composites over metallic alloys in that kind of operation. Wind turbines providing alternative energy sources are getting environmentally more attractive. Their blades are usually made from sandwich structures due to high strength and stiffness to weight ratio, excellent damping to noise and vibration, and resistance to cyclic loadings. On the other hand, the application of composites also shows a fast-growing in civil infrastructure with prefabricated bridge decks. FRP composite bridge decks which can also be made from sandwich panels exhibit many advantages when compared to conventionally used concrete and steel decks such as lightweight, easy and quick installation, resistance to environmental conditions such as corrosion and freeze (Gibson, 2012; Elmarakbi, 2013).

1.2. Manufacturing of Composite Materials

Several methods are available to manufacture FRPCs, such as hand lay-up, vacuum bag, resin transfer molding (RTM), autoclave, resin infusion, pultrusion, filament winding, matching die set compression molding, etc. (Kar, 2017). But, mostly, hand lay-up, vacuum bagging, RTM, vacuum-assisted resin infusion methods are currently used methods for the fabrication of composite materials.

The hand lay-up method, the oldest process, is used for the composite manufacturing carried out on an open mold. This process is simple, but a labor-intensive process, and suitable for low-volume production. For instance, in marine applications, large components like boat hulls can be fabricated with this method. Reinforcing materials such as chopped strand mats or fiber fabrics are placed manually on to the open mold, and resin is sprayed or poured over the reinforcement materials and the impregnation of them is provided manually. The required curing time is 24–48 hours at room temperature. A catalyst and accelerator that are called as hardener are mixed to the resin in a proper fraction in order to satisfy curing. The mixture is carefully stirred to prevent void formations and to obtain homogeneous matrix material. Figure 1.3 shows the schematic view of the hand lay-up process (Kar, 2017).

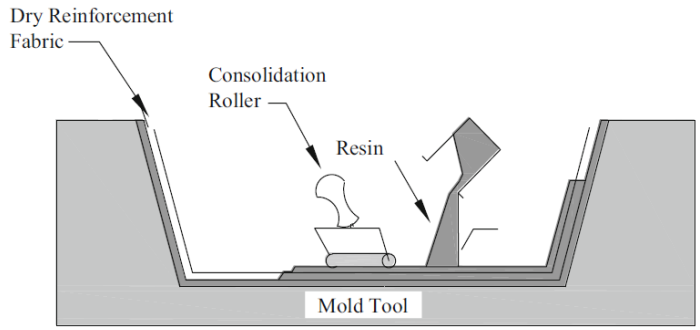


Figure 1.3. Schematic of hand lay-up method (Kar, 2017)

In the vacuum bagging method, the entrapped air during lay-up and excessive resin is removed with a vacuum. After stacking, a peel ply or perforated

release film is laid onto the composite laminate. A breather cloth is placed onto the peel ply, in order to absorb excess resin from the laminate. Lastly, the entire system is enclosed with a vacuum bag and the mold surrounding is covered with sealant tape as presented in Figure 1.4. Then vacuum is applied to composite material under the bag. This process provides a high reinforcement with increased fiber volume fraction and improves adhesion bond strength between the composite layers compared to the hand lay-up process. When compared to the hand lay-up, the method has important advantages such as higher fiber content, better fiber wet out, lower void formation, and decreased volatile emissions. For instance, racing car parts and large cruising boats can be fabricated by using a vacuum bagging method. However, the process has some drawbacks such as labor-intensive, a requirement of better labor skills, loss of seal, process cost (Kar, 2017).

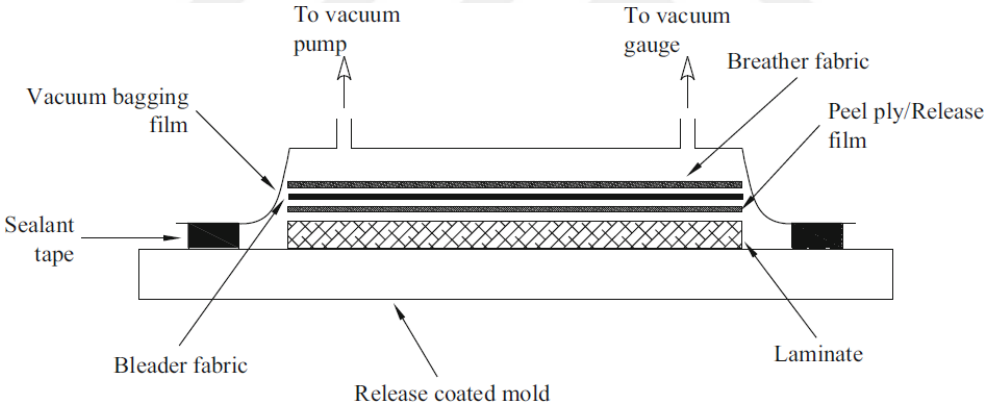


Figure 1.4. Schematic view of the vacuum bag method (Kar, 2017)

Resin transfer molding (RTM) is carried out in a closed mold, and suitable for moderate and high-volume productions. The process mainly contains stacking of the dry reinforcement materials in the base part of the mold, and the other half of the mold is placed over the bottom mold and clamped. The schematic view of the process is presented in Figure 1.5. After closing the molds, a resin including its hardener is injected. High-quality part requirements such as vehicle body parts,

containers, bathtubs, etc. can be achieved by this method. RTM method can be modified with a vacuum assistant for effective resin transfer and impregnation of fiber elements (Kar, 2017).

In vacuum-assisted RTM (VARTM), the manufacturing is carried out on a single mold in which the composite laminates stacked on it. Similar to the vacuum bagging method, peel ply and/or perforated release film is placed over the lamination, and the system covered with a vacuum bag by using sealant tape. The resin impregnation of the dry composite layers is performed with the aid of vacuum supply as seen in Figure 1.6. The vacuum process provides the resin movement. The entrapped air is also removed. The vacuum application increases the fiber concentration and improves adhesion bonding between the composite plies. VARTM technique provides several advantages when compared to the RTM method with lower tooling cost, shorter duration of mold filling by resin. The process efficiency and quality of the final product depend upon sufficient wet-out of the fibers which can be done successfully with a proper resin movement (Kar, 2017).

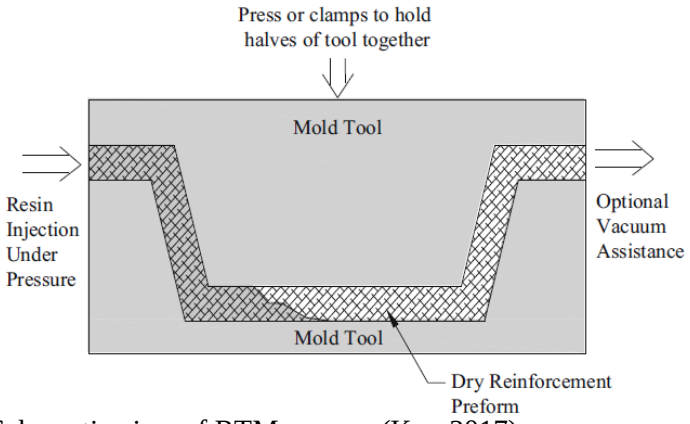


Figure 1.5. Schematic view of RTM process (Kar, 2017)

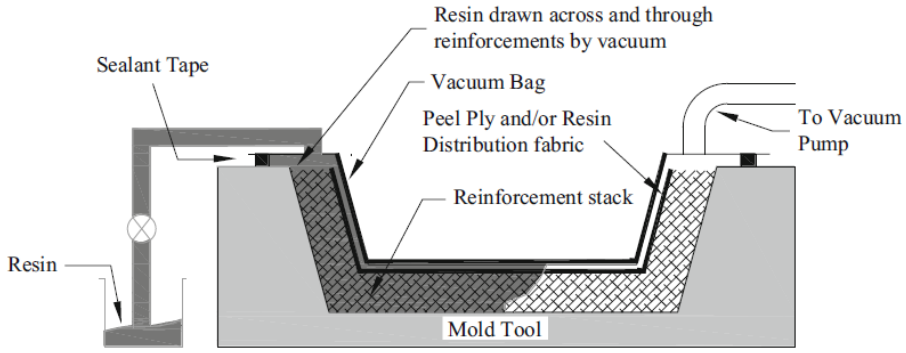


Figure 1.6. Schematic view of the VARTM method (Kar, 2017)

An autoclave manufacturing method can be applied where excellent quality is needed such as in aerospace industries. Because in this method, an increased fiber volume ratio is obtained with minimum void content in the matrix. The curing is carried out under pressure and in a heat-generated autoclave as seen in Figure 1.7. The process parameters of the computer-controlled method depend on the resin system used for lamination. The preparation of the composite materials is similar to the vacuum bagging method. After the composite is ready for curing within the enclosed heat-resisted vacuum bag, the product is placed inside an autoclave. The external sources of vacuum, pressure, and heat provide to densify and consolidate each lamina to form better lamination by removing air and volatiles with the aid of vacuum. In order to prevent any internal fire, nitrogen, or carbon dioxide is used. The process is costly and requires labor-intensive production (Baker et al., 2004; Mallick, 2007; Carlsson and Kardomateas, 2011).

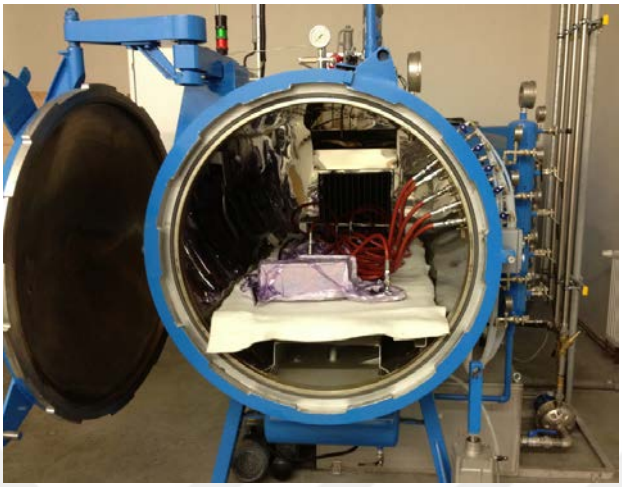


Figure 1.7. Representation of autoclave process (Web page, 2013)

In order to produce cylindrical parts such as pipes and tubes, Filament Winding is used effectively. The process includes wrapped bands of continuous fibers over a mandrel as seen in Figure 1.8. After winding, the curing is performed at an increased temperature of a mandrel. The resin impregnation can be made before, during, or after winding operation. The strength and the stiffness of the finished product depend on the compaction of fiber layers. The major factors have been specified as helix angle, winding tension, conditions of strand bandwidth, resin content, and its distribution and curing cycle (A. McIlhagger et al., 2015).

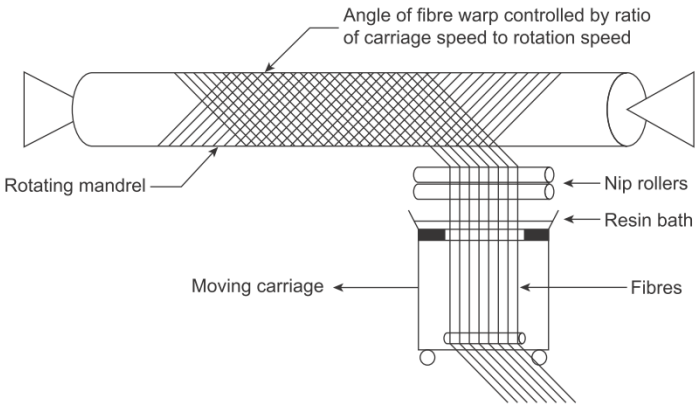


Figure 1.8. Filament winding method (A. McIlhagger et al., 2015)

1.3. Design of Sandwich Structures

The sandwich structures that are one of the hybrid family classes are specially designed for weight critical applications due to their very high bending stiffness among the other laminated composites and conventional engineering materials. As shown in Equation (1.1), the bending rigidity (EI) of a sandwich panel can be increased significantly by using high modulus face sheets (E_f) and/or a thicker core. Separation of the face sheets with thickness t, by an increased core thickness (c), yields higher moment of inertia thus the structure can resist higher bending and buckling loads. Since the density of the core material is relatively low, the increase of its thickness does not add much weight to the whole structure.

$$(EI)_b = E_f \frac{bt^3}{6} + 2bE_f t \left(\frac{c+t}{2}\right)^2 + E_c \frac{bc^3}{12} \tag{1.1}$$

The bending and in-plane loads can almost be carried by the face sheets (also referred to as facings and/or skins) whereas the core stabilizes the face sheets and determines the bending rigidity, compressive and out-of-plane shear behavior (Daniel et al., 2002). Therefore, the face sheets must be stiff and strong against both tensile and compressive loads to resist the bending forces and wrinkling whereas the core materials need to be stiff and strong in thickness direction under the shear forces to resist failures such as wrinkling and indentation (Mallick, 2007).

As shown in Figure 1.9, sandwiches functionally seem like I-beam profiles mostly available in the metal industry. The flanges of I-beam carry the tensile and compressive loads whereas the face sheets similarly perform this function. Likewise, the web between the flanges of I-beam resists to shear forces whereas in sandwich constructions the core material is effective against out-of-plane shear by keeping the top and bottom face sheets together (Diab Group, 2012).

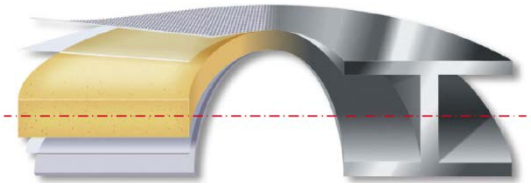


Figure 1.9. The similarity between I-beam and sandwich composite (Diab Group, 2012)

Designing of a sandwich panel depends upon several factors. These are type, density, and thickness of both face sheet and core materials, type of binder, manufacturing, and both curing and post-curing processes and sizes of the sandwich. Therefore, the decision-making process of designing sandwich structures becomes more complex than other types of materials such as laminated FRP composites (SAE International, 2013). From a large number of design parameters, sandwich panels are also designed against the failure types. Face yield and/or face compressive failure, core shear, core crushing, indentation, and de-bonding of the facing and the core are the most common failure modes. For instance, if the face sheets are not thick enough and the core material has relatively high density and thickness, the structure fails due to indentation. Ashby (2011) provides sandwich design principles considering the dominant failure mode. Figure 1.10 shows the failure modes of sandwich panels that are subjected to three-point central bending loading.

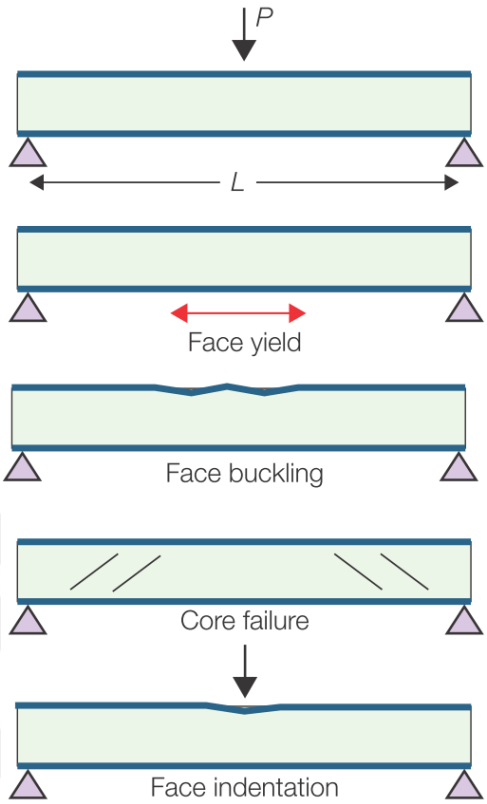


Figure 1.10. Sandwich panel failure modes under bending loading (Ashby, 2011)

In the case of face buckling, the upper facing of the sandwich panel is failed due to compression. It commonly becomes the main failure mode while constructing the sandwich panel with thinner face sheets and low shear strength of core material. Core shear may be prevalent if the face sheets are strong, and the support span length is relatively short. In this case, the transverse shear forces cannot be transferred between the facings. Indentation failure mode must be avoided by determining the minimum sufficient face sheet thickness.

1.4. The constituent of Sandwich Structures

Sandwich structures typically consist of thin and stiff face sheets that are bonded to a lightweight and thicker core by a proper binder called the matrix. Face

sheets can be preferred from thin and strong metallic alloys, fiber-reinforced composites, or fiber metal laminates (FMLs).

The core materials in sandwich structures mainly provide to separate, stabilize, and support the face sheets in order to obtain desired bending rigidity. These carry out of plane loads or transverse shear loads (SAE International, 2013). Core materials are classified into two general categories as cellular and structural. Cellular refers that the material includes open space cells enclosed by walls repetitively to provide space-filling. Cellular foams like metal or polymer foams, honeycomb, and balsa wood have widespread application fields. Web core and/or truss are also structural cores, separate facings, that consist of a continuous web produced with solid material, and due to its various formation types transferring of shear forces becomes more effective. Polymer foams and/or balsa wood provide the same shear properties in two directions, but the web, truss cores, and honeycomb cannot achieve the same or similar properties. The most common polymer foams used for structural sandwiches are polyurethane (PU), polyvinylchloride (PVC), and polymethacrylimide (PMI). These foams are in closed cell form, which makes the structure isotropic and provides better resistance to water penetration (Mallick, 2007).

Matrix material consists of resin and its suitable hardener primarily provides to work of both face sheets and core material together by applying chemical bonding and helps to transfer shear stress between them. For fiber-reinforced composites, the thermoset polymer type matrix materials, i.e. polyester, vinyl ester, and epoxy resin provide better mechanical properties.

2. PREVIOUS STUDIES

The advantages of sandwich structures over the conventional laminated fiber-reinforced composites have attracted the most researchers, and many studies regarding different types of sandwiches are being available in the literature. Because it can be possible to obtain several physical and mechanical features by altering the type, density, thickness of both core and face sheets materials, respectively. For instance, aluminum foam sandwich structures provide good heat and acoustic insulation, and it also has better energy absorption capacity under impact loading (Gibson, 2000; Baştürk and Tanoğlu, 2011; Liu et al., 2014; Xu, 2018). In addition to very thin aluminum (Al) sheets (Harte et al., 2000; Jiang et al., 2015), fiber-reinforced laminated composites can also be used for facings (Styles et al., 2006).

As the sandwich structures can be constructed with various constituent materials (Uzay et al., 2019), the classification of the previous researches can be made from different perspectives considering the type of facings, core material, and/or matrix. On the other hand, as the sandwiches serve different purposes, it may also be classified considering both types of loading such as bending, compressive, impact and etc., and failure modes such as fiber cracks, core shear failure, and matrix failure. In this chapter, the previous researches are going to be summarized based on the type of core material. And failure modes are also going to be summarized briefly.

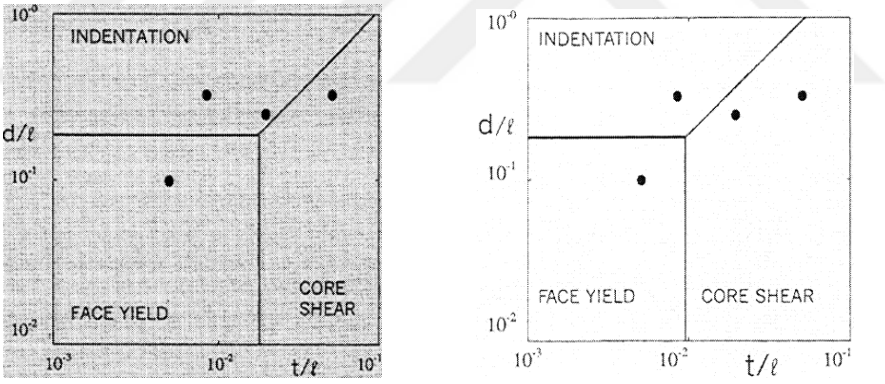
2.1. Utilization of Aluminum (Al) Foam Core for Sandwich Structures

Metallic foams combine the properties which make them attractive for lightweight sandwich panels compared to solid structures. Besides lightweight, it also provides heat and acoustic insulation, and good energy absorption capability, especially for impact loadings. Therefore, metal foams can not only act as a

structural member but also used where the multi-functionality is important (Harte et al., 2000; Baştürk and Tanoğlu, 2011; Liu et al., 2014).

Although aluminum (Al) foams are the most commonly used as core material, zinc, copper, nickel, and steel foams are also available. Their behaviors to creep, multiaxial, and fatigue loadings have been investigated by Gibson (2000) firstly. Aluminum (Al) foam is a cellular solid aluminum structure that includes large volumes of gas-filled pores.

Harte et al. (2000) described the sandwich panel theory by using simple analytical models and carried out experimental tests with sandwich panels having Al skins and Al foam cores. Failure modes were determined as core shearing, face sheet yield, and indentation under static loading conditions. Additionally, theoretical failure maps were presented for both static and fatigue failure conditions as seen in Figure 2.1.



(a) (b)

Figure 2.1. Theoretical failure mode map under a) Static loading, b) Fatigue (d and t are foam and face sheet thickness, respectively, l is the distance from loading to support) (Harte et al., 2000)

Styles et al. (2007) investigated the deformation mechanism of Al foam core (230 kg/m^3) thermoplastic composite facing sandwich structures according to different core thickness values under four-point bending. As it is seen in Figure 2.2, all sandwiches showed an initial linear elastic behavior, then it reached the

maximum load value with a decreasing slope. As the core thickness and the bending rigidity increased, the initial slope of the curve increased. Similarly, the amount of the maximum load increased as the thickness of the core increased. The maximum load of 20 mm thick core specimen was significantly greater than the others.

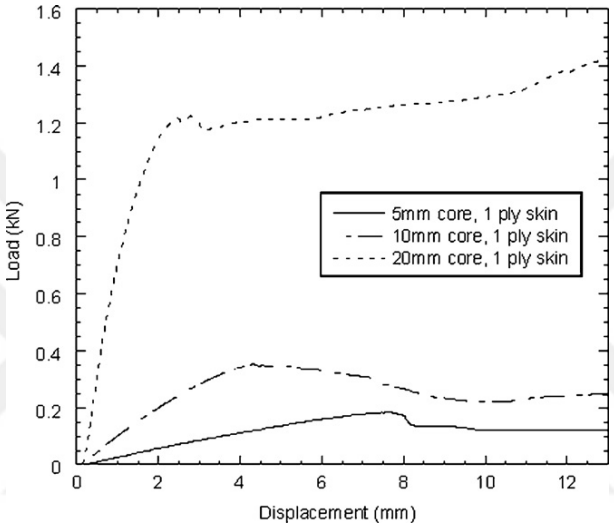


Figure 2.2. Typical load-displacement curve plot for each core thickness (Styles et al., 2007)

It was found out that the thinner specimens failed based on facing wrinkling, face fracture, and core crushing, and some core cracking was seen in thinner foam cores while the thicker specimens failed because of indentation in core. But it was concluded that the incidence of indentation was eliminated by increasing the face sheet thickness.

Jiang et al. (2015) established an analytical approach to predict the failure modes in terms of face sheet yield, core shearing, and indentation. To verify the approach, they used Al foam core and Al face sheets and subjected the sandwich structures to the three-point bending tests as presented in Figure 2.3. The proposed failure prediction models were in good agreement with the experimentally obtained

results. However, for the sandwich structures having thick face sheets, the determination of the load-carrying capacity and the analysis of the indentation failure mode required further improvements.

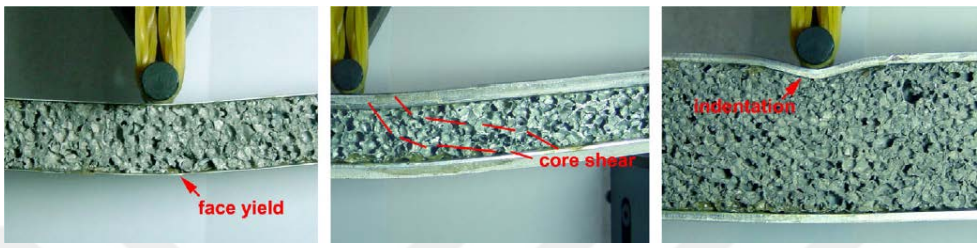


Figure 2.3. Failure modes in quasi-static three-point bending (Jiang et al., 2015)

Kabir et al. (2014) investigated the effect of three-point bending behavior of very thin (0,32 mm) Al face sheets that were constructed with 6 mm and 12 mm Al foam cores, respectively. The sandwich panels having 150 mm x 35 mm size were produced based on different face sheets (low strength and high strength), core materials, and span length (50 mm and 100 mm), respectively. Very thin face sheets primarily yielded by indentation failure mode. In the case of using low strength facings, face yielding also occurred whereas high strength facings caused to core yielding. Table 2.1 gives the results based on high and low strength facings, span length, and core thickness values. The maximum stress in both the face sheets and the core of the sandwich panel and the flexural rigidity were determined for linear elastic behavior based on the elastic beam theory as given in Equations (2.1), (2.2), and (2.3).

Table 2.1. Three-point bending results of Al skin Al foam core sandwiches

σ_{yf} (MPa)	c (mm)	L (mm)	P_{max} (N)	M_{max} (Nm)	$(EI)_{eq}$ (Nm^2)
40	6	50	367,3±34,2	4,6±0,4	16,11
		100	254,5±37	6,3±0,9	
	12	50	504,5±38,1	6,3±0,4	64,12
		100	362,6±29,4	9,1±0,7	
236	6	50	413±22,5	5,2±0,3	16,13
		100	393±62	9,8±1,5	
	12	50	634,4±37,4	7,2±1,3	64,2
		100	549,9±57,9	13,7±1,4	

Equivalent flexural rigidity;

$$(EI)_{eq} = E_f \frac{bt^3}{6} + E_f \frac{bt(c+t)^2}{2} + E_c \frac{bc^3}{12} \tag{2.1}$$

The maximum stress in the sandwich core;

$$(\sigma_c)_{max} = E_c \frac{M_{max} c}{2(EI)} \tag{2.2}$$

The maximum stress in the sandwich face sheets;

$$(\sigma_f)_{max} = E_f \frac{M_{max}(c+2t)}{2(EI)} \tag{2.3}$$

Besides bending properties of Al foam core sandwich structures, the effectiveness of Al foam core on the impact related loadings is also very satisfactory. And it is known that bird strike to an aircraft causes significant hazards such as aircraft structural damage and fatal accidents for human (Allan, 2000). At this point, Al foam core sandwich composites may become a solution to a body structure of an aircraft. To investigate the dynamic behavior of Al foam core sandwiches, researchers developed numerical and experimental studies. Liu et al. (2014) performed a numerical study by simulating bird strike and subjected the modeled bird strike to Al face sheets, and Al foam core sandwich panels. The

numerical bird strike simulation also verified the experimental results. The simulation of a bird strike to any kind of body structure including an aircraft saves many millions of dollars per year and prevents delays considering real damages (Allan, 2000).

Hedayati and Sadighi (2016) numerically simulated a bird strike and made impact loadings to the Al skins (0,8 mm), and to an Al foam core sandwich structure having inner Al plate (0,8 mm) between the face sheets in order to investigate the optimum position of the plate by trying six different cases as seen in Figure 2.4. The inner plate was closer to the top face sheet in the first two cases (a and b), and it was closer to the lower face sheet in the cases of d and e. The optimum configuration was obtained where the plate was inserted in the middle (Figure 2.4(c)). In addition to this, it was suggested that using the high-density foam on the bottom and low-density foam on the top surface provides less deformation for the back face since the middle plate spread the bird strike energy to the high-density foam core.



Figure 2.4. Configurations based on inner plate location: a) Case 1, b) Case 2, c) Case 3, d) Case 4, e) Case 5, f) Case 6 (Hedayati and Sadighi, 2016)

Structural performance such as impact response of Al facings and Al foam core sandwich panels depends upon the bonding capability which is affected by the adhesion surfaces, adhesives, and curing process conditions. Epoxy has often been used as adhesive for the manufacturing of aluminum foam core sandwich panels with metallic facings because of its availability and good bonding ability (Liu et al., 2014).

On the other hand, an advanced hybrid material system, which is called as Fiber Metal Laminate (FML), has mainly been used in aerospace applications due to their relatively lightweight, better impact and damage tolerant characteristics over both laminated fiber-reinforced polymer matrix composites and aluminum alloys (Sinmazçelik et al., 2011; Sadighi et al., 2012; Chai and Manikandan, 2014; Vogelesang and Vlot, 2000; Wu and Yang, 2005; Fontens et al., 2014; Hinz et al., 2009). Liu et al. (2014) designed and manufactured sandwich panels with aluminum foam core and FML face sheets (Al 5005 alloy/E-glass fiber fabrics) to obtain enhanced resistance to impact, and they investigated the bonding capability and impact resistance between both Al sheet-Al foam and E-glass fiber–Al foam, respectively. The configurations were shown in Figure 2.5. Both Al face sheets and Al foam core materials were firstly cleaned with acetone and then subjected to surface treatment by using 15% nitric acid to remove the oxides from the surface and lastly, to remove residual acid on the surface, the materials were subjected to distilled water.

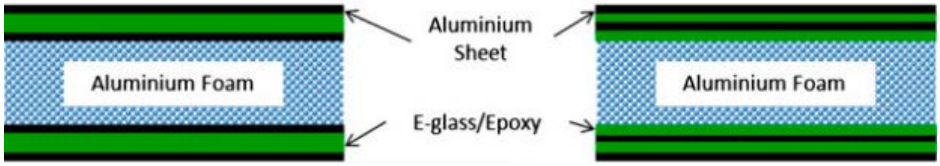
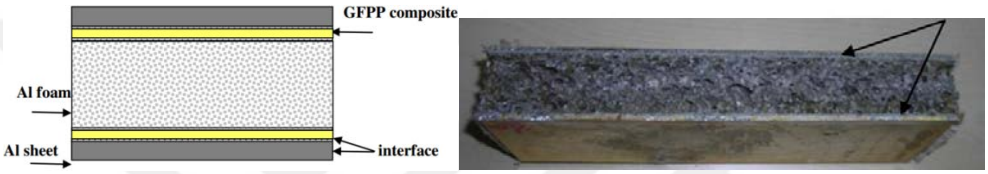


Figure 2.5. Stacking sequence of the panels a) Group 1, b) Group 2 (Liu et al., 2014)

A low-velocity impact test was conducted with drop weight impactor, and according to the deformation on the specimens, energy absorption, bonding capability, and impact resistance were determined. The Group 2 panels absorbed more energy, showed better resistance to impact and good bonding capability.

Baştürk and Tanoğlu (2011) manufactured FML/Al foam (395 kg/m^3, 409 kg/m^3, 456 kg/m^3) sandwich panels (Figure 2.6) by using surface treatment methods (Figure 2.7), silane (ST), chemical treatment and combination of ST with

the addition of polypropylene (PP) based film (PP-g-MA: maleic anhydride-modified polypropylene layer). The manufacturing of the sandwiches was carried out with hot-pressing under 1,5 MPa, at 200°C. They concluded that the modified panels with silane coupling agents and also PP-g-MA-based film layer yielded the best structural performance than epoxy adhesive and glass fiber reinforced polypropylene. The predominant failure modes were found as core shear, face sheet bending, and debonding under the flatwise compression tests.



(a) (b)

Figure 2.6. (a) Schematic representation and (b) Al sheet/GFPP/Al foam sandwich (Baştürk and Tanoğlu, 2011)



(a) (b)

Figure 2.7. 20 wt % PP-g-MA/80 wt % PP blends (a) as fine granules (b) as adhesive film after hot pressing (Baştürk and Tanoğlu, 2011)

2.2. Utilization of Polymer Foam Core for Sandwich Structures

Instead of using metal foams, polymer foam core materials serve the best candidate whenever designing the weight critical components in many industrial applications. The most commonly available polymers are polyurethane (PU), polyvinylchloride (PVC), and polymethacrylimide (PMI). Such foams are closed-cell structures, which makes them isotropic and provides resistance to water

penetration. Wang et al. (2015) also stated that sandwich panels with closed-cell foam cores are getting prevalent in recent years.

Lim et al. (2004) investigated the static and impact failure modes in the foam core sandwiches. As seen in Figure 2.8, the tests were carried out according to different core densities and facing thicknesses. The effects of the parameters were revealed. The specimens were produced from woven plain glass fiber/epoxy prepreg as the face sheet and Divinycell HT grade PVC foam core having the same thickness of 10 mm. The load carrying capabilities were investigated by using three-point bending tests under different span lengths as 100 mm, 150 mm, 200 mm, 250 mm. While the density of the core and/or facing thickness were increased, load capacities of the sandwich panels increased as expected. However, the increase in the thickness of the face sheets caused a change in failure mode. Thinner facings tended to fail by face fracture, but as the thickness increased, it tended to core compression or shear yielding. On the other hand, an obvious change in failure modes was not observed due to the change in core density. It was also found that failure modes under impact loads were obtained as face fracture and core shear. In addition, the panel with thin facings and high-density core lead to the facing compressive fracture because of the high facing stresses.

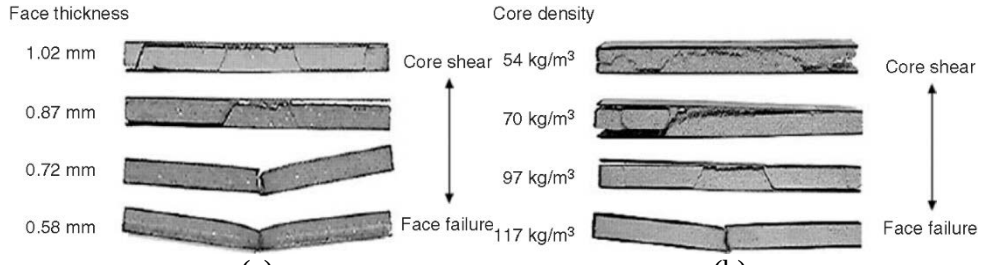


Figure 2.8. Transverse impact results based on; a) face thickness with fixed core density (97 kg/m3), b) core density with fixed thickness (1,02 mm) (width of the bending specimens were 20 mm) (Lim et al., 2004)

Steeves and Fleck (2004) provided analytical expressions to predict the failure modes and to construct the composite sandwich with minimum weight design. The total deflection (δ) of a sandwich beam at the mid-point (Equation 2.4) was specified as the sum of the deflections due to the bending of the facings and the core shear according to three-point bending loading (P).

$$\delta = \frac{PL^3}{48(EI)_{eq}} + \frac{PL}{4(AG)_{eq}} \tag{2.4}$$

Where $(AG)_{eq}$ is the equivalent shear rigidity as follow;

$$(AG)_{eq} = \frac{bd^2G_c}{c} \tag{2.5}$$

The authors represented the four main failure modes for a simply supported sandwich beam under static three-point bending loadings such as micro buckling, wrinkling of the compressive facing, core shearing, and indentation under the loading roller. Each failure mode was described by analytical models and was given in Figure 2.9.

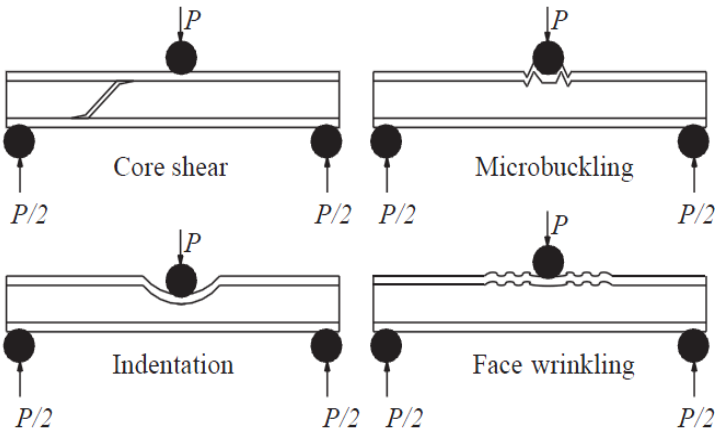


Figure 2.9. Failure modes of sandwiches under three-point bending (Steeves and Fleck, 2004)

Face micro buckling occurs when the axial stress of the facing exposing to compression reaches the face sheet micro buckling strength, σ_f. By neglecting the effect of the core to overall bending strength, the collapse force, P is given as;

$$P = \frac{4bdt_f\sigma_f}{L} \tag{2.6}$$

Face wrinkling was defined as a local elastic instability of the facings involving short-wavelength elastic buckling of the top facing, resisted by the underlying elastic core. A conservative estimate for the facing wrinkling load P was given in Equation 2.7.

$$P = \frac{2bdt_f\sigma_f}{L}\sqrt[3]{\mathrm{E}_f\mathrm{E}_c G_c} \tag{2.7}$$

The factor, 2, in Equation (2.7) was assumed to compensate for the geometrical imperfections of the facings (Allen, 1969).

Daniel et al. (2002) made an investigation about failure modes and their reasons in sandwich structures under three-point, four-point bending, and in-end loading conditions. Possible failure modes were stated as the tensile or compressive failure of the facings, wrinkling of the compressive facing, global buckling, debonding at the facing/core interface, core failure, and indentation under the concentrated loads, see Table 2.2.

Table 2.2. Failure modes in sandwich beams (Daniel et al., 2002)

Mode	Criterion
Face sheet compressive failure	Composite failure criterion (e.g., max. stress, Tsai-Wu)
Face sheet debonding	Max. shear stress of adhesive, or interfacial fracture toughness
Indentation failure	Core state of stress reaches failure condition; critical compressive stress in face sheet under combined local and global bending
Core failure	State of stress in foam reaches failure condition (e.g., Tsai-Wu)
Face sheet wrinkling	Face sheet stress equals critical local buckling stress

The initiation and growth of the various failure modes in sandwich structures depend upon the material properties of its constituent (face sheets, core, adhesive bonding), geometry, size, and type of loading. Due to the nonlinear and inelastic behavior of the constituents and the complex interactions of failure modes, the stress analysis and determination of proper failure criteria in critical regions become difficult. The fatigue life of a structural member is adversely affected by the damage. The magnitude of the reduction in fatigue life is often difficult to establish. For these reasons, many studies that were made under the static, impact, and dynamic loading conditions also proposed numerical and analytical models to save time and sources instead of performing repetitive experiments. These models showed that the results often matched well with experimental studies particularly in the linear-elastic range of the foam-cored sandwich panels (Daniel et al., 2002; Steeves and Fleck, 2004; Lim et al., 2004; Kulkarni et al., 2004; Burman and Zenkert, 1997; Chemami et al., 2011). The failure mechanisms such as face/core debonding can simply be demonstrated in Figure 2.10 (Carlsson and Kardomateas, 2011). However, except for the dynamic loadings such as impact, the debonding is not a matter if there were no fabrication defects (Daniel et al., 2002).

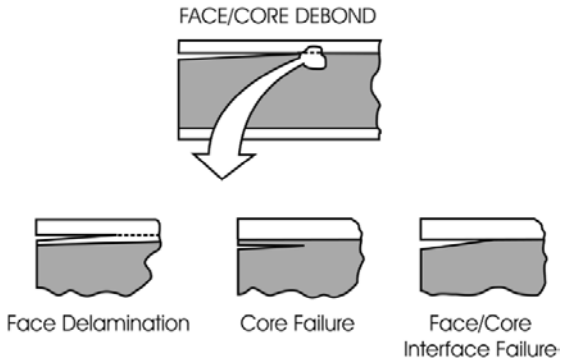


Figure 2.10. Crack growth scenarios in foam core sandwiches (Carlsson and Kardomateas, 2011)

Many researchers have been concentrated on both evaluating the flexural/bending strength, compressive strength, face/core interface shear strength, and investigating the impact behavior especially under the low-velocity impact, and examining the failure mechanisms under the static and fatigue loadings. Yin et al. (2015) used the co-injection RTM process to validate its advantage over a multi-step process and as stated, it provided excellent interface properties which was more feasible and efficient and provided to manufacture the multifunctional sandwich panels in terms of load-bearing, heat insulation, and thermal barrier. To achieve multi-functionality, the sandwich panels were made with plain carbon fiber fabric, 10 mm thick polymethacrylimide (PMI) foam core (110 kg/m^3) and epoxy and phenolic resins, and subjected to in-plane compression test (Table 2.3), three-point bending test (Table 2.4), interface shear test (Table 2.5) with different combinations. The load-displacement curves of the specimens under three-point bending loading were also presented comparatively in Figure 2.11. The average ply number in face sheets was 12.

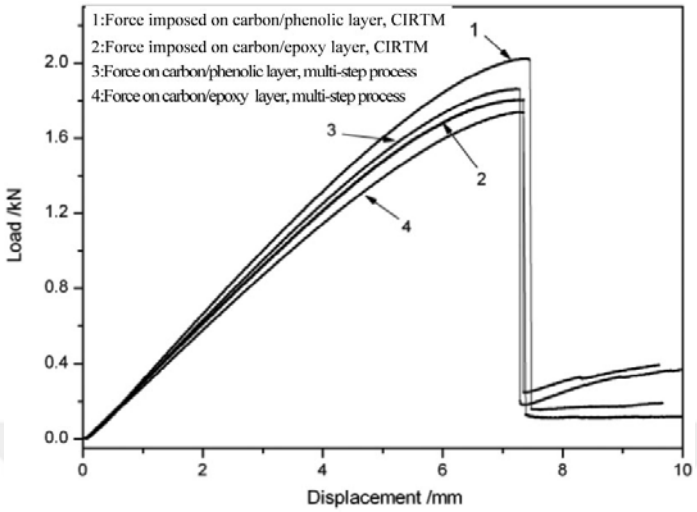


Figure 2.11. Comparative representation of the load-displacement curves (Yin et al., 2015)

Table 2.3. Compression strength and modulus results of the sandwiches based on two different processes (Yin et al., 2015)

Manufacturing process	Compressive strength (MPa)	Coefficient of variance (%)	Compressive modulus, 10^3 (MPa)	Coefficient of variance (%)
Multi-step process	73,4	15,7	7,68	12,4
CIRTM process	86,7	8,1	7,85	9,2

Table 2.4. The flexural strength and modulus results of the sandwiches based on two different processes (Yin et al., 2015)

Manufacturing process	Force on carbon/phenolic layer				Force on carbon/epoxy layer			
	Flexural strength (MPa)	Coeff of var. (%)	Flexural modulus (GPa)	Coef f of var. (%)	Flexural strength (MPa)	Coef f of var. (%)	Flexural modulus (GPa)	Coef f of var. (%)
Multi-step process	105,3	15,7	15,75	12,2	98,8	11,7	14,06	12,8
CIRTM process	114,2	8,2	16,53	8,7	102,1	6,8	14,98	7,6

Table 2.5. Interface shear test results of the sandwich panels based on the processes (Yin et al., 2015)

Manufacturing process	Interface	Interface shear strength (MPa)	Coefficient of variance (%)
Multi-step process	Carbon/epoxy layer/foam core	3,29	20,97
	Carbon/phenolic layer/foam core	3,22	22,98
CIRTM process	Carbon/epoxy layer/foam core	3,82	7,07
	Carbon/phenolic layer/foam core	3,38	9,52

Atas and Sevim (2010) investigated the impact and damage behaviors of sandwich composites by using E glass fiber face sheets having 780 g/m^2 areal density and two different cores, 11,5 mm thick balsa wood (157 kg/m^3) and 10,3 mm thick PVC foam (62 kg/m^3). The primary damage modes were determined as fiber ruptures at top and bottom face sheets, face/core delamination, delamination of adjacent glass fiber/epoxy layers, and core shearing. The debonding was the main damage mode for balsa wood core sandwich since the bonding at balsa and face sheet interface was poor compared to the PVC foam core.

Zhou et al. (2012) used nine polymer foams (PET, PVC) having different densities from 60 kg/m^3 to 200 kg/m^3 at the same thickness of 20 mm with 0,25 mm thick glass fiber facings, and subjected the sandwiches to the low-velocity

impact test. Their objective was to show that perforation resistance was dependent on the foam core properties. The experimental studies were also verified with finite element analysis.

Chemami et al. (2011) manufactured the sandwich panels by using glass fiber/epoxy and 8 mm thick PVC foam (200 kg/m^3) with a vacuum bagging method, and the specimens were subjected to three-point bending test. Figures 2.12 and 2.13 show the static (Figure 2.14) and fatigue (Figure 2.15) failure modes. The tensile stress or compressive in the face sheet, the maximum plane stress in the core, and the shear stress were calculated by the following Equations (2.8 to 2.10).

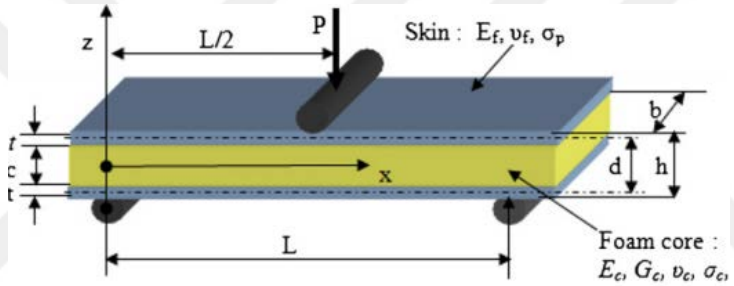


Figure 2.12. Sandwich beam loading in three-point bending test (Chemami et al., 2011)

$$\sigma_f = \frac{PL}{4tdb} \tag{2.8}$$

$$\sigma_c = \frac{PL}{2btd}\frac{E_c}{E_f} \tag{2.9}$$

$$\tau_c = \frac{P}{4D}(E_f td) \tag{2.10}$$



Figure 2.13. Experimental set up (ZWICK Z250/SN5A machine) (Chemami et al., 2011)

Two different facing configurations were fabricated as $[0/90_2/0]$ and $[0_4]$ (2 layers of 90° plies between 1 layer of 0° and 4 layers of 0° glass fibers, respectively). It was found out that three main stages are available in the bending test: linear increase of force with displacement, followed by a nonlinear behavior up to the maximum load. Lastly, there was a sudden drop in the load. The sandwiches with skin cross-laminated $[0/90_2/0]$ were found more rigid. The sandwich configuration of $[0/90_2/0]$ was recommended to use due to its high stiffness and resistance to fatigue compared to $[0_4]$. The unidirectional skin, $[0_4]$, showed delamination between core and top facing then fracture of the core due to shear which also caused a loss of bonding strength between lower facing and core. But the facing with $[0/90_2/0]$ fiber orientation, the top facing undergone to the fracture due to compressive failure.

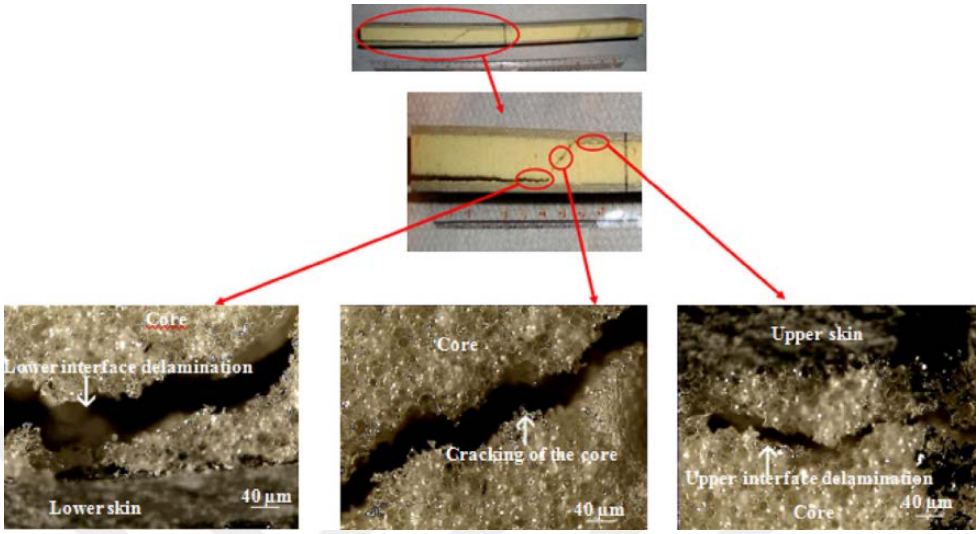


Figure 2.14. Macroscopic and microscopic images of fractured surfaces of the SMS [04] sandwich (Chemami et al., 2011)

Fatigue failure modes were found as core shear and similar for both configurations as it is seen in Figure 2.15. Figure 2.16 shows the crack propagations step by step that started by lower facing delamination and followed by core shearing through the core thickness and ended by upper facing delamination.

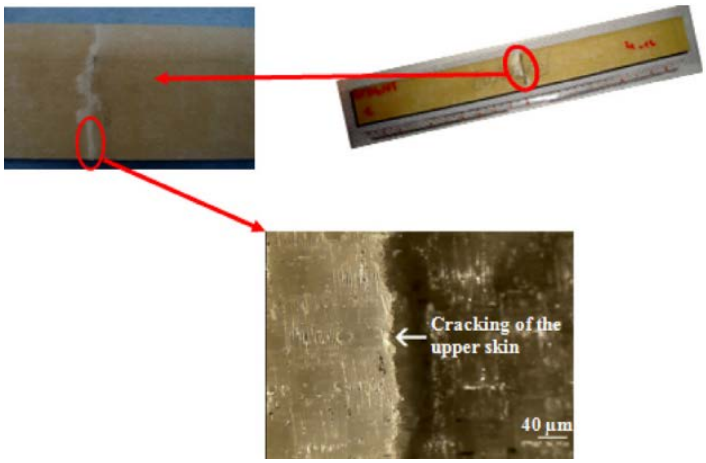


Figure 2.15. Macroscopic and microscopic images of fractured surfaces of the SMS [0/902/0] Sandwich (Chemami et al., 2011)

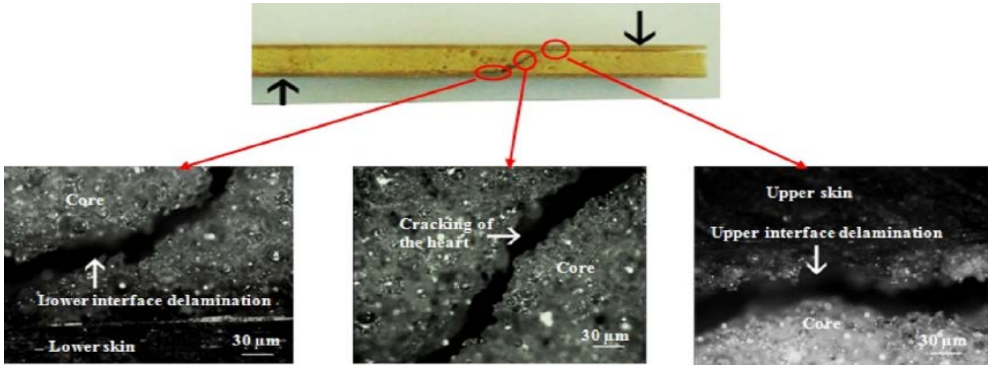
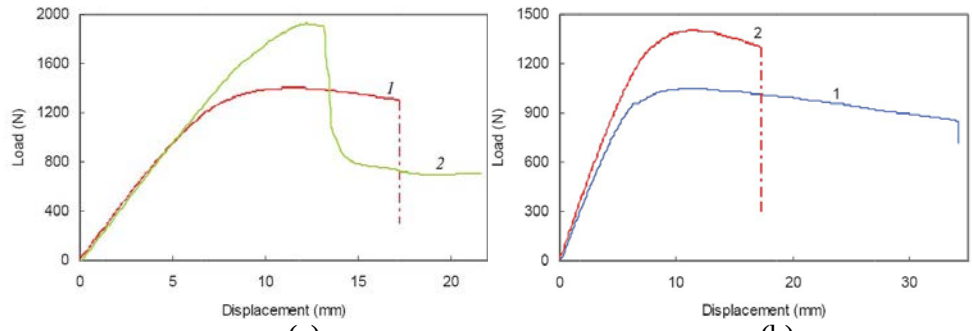


Figure 2.16. Macroscopic and microscopic images of the crack growing during the fatigue test of the sandwich SMS [0/902/0] (Chemami et al., 2011)

Bezazi et al. (2007) manufactured glass fiber (300 g/m^2) sandwich panels with PVC foam core materials having two different density (60 kg/m^3 and 80 kg/m^3) and two different thicknesses (15 mm and 25 mm) values, respectively. The sandwiches were subjected to quasi-static three-point bending tests. The stiffest results were found with a higher density foam core. In addition, the specimens having 15 mm and 25 mm thick cores, respectively, with 80 kg/m^3 density showed the same stiffness up to a certain mid-point deflection as presented in Figure 2.17a. And the effect of the core density was presented in Figure 2.17b. According to the examination of sandwiches after tests, it was observed that high-density foam core sandwich structure primarily showed shear failure whereas low-density foam core sandwich specimens failed due to wrinkling of the upper face sheet.



(a) (b)

Figure 2.17. Effect of; a) core thickness at density of 80 kg/m3(1: 25 mm, 2: 15 mm), b) core density (1: 60 kg/m3, 2: 80 kg/m3) (Bezazi et al., 2007)

The effectiveness of sandwich structures strongly depends on the bonding capability of the face/core interface. Inadequate bonding and/or lack of bonding surfaces adversely affect shear stress transfer between the face sheets throughout the core. It is important to provide sufficient adhesion of the facings to the core particularly in large panel applications. Because if the debonding of the layers occurs, it tends to grow over a large area. Therefore, inadequate wet out the layers must be prevented since it results in poor facing to core bonding. For this reason, various studies were carried out to increase the adhesion behavior of the interface such as reducing the viscosity of the resin by increasing the process temperature. But in this case, the polymerization with the aid of a particular hardener can start very early before the impregnation of all stacking surface layers completed. Therefore, more attention is required while increasing the resin temperature. Truxel et al. (2006) examined the face/core interface bonding by using different resin infusion techniques (Figures 2.18 and 2.19). The manufacturing of the sandwich panels was carried out with glass fiber vinyl ester resin and different core materials, PVC (200 kg/m^3) and Balsa wood (155 kg/m^3) having the same thickness of 25,4 mm.

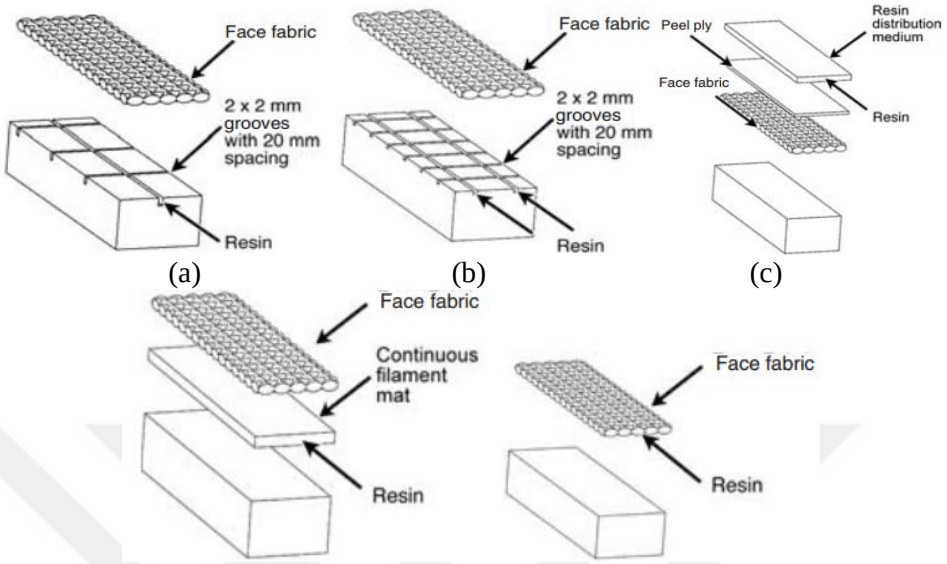


Figure 2.18. Sandwich panels configurations; a) 2 x 4 mm grooves, spaced 40 mm (2 x 4(40)); b) 2 x 2 mm grooves, spaced 20 mm (2 x 2(20)); c) resin distribution medium; d) continuous filament mat; and e) no infusion aid but excess 2,4-P inhibitor (2,4-P) (Truxel et

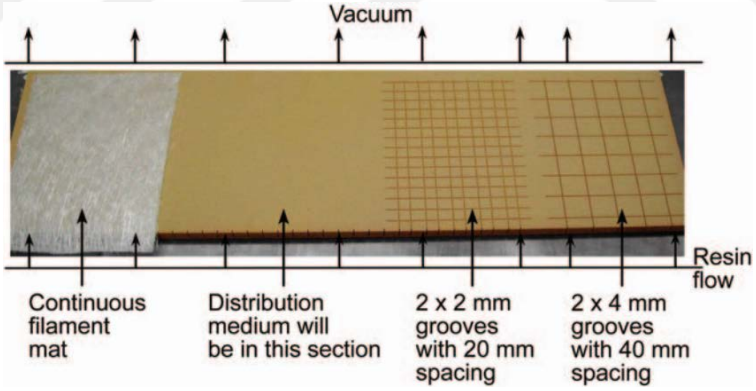
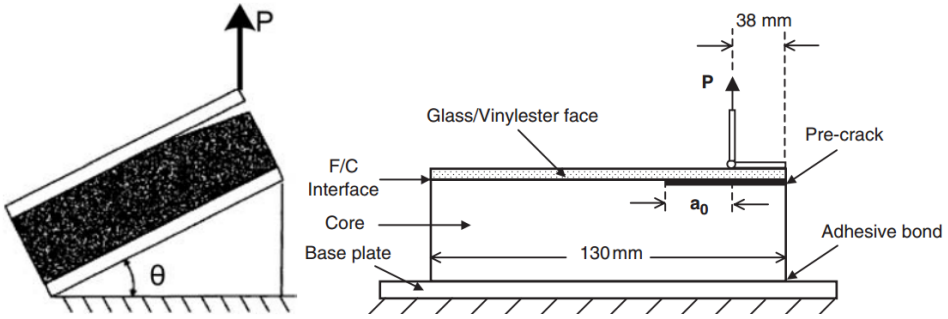


Figure 2.19. Preparation of the facing/core interface using different methods on the top surface of the foam (before infusion) (Truxel et al., 2006)

The face/core interface adhesion capability was tested by a debond fracture testing method using a tilted sandwich debond (TSD) specimen as seen in Figure 2.20.



(a) (b)

Figure 2.20. a) Geometry and loading of the TSD specimen, b) Sketch of the TSD test setup (Truxel et al., 2006)

It was concluded that specimens with grooved cores, especially with 4 mm deep grooves showed high fracture resistance to crack propagation compared to non-grooved regions which caused low interface toughness. The specimens with continuous filament mat between the facings and the core yielded the highest fracture toughness. The addition of continuous fiber mat (CFM) and/or chopped strand mat (CSM) may improve the toughness of the sandwich's facing/core interface. With the aid of such a mat, a transition region can be provided between the high modulus facings and the low modulus core. Thus, the adhesion of facings to the core may be improved. It is very important to prepare the bonding surfaces of the core for the mechanical behavior of the structure under both static and dynamic loadings.

Imielinska et al. (2007) investigated the effect of bonding type of E-glass fiber/polyester facings PVC foam core (20 mm thick, 80 kg/m^3) sandwich structures based on low-velocity impact behavior. In addition to matrix resin, two different adhesives were used for facings/core bonding. It was observed that facing/core bonding via matrix was a better way than that of using an adhesive due to less frequent transverse core fracture. On the other hand, bonding with adhesives showed less extensive delamination area in the top facing compared to resin-bonded sandwich specimens as presented in Figure 2.21. Because the growth of

crack can be prevented at the filler particles due to impact energy absorption capacity of adhesives.

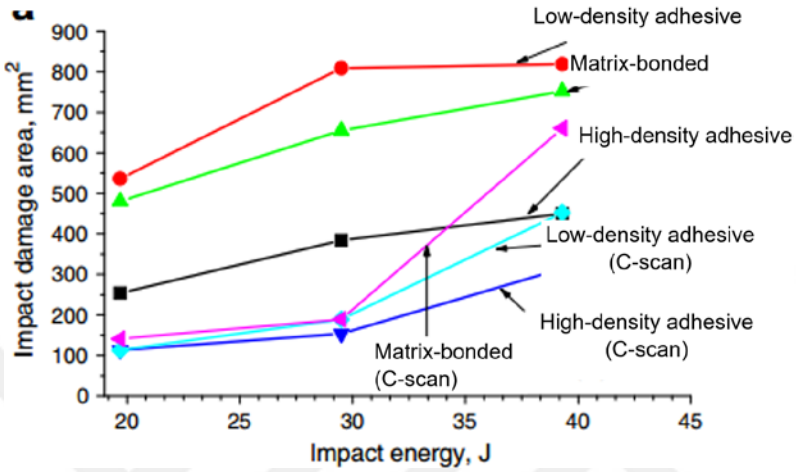


Figure 2.21. Visual inspection and C-scan results of impact damage area based on impact energy values of three types of sandwiches (Imielinska et al., 2007)

Although sandwich structures have very high bending stiffness, lightweight, resistance to heat and acoustic, and simple reparation comparing to conventional laminated FRP composites, they are not good at against to impact loads and can be exposed to various impacts such as bird strikes, hail storms, tool drops, and runway debris during the operation. These sudden loads cause a decrease in the structural strength. Ozdemir et al. (2015) investigated the core thickness effect (5, 10, and 15 mm) under low-velocity impact tests by using sandwich structures with glass fiber face sheets and two different cores, PET (60 kg/m^3) and PVC (65 kg/m^3) foam. Deformations types were also compared to the laminated composites without core material visually. It was concluded that the effect of relatively thin cores on contact force and rigidity of specimen was not significant, because core thickness of 5 mm showed almost the same impact properties with conventional laminated composites due to less contact time to deform the core. The specimens having a thicker core absorbed more energy. PVC

foam core specimens showed higher bending stiffness than PET foam core specimens did.

Fatigue failure modes usually show similarity to that of occurred in static and impact loading. Several failure modes are available in sandwich beams under both static and impact loads, and these are dependent on the material properties and loading types. However, under the cyclic fatigue loading, the core shear failure is the most encountered failure mode of the foam core sandwiches. Because the residual shear strength of the core decreases due to cyclic loading (Sharma et al., 2006). Therefore, bending fatigue failure of the sandwich composites can be controlled by the failure of core material as also stated by Kulkarni et al. (2004). They investigated fatigue failure behavior in sandwich specimens which were made of glass fiber/epoxy, and 12,7 mm thick PVC foam (75 kg/m^3) manufactured by using the co-injection RTM process which provides simultaneous resin infusion to both top and bottom facings. Fatigue tests were performed using three-point bending tests. Failure mode was found as a core shear. Three distinct damage events that were core–facing debond, core shear, bottom facing-core debond were observed until the specimen failed. Initiation of the crack and its propagation just below the top facing/core interface on the compression side of the composite was carried out in damage event (1) and it occupied about 85% of the fatigue life. Damage event (2) was the core shear, which occurred rapidly, and only about 7–8% of the fatigue life was occupied. Damage event (3) consisted of delamination at the bottom facing/core interface and the separation of the core material from the facings occurred. As the propagation of core shear was at a faster rate, the remaining 7–8% of the fatigue life was occupied. The tension side of the facing/core interface was obviously debonded from each other, causing fast crack propagation in the last stage of the failure. It was also concluded that the dispersion in fatigue was significantly smaller in foam core sandwiches when compared to other composite materials.

Atas and Potoğlu (2016) investigated the face sheet thickness effect on the impact resistance of the glass/epoxy/foam core sandwich structures. PVC (60 kg/m^3) and PET (105 kg/m^3) polymer foam core with 10 mm thickness and ±45° glass fiber facings having 780 g/m^2 areal density for each sample and one-two-three-four plies were used, respectively. According to the drop weight tests, the PVC and PET core sandwich structures did not show a distinct difference on the damaged surface. Perforation energy of the sandwiches was increased linearly with increasing of the facing thickness irrespective of the core type.

Al-Shamary et al. (2016) used E-glass fiber fabrics (300 gr/m^2) as face sheets and five mm thick PVC foam core (60 kg/m^3) to manufacture the sandwich composites. The sandwich structures were manufactured with single-core, two core-one inner face sheet, and three core-two inner face sheets, respectively as seen in Figure 2.22. According to the low-velocity impact tests, the resistance to impact load and the energy absorption capacity were found as improved for the sandwiches having inner facing and inner core.

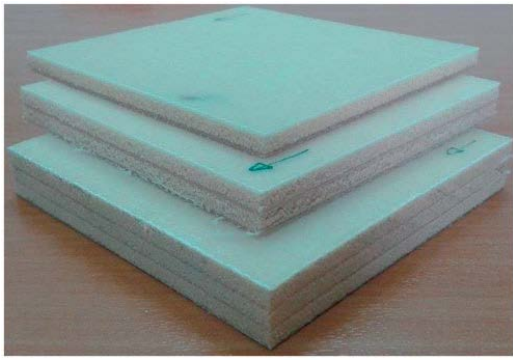


Figure 2.22. One-core, two-core, and three-core sandwich structures (Al-Shamary et al., 2016)

Garay et al. (2016) investigated the effect of both core type (PVC and PET; having the same thickness and density of 12 mm and 80 kg/m^3, respectively) and different face sheets (glass fiber fabrics or mats) on mechanical properties of the

sandwich structures by subjecting the specimens to flexural, compression (flatwise and edgewise), and Shore-D hardness tests. The glass fiber mat and 0/90 bidirectional plain fabric forms were 300 g/m^{2}and 300 g/m^2, respectively. Flatwise compressive, flatwise tensile, and shear strength properties were obtained higher for PVC foam core sandwiches and, in addition to this, the fabric forms of glass fiber face sheet sandwich structures provided slightly better overall results than that of mat facings. The results were given comparatively in Table 2.7-2.8.

2.3. Utilization of Other Core Materials for Sandwich Structures

Besides aluminum and polymer foam cores, there are a few further core materials are available such as corrugated structure, balsa wood, truss type core, and honeycomb. Yan et al. (2014) fabricated sandwich panels by using aluminum foam-filled corrugated core material and subjected them to quasi-static three-point bending tests to examine the bending behavior of aluminum foam-filled corrugated core by comparing with the non-filled corrugated core as illustrated in Figure 2.23. Both the facings and core web materials were stainless steel and the density of aluminum foam was 540 kg/m^3.

Table 2.6. Barcol hardness and flatwise compressive test results (M:mat; C:Cloth) (Garay et al., 2016)

Test	Samples					
	PET-2M	**PET-3M**	**PET-4M**	**PET-2C**	**PET-3C**	**PET-4C**
Barcol hardness	48 (±3)	53 (±5)	54 (±5)	40 (±4)	57 (±3)	55 (±5)
Flatwise compressive strength (MPa)	1,50 (±0,31)	1,62 (±0,40)	1,67 (±0,20)	1,17 (±0,36)	1,52 (±0,18)	1,74 (±0,20)
Test	**Samples**					
	PET-2M	**PET-3M**	**PET-4M**	**PET-2C**	**PET-3C**	**PET-4C**
Barcol hardness	47 (±6)	50 (±4)	51 (±4)	41 (±4)	44 (±3)	47 (±3)
Flatwise compressive strength (MPa)	1,50 (±0,31)	1,62 (±0,40)	1,67 (±0,20)	1,17 (±0,36)	1,52 (±0,18)	1,74 (±0,20)

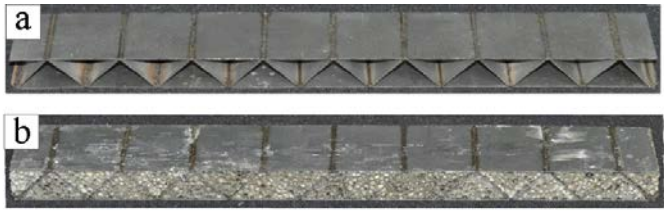


Figure 2.23. Sandwich panels with; a) non-filled corrugated core, b) aluminum foam-filled corrugated foam (Yan et al., 2014)

Table 2.7. Core shear ultimate and facing stresses (Garay et al., 2016)

Test	Samples					
	PET-2M	**PET-3M**	**PET-4M**	**PET-2C**	**PET-3C**	**PET-4C**
Core shear ultimate stress (MPa)	0,78 (±0,03)	0,83 (±0,01)	0,83 (±0,02)	0,80 (±0,08)	0,74 (±0,02)	0,75 (±0,03)
Facing stress (MPa)	39,05 (±0,15)	41,88 (±0,07)	45,71 (±0,20)	39,61 (±0,18)	40,11 (±0,21)	46,18 (±0,11)
Test	**Samples**					
	PET-2M	**PET-3M**	**PET-4M**	**PET-2C**	**PET-3C**	**PET-4C**
Core shear ultimate stress (MPa)	1,05 (±0,01)	1,17 (±0,06)	1,18 (±0,04)	1,15 (±0,07)	1,11 (±0,04)	1,18 (±0,01)
Facing stress (MPa)	39,82 (±0,10)	44,24 (±0,14)	45,98 (±0,18)	43,12 (±0,24)	46,91 (±0,23)	48,00 (±0,21)

The load-displacement curves of two different sandwiches were compared in Figure 2.24. and it was concluded that higher bending load carrying capacity and superior stiffness of the structure were obtained.

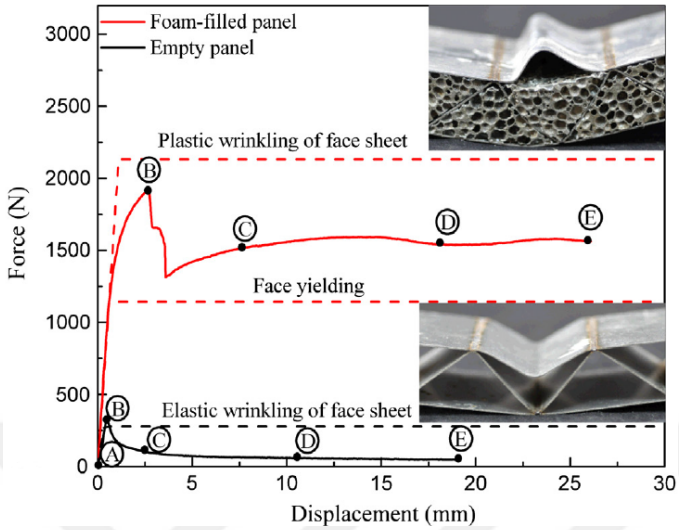


Figure 2.24. Comparison of both aluminum foam-filled and empty corrugated core sandwich panels (Yan et al., 2014)

Li and Wang (2017) manufactured 3D printed core material in the form of truss, conventional honeycomb, and re-entrant honeycomb as presented in Figure 2.25. They constructed the sandwich panels with different facings such as woven and unidirectional carbon fiber and different core materials, respectively. The conducted three-point bending results showed that truss and conventional honeycomb core sandwiches failed due to localized stress concentration while re-entrant honeycomb yielded homogeneous stress distribution. However, the flexural strength of the truss core sandwich panel was found higher compared to others and the sandwich having re-entrant honeycomb core was the least.

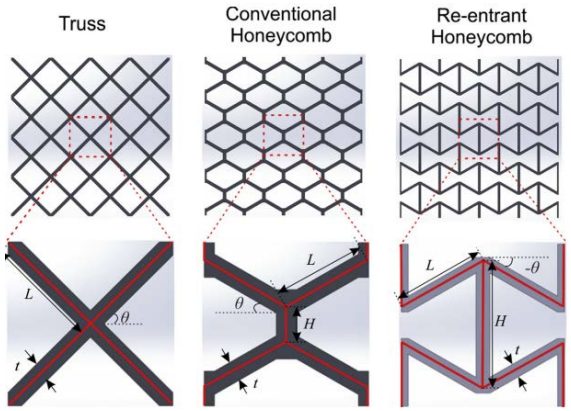


Figure 2.25. The shape of truss, conventional and re-entrant honeycombs (Li and Wang, 2017)

Sandwich structures made from honeycomb core serve extremely high performance to weight ratio in terms of compressive behavior. Although honeycomb core sandwiches have excellent structural performance potential, due to high maintenance costs, there is an increasing demand by airlines to find out alternatives. The high maintenance cost is mostly associated with the possibility of water filling up to honeycomb cores from the porous surfaces under certain situations. The water in honeycomb cells may freeze and expand at low operating temperatures and then it can damage the adjacent honeycomb cells (Herbeck et al., 2002). A study mentioned by Vinson (2001) which was made by Bitzer in 1992 stated that 8% of the wetted surface of Boeing 707 is sandwich while 46% of the wetted surface of Boeing 757/767 is honeycomb core sandwich panel (Vinson, 2001). In comparison with other core materials, the treatments of honeycomb edges are difficult since the material cannot be formed as easily as foam or balsa wood. Therefore, some particular treatments are required for fasteners, as honeycomb has negligible screw retention. Moreover, although honeycomb core has a higher strength to weight ratio, balsa wood and/or solid foam cores are in full contact with face sheets and fortunately, the impact loads spread over a larger area than honeycomb (Black, 2013). Consequently, foam cores can be better alternatives for

sandwich structures and they can be used for both as a cost reduction in production and structural applications instead of honeycombs.

2.4. Numerical Analysis for Sandwich Structures

Numerical analysis carried by finite element methods is commonly used in industrial fields of automotive, aviation, defense, energy, etc. Computer-aided design (CAD) tools provide three-dimensional (3D) modeling of the structural member for the finite element analysis (FEA). The results obtained by FEA reduce cost, save time and resources caused by experimental studies and suggest optimal material selection, geometry, ply number, and layer thicknesses of the structure. In the development of the composite materials such as sandwich structures, determining the suitable configurations for a particular usage area requires complex manufacturing processes and high cost. Therefore, using numerical methods for that kind of production is inevitable. According to the analysis results, optimal sandwich panels such as having maximum strength with minimum weight configuration can be determined and then manufactured instead of manufacturing all configuration types with trial and error.

As the sandwich structures are hybrid composites, their mechanical properties cannot be shown uniform in different section geometries. Borsellino et al. (2004) stated that modeling of the sandwiches was difficult since they could not provide isotropic property. Moreover, it was also manifested that modeling and FEA of the sandwich structures could not satisfy reliable and/or correct results due to limited features of the mechanical properties which were required for design description. However, although there was an inconsistency between experimental and numerical results at the plastic deformation region (Figure 2.26), FEA became useful with a good estimation of geometry, ply number, and stacking sequence.

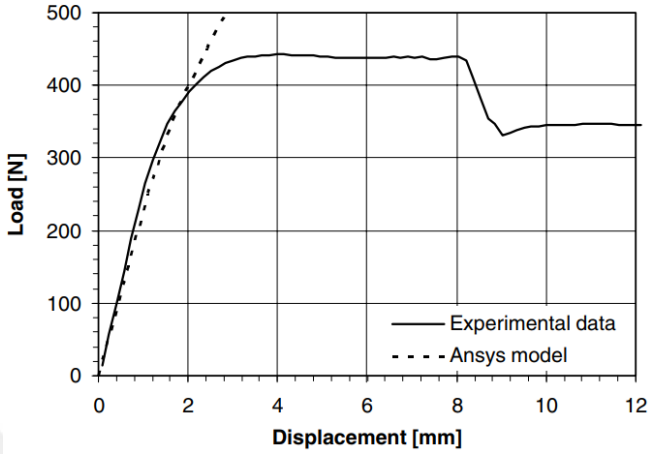


Figure 2.26. Comparison of load-displacement curves obtained by both experimentally and numerically (Borsellino et al. 2004)

Turgut (2007) manufactured a sandwich aircraft wing and subjected to FEA by using MSC Patran 2006 and MD Nastran 2006 software. He recommended that the modeling of the structure should be made on a large scale defining the mechanical properties in detail and creating a more complex shape for the geometry.

Herranen et al. (2012) used different types of core materials, PET, PMI, HDPE, with three different thickness values (15-18-20 mm) and fabricated sandwich panels with glass fiber face sheets. Then the sandwiches were subjected to FEA using ANSYS APDL software in order to determine the optimum core material under four-point bending loading. While PET and PMI foam core sandwiches yielded similar results to experimentally obtained results, the HDPE core sandwich gave quite different values.

Venugopal et al. (2013) modeled a honeycomb core sandwich structure with carbon fiber facings and analyzed under static four-point bending loading by using ANSYS software. When the FEA and experimental results were compared, there was an 11.27% error between them.

Mostafa et al. (2014) made experimental, theoretical, and numerical investigations of flexural behavior of sandwich panels having glass fiber composite

face sheets and 30 mm thick PVC foam core (100 kg/m^3) material under four-point bending loading. The simulation of numerical finite element analysis was performed with the ABAQUS FE program. They considered the construction of the sandwich panel as cohesive contact. Tsai-Wu failure criteria was considered for the nonlinear behavior region of the sandwich structure. The load-displacement curves obtained by experimentally, theoretically, and numerically was shown comparatively in Figure 2.27. Although the theoretical solution was partially agreed with the experimental results in the linear elastic region, the numerical solution fitted well to the experimental load-displacement curve.

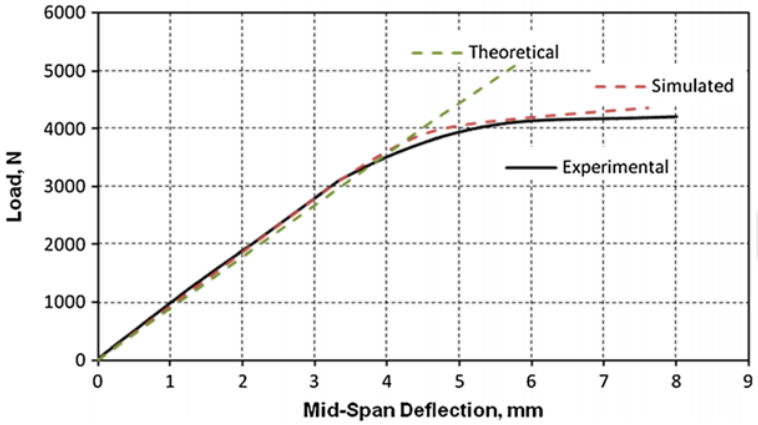


Figure 2.27. Comparison of the load-displacement curves obtained from experiments, theoretical and numerical solutions (Mostafa et al., 2014)

2.5. Current Developments for Sandwich Core Materials

The further developments to reduce the weight of the sandwich structures without sacrificing their effectiveness in flexure can be possible by making modifications and/or considerations in designing the core materials. For instance, carbon fiber lattice core material showed superior mechanical properties compared to metallic ones (Fan et al., 2010). The manufacturing process and the sandwich products were presented in Figure 2.28 and 2.29, respectively.

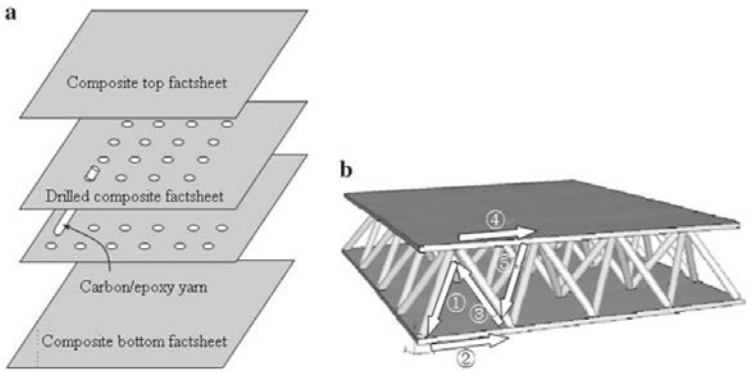


Figure 2.28. Manufacturing process of carbon fiber lattice core sandwich panel (Yan et al., 2010)



Figure 2.29. Carbon fiber lattice core sandwich products; a) panel, b) shell, c) cylinder, d) double-layer panel (Yan et al., 2010)

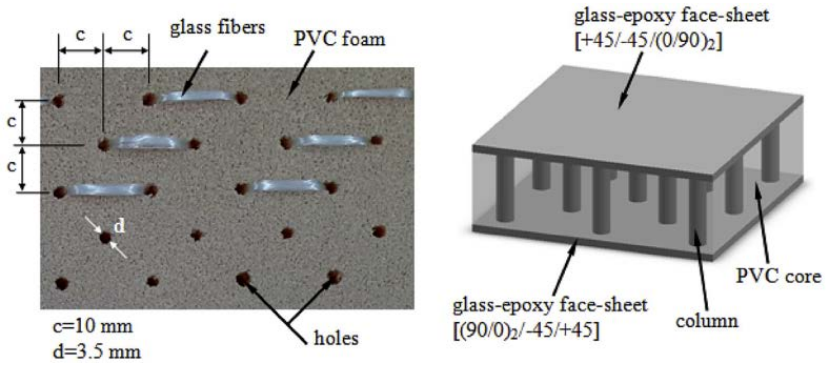
Arbaoni et al. (2015) indicated that they developed a new core material called YmaCell. It was reported as original cellular composite material consists of polypropylene cells coated by epoxy resin. The core materials developed for the sandwich panels were compared with Airex thermoplastic foam and polypropylene honeycomb sandwiches constructed with a different type of glass/epoxy and carbon/epoxy face sheets. Figure 2.30 presents the core materials.



Figure 2.30. Core materials; a) YmaCell, b) polypropylene honeycomb, c) Airex foam (Arbaoni et al., 2015)

Four-point bending results showed that the sandwich panels with the developed new core material exhibited the highest bending rigidity. But when the density and shear properties were investigated, the density of the developed core material was higher than the others. As it is well-known, the increase in density yields better shear properties for the foam core materials and thus yields to obtain better stiffness as well.

Yalkin et al. (2015) used PVC foam core (60 kg/m^3) and unidirectional glass fiber fabrics (300 g/m^2) to fabricate sandwich panels. They investigated the effects of both perforation and stitching on the mechanical properties. Stitching was carried out by glass fiber tows in a specified order as seen in Figure 2.31. Three-point bending results of the stitched foam core sandwiches were presented compared to both plain foam core and perforated foam core sandwiched in Figure 2.32.



(a) (b)

Figure 2.31. a) Stitching of the perforated core, b) developed sandwich panel (Yalkin et al., 2015)

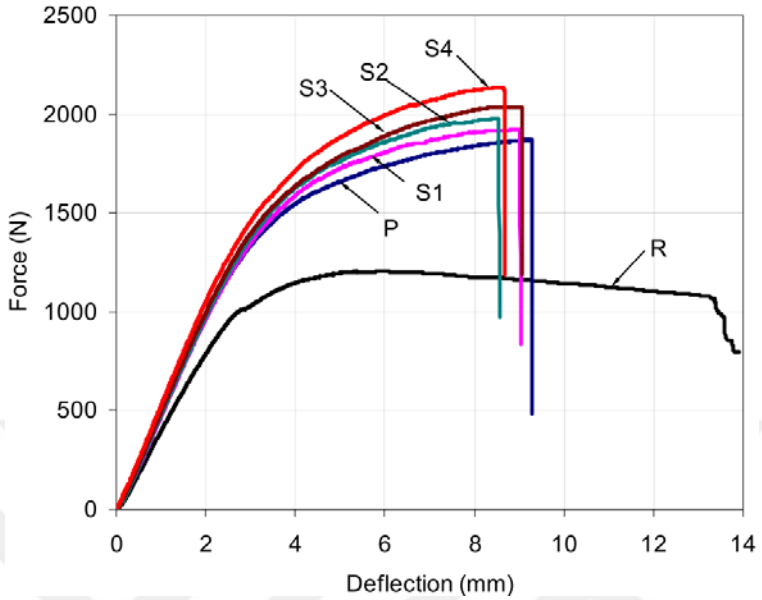


Figure 2.32. Load-displacement curves of the sandwiches (Yalkin et al., 2015) (R: plain foam core, P: perforated, S1: 600-tex stitched, S2: 1200 tex stitched, S3: 1800 tex stitched, S4: 2400 tex stitched)

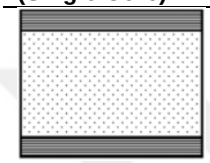
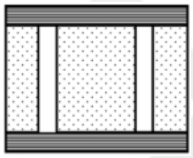
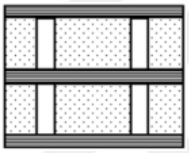
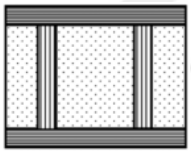
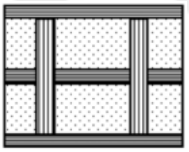
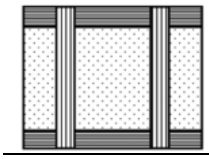
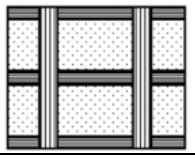
Yalkin et al. (2017) made some modifications to the PVC foam core (60 kg/m^3) and the whole sandwich structure as well. For this purpose, single-core perforated, divided core perforated, single-core stitched, and divided core-stitched sandwiches were manufactured as presented in Table 2.9 and the configurations were subjected to tensile and compression tests, respectively. The single-core was 20 mm thick, while each divided core was 10 mm thick.

Tensile and compression tests were made to each configuration. And they concluded that stitched core provided the highest compressive strength and better tensile strength over the other configurations. In addition, dividing the core did not show a substantial effect on the failure modes of the sandwich structures.

Santhanakrishnan et al. (2018) produced different pile-oriented stitched foam core and investigated the shear strength of the woven glass fiber facings sandwiches having unstitched and stitched foam core materials. The used core material was 10 mm thick PVC foam having a density of 80 kg/m^3. The stitching of

the foam core was made by glass fiber yarns according to different pile orientations of 90º, 45º, 90º/45º, and 90º/45º/90º, respectively. The load-displacement curves obtained from the shear test were presented in Figure 2.33 and the results were given in Table 7.

Table 2.8. Specifications of the sandwich composite specimens (Yalkin et al., 2017)

Image (Single Core)	Face sheet	Column Material	Image (Divided Core)	Face sheet	Column Material
	Glass /epoxy	None		Glass /epoxy	None
Perforated core 	Glass /epoxy	Epoxy	**Perforated core** 	Glass /epoxy	Epoxy
Stitched core 	Glass /epoxy	Glass /epoxy	**Stitched core** 	Glass /epoxy	Glass /epoxy
Stitched core and face sheet 	Glass /epoxy	Glass /epoxy	**Stitched core and face sheet** 	Glass /epoxy	Glass /epoxy

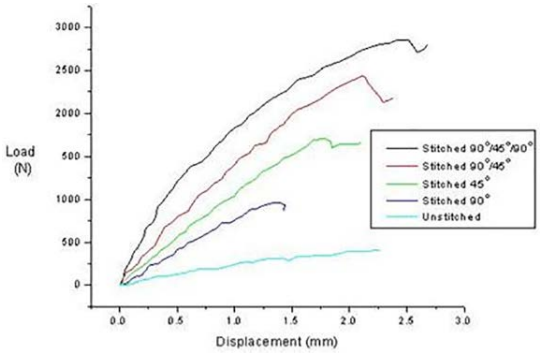


Figure 2.33. Load-displacement curves of stitched and unstitched and foam core sandwiches (Santhanakrishnan et al., 2018)

Table 2.9. Shear properties of stitched and unstitched foam core sandwiches (Santhanakrishnan et al., 2018)

SandwichPanel	Ult. Shear Strength (kPa)	Shear Modulus (MPa)
Unstitched	420	1,75
Stitched- 45°	1686	11,24
Stitched- 90°	963	8,78
Stitched- 90°/45°	2443	13,75
Stitched- 90°/45°/90°	2844	16,32

Taghizadeh et al. (2019) studied the effect of different corrugated core shapes with filled PVC foam (80 kg/m^3) material on sandwich panels. As seen in Figure 2.34, rectangular, triangular, and trapezoidal corrugated cores are used. The core shapes were manufactured by woven glass/epoxy similar to face sheets. Especially rectangular and trapezoidal corrugated and PVC foam-filled sandwiches showed superior structural efficiency compared to non-corrugated, plain foam core sandwich panel.

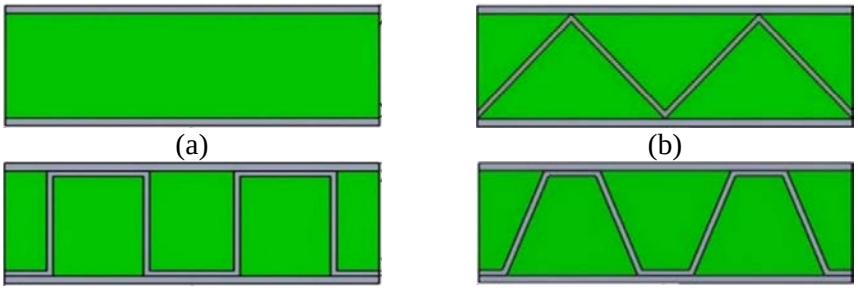


Figure 2.34. Sandwich panels with; a) no-corrugated, plain foam core, b) triangular corrugated core, c) rectangular corrugated core, d) trapezoidal corrugated core (Taghizadeh et al. 2019)

2.6. Advanced Technologies for Composite Manufacturing

As stated by Fan et al., (2010), the further developments for improving the effectiveness of the sandwich structures strongly depend on the manufacturing methods based on cost-effective, automated with mechanization and controlling the imperfections.

2.6.1. Advances in Lay-up Processes

The hand lay-up process has been automated by using a chopper gun and a spray. As seen in Figure 2.35, a machine tool that can be used by hand-held or a robot arm. The process can accelerate the manufacturing time with the low-cost operation and reduce the manual work and labor cost. It is possible to mix the resin and its hardener in a reservoir and allow it to distribute chopped fibers and matrix material simultaneously directly onto the mold surface. Although continuous fiber is feeding to chopper guns, the fibers are sprayed as chopped glass fiber which is the main drawback and cannot provide homogeneous mechanical properties for the finished product.

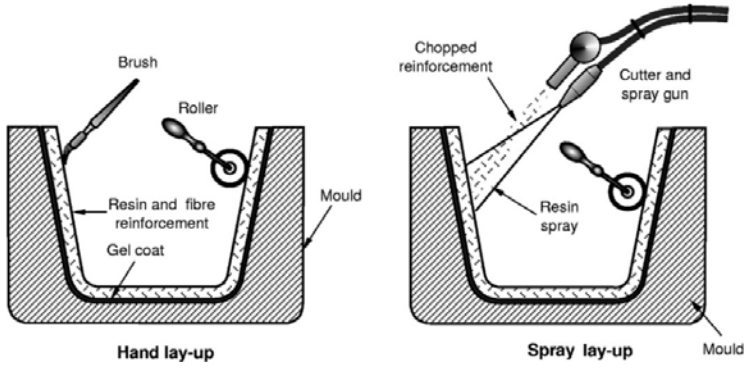
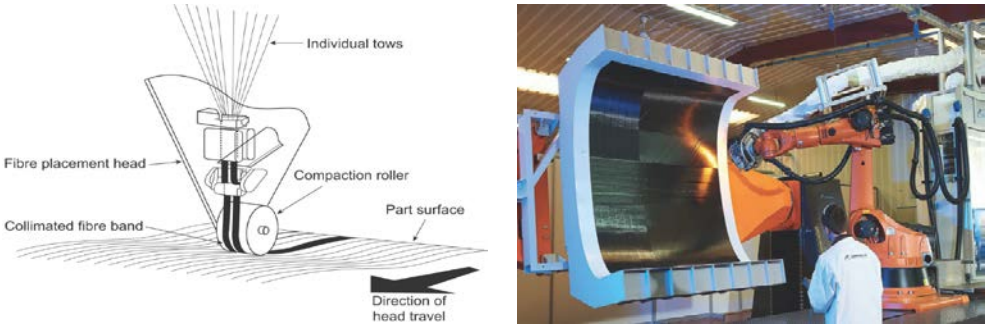


Figure 2.35. Hand lay-up vs. spray-up manufacturing methods (Swift and Booker, 2013)

Using prepregs is also a better alternative to wet lay-up processes for advanced structures such as sandwich panels for obtaining well-impregnated resin, and increased mechanical properties for the final product. Low void contents are obtained in face sheets laminated by prepregs (Karlsson and TomasAström, 1997). For aircraft structures such as wing skins and fuselages, the production and mechanical properties must be excellent. Therefore, prepreg materials with autoclave curing are the best process combination for that kind of application fields. In order to increase production rates, improve shape tolerances, and dimensional accuracy, automated processes have been developed such as automated fiber placement (AFP) and automated tape layup (ATL). AFP process was developed to overcome the drawbacks of ATL (Crosky et al., 2015) that lays up the prepregs either onto a flat or a cylindrical mandrel by using multi-head robot machinery (A. McIlhagger et al., 2015) as represented in Figure 2.36. It was reported that the significant gain for the cost-effectiveness of AFP is low material scrap rate besides reduced labor cost (Crosky et al., 2015).



(a) (b)

Figure 2.36. a) AFP process (A. McIlhagger et al., 2015), b) Image of the AFP (Crosky et al., 2015)

2.6.2. Advances in Pultrusion Method

Pultrusion is a cost-effectively used and automated manufacturing process for continuous and constant cross-sectional composite profiles. As presented from Figure 2.37, continuous fibers are drawn through a resin tank and moved to a heated die having a final shape of the product. As the resin-impregnated fibers pass through the die, the composite material is assumed to form to final shape and cured. After curing and leaving the die, the product is cut properly.

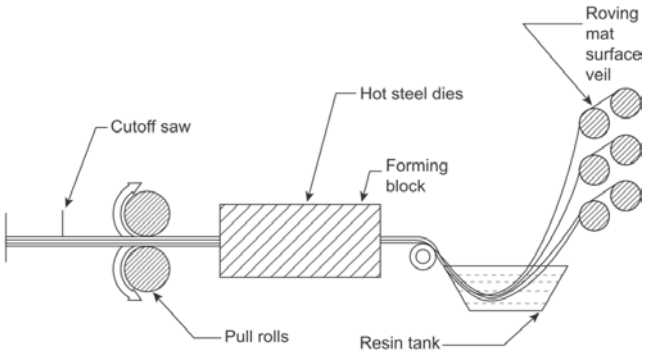


Figure 2.37. Pultrusion method (A. McIlhagger et al., 2015)

2.6.3. Advances in Stitching Machines

Santhanakrishnan et al., (2018) designed a stitching machine for the sandwich core materials as shown in Figure 2.38. The machine also provided to

make different pile orientation in the stitching process, which allow to find out optimal mechanical properties.

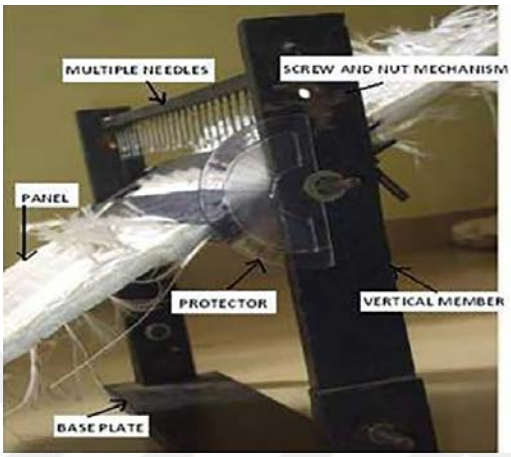


Figure 2.38. Image of Stitching machine (Santhanakrishnan et al., 2018)

2.6.4. Advances in Hot Press Molding Method

Mei et al. (2017) developed a novel manufacturing method by hot press molding for fabricating carbon fiber reinforced tetrahedral truss core sandwich panels. The process is illustrated in Figure 2.39.

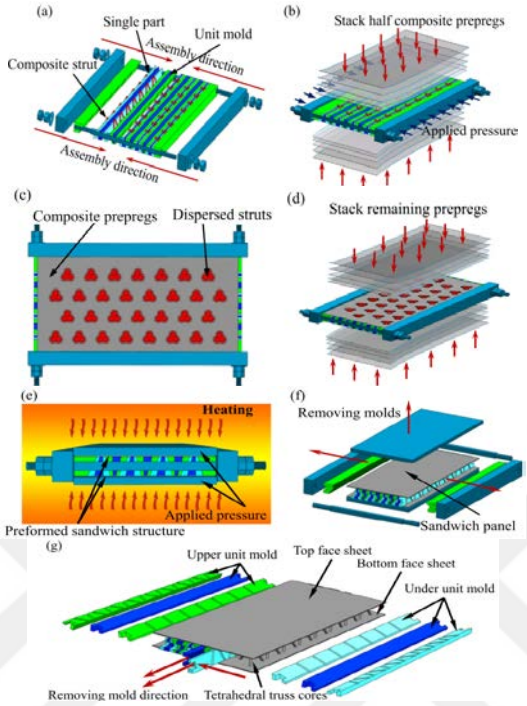


Figure 2.39. Manufacturing process with developed hot press molding; a) placing the prepared composite strut into corresponding position, b) lay-up of five layers of carbon/epoxy prepregs on the mold, c) dispersing end of the struts by penetrating them into prepreg

2.6.5. Same Qualified Resin Transfer Molding (SQRTM)

SQRTM is a newly developed composite manufacturing method consists of the prepreg lay-up and liquid resin transfer molding. The method was first developed and commercialized by Radius Engineering in order to provide net shape composite products. Figure 2.40 presents the difference between traditional and net shape productions.



(a) (b)

Figure 2.40. a) traditional production of composite parts, b) net shape, single part composite production (Website, 2019)

SQRTM is also known as the out-of-autoclave process and it has several advantages over the autoclave process. With the aid of SQRTM, large and complex parts can be produced with final shapes with reduced cost. The method differs from the RTM method with prepreg lay-up and the injected resin to the RTM system is the same as that existed in prepreg as shown in Figure 2.41. This allows using of high qualified toughened materials such as tough resins and toughened agents. The injected resin creates hydrostatic pressure to composite laminate and eliminates the formation of void contents, which improves both quality of the final product and its mechanical properties. By the way, control of the composite quality is easier than the autoclave process due to its complex dependent variables. In addition, the curing in the SQRTM method is approximately two hours shorter than in autoclave as the sheen in Figure 2.42. On the other hand, the method has advantages over the RTM technique. Thickness variations in the final part, dimensional accuracy, and surface quality are improved with the aid of SQRTM. Therefore, the SQRTM process has been most suitable and preferable for aerospace industries to produce structural members. (Website, 2019; Website, 201?)

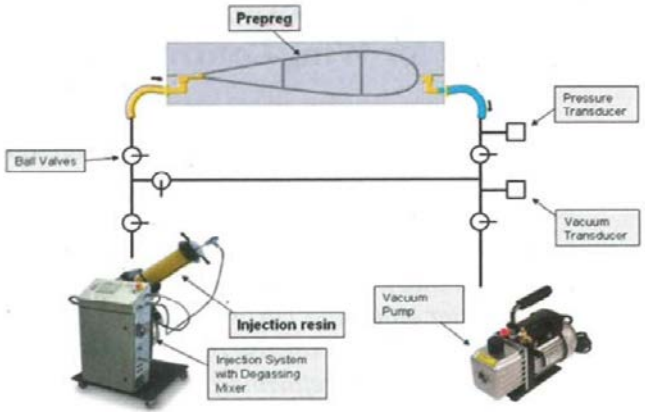


Figure 2.41. Schematic presentation of SQRTM process (Gueuning and Mathieu, 2016)

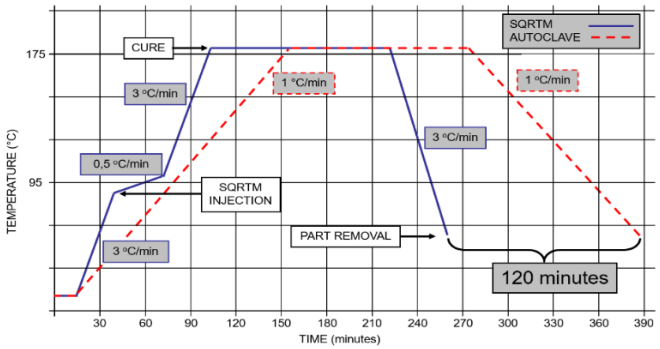


Figure 2.42. Comparative demonstration of curing cycles both in SQRTM and autoclave (Website, 2019)

2.7. Significance and Goal of the Study

Sandwich composites have arisen as important structural members due to their excellent stiffness to weight ratio, better impact resistance, resistance to environmental conditions, etc. When the literature is scrutinized, most of the researchers have investigated the behavior and their failure modes of the sandwiches under static or dynamic loadings. The previous studies generally serve the results of mechanical tests based on the effect of different constituents and their different thickness and density, i.e. facing properties, core densities and thicknesses, and matrix surroundings. However, the researches which makes the structure more rigid under bending loadings are only limited to usage of commonly existed materials, and very few researchers have interested in different design constructions and considerations. In this thesis work, the effect of bending characteristics of woven plain carbon fiber sandwich structures having extremely low-density PVC foam core and inner wire mesh stainless steel have been investigated. In the literature usage of the wire mesh steels having very fine sizes and extremely low-density foam core such as 48 kg/m^3 in sandwich panel applications have not been encountered yet.

Very recently, porous wire mesh steels were used in civil engineering applications as reinforcement material in sandwich concretes (Joseph et al., 2017; Matalkah et al., 2017), as a good absorber under the impact (Shao et al., 2018), and

in mechanical engineering applications in order to improve heat transfer (Kurian et al., 2016 and 2017). Wire mesh steels, in a porous form, are available from very fine to coarse sizes at various wire diameters.

Based on the results obtained by Joseph et al. (2017) and Matalkah et al. (2017), stacking the wire mesh stainless steel in sandwich structures has positively affected the bending rigidity of the specimens. However, the used wire mesh sizes were very coarse size. Besides the improvement of bending stiffness, the wire mesh layers may be considered to increase load-carrying capacity over a larger mid-span displacement, and also it may be used to eliminate or reduce the indentation failure of the structure. Since the indentation is a local concentrated load on foam-cored sandwich panels, it was reported as a serious problem by Daniel et al. (2002).

As it is presented in Figure 2.43, Ashby (2011) introduces an advanced material selection technique by providing material charts considering the desired mechanical properties. Figure 2.43 represents Young's modulus versus the density chart of all material families. The chart draws particular attention to the large holes. The direction of material development is also indicated in the chart with an arrow. One approach to fill these holes is to develop hybrid materials that have the desired property profile. Therefore, the produced sandwich panels in this thesis work directly contribute to the material universe. For instance, Finnegan et al. (2007) contributed by a research study to fill the holes in the material universe by introducing pyramidal truss core sandwiches for high strength, lightweight structural design. Therefore, one of the main purposes of the Ph.D. study is to develop lightweight, stiff, and strong composite sandwich panels and to fill the holes in the material universe.

The second main intention of the study is to develop multifunctional sandwich structures by using very fine stainless-steel wire mesh sheets (100 and 200 mesh sizes). Face sheets of the sandwich panels are going to be hybridized with wire mesh sheets. This hybridization does not only improve bending stiffness but also controls the failure behavior of the structure by eliminating the sudden

fracture of carbon fiber face sheets. Therefore, the highly brittle behavior of the carbon fiber laminates during failure can be compensated by stacking the wire mesh sheets within the facings. In this respect, the study is going to provide a novelty for the literature and industrial applications. In addition to this, hybridization of sandwich facings with very fine wire mesh sheets can also be a good alternative for Fiber Metal Laminates (FMLs). Because the lap shear strength between fiber-reinforced composites and metal alloys can be very weak unless some surface treatment processes are applied to metal surfaces in order to improve adhesion bonding capability. In the case of using wire mesh sheets, additional processes such as anodizing, mechanically grinding, acid etching, etc. may not be required because of the porous form of wire mesh sheets. The previous studies have also shown that wire mesh layers contributed to the bending rigidity of the structure in civil engineering applications. Therefore, the effect of wire mesh sheets in the hybridization of sandwich facings is going to be investigated considering both bending stiffness and failure behavior of the sandwich panels, it is predicted that the developed sandwiches can be a suitable candidate for mechanical engineering fields.

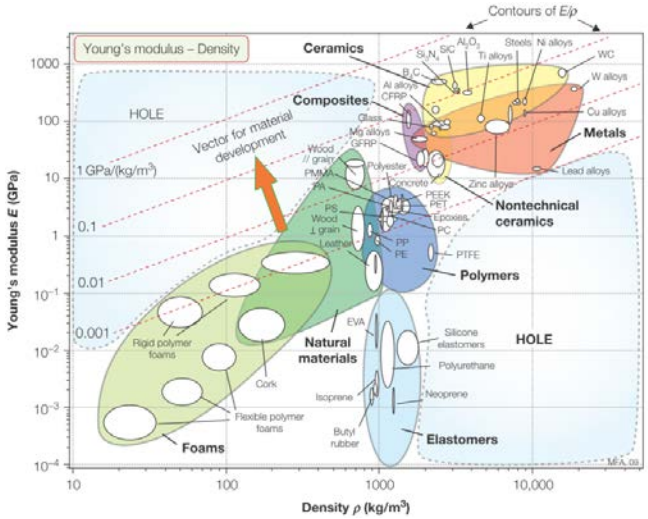


Figure 2.43. Young modulus vs. density chart of the material families (Ashby, 2011)

Testing and development of the sandwich panels are going to be carried out based on the investigation of flexural characteristics. Therefore, other kinds of testing methods such as low-velocity impact tests are not within the scope of the work.

Besides the main intentions given above, the study also highlights the followings:

- The use of woven plain carbon fiber fabrics and rigid closed-cell polymer foam (PVC) as face sheets and core, respectively. Because, that kind of combination for sandwich applications has become more prevalent and differed from the most of the existed literature (Wang et al., 2015). The material combination of polymeric foams and fiber-reinforced composites finds widespread application in the marine industry such as shipbuilding and boats (Stevees and Fleck, 2004). It is anticipated that the use of selected material combinations for face sheets and core is going to provide certain advantages. The core material has identical shear properties through the thickness and hence, the shear properties such as core shear modulus, shear stress, transverse shear rigidity can be evaluated identically between the face sheets. On the other hand, using woven plain carbon fiber fabrics in the manufacturing process is going to ease the fabrication of sandwich panels. In the hand lay-up process, especially the resin impregnation of unidirectional fibers in different angular orientations becomes very difficult. Consequently, it adversely affects the structural effectiveness of the sandwich product.
- The density of the core material used throughout the study is 48 kg/m^3. Up to date, in the literature, the lowest density used for the core of sandwich structures was 54 kg/m^3. Gupta et al. (2019) also stated that the most commonly found PVC foams' densities in both the literature and applications are in the range of 60-350 kg/m^3. Therefore, the study also

aims to increase specific bending stiffness (EI/ρ) by lowering the weight of the structure as much as possible. This will also provide a better E/ρ ratio.

- Besides the physical and mechanical advantages of the constituents, usage of the extremely low-density foam core with stiff and strong carbon fiber face sheets is going to allow to fabricate economically justifiable unique sandwich panels.

The followings are the considered activities and principal tasks that are carried out in this thesis work:

- ✓ Proper selection of the sandwich constituent materials to fill holes in the material universe by introducing lightweight, stiff, and strong sandwich composites.
- ✓ The selection of appropriate wire mesh sizes can improve the bending behavior of the produced sandwich panels.
- ✓ Determination of the manufacturing method that is suitable for sandwich fabrications especially in laboratory ambient, and setting up the manufacturing equipment.
- ✓ Decision making for lamination of the face sheets considering the stacking sequence of wire mesh sheets and carbon fiber fabrics. Construction of experimental design for these purposes.
- ✓ Designing the geometry and performing three-point bending tests of the sandwich panels are going to be carried out based on clearly identified circumstances, according to ASTM standards. Because, the literature survey has shown that many of the experimental studies were carried out with different geometrical dimensions, testing conditions without indicating any technical standard. The results obtained from that kind of studies have provided different values from each other and even they

provide conflicting or inconsistent results. This is also stated by Wang et al. (2015). Therefore, in this thesis work, the construction and testing of the sandwich panels are going to be made based on ASTM standards.

The following standards have been met in this work for the tests, manufacturing, and other related requirements.

- ✓ ASTM C393 *("Core Shear Properties of Sandwich Constructions by Beam Flexure"),*
- ✓ D7249 *("Facing Properties of Sandwich Constructions by Long Beam Flexure"),*
- ✓ D7250 *("Determining Sandwich Beam Flexural and Shear Stiffness"),*
- ✓ D3039 *("Tensile Properties of Polymer Matrix Composite Materials").*
- ✓ The bending stiffness of sandwich panels is going to be determined considering sandwich beam theory as given in Chapter 1 (Equation 1). In addition to this, ASTM D7250 Standard also provides an analytical approach to determine bending characteristics of the sandwiches. Up to date, the usage of the ASTM D7250 Standard approach for evaluating the bending and/or shear stiffness has been very limited.
- ✓ Evaluation of the testing results based on both ASTM standards and classical sandwich beam theory approaches.
- ✓ Examining bending behavior and failure modes of the sandwich structures.
- ✓ Investigation of the effects of wire mesh sheets on the developed sandwich panels.
- ✓ Examining of statistical significance of the experimental parameters with their levels and finding out the most effective parameter for experimentally obtained testing results.
- ✓ Determining the location of developed sandwich panels in the material universe considering E/ρ ratio.

3. MATERIAL AND METHOD

This study consists of the fabrication of sandwich composites, mechanical tests in terms of three-point bending, and tensile. This is followed by numerical analysis for validation of the experimental results, determining the statistical significance of the test values using design of experiment techniques, and discovering failure mode analysis after tests.

3.1. Materials Used for the Sandwich Panels

The sandwich composites that were manufactured in this thesis work consist of woven plain carbon fiber fabrics, stainless steel wire mesh sheets, closed-cell rigid polyvinylchloride (PVC) foam core, epoxy resin, and its hardener. In addition, other consumable materials for sandwich manufacturing processes were procured and used. All of the materials used in this work are provided in the following sections.

3.1.1. Carbon Fiber Fabrics

Carbon fiber fabrics were used for the lamination of the facings of the sandwich panels. Woven plain, continuous carbon fiber fabrics, which were procured from the market (Dost Kimya Inc.) were used in the study. The physical and mechanical properties of the carbon fiber fabrics are given in Table 3.1.

Table 3.1. Physical and mechanical properties of woven plain continuous carbon fiber fabric (TDS, Dost Kimya Inc., 2014)

Physical and Mechanical Property	Value
Fabric Description	Woven, 3K Plain, Continuous
Areal Weight	200 g/m^2
Thickness	0,20 mm
Density	1790 kg/m^3
Tensile Strength	3800 MPa
Tensile Modulus	240 GPa
Tensile Strain	1.6 %

Woven fabrics provide better dimensional stability in both weft and warp directions (cross-ply with 0° and 90°) compared to unidirectional reinforcements (Dixit et al., 2014). Therefore, they can provide higher out of plane strength, i.e. transverse tensile, to the composite structures (Priyanka et al., 2017). The fabrication time while using woven fabrics is also relatively short due to the stability of the fibers. Woven fabrics can be classified as plain, satin and twill weaves as shown in Figure 3.1 (Gay, 2015).

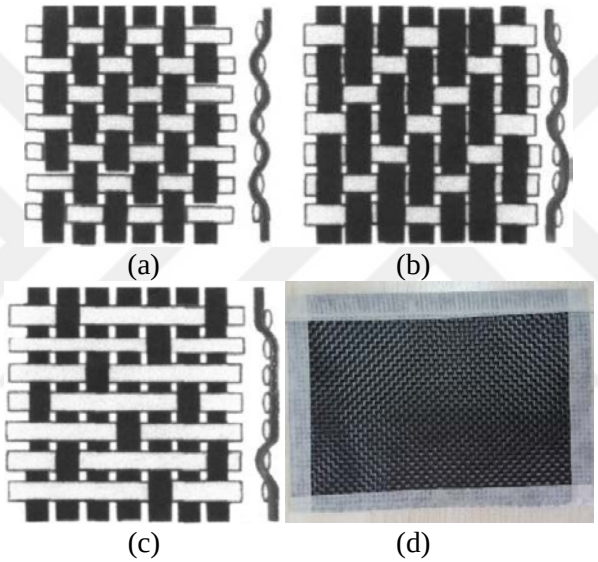


Figure 3.1. Woven fabrics; a) plain, b) twill, c) satin, d) image of plain weave woven fabric used in this study (Gay, 2015)

3.1.2. Core Material

As the core materials play an important role in sandwich structures under the static and dynamic loadings, the selection should be made carefully. The core material of the sandwich panels manufactured in this study was selected as linear cross-linked, closed-cell, rigid, industrial polyvinylchloride (PVC) foam due to its high chemical and flammability resistance, and low cost (Al-Shamary et al., 2016). The closed-cell form makes the structure isotropic and can resist moisture and

water penetration (Carlsson and Kardomateas, 2011). In addition to these advantages, Zhou et al. (2012) reported that linear cross-linked PVC foams at low densities provided higher perforation resistance, and it is important especially for the sandwiches having thinner face sheets. In recent years, this kind of foam core material has particularly been used in marine and aerospace applications due to their benefits mentioned above. And it is also possible to use for the weight critical fields where structural rigidity is important such as body parts of the vehicles, the interior body of airplanes, lift machines, sports goods, etc. Table 3.2 gives the physical and mechanical properties of the foam core used in this thesis work. As seen in Table 3.2, the density property of the foam is lower than the ones experienced so far in the sandwich composites given in the literature. It is intended that the selected low-density foam can provide further opportunities to reduce the weight of lightweight sandwich panels without sacrificing the mechanical load-carrying capacities. To investigate this, bending characteristics and failure modes of the lightweight sandwich panels will be subjected to a systematic testing program to evaluate the gain obtained for stiffness to weight ratio or specific stiffness and bending performance.

Table 3.2. Physical and mechanical properties of PVC foam core material (TDS, Airex C70)

Physical and Mechanical Properties	**Value**
Description	Airex C70.48
Density	48 kg/m^3
Thickness	10 mm – 20 mm - 30 mm
Compressive strength	0.60 MPa
Compressive modulus	48 MPa
Tensile strength	0.95 MPa
Tensile modulus	35 MPa
Shear strength	0.55 MPa
Shear modulus	16 MPa

As it is seen from Table 3.2, foam materials with three different thicknesses were considered and used in the study to examine the effect of PVC foam thickness under bending loading as a core material.

3.1.3. Matrix Material

The lamination of face sheets and core material to construct the sandwich panels was carried out with polymer matrix surrounding. Epoxy resin and its proper hardener were used to prepare the matrix material. MGS^{TM} L160 epoxy resin and H160 hardener were procured from the market (Dost Kimya Inc.). This combination is suitable for the construction or manufacturing of the sandwich panels where the bending stiffness to weight ratio is important such as boat and shipbuilding, airplane models, body parts of a vehicle, sports equipment, etc. The physical and mechanical properties of the epoxy resin and its hardener are given in Table 3.3. However, the matrix, epoxy, and hardener mixture in a proper weight ratio, yielded a density of 1,18 kg/m^3 to 1,20 kg/m^3 (TDS, Hexion, 2006).

Table 3.3. Physical and Mechanical Properties of the epoxy resin and its hardener (TDS, Hexion, 2006)

Physical and Mechanical Properties	**Epoxy resin**	**Hardener**
Density	1.13-1.17 kg/m^3	0.96-1.00 kg/m^3
Viscosity	700-900mPa.s	10-50mPa.s
The Matrix Properties		
Density	1,18-1,20 kg/m^3	
Flexural strength	110-140MPa	
Modulus of elasticity	3.2-3.5GPa	
Tensile strength	70-80MPa	
Compressive strength	80-100MPa	

3.1.4. Stainless Steel Wire Mesh Sheets

AISI 304 Stainless steel wire mesh sheets were also used in the construction of the developed panels. The intention is to improve both the bending load-carrying capacities, improved bending behavior during failure, and reduction

of punctures. Therefore, AISI 304 stainless steel wire mesh sheets were located in different layer position and layer combinations in the panels to investigate its effect on both the bending characteristics and the failure behavior of very low-density PVC foam core carbon fiber sandwich structures. Two different mesh sizes that are 100 mesh (100 openings in one inch) and 200 mesh (200 openings in one inch) stainless steel sheets were used. The image of the materials was taken with a macroscopic photograph and stereomicroscope in detail as shown in Figure 3.2. The chemical composition and mechanical properties of the wire mesh sheets are given in Table 3.4 and 3.5.



(a) (b)

Figure 3.2. Stainless steel wire mesh; a) 100 mesh, b) 200 mesh

Table 3.4. Chemical composition of wire mesh (CES Selector, 2016)

Material	C%	Cr%	Fe%	Mn %	Ni%	P%	S%	Si %
304 stainless steel mesh film	0-0,08	18-20	65,8-74	0-2	8-11	0-0,045	0-0,03	0-1

Table 3.5. Physical and Mechanical Properties of the wire mesh film (CES Selector, 2016)

Physical and Mechanical Properties	**AISI 304 stainless steel wire mesh**
Density	7850-8060kg/m^3
Wire thickness (100 mesh)	0,1 mm
Wire thickness (200 mesh)	0,05 mm
Young's modulus	190-203GPa
Yield strength	205-310 MPa
Ultimate Tensile Strength	510-620 MPa
Elongation	45-60 % strain
Compression strength	205-310 MPa
Shear modulus	74-81GPa
Poisson's ratio	0,265-0,275
Hardness, Vickers (HV)	170-210

3.2. Equipment and Pre-processes for Sandwich Manufacturing

Vacuum bagging has been preferred for the manufacturing method since it is more suitable for laboratory conditions, provides ease of application, and requires experience for labor skills. The equipment and preparation of the composite materials during pre-processing are going to be discussed in the following sections.

3.2.1. Vacuum Pump

According to the preferred manufacturing process, a vacuum pump is used to obtain the final sandwich product. Curing under a vacuum atmosphere provides better mechanical properties due to higher fiber to matrix volume fraction. The sandwich composites fabricated in this thesis work were cured via RC-8D, 50 Hz, standard vacuum pump, shown in Figure 3.3. The technical specifications are given in Table 3.6.



Figure 3.3. The vacuum pump used for the fabrication of the sandwich panels

Table 3.6. Technical specifications of the Vacuum Pump

Specification	Corresponding Value
Number of stages	2
Nominal capacity speed	8,5 m^3/h
Total final pressure (Abs)	0,01 mbar
Partial final pressure (Abs)	0,005 mbar, (3,7 micron)
Motor power	0,37 kW
Nominal r.p.m	1400 n/min
Noise level	52 dB (A)
Weight	13,2 kg
Oil type	SW60
Oil quantity	0,35 dm^3

3.2.2. Chemical Treatment Solution

Before stacking the composite layers during fabrication, metal wire mesh sheets were subjected to chemical treatment. The surface of the AISI 304 stainless steel wire mesh sheets was chemically treated by using alkaline-based caustic soda, sodium hydroxide (NaOH). The process is carried out for surface degreasing, and cleaning as well with the aid of an alcohol bath. The image of caustic soda used in this study is presented in Figure 3.4.



Figure 3.4. Caustic soda

3.2.3. Preparation of Composite Materials and Consumables

Preparation of the carbon fiber fabrics and the foam core material were made according to the design of the sandwich panels considering their geometry and testing conditions, which are specified in related ASTM standards. On the other hand, the polymer matrix was prepared based on the weight ratio by using precision scales.

The consumable materials for the application of vacuum bagging technique are vacuum bag, perforated release film, breather cloth, spiral hose, vacuum hose, sealant tape. The vacuum bag must be durable against tearing and environmental conditions. The perforated release film must not be adhered to the surface of the sandwich product after curing. Breather cloth is used to collect the excessive resin within the vacuum bag with the aid of a spiral hose. The sandwich product must be kept in an enclosed vacuum bag with the aid of sealant tape. Vacuum hose is employed to provide adequate tightness and to remove entrapped air within the vacuum bag.

3.3. Fabrication of Sandwich Composites

The sandwich composites were manufactured with hand lay-up followed by a vacuum bagging method. In this type of manufacturing method, all fiber fabrics and core material are impregnated by matrix material at each layer. After the impregnation of sandwich constituents by hand lay-up, it is enclosed by a

vacuum bag for the curing process. In addition, a release film and breather cloth placed on the sandwich are also used inside the bag. The process is more suitable for small batch production due to its simplicity and cost-effectiveness but the quality of the product depends upon the labor skill. The manufacturing is carried out on an open mold as it is recommended by Balasubramanian (2014).

A schematic view of the process is demonstrated in Figure 3.5. The facings either may be manufactured separately and then they bonded to a core or the sandwich may be co-cured. In this study, the latter was applied.

Before the start of the production, determination of the weight ratios for facings, foam core and matrix materials are essential in order to provide sufficient resin impregnation to each layer. The amount of matrix material was sufficiently prepared considering the total weight of fabrics and foam core materials. And the weight ratio of the epoxy resin to its hardener was set to 100:25. The mixture of epoxy and hardener was carefully stirred by avoiding the formation of air bubbles to obtain a homogeneous polymer matrix. Then, all the layers including fiber fabrics, core material, and wire mesh sheets sequentially stacked by hand lay-up resin impregnation. The fiber facings of the sandwich composites are arranged as symmetrical and the wire mesh sheets were placed either at the upper facing-core interface or under the first fiber fabric of the upper facing or combination of both cases. The lamination of all layers was carried out simultaneously and the process is co-cured after the manufacturing. During the hand lay-up process, utmost importance was given to eliminate air bubbles between the composite layers. This is because the effectiveness of the sandwich structures is directly related to good chemical bonding of the layers. Insufficient cross-linking and/or lack of bonding adversely affect the transmission of shear stress between the facings and the core. After stacking all the layers (complete wet out), a perforated release film, which excludes air bubbles from the structure during curing, and provides ease of handling for the sandwich production after curing, was placed over the composite sandwich. It also allows to drain or release the excessive resin throughout the

perforations. Over the perforated release film, a breather cloth was placed to transmit gases, and collect the excessive resin properly. Finally, the sandwich structure was enclosed by a sealed tape, and kept inside a vacuum bag as suggested by Dutton et al. (2004).

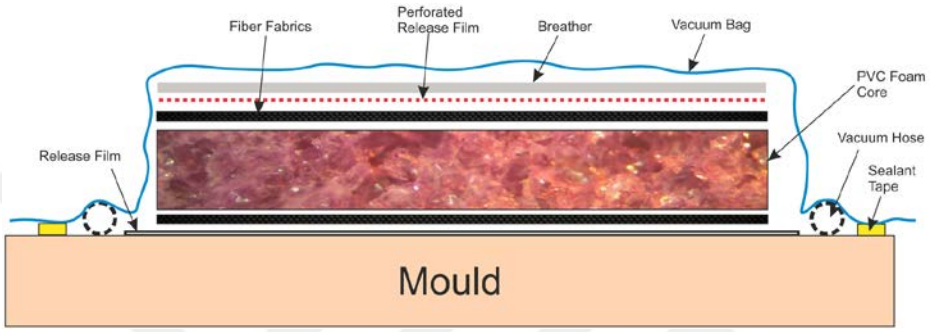


Figure 3.5. A schematic view of the manufacturing process

The curing process was carried out under a 0,01 mbar vacuum process for approximately six hours, and then, the pump was turned off when there is no evidence of resin being bleed from the outlet of the vacuum bag. Then the manufactured sandwich panels were kept under vacuum atmosphere at room temperature for 24 hours. Figure 3.6 shows the production steps carried out in this study.



Figure 3.6. The production steps of sandwich composite panel

The most important drawback of the vacuum bagging method is the possibility of excessive resin in the structure, and high void content particularly at corners (Peters, 1998). Therefore, during hand lay-up, a roll tool was used to spread resin and minimize the trapped gases between the layers. Extended margins were also given to the produced sandwich panels to protect the specimens from any defects as mentioned in Section 3.4.

Based on the manufacturing method, the produced sandwich panels are demonstrated in Figure 3.7 by a flow chart considering the combinations of the investigated sandwich structures.

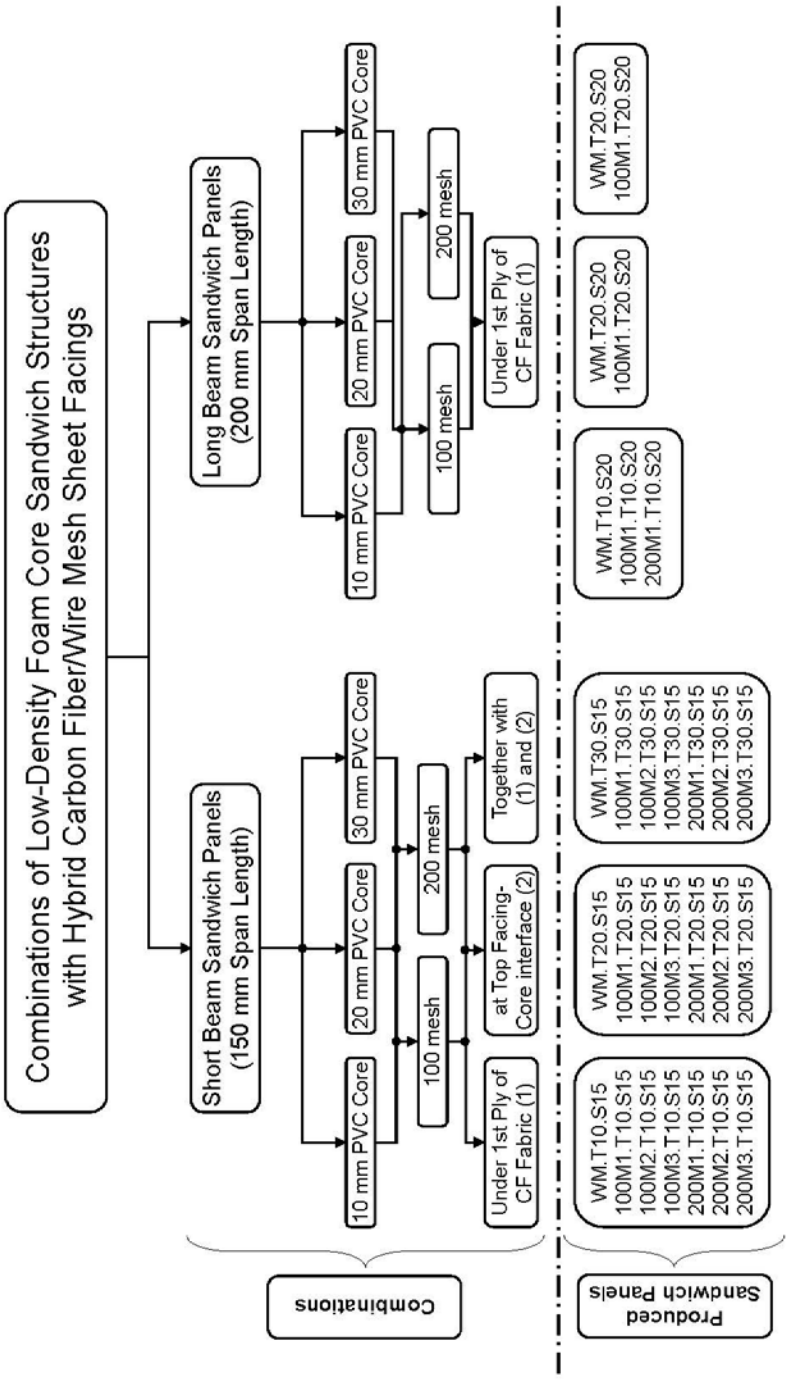


Figure 3.7. Flowchart of the produced sandwich configurations

3.4. Determination of Fiber Volume Fraction (V_f %)

The mechanical properties such as strength and modulus of fiber-reinforced polymer composites are mostly affected by the fiber volume fraction (V_f) in the composite structure (Mallick, 2007). Fiber volume fraction strongly depends upon the type of manufacturing process. The strength properties and the quality of the product fabricated by conventional methods are obtained as relatively low when compared to the most developed techniques such as the autoclave curing method. Poor labor skills may also adversely affect the V_f during the stacking of the layers. Although the hand lay-up vacuum bagging method is cost-effective and more suitable for considerably low volume productions, its fiber V_f is relatively low (Carlsson and Kardomateas, 2011).

In this study, V_f of the sandwich panels was determined by using burn off tests. This test was performed in an industrial muffle furnace by burning the facings of the sandwich panels. The burn-off test specimens were obtained from the produced sandwich panels which had been subjected to three-point bending tests. A sample was taken from a sandwich face sheets, and its weight was measured firstly. The core material was removed from the surface of the face sheets. Then the sample was burned in the preheated muffle furnace at a temperature of 600 °C for 60 minutes as suggested in the literature (McDonough et al., 2004). After the process was completed, the sample mass was measured again and the mass of the matrix material was determined experimentally. During the burn-off, the matrix material disappeared and only the fiber elements remained. Then the fiber V_F can be calculated from the Equation (15). In this equation; ρ_m and ρ_f are the density of matrix and fiber materials, respectively; m_f and m_m are mass of the fiber and matrix materials, respectively. However, Equation (3.1) is modified for the sandwiches having hybrid facing such as consisting of wire mesh sheets. For this reason, the wire mesh sheet is considered as a reinforcement material, and its volume fraction can be determined by using Equation (16). In this

case, the effect of wire mesh sheets can be added and hence the results become more accurate.

$$V_f = \frac{{}^{m_f}/_{\rho_f}}{\frac{m_m}{\rho_m} + \frac{m_f}{\rho_f}} \tag{3.1}$$

$$V_T = V_F + V_{WM} + V_M \tag{3.2}$$

3.5. Design of Experiments

In this thesis work, the effects of different parameters on bending characteristics of sandwich structures have been investigated. In order to arrange a large number of tests, and to perform the tests systematically, the design of the experiments tool was applied using software called Design of Expert. In addition, the examinations of the test results were also carried out with the suggested method of design of experiments by constructing suitable models. In this study, the factors and their levels were determined and given in Table 3.7.

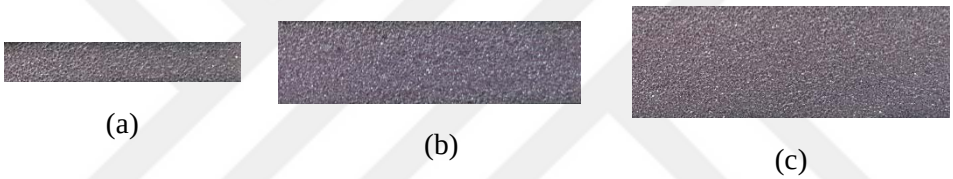
Table 3.7. The parameters and their levels considered in this study

Parameters	**Levels**		
	I	**II**	**III**
Core thickness	10 mm	20 mm	30 mm
Wire mesh sizes	0 (without wire mesh)	100-mesh	200-mesh
Stacking sequence of wire mesh sheets	at core-upper facing interface	Under 1st ply of upper facing	both of level I and II
Span length	150 mm (Short beam)	200 mm (Long beam)	---

In order to analyze the effects of these parameters given in Table 3.7, statistical variance analysis (two-way ANOVA) with the central composite design of experiments was carried out by using Response Surface Methodology (RSM). The individual effects and interactions of independent variable parameters considered during manufacturing were investigated for all the bending characteristics.

3.5.1. Core Thickness

The core thickness effect on flexural characteristics was investigated considering three thickness values, which are 10 mm, 20 mm, and 30 mm as shown in Figure 3.9.



(a) (b) (c)

Figure 3.8. Core material thickness; a) 10 mm, b) 20 mm, c) 30 mm

3.5.2. Wire Mesh Size

In order to investigate the effect of wire mesh sheets on bending characteristics of the sandwich composites, two different wire mesh sizes that are 100 mesh and 200 mesh were used as seen in Figure 3.2. The thickness of these wire mesh sheets has already been given in Section 3.1.4.

3.5.3. Stacking Sequence of Wire Mesh Sheets

In sandwich construction, the effect of layer position of stainless-steel wire mesh sheets to the bending characteristics are going to be investigated considering the following configurations (Figure 3.10) for three different core thicknesses in this work.

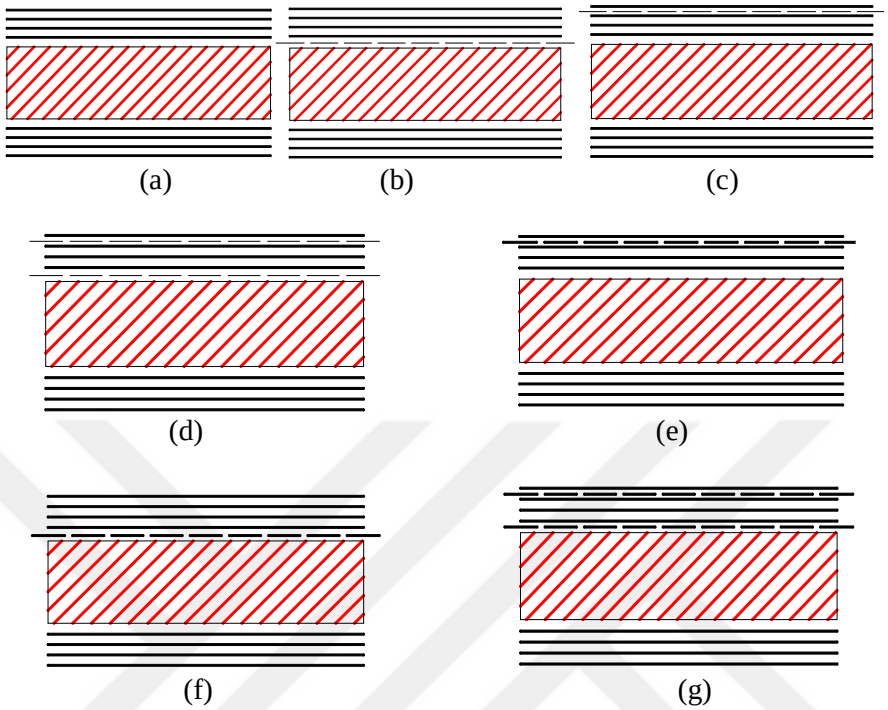


Figure 3.9. Layer position of stainless steel wire mesh sheets; a) without wire mesh, b) 200 mesh at interface, c) 200 mesh under 1st ply, d) combination of b and c, e) 100 mesh under 1st ply, f) 100 mesh at interface, g) combination of e and f

3.5.4. Span Length

The bending characteristics of a sandwich structure are directly affected by the geometry. And, one of the geometrical parameters is the length of span in three-point bending testing between the supports. In this study, the tests were carried out based on two different span length values that are 150 mm for short length and 200 mm for the long length. The short length (200 mm) and the long length beam (250 mm) sandwich panels were fabricated in order to examine the differentiation in failure modes (see Figure 3.11). In addition to this, ASTM D7250 Standard provides an analytical approach that allows determining the flexural stiffness, transverse shear rigidity, and core shear modulus irrespective of facing modulus data in the case of testing sandwich panels in two different (150 and 200 mm) span

lengths. However, the productions were performed progressively. The shorts beam sandwich panels were fabricated firstly for all configurations. Then the fabrications of the long beams were carried out only for the selected configurations. The decisions of the selected configurations were made based on the three-point bending results of the short beam sandwich panels. After investigating the bending behavior of short beam sandwiches, the effective configurations were determined considering the core thickness, stacking sequence of wire mesh sheets, and mesh size.

In this thesis work, the approach provided by ASTM is going to be used and the results are going to be compared with the results obtained by the classical sandwich theory. The schematic views of the sandwich panels are given in Figure 3.11.

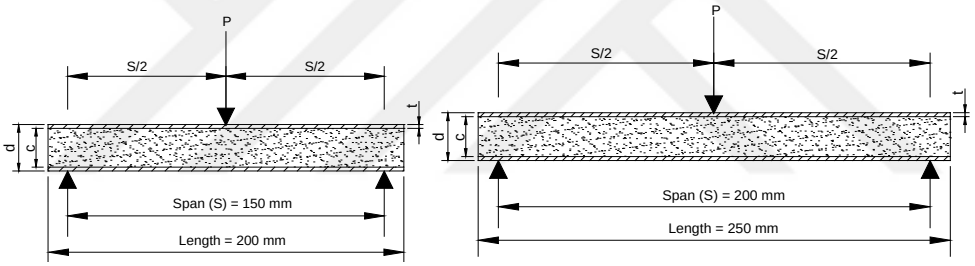


Figure 3.10. Schematic views based on span length, a) 150 mm, b) 200 mm

3.6. Preparation of Test Specimens

Two different mechanical tests were carried out in this thesis work. These are tensile and three-point bending tests. Tensile tests were done to obtain the face sheet properties in terms of tensile stress, tensile strain, and modulus. This is because, in sandwich beam theory, the determination of flexural stiffness of a sandwich panel depends upon the modulus of facing material.

Tensile tests were carried out based on ASTM D3039 Standard whereas three-point bending tests were performed based on ASTM C393, ASTM D7249, and ASTM D7250 standards. The geometries of the specimens have been specified in the corresponding standards. According to the dimensions of the specimens, the

overall composite panel sizes were determined for the production. In Figure 3.12, produced overall composite panel sizes for tensile tests were schematically represented including the specimen dimensions (15x250).

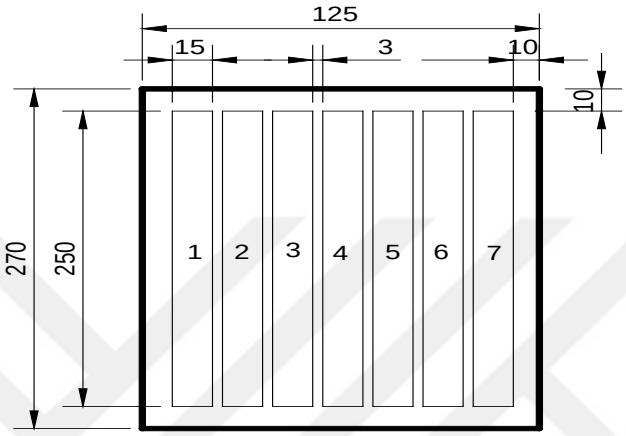


Figure 3.11. Schematic representation of tensile test specimen and composite lamination dimensions

As it is seen from Figure 3.12, the overall composite panel lamination sizes of the productions are 125 mm x 270 mm and the obtained test specimens are 15 mm in width and 250 mm in length according to ASTM D3039 Standard. ASTM standards recommend using at least five specimens to obtain accurate results. Therefore, the seven specimens per each configuration were tested to verify the consistency of test results.

In order to perform the tests accurately, the specimens were tabbed. The tab elements were manufactured from glass/epoxy polymer composites by using an open mold vacuum bagging method. The tabs are used to avoid unexpected failures during tests and they provide better clamping at the fixture of the tensile test machine. The tabs are 56 mm in length as specified in the ASTM standard. They were adhered to the specimens by using an epoxy-based adhesive called Araldite (TDS, Araldite 2015). Figure 3.13 shows the schematic view of the tensile test specimen, the tab formation, and the photo of the produced test specimen.

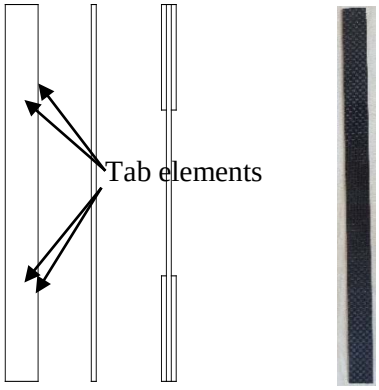


Figure 3.12. a) schematic view of the tensile test specimen (untabbed), b) the tab formation, c) produced test specimen

For three-point bending tests, the sandwich specimens with short and long beams were obtained from the panels having a size of 220 mm x 282 mm and 270 mm x 282 mm, respectively as presented in Figure 3.14. The short beam sandwiches (200 mm length) which have 150 mm span length according to ASTM C393 Standard were obtained from the smaller width panel whereas long beam sandwiches (250 mm length) having 200 mm span length obtained from the larger width panel according to ASTM D7249 Standard. As it is seen from the figure, five specimens were tested for each sandwich configurations.

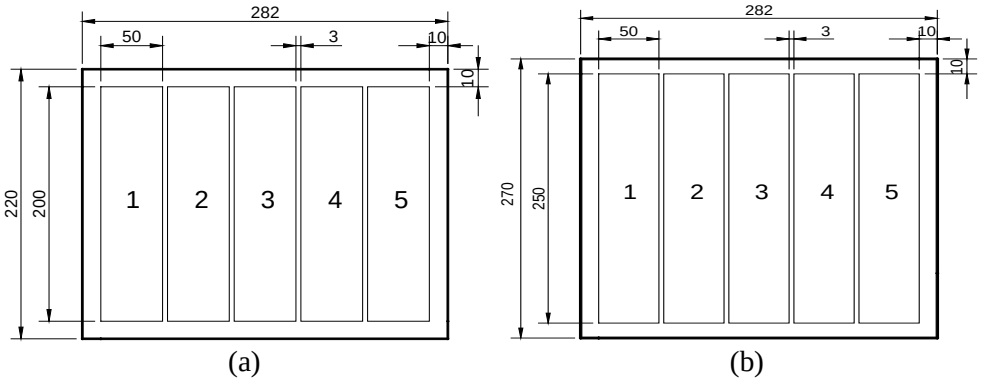


Figure 3.13. Schematic representation of sandwich specimens and their panel dimensions, a) short beam, b) long beam

The sandwich panels produced in this thesis work were defined by the codes considering the experimental parameters. The samples' code of the sandwich panels was presented in Figure 3.15.

For example, the coding of WM.T10.S15 represents sandwich specimens without wire mesh (WM), having 10 mm core thickness (T) and subjected to three-point bending tests at a span (S) length of 150 mm respectively. The method for coding used in this work is provided in Figure 3.15. A sandwich coded by 100M1.T20.S15 includes 100 mesh stainless steel sheet exists under the 1st ply of upper facing, has 20 mm thick foam core and is subjected to bending test at a span length of 150 mm. In another example, 200M3.T30.S20 means the sandwich panels having 200 mesh sheets included both at the core-upper facing interface and under the first ply of upper facing, 30 mm thick core, and its span length is 200 mm during tests (see Figure 3.15).

3.7. Tensile Tests

Tensile tests are required to determine the mechanical properties of the facing materials in terms of tensile strength and modulus, which are necessary to calculate the bending characteristic of the sandwich structures.

Tensile tests were performed according to ASTM D3039 Standard by using 100 kN Instron 8801 universal testing machine at a speed of 2 mm/min. During the tests, a dial gauge indicator was attached to the testing machine (Figure 3.16) to obtain a reference surface. This technique was used to determine the tensile strain of the specimens.

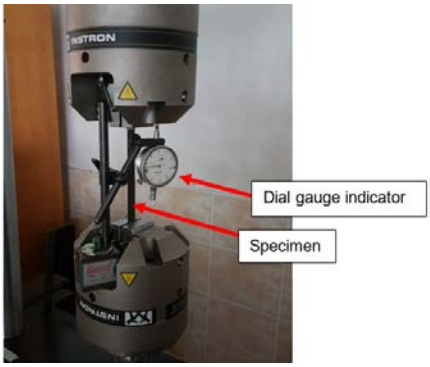
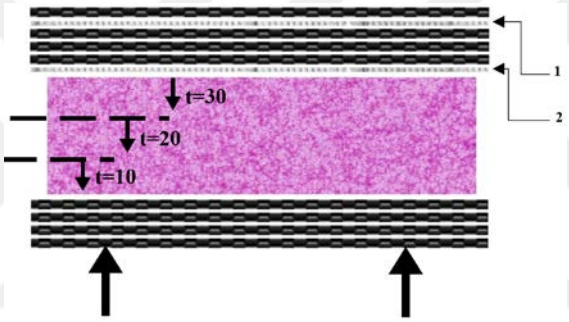
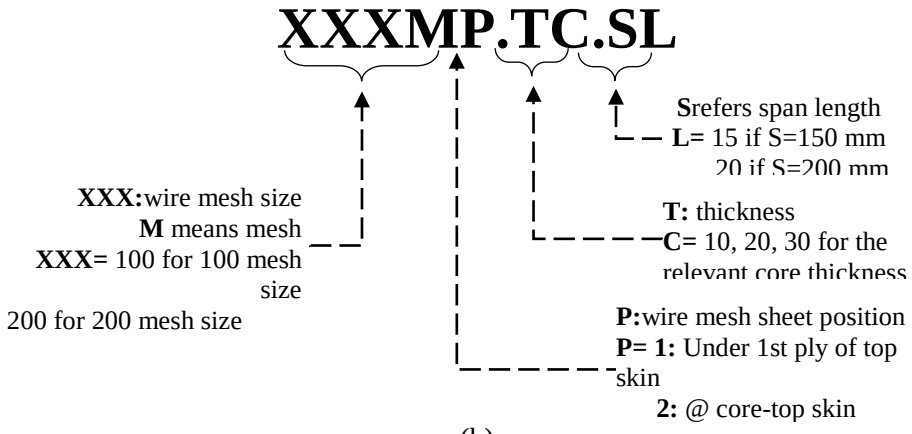


Figure 3.14. Attaching the dial gauge indicator to the tensile testing machine for measuring of strain during the tensile loading



(a)



(b)

Figure 3.15 a) Sandwich panel schematic representation, b) Samples' code system (Note: sandwiches which do not include any wire mesh sheets are named as "WM.TC.SL")

3.8. Three-point Bending Tests

Three-point bending tests were carried out based on ASTM C393, ASTM D7249, and ASTM D7250 standards in order to obtain bending characteristics depending upon the load-carrying capacity of the sandwich composites produced in this work. ASTM C393 provides to determine sandwich core shear properties in terms of core shear ultimate strength, core shear yield stress, and facing stress. ASTM D7249 is related to facing properties of long beam sandwiches. ASTM D7250 is used to determine the flexural and shear stiffness properties of the sandwich structures.

The tests were performed by using 100 kN Shimadzu Autograph (AG IS) universal testing machine and the crosshead speed was set to 2 mm/min. This is because ASTM standards dictate that failure of the structure is desired to develop or occur within three to six minutes. Therefore, after doing several trials the crosshead speed was determined as 2 mm/min. The test set-up was displaced in Figure 3.17.

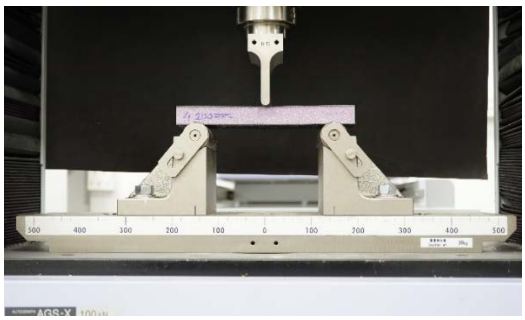


Figure 3.16. Three-point bending test of a short beam sandwich specimen

3.9. Analytical and Experimental Approaches for Bending Characteristics

The flexural characteristics can be evaluated experimentally according to Equations (3.3) to (3.10) provided by ASTM standards. Besides calculating the flexural and shear stiffness values, three-point bending tests also help to calculate core shear stress and compressive strength of the face sheets. Evaluation of these

mechanical properties is necessary in order to determine the failure mode that can be carried out during the test. Core shearing, indentation, and/or face sheet compression failure behaviors can be occurred due to the change of geometrical dimensions of sandwich panels. And they may not occur simultaneously. Therefore, the type of failure mode should be investigated (Carlsson and Kardomateas, 2011).

3.9.1. Core shear ultimate stress (MPa)

$$F_s^{ult} = \frac{P_{max}}{(d+c)b} \quad (3.3)$$

Where;

F_s^{ult} = core shear ultimate stress, MPa,

P_{max}= maximum force, N (before failure),

d = sandwich thickness, mm,

c = core thickness, mm,

b = sandwich width, mm,

3.9.2. Core shear yield stress (MPa)

$$F_s^{yield} = \frac{P_{yield}}{(d+c)b} \quad (3.4)$$

Where;

F_s^{yield} = core shear yield strength, MPa,

P_{yield}= force at 2% offset shear strain, N

3.9.3. Facing stress (MPa)*

$$\sigma = \frac{P_{max}.S}{2t.(d+c).b} \quad (3.5)$$

Where;

σ = facing stress, MPa,

S = span length, mm

t = facing thickness, mm

*: the facing stress is only used when the core shear failures or face-core debonding occurs. Otherwise Equations (3.6) and (3.7) given below are used to find ultimate facing strength.

3.9.4. Facing 1 and facing 2 ultimate stress (MPa)

$$F_1^u = \frac{P_{max}\, S(1-L/S)}{4(d-t_1/2-t_2/2)bt_1} \quad (3.6)$$

$$F_2^u = \frac{P_{max}\, S(1-L/S)}{4(d-t_1/2-t_2/2)bt_2} \quad (3.7)$$

Where;

F_1^u = facing 1 ultimate stress, MPa,

F_2^u = facing 2 ultimate stress, MPa,

t_1 = nominal facing 1 thickness, mm,

t_2 = nominal facing 2 thickness, mm

L= loading span length, mm (L= 0 for three-point bending loading)

3.9.5. Flexural stiffness (N.mm^2)

Flexural stiffness, D (E.I) is a bending characteristic of the sandwich structures that can be defined as the resistance of the structure to deflection under bending loading that exerts as out of the plane. The core material in a sandwich transmits the shear loads and holds the top and bottom facings far away from the neutral axis of the structure to maximize the flexural stiffness (Sharma et al., 2006).

ASTM D 7250 Standard suggests an approach in order to calculate flexural stiffness based on the data obtained from the sandwich panels' force and mid-span displacement curves. Two different configurations are to be considered such as one three-point bending test and one four-point bending test or two different configurations can be selected from three-point bending tests in the case of testing under two different span lengths. Therefore, two different span lengths were considered in this work to obtain configuration #1 and configuration #2.

The data is selected from the linear elastic region of the sandwich bending behavior. Figure 3.18 shows the determination of the nonlinearity offset provided by ASTM. Firstly, a tangent line is drawn to the load-displacement curve of the sandwich structure, and an offset line is created to it. The intersection point of the load-displacement curve and linearity offset becomes yield point; thus, both the force and its corresponding mid-span displacement can be obtained. But, according to the expression given in Equation (3.8), the determination of the nonlinearity offset has to satisfy the expected condition that should not be larger than 10%.

$$\%\text{Offset} = \frac{\text{Displacement @ Pyield} - \text{Linearized displacement}}{\text{Displacement @ Pyield} - \text{Toe correction}} \tag{3.8}$$

$$D = \frac{P_1.{S_1}^3(1-{S_2}^2/{S_1}^2)}{48\Delta_1.(1-P_1.S_1.\Delta_2/P_2.S_2.\Delta_1)} \tag{3.9}$$

Where;

D = flexural stiffness, Nmm^2,

P_1= total applied force, N, for configuration #1

P_2= total applied force, N, for configuration #2

S_1= support span length, mm, for configuration #1

S_2= support span length, mm, for configuration #2

Δ_1 = beam mid-span deflection, mm, for configuration #1 corresponding to P_1

Δ_2 = beam mid-span deflection, mm, for configuration #2 corresponding to P_2

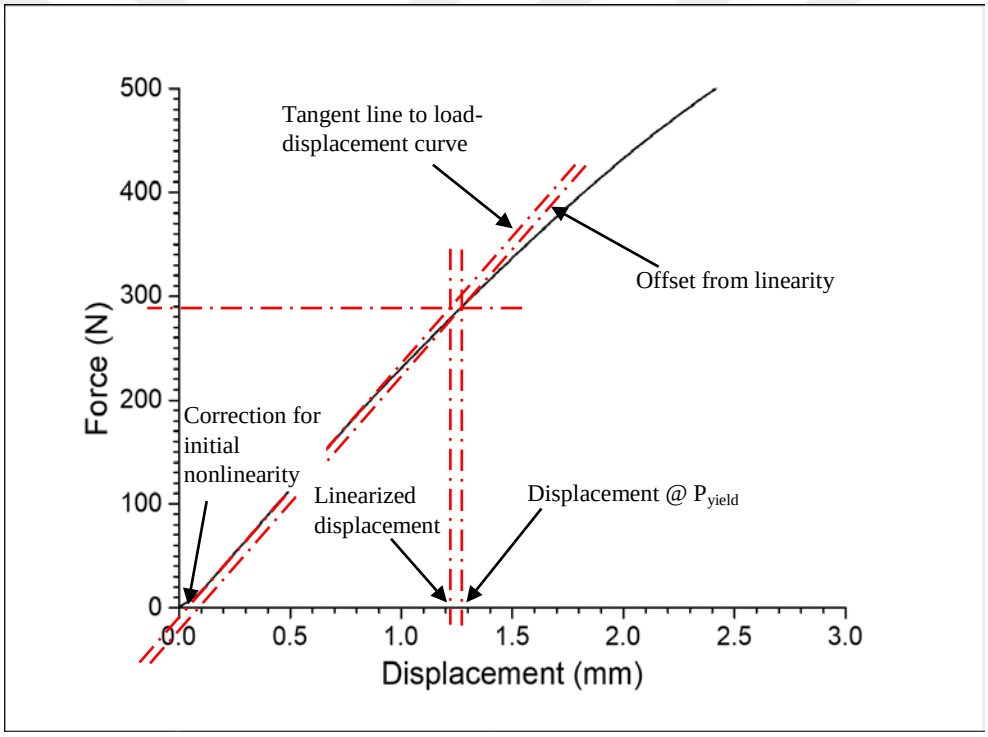


Figure 3.17. Determination of nonlinearity offset

3.9.6. Transverse shear rigidity (N)

While a sandwich beam is subjected to bending loading, transverse shear forces (U), which is given in Equation (3.10), are also developed besides bending moments. This kind of force can fail due to transverse shear stresses referred to as

interlaminar shear stresses and corresponding deflections (Gibson, 2012). In order to ensure that the facings and the core behave as an integrated laminate, the core material must have sufficient transverse shear rigidity (Baker et al., 2004). Using thicker core material does not increase the sandwich weight so much since it has a relatively low density. But if the span length to the face sheet thickness is not high enough, the failures can happen because of the transverse shear effect since the core material has lower shear (G) modulus, which is given in Equation (3.11), as well (Mallick, 2007).

$$U = \frac{P_1.S_1.(S_1{}^2/S_2{}^2-1)}{4\Delta_1.\left((P_1.S_1{}^3.\Delta_2/P_2.S_2{}^3.\Delta_1)-1\right)} \quad (3.10)$$

Where;

U= transverse shear rigidity, N

3.9.7. Core shear modulus (MPa)

$$G = \frac{U.(d-2t)}{(d-t)^2.b} \quad (3.11)$$

Where;

G= core shear modulus, MPa

According to the approaches provided above, analytic determination of the flexural stiffness and the transverse shear rigidity requires tests to perform in two different configurations in terms of different span lengths such as 150 mm and 200 mm.

In the case of using analytical sandwich beam theory, Equations (3.12) to (3.16) are provided in the literature for flexural characteristics of the sandwich composites under three-point bending loadings. The flexural stiffness that can be obtained by the sandwich beam theory has already been given in the previous sections. Contrary to the experimental approach provided by ASTM standards,

flexural stiffness depends upon the facings and the core materials' modulus data and sandwich geometry whereas ASTM standard requires to perform tests in two different configurations having different span lengths.

Based on the analytical sandwich beam theory:

3.9.8. Bending strength of the core

$$\sigma_{max} = E_c \frac{M_{max} c}{2(EI)} \quad (3.12)$$

Where;

σ_{max} = bending strength of the core, MPa,

$M_{max} = P_{max}.S/4$, Nmm,

E_c = core Young's modulus

(EI) = equivalent flexural rigidity that is the same as "D" in the ASTM approach.

3.9.9. The maximum stress in the face sheets of sandwich panels

$$\left(\sigma_f\right)_{max} = E_f \frac{M_{max}(c+2t)}{2(EI)} \quad (3.13)$$

Where;

c and t are the core and the facing thicknesses, respectively

$\left(\sigma_f\right)_{max}$ = face sheet maximum stress, MPa,

E_f = face sheet Young's modulus, GPa

3.9.10. Core shear stress

$$\tau_{xy} = \frac{-\mathrm{P}}{2\mathrm{b}h_c} \quad (3.14)$$

Where P is the bending force, b and h_c are the sandwich specimen width and the core thickness, respectively. τ_{xy} is the core shear stress. It is assumed that the core carries the shear forces (Carlsson and Kardomateas, 2011).

3.9.11. Maximum bending stress of face sheet

$$(\sigma_x)_{max} = \frac{P.L}{4b.(h_f+h_c).h_f} \quad (3.15)$$

$(\sigma_x)_{max}$ and τ_{xy} can be rated as given in Equation (3.16) for determining the sandwich geometry where a transition in the failure mode takes place either from core shear to face sheet compression or vice versa (Carlsson and Kardomateas, 2011).

$$\frac{(\sigma_x)_{max}}{\tau_{xy}} = \frac{L}{2h_f(1+h_f/h_c)} \quad (3.16)$$

Sandwich structures particularly having foam core and fiber-reinforced composite face sheets are mainly designed to carry bending loads due to their very high strength to weight ratio. Therefore, the evaluation of the optimum bending stiffness depends on mostly core density and sandwich geometry. Carlsson andKardomateas (2011) provided an analytical expression to show the relationship between weight and geometry of a sandwich panel to obtain optimum bending stiffness as given in Equation (3.17).

$$\frac{W}{bl} = 2h_f\rho_f + h_c\rho_c \quad (3.17)$$

Where W is the sandwich weight, b and l are the sandwich width and length, respectively. h_f and h_c are the facings and the core thicknesses, respectively, and ρ_f and ρ_c are the density of face sheet and core materials, respectively.

Although relatively thicker facing sandwiches carry larger amounts of load, it is recommended that designing a sandwich having thin and high modulus face sheets with low-density core material is desired because of obtaining high bending stiffness from a lightweight sandwich (Carlsson and Kardomateas, 2011).

3.10. Examination of the Failure Modes

The failure modes and the collapse force that predicts maximum bending loading before failure should be examined according to sandwich design principles after subjecting the specimens to three-point bending tests. This examination is essential to determine the behavior of sandwich structures under a particular loading. It also helps the designer to select more suitable constituent materials and geometry for the further sandwich constructions. For instance, by comparing the strength of the materials with their stress values in terms of shear stress and facing compressive stress, the proper geometry can be determined for the desired failure mode. The commonly seen failure modes are due to core shear, face sheet fractures due to compressive forces, face wrinkling, and indentation. In this study, failure modes of the sandwiches after three-point bending tests were investigated and primary failure modes were addressed.

4. RESULTS AND DISCUSSION

4.1. Fiber Volume Fractions of the Sandwich Panels

Burn off tests were carried out to facings of sandwich panels to determine fiber volume fraction (V_f) values as mechanical properties of composite materials are strongly affected by their V_f. Table 4.1 presents measurement results, determination of matrix, fiber and wire mesh sheet weights, and percent volume fractions of fiber and wire mesh layers (V_F% and V_{WM}%). In the table, volume fractions are calculated only for short span length sandwiches since the long span sandwich panels have the same results.

Table 4.1. Fiber and wire mesh volume fractions (V_F% and V_{WM}%) of the produced sandwich panels

Sandwich Panels	**Sandwich Sample Mass (g)**				**V_F %**	**V_{WM} %**	**V_F + V_{WM} (%)**
	Face sheets (Before burn-off)	Carbon fiber (After burn off)	Matrix	Wire mesh			
WM.T10.S15	7,0423	4,3515	2,6908	0	51,8	0,0	51,8
100M1.T10.S15	12,465	6,1327	4,388	1,944	46,6	3,3	49,9
100M2.T10.S15	11,702	6,4712	4,072	1,946	49,7	3,3	53,0
100M3.T10.S15	14,8355	6,1194	4,8488	3,867	42,9	6,1	48,9
200M1.T10.S15	10,8177	5,9002	3,9122	1,005	49,1	1,9	51,0
200M2.T10.S15	11,1167	6,1248	3,9588	1,033	49,8	1,9	51,6
200M3.T10.S15	13,26	6,1658	5,11	2,046	43,1	3,2	46,3
WM.T20.S15	10,0221	5,9456	4,0765	0	49,2	0,0	49,2
100M1.T20.S15	9,7986	4,945	3,3651	1,489	47,8	3,2	51,0
100M2.T20.S15	10,2222	5,0459	3,6406	1,536	46,4	3,2	49,6
100M3.T20.S15	11,6399	5,0512	3,5755	3,013	45,5	6,1	51,6
200M1.T20.S15	8,694	5,0338	2,8555	0,805	52,9	1,9	54,8
200M2.T20.S15	7,9057	4,0831	3,1013	0,721	45,8	1,8	47,6
200M3.T20.S15	9,919	4,8569	3,4684	1,594	46,6	3,4	50,0
WM.T30.S15	5,4224	3,292	2,1304	0	50,7	0,0	50,7
100M1.T30.S15	11,9776	5,7061	4,4207	1,841	44,7	3,2	47,9
100M2.T30.S15	12,3913	6,4709	4,0025	1,918	50,1	3,3	53,4
100M3.T30.S15	14,2058	5,9807	4,4205	3,805	44,4	6,3	50,7
200M1.T30.S15	11,6291	6,0936	4,5116	1,024	46,5	1,7	48,2
200M2.T30.S15	10,9079	6,0815	3,8502	0,976	50,3	1,8	52,1
200M3.T30.S15	8,3729	6,1339	4,5129	2,103	45,8	3,5	49,3

4.2. Thickness and Weight of the Sandwich Panels

The produced sandwich panels were measured to determine their thickness and weight. This is made in order to show the consistency of the productions thus, the results of the tests can be better evaluated. Table 4.2 presents the average values of the measurement results for each configuration sample. The standard deviations (std) are also given in Table 4.2 in parenthesis with "std". the difference between the standard deviation values are due to the manufacturing conditions. As mentioned in the previous chapters, each panel has five specimens.

Table 4.2. Average values of thickness (mm) and weight (g) measurements

Sandwich code	Average Thickness (mm)(std)	Average Weight (g) (std)	Sandwich code	Average Thickness (mm) (std)	Average Weight (g) (std)
WM.T10.S15	11,05 (0,06)	29,41 (0,23)	WM.T30.S15	31,33 (0,03)	38,70 (0,27)
100M1.T10.S15	11,17 (0,02)	34,98 (0,27)	100M1.T30.S15	31,50 (0,04)	46,13 (0,27)
100M2.T10.S15	11,25 (0,03)	36,08 (0,29)	100M2.T30.S15	31,49 (0,04)	45,59 (0,17)
100M3.T10.S15	11,30 (0,04)	41,33 (0,21)	100M3.T30.S15	31,55 (0,05)	49,46 (0,16)
200M1.T10.S15	11,10 (0,01)	32,94 (0,24)	200M1.T30.S15	31,42 (0,07)	42,88 (0,36)
200M2.T10.S15	11,11 (0,02)	32,59 (0,26)	200M2.T30.S15	31,48 (0,02)	42,72 (0,18)
200M3.T10.S15	11,30 (0,04)	37,94 (0,20)	200M3.T30.S15	31,51 (0,02)	45,21 (0,39)
WM.T20.S15	21,03 (0,03)	34,45 (0,31)	WM.T10.S20	11,10 (0,04)	38,21 (0,28)
100M1.T20.S15	21,21 (0,04)	40,36 (0,16)	100M1.T10.S20	11,22 (0,03)	45,17 (0,36)
100M2.T20.S15	21,30 (0,02)	40,94 (0,23)	200M1.T10.S20	11,14 (0,04)	41,68 (0,21)
100M3.T20.S15	21,49 (0,01)	45,52 (0,31)	WM.T20.S20	21,10 (0,09)	45,94 (0,69)
200M1.T20.S15	21,35 (0,03)	36,34 (0,50)	100M1.T20.S20	21,24 (0,08)	52,16 (0,21)
200M2.T20.S15	21,35 (0,07)	36,95 (0,22)	WM.T30.S20	31,36 (0,05)	49,59 (0,31)
200M3.T20.S15	21,5 (0,05)	40,41 (0,17)	100M1.T30.S20	31,53 (0,08)	56,14 (0,23)

4.3. Tensile Test Results

Tensile tests were performed to obtain mechanical properties of the sandwich face sheets. This is because the results of the tensile tests are going to be used to evaluate the flexural characteristics of the sandwiches.

As it was presented in the previous chapter seven different configurations exist for sandwich face sheets consisting of four layers of woven plain carbon fiber fabrics with and without stainless steel wire mesh sheets. These are without wire mesh sheet (WM), 100M1, and 200M1 (wire mesh layer under the first carbon fiber fabric layer of top facing), with a size of 100M2 and 200M2 (wire mesh layer between top facing and foam core interface). And combinations of M1 and M2 configurations (100M3 and 200M3) are produced. The seven configurations were subjected to tensile tests at a crosshead speed of 2 mm/min as recommended by ASTM D3039 Standard. Figures 4.1-4.7 show the load-extension curves that are plotted on a graph with load measured on the vertical axis and extension on the horizontal axis by using the raw data provided by the tensile test software. As seen from the figures, each configuration was tested with five replications to satisfy the consistency of the results.

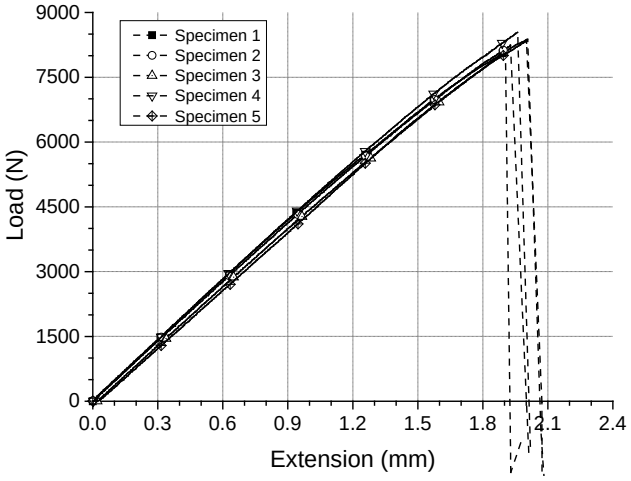


Figure 4.1. Load-extension curves of WM face sheets

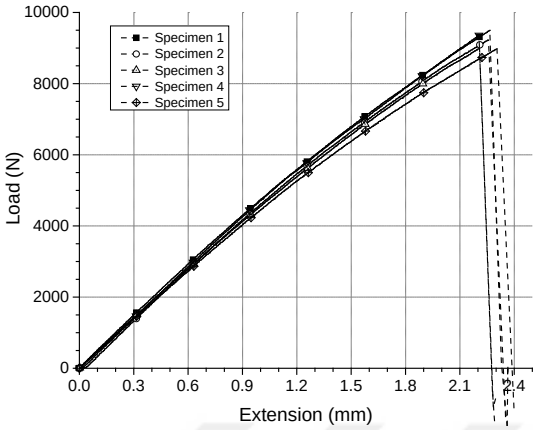


Figure 4.2. Load-extension curves of 100M1 face sheets

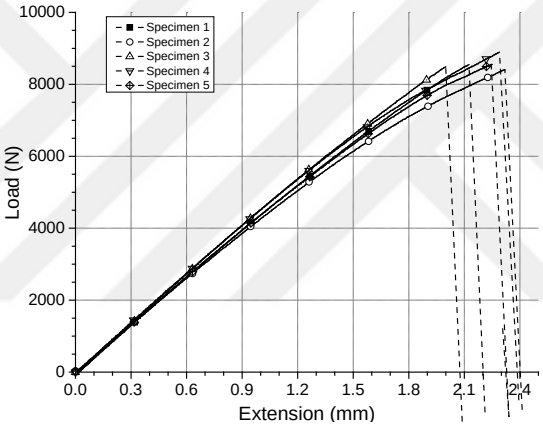


Figure 4.3. Load-extension curves of 100M2 face sheets

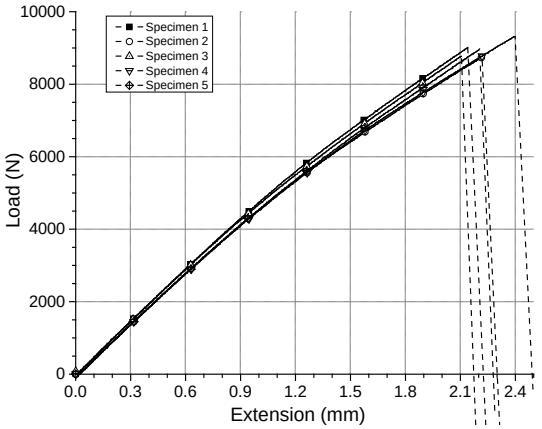


Figure 4.4. Load-extension curves of 100M3 face sheets

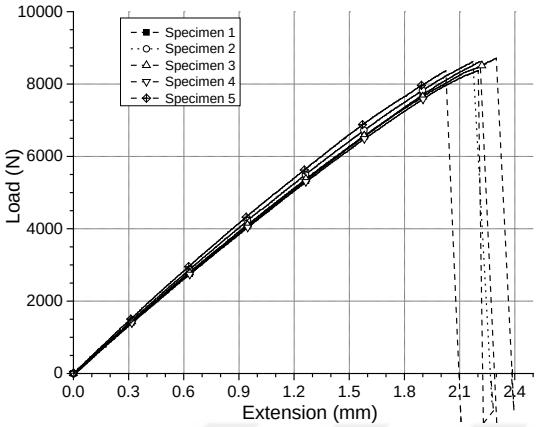


Figure 4.5. Load-extension curves of 200M1 face sheets

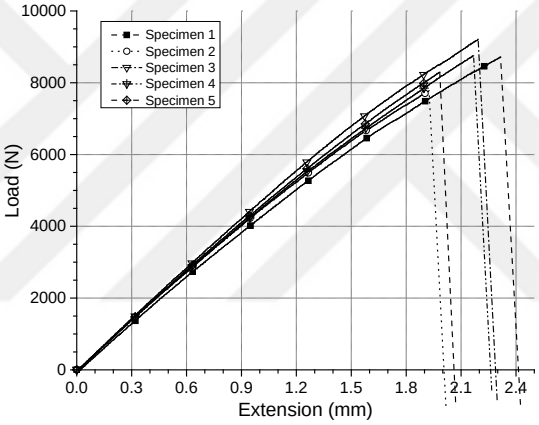


Figure 4.6. Load-extension curves of 200M2 face sheets

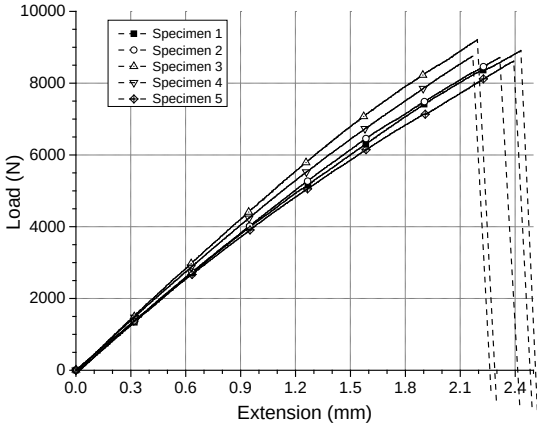


Figure 4.7. Load-extension curves of 200M3 face sheets

The maximum tensile load carrying capacities were determined for each of the face sheet configurations from the load-extension curves of the specimens. The results are given in Tables 4.3-4.4 based on the wire mesh size. The standard deviations are written below the load in parenthesis.

Table 4.3. Maximum load-carrying capacities of face sheets with 100-mesh and without wire mesh sheet

Face Sheet Configuration	**WM**	**100M1**	**100M2**	**100M3**
Maximum Load, N (std. dev.)	8313,97 (158,86)	9208,42 (203,19)	8578,67 (165,98)	8964,26 (203,66)

Table 4.4. Maximum load-carrying capacities of face sheets with 200-mesh and without wire mesh sheet

Face Sheet Configuration	**WM**	**200M1**	**200M2**	**200M3**
Maximum Load, N (std. dev.)	8313,97 (158,86)	8538,03 (142,39)	8550,20 (483,45)	8842,29 (207,86)

The face sheets without any wire mesh sheets can carry approximately 8,3 kN tensile load. However, in the case of using stainless steel wire mesh sheets, the load-carrying capacities were improved. For instance, 100M1 configuration, which has a 100-mesh wire sheet under the first carbon fiber fabric layer of composite facing, increased the tensile load by 10,76% whereas 200M1 configuration carried 2,7% higher tensile load when compared to WM face sheet.

After obtaining the load-extension curves, the ultimate tensile stresses and strains of each configuration were calculated according to the ratio of axial tensile load to the cross-sectional area of the facing materials. Each configuration is 15 mm wide identically but their thicknesses slightly vary due to the nature of the sandwich manufacturing process. The thicknesses were measured using a micrometer, and mean values of the results were recorded as follows: WM= 0,82 mm; 100M1= 0,90 mm; 100M2= 0,91 mm; 100M3= 1,06 mm; 200M1= 0,87mm; 200M2= 0,89mm; 200M3= 1,01 mm. The variations in measurements have been

caused by the size and the number of wire mesh sheets and stacking configurations during manufacturing. In order to determine the strain values, a dial gauge indicator was used as presented in the previous chapter. The ultimate stresses were calculated using the data corresponding to each configuration, and stress-strain values were plotted as given in Figures 4.8-4.14.

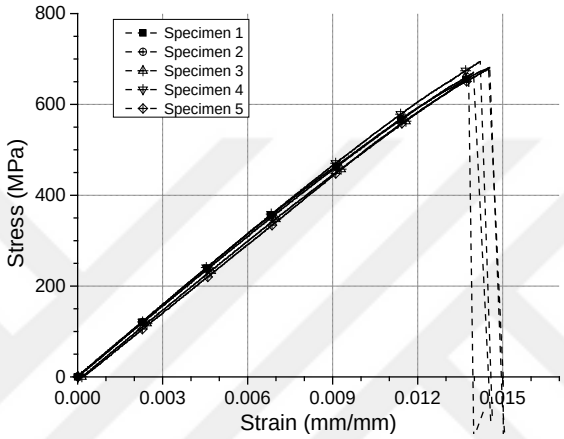


Figure 4.8. Stress-strain curves of WM face sheets

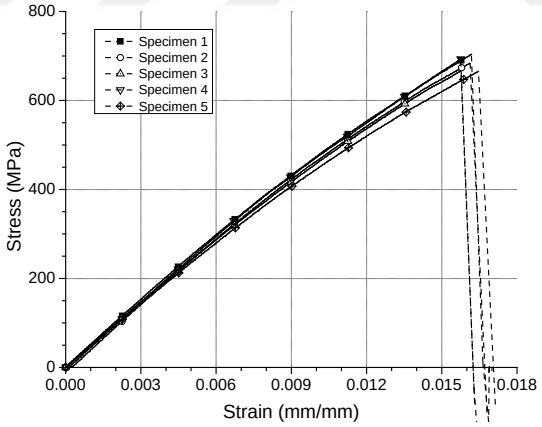


Figure 4.9. Stress-strain curves of 100M1 face sheets

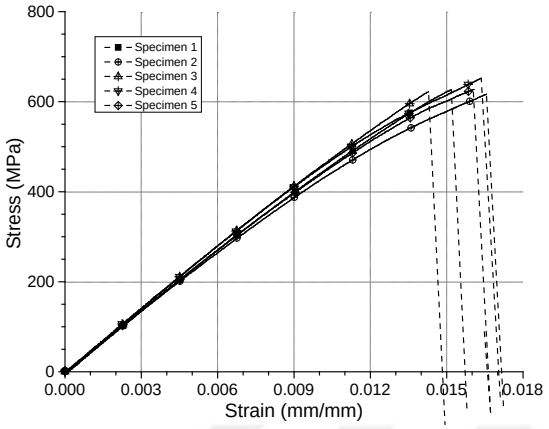


Figure 4.10. Stress-strain curves of 100M2 face sheets

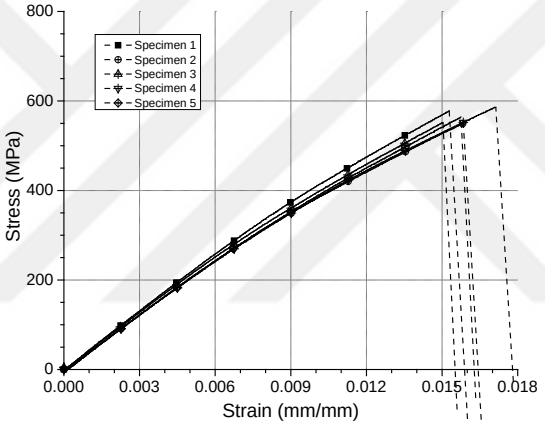


Figure 4.11. Stress-strain curves of 100M3 face sheets

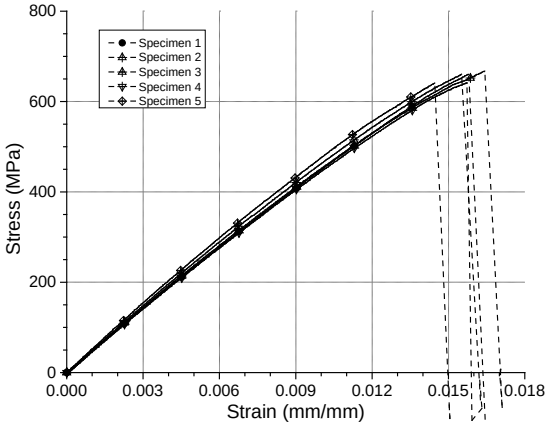


Figure 4.12. Stress-strain curves of 200M1 face sheets

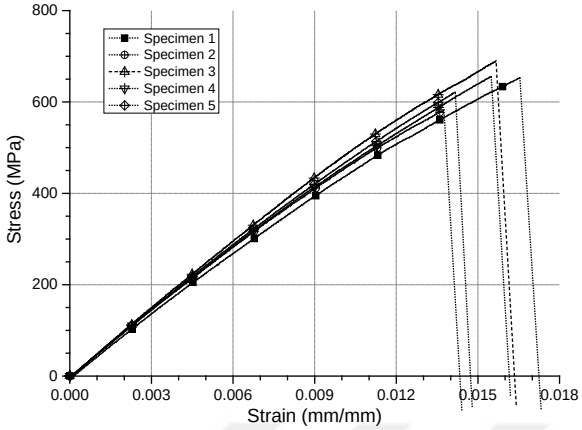


Figure 4.13. Stress-strain curves of 200M2 face sheets

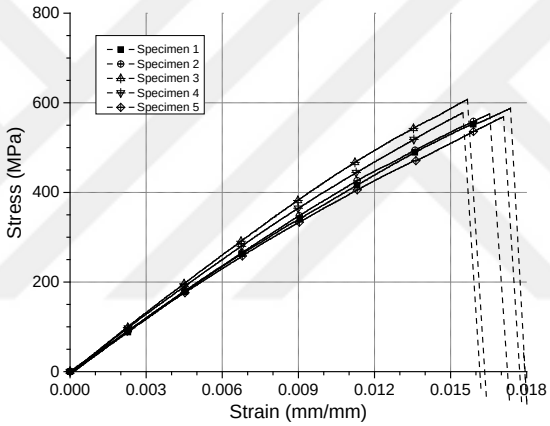


Figure 4.14. Stress-strain curves of 200M3 face sheets

According to the stress-strain data, the maximum tensile strength values were determined for each of the facing configurations. In addition, the tensile modulus of elasticity of the materials was calculated based on the linear elastic range of the stress-strain data. Tables 4.5 and 4.6 show the average values of both the maximum tensile strength and tensile modulus of the facings depending upon the wire mesh size. The standard deviations were also given in parenthesis under the strength and modulus data, respectively.

The pure carbon fiber face sheet (WM), which does not include any wire mesh sheet, has a tensile strength of 675,93 MPa. Although wire mesh sheets have

significantly contributed to the tensile load carrying capacities of the facing materials, the contribution to the tensile strength for most of the configurations was lower. Only the configurations of 100M1 increased the tensile strength of the facing materials. And 200M1 and 200M2 yielded very close results to WM configuration. The findings provided that the rest of the configurations have lower tensile strength due to an increased cross-sectional area of the face sheets and increased strain rates. The load-carrying capacities and tensile strength results are illustrated comparatively in Figure 4.15 according to the face sheet configurations.

The tensile modulus of the facing materials was calculated based on the linear elastic range of stress-strain curve according to the ratio of tensile stress to strain value. For WM facing, the tensile modulus was obtained as 50,75 GPa. In the case of using 200-mesh wire sheets (200M1, 200M2, and 200M3), the results were approximately equal and/or lower than WM configurations. However, 100M1 yielded a larger modulus. This is because the face sheet configurations having a wire mesh size of 200 and the configurations of 100M2 and 100M3 resulted in higher strain rates than WM facings. Although 100M1 sandwiches resulted in higher strain rates than WM facings, their load carrying capacities were considerably found larger than others (see Figure 4.15). According to the literature (Swolfs, Gorbatikh, and Verpoest, 2014), hybridization is primarily made to increase failure strain instead of strength and stiffness properties. This objective is achieved due to the bridging effect. When the carbon fibers started to break, the wire mesh sheet played a major role between the fibers by retarding the crack growth. The face sheet configuration of M1 provided better results than M2. Because the wire mesh sheet was stacked between fiber fabrics in the case of M1, whilst it was stacked at the outermost side of the carbon fiber facings in the case of M2, which was bonded to the core material of the sandwich later. For this reason, the tensile properties of M1 are obtained higher than those of M2 and M3. Nevertheless, as the wire thickness of the 200-mesh sheet is half of the 100-mesh, 200M1 configuration did not exhibit such high results as 100M1.

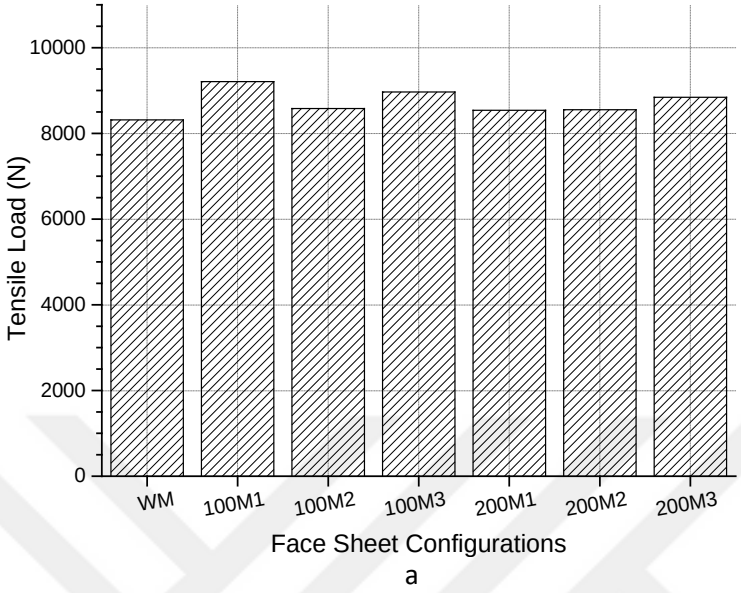
The obtained stress-strain data and tensile modulus of the face sheet configurations are going to be used for the evaluation of the flexural characteristics of sandwich panels.

Table 4.5. Tensile strength and tensile modulus of the facings with 100-mesh and without wire mesh sheet

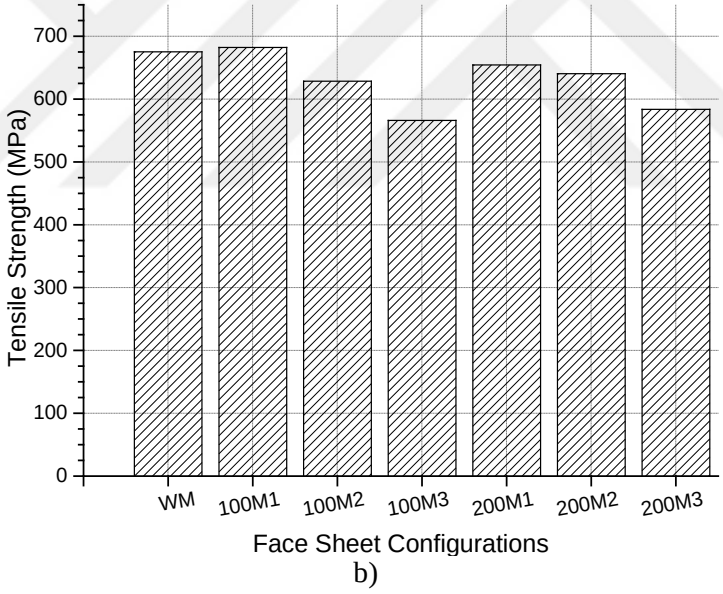
Face Sheet Configuration	WM	100M1	100M2	100M3
Tensile Strength, MPa	675,93	682,11	628,47	565,97
(std. dev.)	(12,91)	(15,15)	(12,16)	(14,02)
Tensile Modulus, GPa	50,75	52,00	46,24	41,90
(std. dev.)	(0,84)	(0,82)	(0,95)	(1,24)

Table 4.6. Tensile strength and modulus of the facings with 200-mesh and without wire mesh sheet

Face Sheet Configuration	WM	200M1	200M2	200M3
Tensile Strength, MPa	675,93	654,26	640,46	583,65
(std. dev.)	(12,91)	(10,91)	(36,21)	(13,72)
Tensile Modulus, GPa	50,75	49,22	47,95	42,49
(std. dev.)	(0,84)	(1,06)	(1,77)	(1,26)



a



b)

Figure 4.15. a) Maximum tensile load of the facings b) Maximum tensile strength of the facings

4.4. Three-point Bending Test Results of Short-span Sandwich Beams

Quasi-static three-point bending tests, performed at 2 mm/min crosshead speed, provided load and mid-span deflection data for all configurations, the results are given in this section. The results were presented by plotting on a graph with a load against deflection curves depending upon the sandwich core thickness values. Each test was performed using five replications.

4.4.1. Load-Deflection Curves of 10 mm Thick Core Sandwich Panels

Load-deflection curves of the sandwich composites under three-point bending tests having 10 mm foam core were given individually according to each sandwich code. Five specimens were shown in Figures 4.16 to 4.22 for each of the configurations tested at a span length of 150 mm.

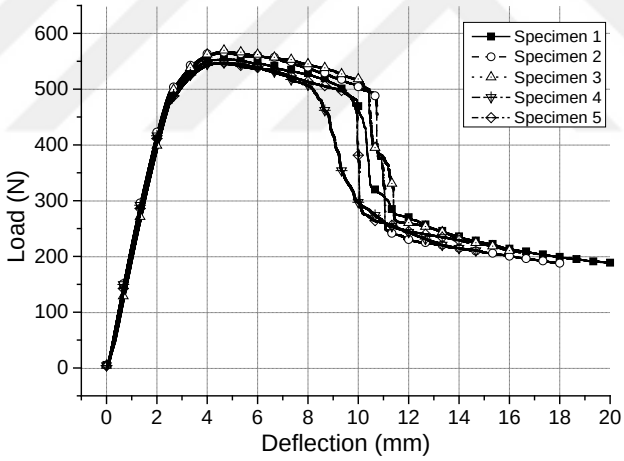


Figure 4.16. Load – deflection curves WM.T10.S15 sandwich specimens

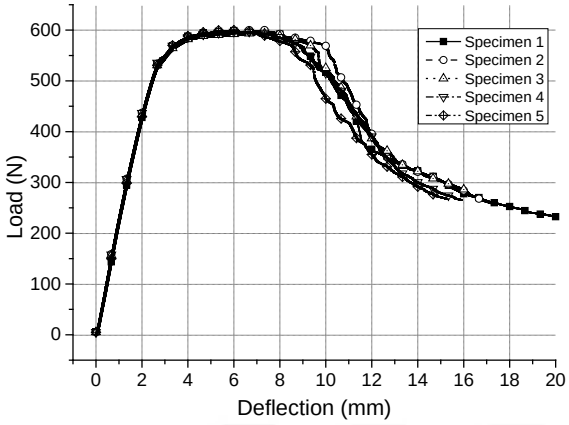


Figure 4.17. Load – deflection curves 100M1.T10.S15 sandwich specimens

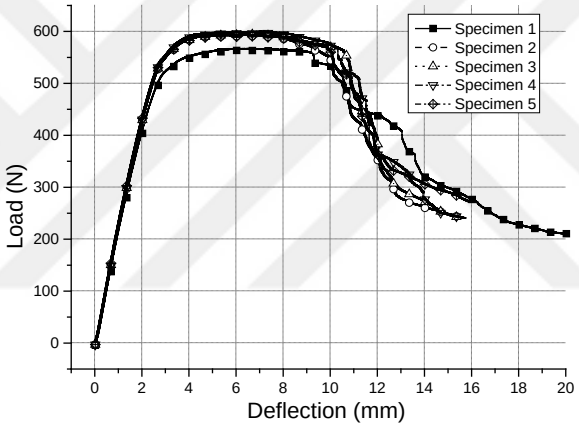


Figure 4.18. Load – deflection curves 200M1.T10.S15 sandwich specimens

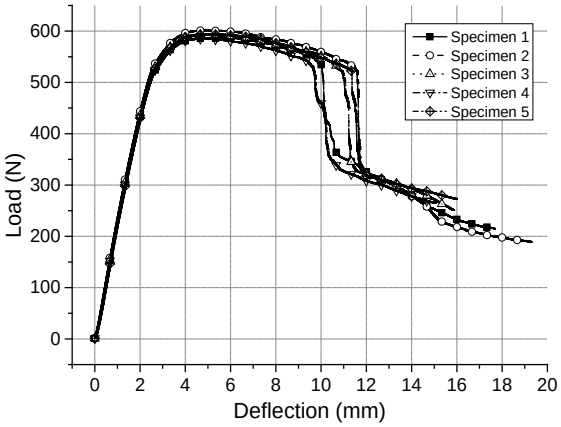


Figure 4.19. Load – deflection curves 100M2.T10.S15 sandwich specimens

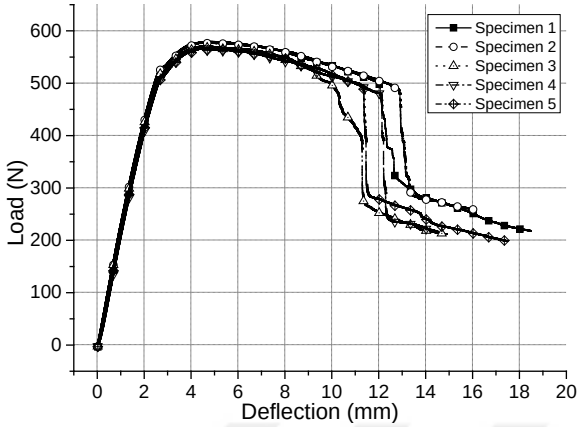


Figure 4.20. Load – deflection curves 200M2.T10.S15 sandwich specimens

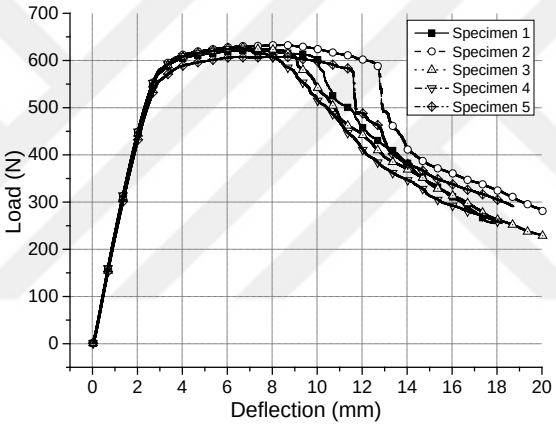


Figure 4.21. Load – deflection curves 100M3.T10.S15 sandwich specimens

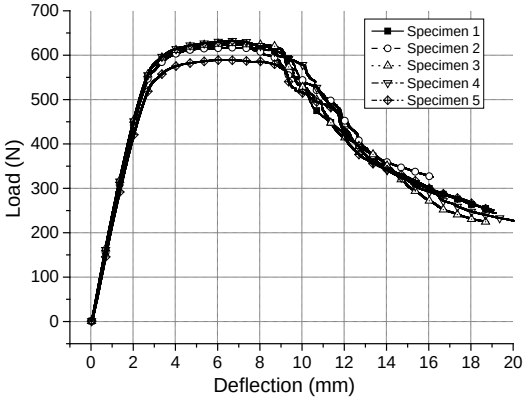


Figure 4.22. Load – deflection curves 200M3.T10.S15 sandwich specimens

As it is seen from the figures above, the results for five replications in each plot are seen to be consistent with each other. This may also indicate the proper and consistent production of specimens. The load-deflection curve of WM sandwich panel, which is given in Figure 4.16, has firstly shown a linear increase in slope up to 450 N, then the slope continued with a nonlinear and gradual increase up to a maximum point of 540 N. After the maximum load was reached, the force is decreased slowly from a mid-span displacement of ~4 mm to ~10mm. At this interval fibers and matrix failures are initiated. But the load is carried by the upper face sheet, and core crushing occurs between the facings. Lastly, a sudden drop in force is observed due to upper face sheet compressive failure at a mid-span deflection of ~10 mm. On the other hand, in the case of using either 100-mesh or 200-mesh wire sheets, sandwich panels carried a larger amount of bending load when compared to WM sandwich panels. Table 4.7 shows the average values of the maximum bending load carrying capacities (P_{max}) of the sandwich panels and corresponding mid-span (MS) deflection values according to the sandwich panel code system of the work. The standard deviations are presented in parenthesis.

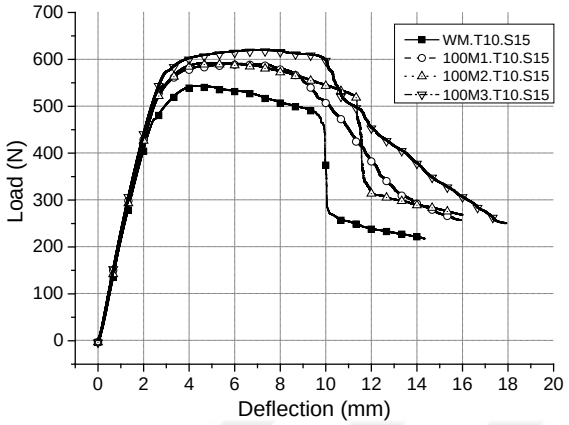
Table 4.7. Maximum load-carrying capacities and MS deflection of the sandwich panels

Sandwich panel code	Maximum Load and Corresponding Mid-span (MS) Deflection	
	P_{max} (N) (std)	MS Displacement (mm)
WM.T10.S15	554,36 (8,76)	4,613
100M1.T10.S15	594,56 (2,40)	6,540
100M2.T10.S15	592,52 (5,75)	5,001
100M3.T10.S15	623,61 (8,49)	7,379
200M1.T10.S15	592,14 (11,87)	6,591
200M2.T10.S15	573,60 (5,49)	4,659
200M3.T10.S15	618,42 (15,34)	6,768

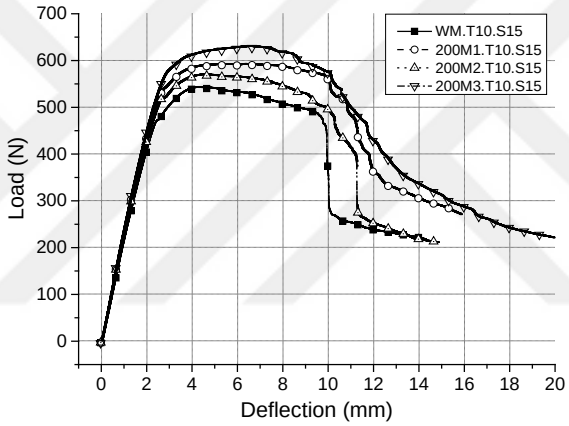
In addition to increased bending force, the type of wire mesh sheet has also positively affected the sandwich behavior under three-point bending loadings. In

the first stage, a higher linear increase in slope is seen. And, the distance between the end of the linear increase and the maximum point of the bending force is very close when compared to WM sandwich panels. After the maximum point is reached, contrarily to WM specimens, the existence of wire mesh sheets provided constant load carrying capacity with a larger plateau in between ~4 mm to ~10 mm deflection interval. Figures 4.17 to 4.22 also show that the facings having a wire mesh layer provided higher resistance to the bending force. It also prevented a sudden drop of bending force as it was the case for without mesh (WM) sandwiches. Contrary to WM sandwich panels, the meshed type failed with a gradual decreased bending force slope instead of a sudden one. While both of the mesh sizes of 100 and 200 provided increased bending stiffness, the 100 mesh wire sheets were found better. Using two layers of 100 and/or 200-mesh sizes wire sheets at the upper facing-core interface, and under the first ply of upper facing are the most effective configurations among the 10 mm thick foam core sandwiches when considering the bending load capacities (Figures 4.21-4.22). Secondly, using wire mesh sheets under the first ply of upper facing is found to be more effective than using at the facing-core interface especially in the case of using 200-mesh size.

From each of the corresponding figures given above, a quasi-average estimation of force-deflection curves were obtained for WM, 100-mesh, and 200-mesh sizes. Although five specimens were tested for each configuration, one curve, which is the closest curve to the average, was selected for the comparison, as this is the representative one and recommended by Sadeghian et al. (2018). Figure 4.23 compares quasi-average values of the test results without and with wire mesh sheets. Figure 4.23 (a) provides the comparison between WM and 100-mesh sizes, whilst Figure 4.23 (b) compares WM and 200-mesh sized sandwich specimens.



(a)



(b)

Figure 4.23. Comparison of the 10 mm thick foam core sandwiches with and without wire mesh; a) WM and 100-mesh, b) WM and 200-mesh

In order to see the effect of wire mesh sheets on the bending behavior of sandwich structures more clearly, it is better to compare the load-carrying capacities of the sandwich panels at a particular mid-span deflection value where the force suddenly drops for the WM sandwiches. The sudden failure for WM sandwich panels happened at an approximate mid-span deflection of 10 mm. Table 4.8 shows the maximum load-carrying capacities of sandwich panels and the load-carrying capacities at an approximate MS deflection of 10 mm comparatively. And Figure 4.24 reveals the significant effect of wire mesh sheets during the failure of

sandwich panels by displaying the difference between maximum bending load and the bending load at 10 mm mid-span deflection where the WM sandwich failed due to sudden drop in the bending force. As seen in Table 4.8, due to the drop in bending force, the load-carrying capacity was decreased by 44,67%. On the other hand, the reduction in bending load capacities of sandwich panels having wire mesh sheets was obtained very small compared to WM sandwich panels at the same deflection value. The wire mesh sheets do not only prevent sudden drops in bending force but also enabled them to carry higher loads for a particular deflection even after the failure. Because, when a sudden failure occurred for WM sandwiches, the panels having wire mesh sheets still carried a larger amount of bending force, and the reduction in force occurred very slowly with the downward slope of the longer displacements. Moreover, high load carrying capacities were obtained with very small weight penalties. For instance, although 200M1.T10.S15 sandwich panel has a 12% higher weight than the WM.T10.S15 sandwich, it carried 85,75% more bending load.

Table 4.8. Load-carrying capacities of sandwich panels after 10 mm thick core WM sandwiches underwent to sudden failure at MS deflection of ~10 mm

Sandwich Configurations	Maximum Load (N)	Load (N) at ~10,0 mm MS Deflection	Percent (%) Reduction in Bending Load
Without wire mesh (WM)	554,36	306,73	44,67
100M1	594,56	527,53	11,27
100M2	592,52	501,59	15,35
100M3	623,61	607,08	2,65
200M1	592,14	569,76	3,78
200M2	573,60	512,89	10,58
200M3	618,42	585,61	5,31

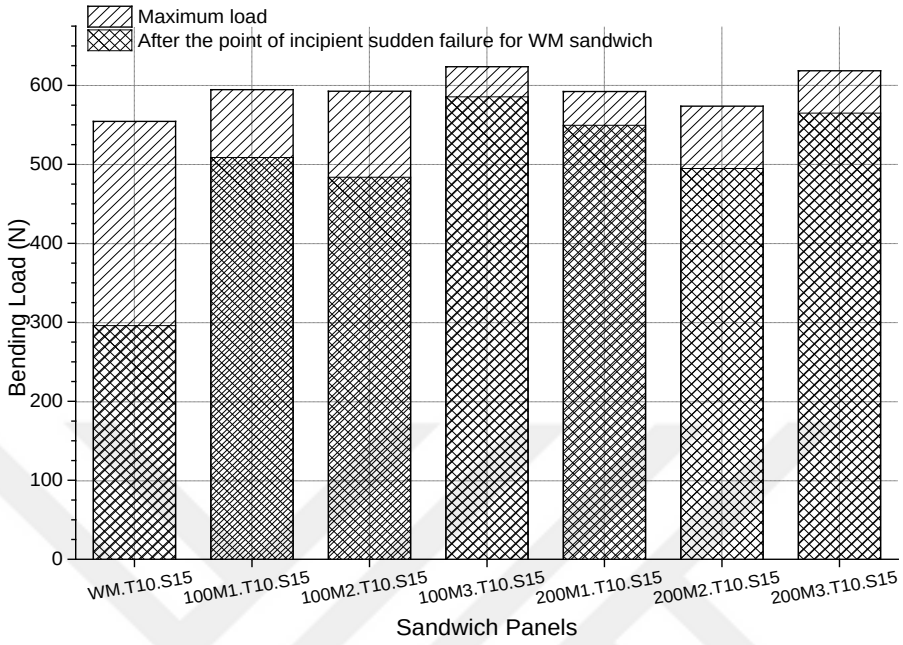


Figure 4.24. Reduction in bending load between the maximum point and 10 mm MS deflection

4.4.2. Load-Deflection Curves of 20 mm Thick Core Sandwich Panels

The load-deflection curves of the 20 mm thick foam core sandwich panels obtained by the test are presented in Figure 4.25 to 4.31.

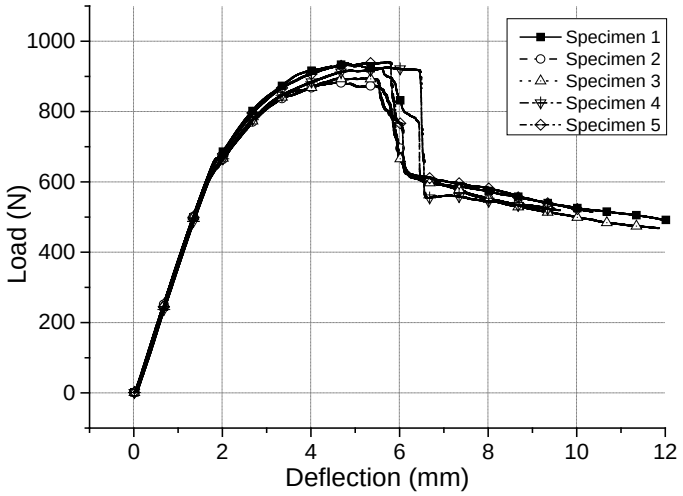


Figure 4.25. Load – deflection curves WM.T20.S15 sandwich specimens

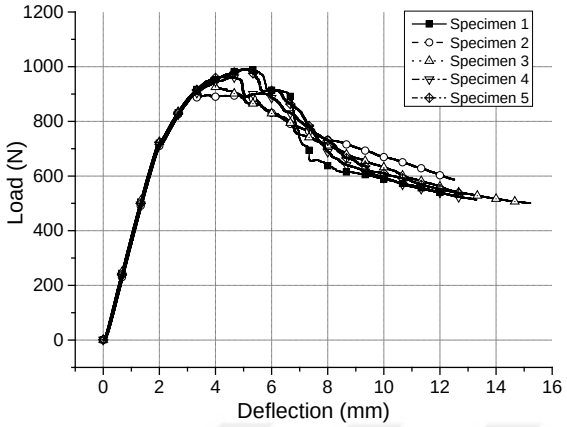


Figure 4.26. Load – deflection curves 100M1.T20.S15 sandwich specimens

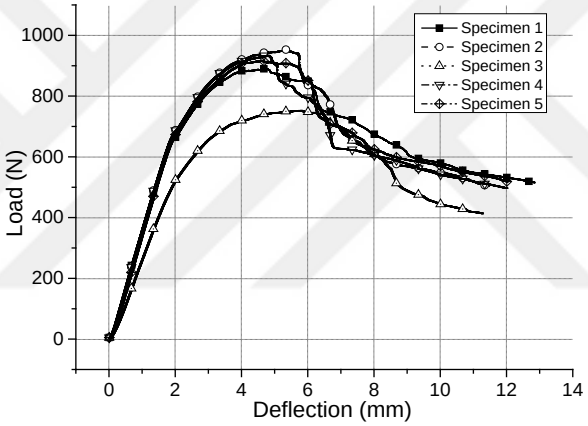


Figure 4.27. Load – deflection curves 200M1.T20.S15 sandwich specimens

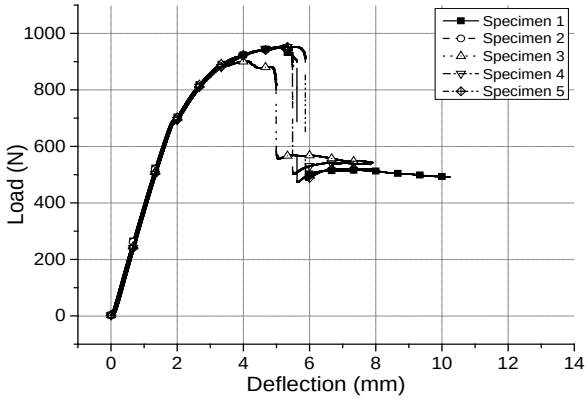


Figure 4.28. Load – deflection curves 100M2.T20.S15 sandwich specimens

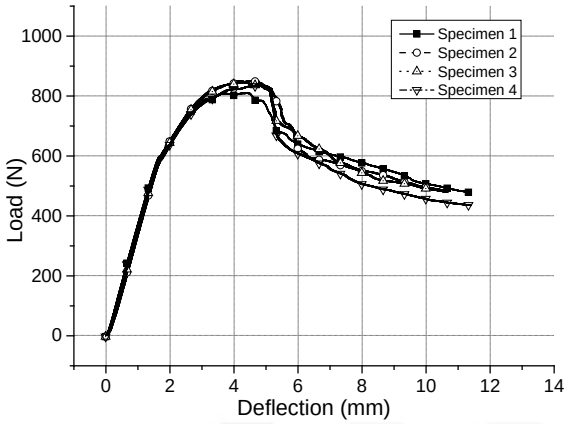


Figure 4.29. Load – deflection curves 200M2.T20.S15 sandwich specimens

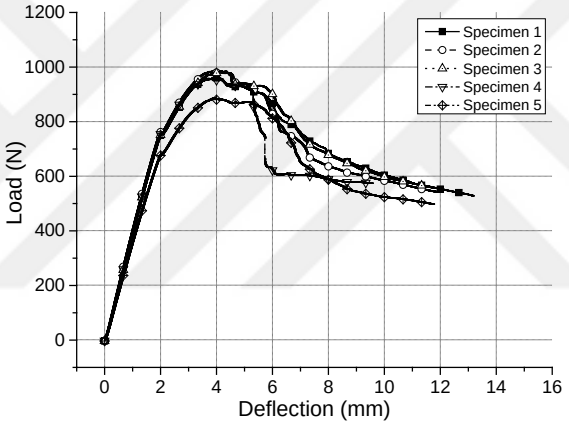


Figure 4.30. Load – deflection curves 100M3.T20.S15 sandwich specimens

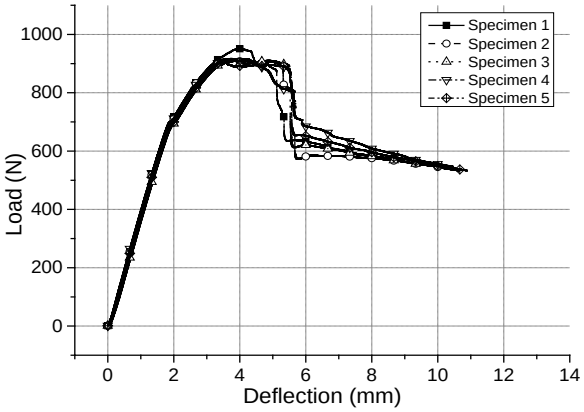


Figure 4.31. Load – deflection curves 200M3.T20.S15 sandwich specimens

Table 4.9 shows the average values of the maximum bending load carrying capacities (P_{max}) of the sandwich panels and corresponding mid-span (MS) deflection values according to the sandwich panel code system of the work. The standard deviations are presented in parenthesis.

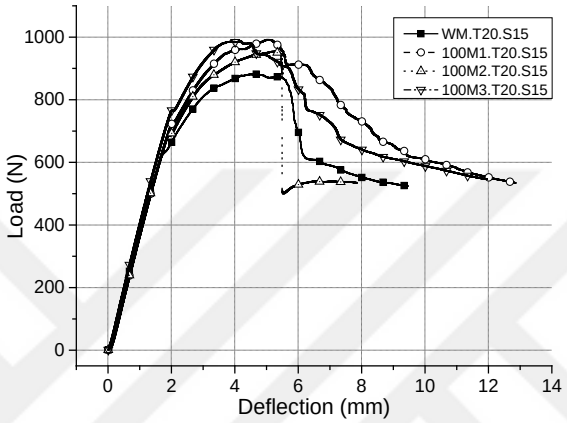
Table 4.9. Maximum load-carrying capacities and MS deflection of the 20 mm thick core sandwich panels

Sandwich panel code	Maximum Load and Corresponding Mid-span (MS) Deflection	
	P_{max} (N)	MS Displacement (mm)
WM.T20.S15	916,15 (23,56)	5,115
100M1.T20.S15	960,13 (31,74)	4,409
100M2.T20.S15	938,36 (22,37)	4,997
100M3.T20.S15	957,53 (36,39)	4,018
200M1.T20.S15	920,70 (22,83)	4,885
200M2.T20.S15	837,67 (18,54)	4,521
200M3.T20.S15	921,96 (14,97)	3,843

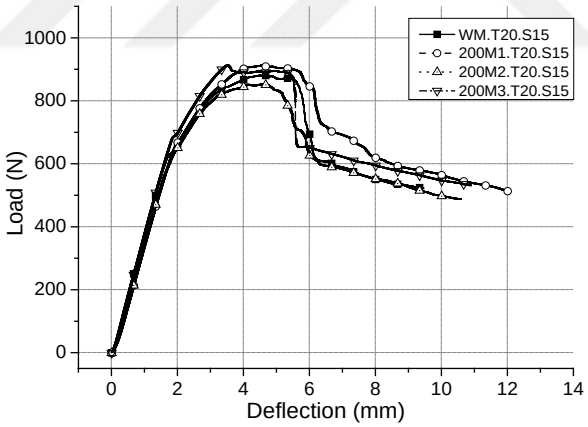
The bending behavior of sandwich panels with 20 mm thick foam core was found to be partially similar to ones with the 10 mm thick core. The plots provided a linear load increase in the elastic region initially, and this is followed by a nonlinear increase up to the maximum point of bending force. This behavior is also the same for 10 mm thick foam core sandwiches. But, the amount of deflection between the end of the linear elastic region and nonlinear point of maximum bending load was smaller than the sandwich panels with 10 mm thick foam core. And after the maximum point is reached, 20 mm thick foam core sandwiches start to fail. Both WM and sandwiches with wire mesh sheets showed sudden drops in force. This is because the sandwiches have a tendency to fail based on indentation. As the thickness ratio of facing to core (t/c) decreases, the indentation becomes a primary failure mode due to the weakness of facing.

After obtaining plots for each of the sandwich panel configurations, a quasi-average estimation of load-deflection placement curve was obtained for WM,

100-mesh, and 200-mesh sizes. As given in Figure 4.32 (a), the comparison was made between sandwiches having no-wire mesh sheet and 100-mesh wire sheets facings. And Figure 4.32 (b) provides the quasi-average estimation values for sandwiches with WM and 200-mesh steel wire sheets facings.



(a)



(b)

Figure 4.32. Comparison of the 20 thick foam core sandwich panels with and without mesh; a) WM and 100-mesh, b) WM and 200-mesh

Although there is a considerable difference between each of the configurations for 10 mm thick core sandwiches, less improvement is observed for the sandwiches having 20 mm thick foam core. The existence of 100-mesh wire

sheets in sandwich panels provided better results for 20 mm foam core. In general, the most effective configuration is obtained as the sandwich having a 100-mesh wire sheet (under the first ply of upper facing). Actually, 100M3 configuration provided the best results but the existence of two-wire mesh sheet layers highly increased the total weight of the sandwich. Also, the use of 200 mesh for the same configuration contributed to failure behavior but the improvement is less compared to the one with a 100-mesh steel wire sheet. The effects of wire mesh sheets to 20 mm thick foam core sandwiches were examined in detail. The procedure is the same as the 10 mm core thickness that performed in the previous section. Firstly, the initiation point of the sudden failure of the WM sandwich panel was determined approximately at an MS deflection of 6,29 mm. Then the bending load-carrying capacities were found for all sandwich configurations at that deflection and given in Table 4.10.

Table 4.10. Load-carrying capacities of sandwich panels after 20 mm thick core WM sandwiches underwent to sudden failure at MS deflection of ~6,29 mm

Sandwich Configurations	Maximum Load (N)	Load (N) at ~6,29 mm MS Deflection	Percent (%) Reduction in Bending Load
WM.T20.S15	916,15	633,00	30,91
100M1.T20.S15	960,13	912,67	4,94
100M2.T20.S15	938,36	553,63	41,00
100M3.T20.S15	957,53	819,89	14,37
200M1.T20.S15	920,70	788,57	14,35
200M2.T20.S15	837,67	630,72	24,71
200M3.T20.S15	921,96	663,21	28,07

As seen from the table, the sudden drop in the bending force of the WM.T20.S15 sandwich caused a reduction in load capacity by 30,91%. The minimum decrease in load capacity (4,94%) was obtained for 100M1.T20.S15 sandwich panels. At the same deflection, 100M1.T20.S15 sandwich carried 44,18% higher bending load

compared to WM.T20.S15 although the weight penalty is about 17%. Figure 4.33 shows the effects of wire mesh sheets to the sandwich panels by presenting both the maximum load-carrying capacities and bending load obtained at 6,29 mm deflection.

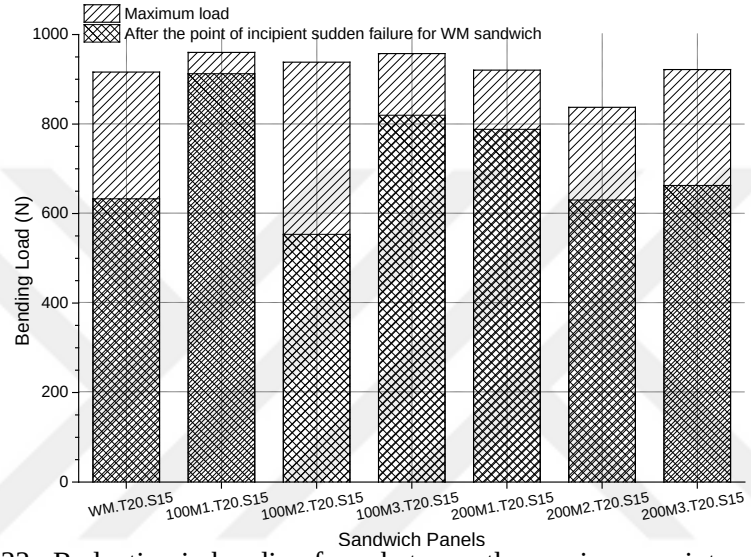


Figure 4.33. Reduction in bending force between the maximum point and 6,29 mm MS deflection

4.4.3. Load-Deflection Curves of 30 mm Thick Core Sandwich Panels

The load-deflection curves of the 30 mm thick foam core sandwich panels having five specimens are presented in Figures from 4.34 to 4.40.

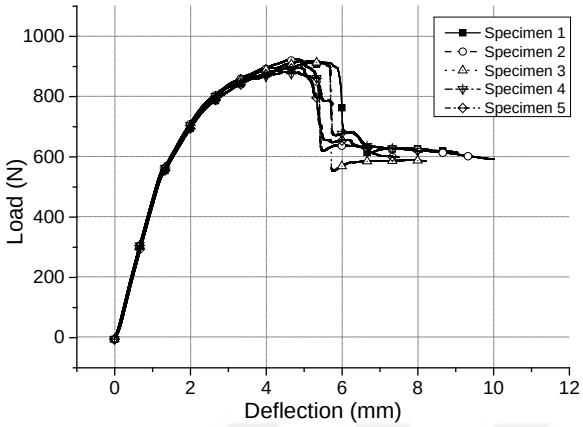


Figure 4.34. Load-deflection curves WM.T30.S15 sandwich specimens

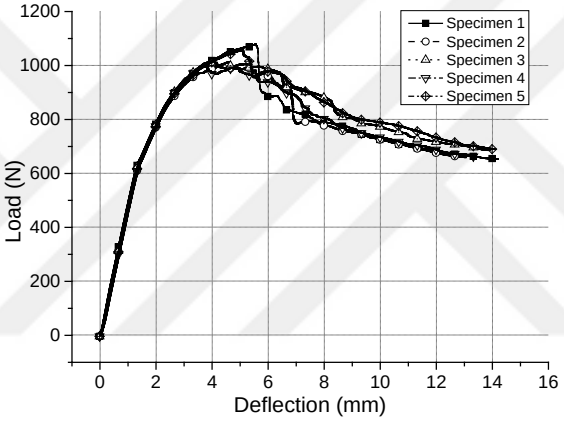


Figure 4.35. Load-deflection curves 100M1.T30.S15 sandwich specimens

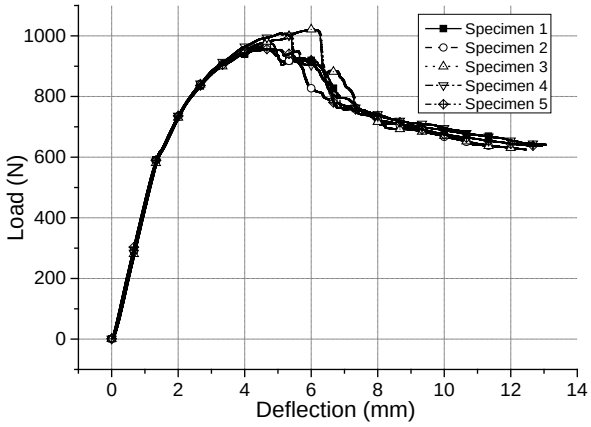


Figure 4.36. Load-deflection curves 200M1.T30.S15 sandwich specimens

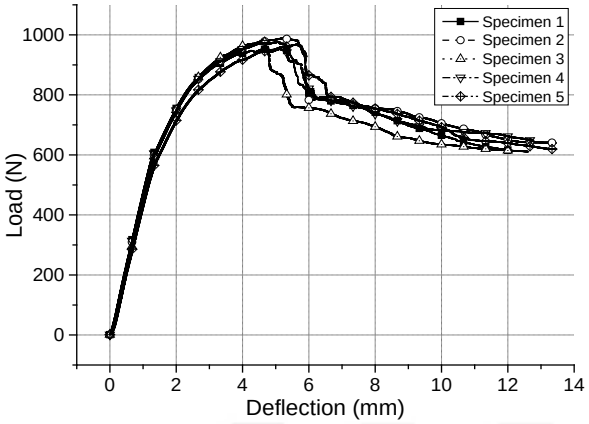


Figure 4.37. Load-deflection curves 100M2.T30.S15 sandwich specimens

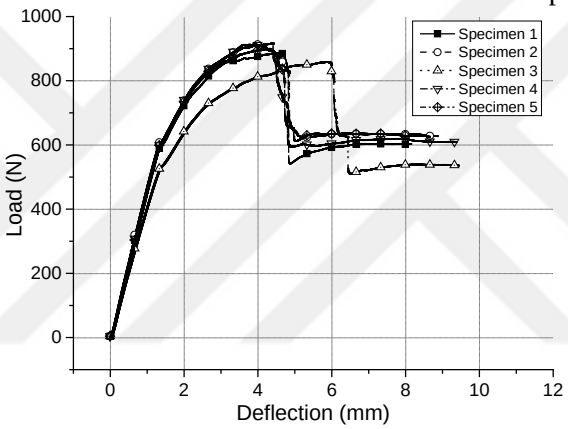


Figure 4.38. Load-deflection curves 200M2.T30.S15 sandwich specimens

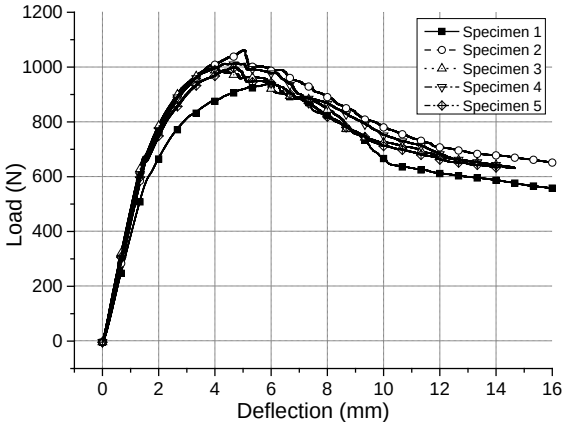


Figure 4.39. Load-deflection curves 100M3.T30.S15 sandwich specimens

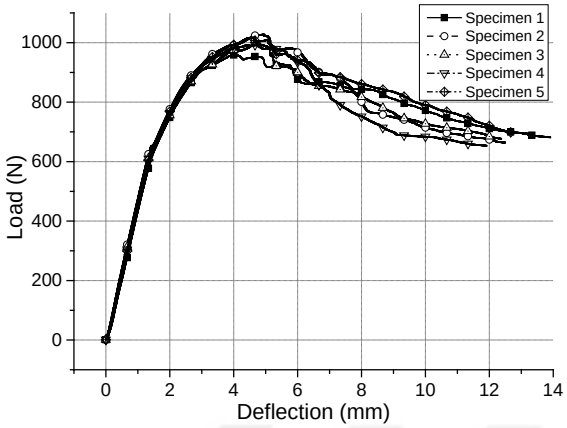


Figure 4.40. Load-deflection curves of 200M3.T30.S15 sandwich specimens

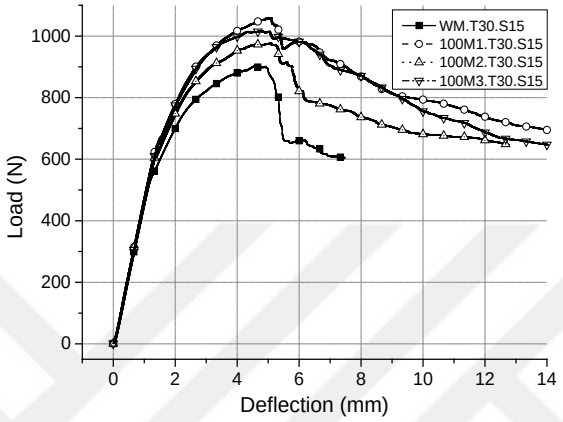
The maximum bending load carrying capacities (P_{max}) of the sandwiches were determined and their average values are presented in Table 4.11 together with corresponding MS deflection values according to the sandwich panel code system. The standard deviations are given in parenthesis.

Table 4.11. Maximum load-carrying capacities and MS deflection of the sandwich panels for 30 mm thick foam core

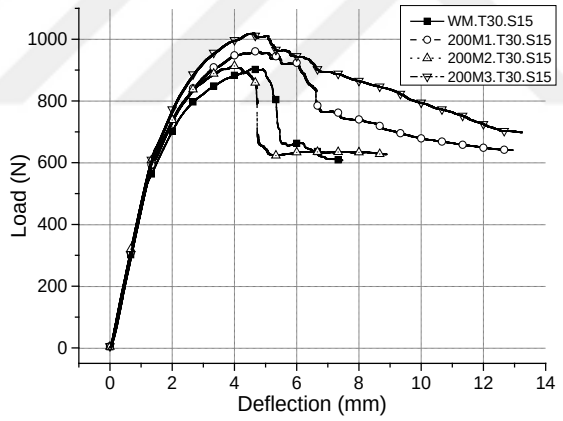
Sandwich panel code	**Maximum Load and Corresponding Mid-span (MS) Deflection**	
	P_{max} (N)	**MS deflection (mm)**
WM.T30.S15	911,99 (15,59)	4,939
100M1.T30.S15	1033,19 (31,64)	4,863
100M2.T30.S15	974,29 (12,84)	5,13
100M3.T30.S15	1005,02 (38,91)	4,867
200M1.T30.S15	985,96 (24,98)	4,829
200M2.T30.S15	893,63 (21,31)	4,614
200M3.T30.S15	1000,31 (23,12)	4,623

Since the consistency of the results among each configuration was achieved, a quasi-average curve was determined and used to make a comparison between specimens with and without wire mesh sheets. The intention was to see the effect of both size and stacking position of the wire mesh sheets in the

lamination of facings. Figure 4.41 (a) provides the comparison between WM and 100-mesh sizes, whilst the Fig 4.41 (b) compares WM and 200-mesh sized sandwich specimens.



(a)



(b)

Figure 4.41. Comparison of the 30 mm thick foam core sandwiches with and without mesh; a) WM and 100-mesh, b) WM and 200-mesh

The plots for bending behavior of 30 mm thick sandwiches show that the bending force of sandwich panels initially increases linearly, and this is then followed by a nonlinear increase up to a maximum point of bending force. The amount of deflection between the end of the linear point and the maximum bending

point is larger than both 10 mm and 20 mm thick foam core sandwiches as these are seen in Figure 4.43, in Section 4.4.4.

After the maximum bending force is reached, a sudden drop of force occurs at an approximate MS deflection of 5,59 mm. This is because the indentation creates and controls the failure. However, unlikely to sandwiches with 20 mm thick core, the wire mesh sheets considerably improved the three-point bending behavior of the sandwich structures having 30 mm thick foam core. Wire mesh sheets, except for the configuration of 200M2, provided three improvements. These are larger bending load carrying capacity, improved stiffness, and preventing sudden drop of bending force. As seen from Table 4.12, the bending load capacity of the WM.T30.S15 sandwich panel was decreased by 25,37% whereas there was only a 4,28% reduction for 100M1.T30.S15 sandwich panel and it carried 45,32% higher bending load at the same deflection point where WM configuration started to fail. The difference between the maximum bending load and the load obtained at a deflection of 5,59 mm which is the initiation point of sudden failure of WM sandwiches is presented in Figure 4.42 for whole sandwich configurations.

Table 4.12. Load-carrying capacities of sandwich panels after 30 mm thick core WM sandwiches underwent to sudden failure at MS deflection of ~5,59 mm

Sandwich Configurations	Maximum Load (N)	Load (N) at ~5,59 mm MS deflection	Percent (%) Reduction in Bending Load
WM.T30.S15	911,99	680,58	25,37
100M1.T30.S15	1033,19	989,00	4,28
100M2.T30.S15	974,29	917,24	5,86
100M3.T30.S15	1005,02	1000,25	0,47
200M1.T30.S15	985,96	924,28	6,26
200M2.T30.S15	893,63	640,28	28,35
200M3.T30.S15	1000,31	961,90	3,84

When all the figures are closely scrutinized, it is clearly seen that only the sandwiches having a 10 mm foam core are more likely to bend. Increasing the core

thickness changes bending behavior as well as failure modes of the panels. After reaching the maximum point of bending load, 10 mm foam core sandwich panels still carried the bending loads for a particular amount of deflection with a small decrease in force/deflection slope. In the case of 20 mm and/or 30 mm thick foam core, a sudden drop of the force occurred when the bending force reached to the maximum. This is because the thicker cores provide more rigidity, and resist bending in a better way due to the moment of inertia increase of the structure about the axis normal to the plane of bending. In addition, as the thickness ratio of facing to core decreases, the failure mode changes from core shearing to indentation. However, the existing of wire mesh sheets increased the maximum forces against bending loads throughout all sandwich panels except one or two configurations which did not contribute to the bending properties. The mesh sheets also prevented the sudden force drop when a sandwich reaches a maximum point in bending force. When the wire mesh configurations were examined from Figures 4.24, 4.33, and 4.42, it can be seen that M2 configurations are the least effective ones except for 100M2.T10.S15 sandwich panel. Therefore, the drop in bending force is greater. On the other hand, since M3 configurations have two wire mesh sheets in sandwich facings, their weight penalties are larger. Because of that reason, M1 configurations are better candidates to contribute to the bending behavior of the sandwiches. In the case of sandwich panels without wire mesh sheets, the main reason for the sudden force drop is due to the brittle nature of carbon fibers.

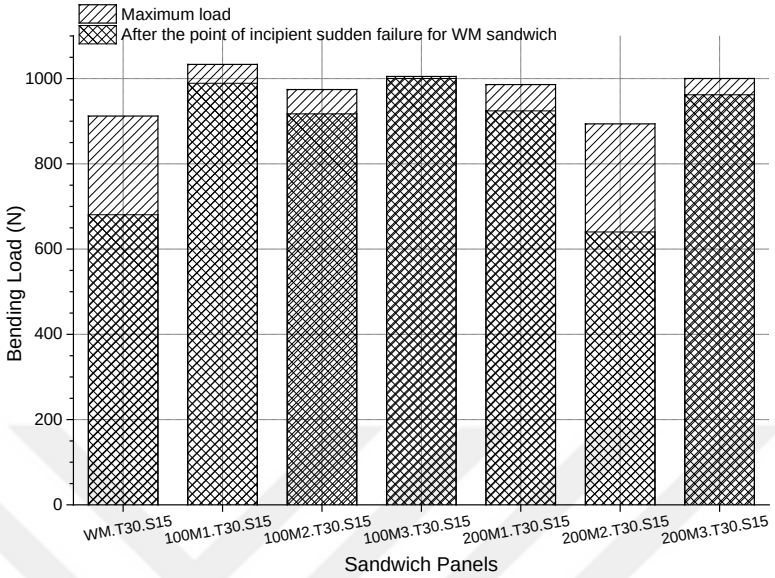
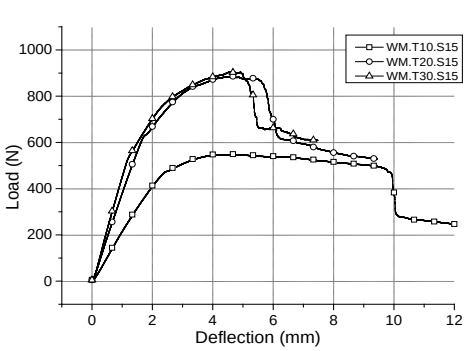


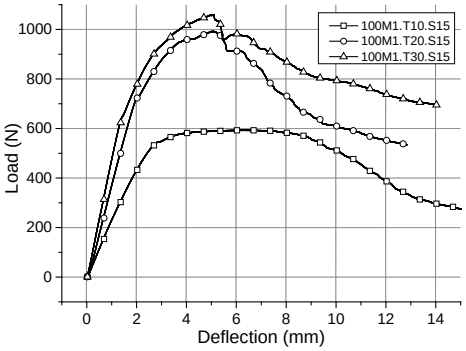
Figure 4.42. Reduction in bending force between the maximum point and 5,59 mm MS deflection

4.4.4. Comparison of the Sandwich Panels Based on the Core Thickness

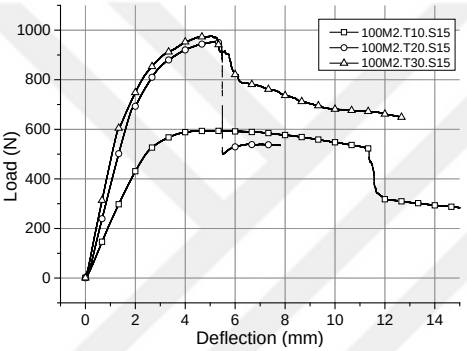
A comparison of the sandwiches based on the core thickness is discussed in this section. The load-deflection curves of the sandwich panels are rearranged based on the core thicknesses of the panels and are presented in Figure 4.43 to illustrate the effect of the core thickness.


WM.T10.S15
WM.T20.S15
WM.T30.S15
Load (N)
Deflection (mm)

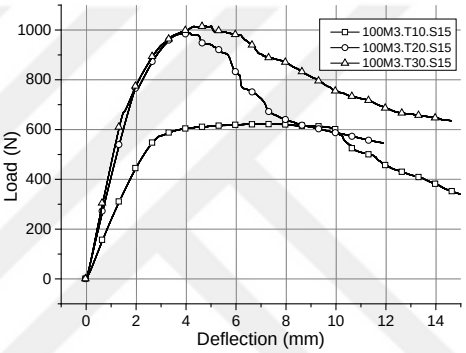
(a)


100M1.T10.S15
100M1.T20.S15
100M1.T30.S15
Load (N)
Deflection (mm)

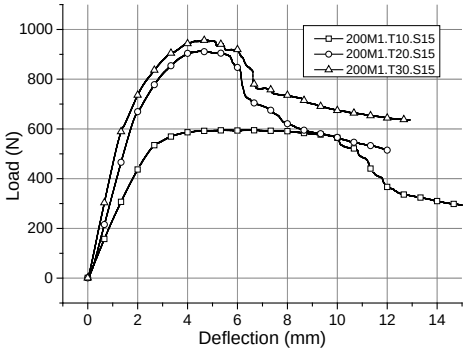
(b)


100M2.T10.S15
100M2.T20.S15
100M2.T30.S15
Load (N)
Deflection (mm)

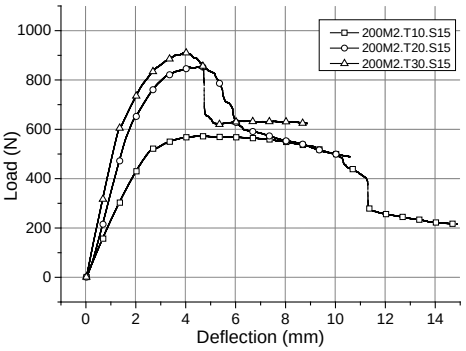
(c)


100M3.T10.S15
100M3.T20.S15
100M3.T30.S15
Load (N)
Deflection (mm)

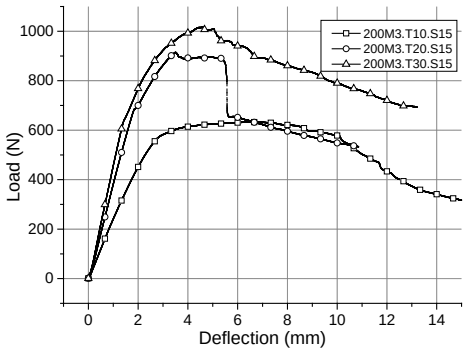
(d)


200M1.T10.S15
200M1.T20.S15
200M1.T30.S15
Load (N)
Deflection (mm)

(e)


200M2.T10.S15
200M2.T20.S15
200M2.T30.S15
Load (N)
Deflection (mm)

(f)



(g)

Figure 4.43. Comparison of the sandwich panels based on the core thickness. (Configurations: a) WM, b) 100M1, c) 100M2, d) 100M3, e) 200M1, f) 200M2, g) 200M3)

When the results in Figure 4.43 are examined, it can be seen that the increase in the core thickness provides better bending rigidity. However, although there has been a constant linear relationship among the core thickness values of 10 mm, 20 mm and 30 mm, the bending behavior of the panels for rigidity does not show a linear trend. For the WM sandwiches, the bending behaviors of both 20 mm and 30 mm thick core sandwich panels were found very similar to each other even they have the same face sheet configuration. Because when a 10 mm core was used, the sandwich specimens were failed due to core shearing. But by using a thicker core, the failure mode was changed from the core shear to the indentation. Therefore, 30 mm thick core sandwich panels carried approximately the same bending load comparing to 20 mm thick foam core sandwiches due to indentation failure. However, the use of wire mesh sheets mostly improved the bending behavior of 30 mm thick core sandwich panels, and significantly changed the load-deflection curves when compared to 20 mm thick core sandwiches (see Figures 4.33 and 4.42).

Actually, using the wire mesh sheets at the top facing-core interface (configuration of M2) did not contribute a significant mechanical behavior for the three different core thicknesses of the study. In the case of using wire mesh sheets

under the first carbon fiber fabric ply of the upper face sheet (configuration of M1) has provided better results in terms of both bending characteristics and failure modes.

The sandwich panels having 30 mm core thickness provided the highest flexural stiffness but the difference in the load-deflection curve between 30 mm and 20 mm thick core sandwiches is very close to each other and increasing core thickness did not contribute to bending load capacity. This is due to the failure behavior of the sandwich structures. As the face sheet-core thickness ratio (t/c) decreases, the sandwich panels failed based on the indentation failure mode. Therefore, in order to avoid indentation failure, there is a thickness limit for the core, and using a 20 mm thick core is better than 30 mm particularly for WM sandwiches.

A preliminary study was also carried out by using a thicker face sheet with a 20 mm thick core. Six carbon fiber fabric plies were used for facings in the manufacturing of sandwich panels. The production of the sandwich panels, which has six carbon fiber fabric plies for face sheets, was only manufactured for WM configuration in order to see the effect of face sheet to core thickness *(t/c)* ratio on the bending behavior of sandwiches. The load-deflection curves are given comparatively in Figure 4.44.

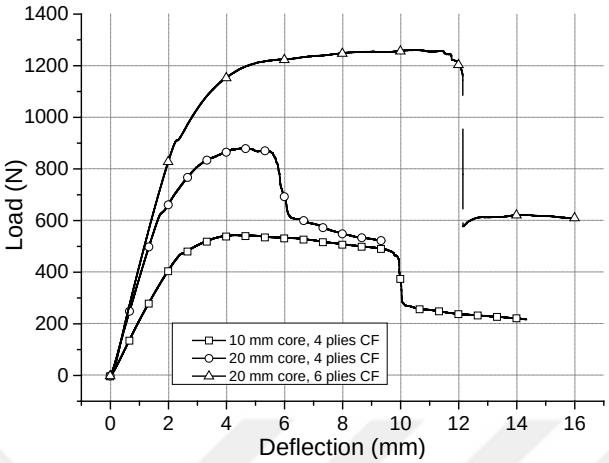


Figure 4.44. Comparison of sandwich load-deflection curves based on both facing and core thickness

As seen from Figure 4.44, when the load-deflection curves of 20 mm thick core sandwiches are compared for the core thicknesses, the flexural stiffness is increased by using thicker face sheets. However, the initial stiffness of both six and four plies of carbon fiber fabric sandwiches with a 20 mm thick core provides similar mechanical behaviors up to about 300 N. Then, thicker facing specimen demonstrates the highest peak load carrying capacity and shows longer horizontal plateau at the peak load than thinner facing. In addition, the maximum bending load-carrying capacity increased by approximately 43%. However, there is a significant sudden drop in the force during failure. In addition to this, the load capacities were found quite similar after the failure of both thin and thick facing sandwiches. Sandwich panels with thicker facings were also tended to provide larger deflection with a longer plateau under bending loading compared to those of thin facings sandwiches. Core shear failures occurred in thicker specimens before fracture of top facing. This corresponds with the observed behaviors of the literature. It was reported that thicker facing increases the shear stress in the core and results in shear cracks whereas thinner skin underwent indentation failure (Styles et al., 2007). But the increase of weight due to six carbon fiber plies facings

is approximately 48,5% compared to that of four plies for facings whilst the improvement of bending load capacity is 43%. Although the bending force increased with the increase of facing to foam core thickness (*t/c)* by using six plies of carbon fiber fabrics instead of four layers, it also yielded large weight penalties. On the other hand, as presented in Figure 4.45, increasing core thickness from 10 mm to 20 mm for four plies facings provided 65,3% higher bending load capacity whereas the weight increase was only about 17%. Therefore, the structural effectiveness of sandwich panels strongly depends on geometrical sizes and material selection. For this reason, the use of wire mesh sheets may become a proper solution to improve bending characteristics with a minimum weight increase.

4.5. Three-point Bending Test Results of Long-span Sandwich Beams

As mentioned in Chapter 3 (Section 3.4.4), the long-span sandwich panels were fabricated after the results of short-span sandwiches had been obtained. According to the results obtained from the bending behavior of the short-span sandwich beams under three-point bending tests, the following configurations were specified for further investigations. Their sandwich codes are: WM.T10.S20, 100M1.T10.S20, 200M1.T10.S20, WM.T20.S20, 100M1.T20.S20, WM.T30.S.20, 100M1.T30.S20. The configurations were limited to a few. Because the use of the wire mesh sheets at the top facing-core interface did not provide a significant effect on the bending behavior of the sandwich specimens. Furthermore, in the case of using two wire mesh sheets in the facing eliminates the weight advantage and causing drawback effects. In addition, the results of tensile tests indicated that tensile properties of 100M1 configuration provided improved properties than other facing configurations. Therefore, the long-span sandwich beams (250 mm in length) including only one wire mesh sheet stacked under the first carbon fiber ply of top facing were fabricated. The sizes of the wire mesh sheets are 100-mesh and

200-mesh for 10 mm, and 100-mesh for both 20 mm and 30 mm thick core sandwiches, respectively. 200-mesh wire sheets were not considered due to obtained bending test results of short beams. In addition, the long-span sandwich panels were also fabricated without any kind of wire mesh (WM) sheets in order to reveal the effect of wire mesh. This also provides to establish baseline reference data for the comparison of the test parameters.

Testing of the long-span sandwich beams is also required to investigate failure modes. It will reveal the transition from core shearing to the facing failures. Moreover, ASTM D7250 standard provides an approach for the evaluation of sandwich bending and shear stiffness values based on the results of both short and long-span sandwich beams. Therefore, long-span sandwich panels having a length of 250 mm were manufactured with identical facings and widths to short-span specimens, and the obtained sandwich beams were subjected to three-point bending tests. However, the productions were carried out for seven different configurations (WM.T10.S20, 100M1.T10.S20, 200M1.T10.S20, WM.T20.S20, 100M1.T20.S20, WM.T30.S.20, 100M1.T30.S20) as discussed above. Figures from 4.45 to 4.51 provide the three-point bending test results of the long-span sandwiches in the form of load versus deflection curves.

The maximum load-carrying capacities were determined, and their average values are given in Table 4.13 together with the standard deviations and corresponding MS deflections. Examination of the load-deflection diagrams of the short-span and long-span beams reveals that load-carrying capacities of the long-span beams decreased due to increased support span length under three-point bending tests as expected. This corresponds with the findings of Sadeghian (2018).

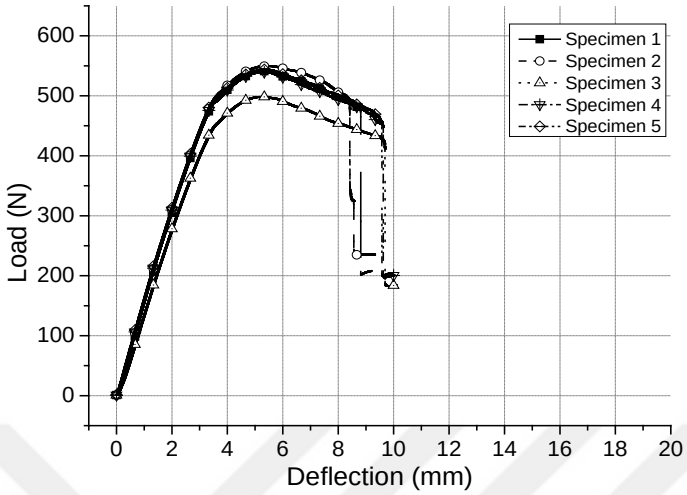


Figure 4.45. Load-deflection curves of WM.T10.S20 sandwich specimens

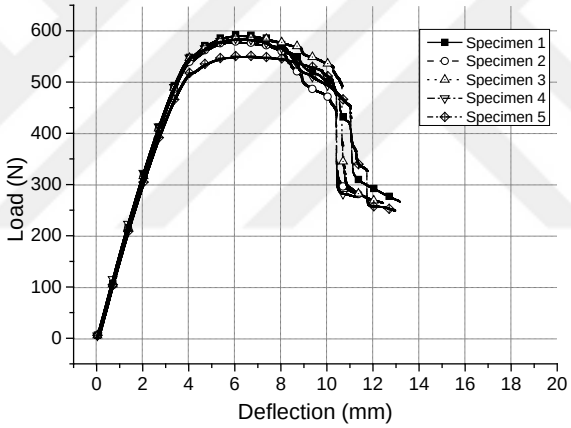


Figure 4 46. Load- deflection curves of 100M1.T10.S20 sandwich specimens

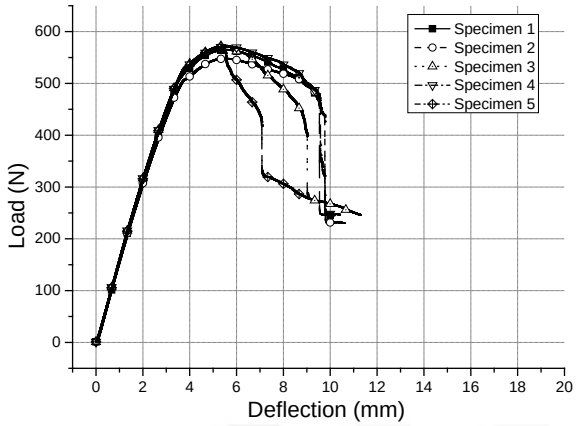


Figure 4.47. Load- deflection curves of 200M1.T10.S20 sandwich specimens

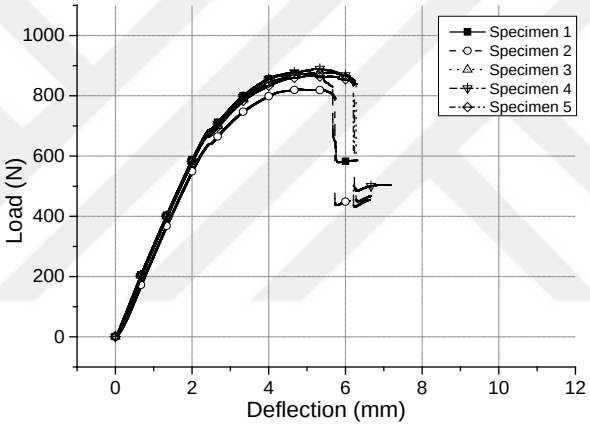


Figure 4.48. Load- deflection curves of WM.T20.S20 sandwich specimens

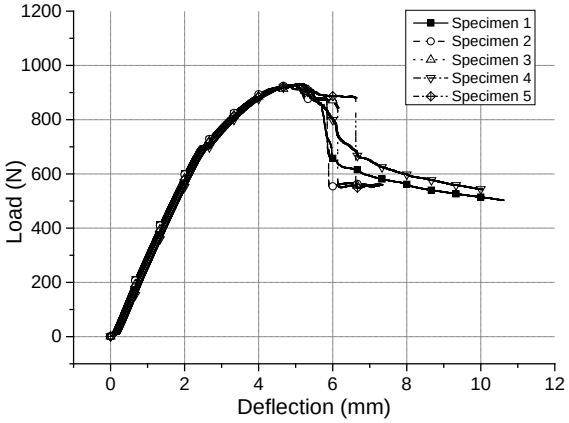


Figure 4.49. Load- deflection curves of 100M1.T20.S20 sandwich specimens

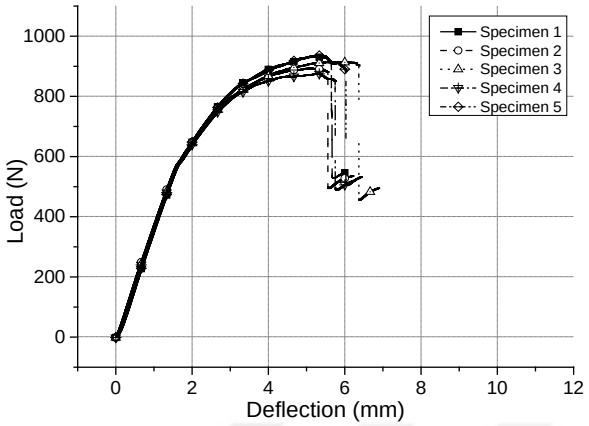


Figure 4.50. Load- deflection curves of WM.T30.S20 sandwich specimens

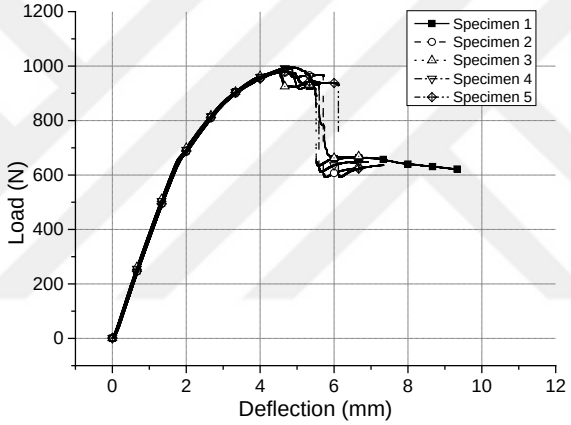


Figure 4.51. Load- deflection curves of 100M1.T30.S20 sandwich specimens

Table 4.13. Maximum load-carrying capacities and MS deflections of the long-span sandwich panels

Sandwich panel code	Maximum Load and Corresponding Mid-span (MS) Deflection	
	P_{max}(N)	MS Deflection (mm)
WM.T10.S20	535,07 (18,38)	5,334
100M1.T10.S20	574,88 (14,36)	6,201
200M1.T10.S20	566,20 (9,29)	5,528
WM.T20.S20	867,73 (24,31)	5,108
100M1.T20.S20	928,40 (4,24)	5,031
WM.T30.S20	912,95 (23,04)	5,248
100M1.T30.S20	985,34 (6,96)	4,626

The above figures and Table 4.13 show that the use of wire mesh sheets increases the bending load-carrying capacities. However, the bending behavior of the sandwich panels in both linear elastic and non-linear sections are found similar to those used in their short-span counterparts for each of the core thicknesses. Although wire mesh sheets favorably affected the failure of short-span sandwich panels, a similar effect was not obtained for the long-span sandwiches. For instance, using the wire mesh sheets for 10 mm thick core short beam sandwiches provided a longer plateau after the maximum bending load was reached. But, as it is seen in Figure 4.52, after the maximum bending load was reached, the force decreases with a negative slope before a sudden drop. This is due to the larger distance between the supports. If a sandwich panel is subjected to bending loading at a particularly long-span length, the failure mode occurs as face sheet yielding or fracture. This coincides with the findings of Sadeghian, (2018). Therefore, the wire mesh sheets do not contribute to fracture resistance or face yielding.

Figures 4.52 to 4.54 contain rearranged test results of Figures 4.45 to 4.51 based on the core thickness. This arrangement of the load-deflection curves of the sandwich panels allows evaluating the effect of wire mesh sheets by relative comparison.

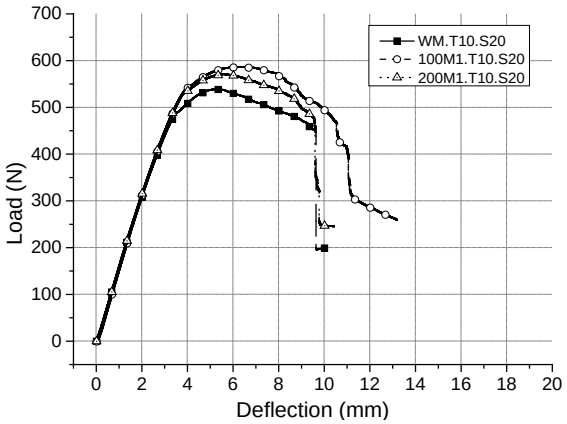


Figure 4.52. Load-deflection curves of 10 mm thick long-span sandwich beams

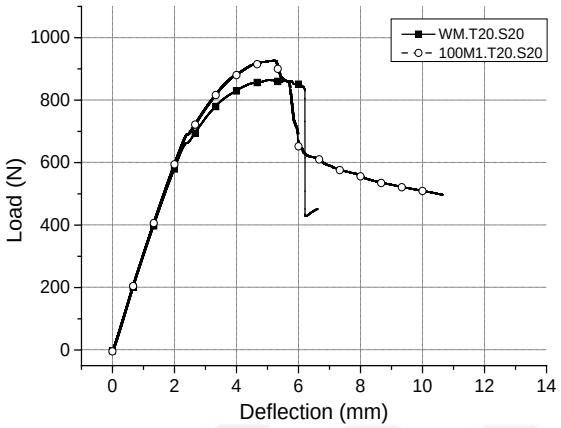


Figure 4.53. Load-deflection curves of 20 mm thick long-span sandwich beams

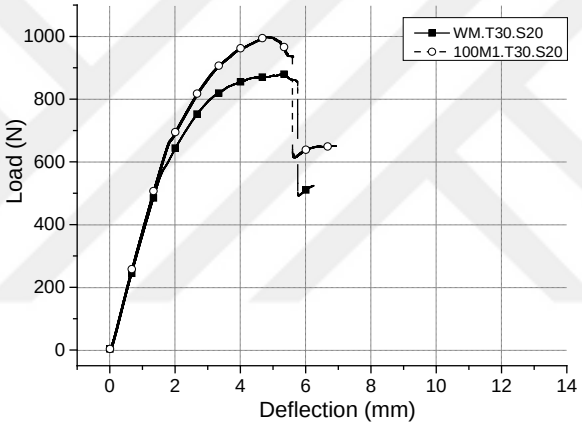


Figure 4.54. Load-deflection curves of 30 mm thick long-span sandwich beams

The effects of wire mesh sheets to the long beam sandwiches were investigated by comparing of the sandwich panels' maximum load capacity and the bending load at a particular deflection point, which is the initiation point of sudden failure for the long WM sandwich panels. Therefore, when WM sandwiches failed due to sudden drop in bending force, the effect of wire mesh sheets on bending load-carrying capacity at the same deflection value can be revealed clearly, as this approach was applied for all short-span sandwich specimens in the previous sections. The sudden failures for WM sandwiches occurred at an approximate deflection value of 9,6 mm, 6,22 mm, and 5,75 mm for 10, 20, and 30 mm thick core sandwich panels,

respectively. When the data in Tables 4.13 and 4.14 were compared, WM sandwiches lose the load-carrying capacity by 63,63% after the sudden failure in bending. When the WM sandwich panels were failed at the specified deflection points, 100M1 sandwiches still contributed to the maximum bending load capacity by 157,20%, 45,04% and 24,74% for 10 mm, 20 mm and 30 mm thick core sandwiches. Figure 4.55 shows the maximum bending load and the load at a particular deflection point where WM sandwiches exposed to sudden failure for the long-span beam sandwiches.

Table 4.14. Load carrying capacities of long-span sandwich panels after WM sandwiches underwent sudden failure

Sandwich Configurations	**Bending Load Capacity (N) of Sandwiches at Initiation Point of Sudden Failure for WM Sandwiches**		
	10 mm Thick Core (failure at ~9,6 mm)	20 mm Thick Core (failure at ~6,22 mm)	30 mm Thick Core (failure at ~5,75 mm)
WM	197,89	433,76	493,51
100M1	508,97	629,14	615,58
200M1	344,90	---	---

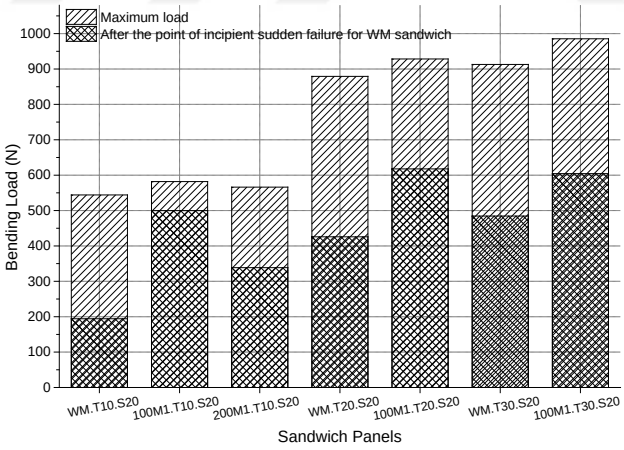


Figure 4.55. Comparison of the maximum load capacity and the load at where WM sandwiches underwent to failure for long-span sandwiches

4.6. Comparison of the Bending Test Results of Both Short and Long-span Sandwich Panels

When the effect of span length is investigated, it can be seen that the maximum bending load-carrying capacities of the sandwich panels are close to each other for different core thickness values as seen in Figure 4.56. But, the bending stiffness of the long-span beam sandwiches was found slightly lower than the short-span beam sandwiches as expected.

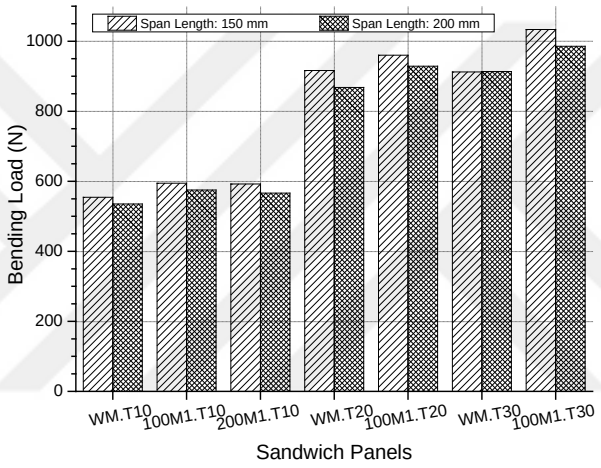
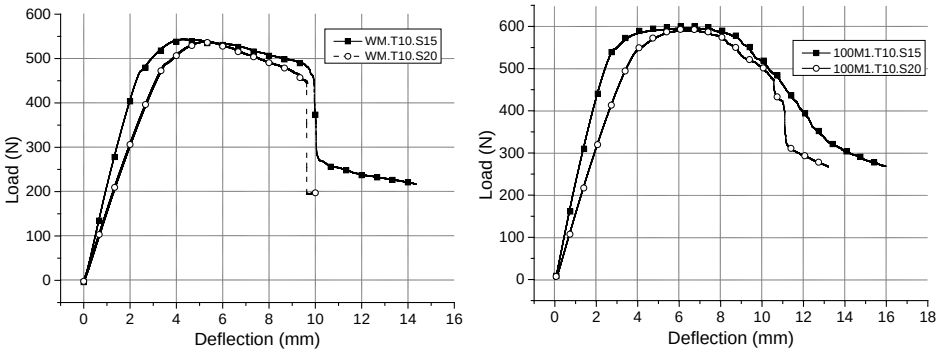
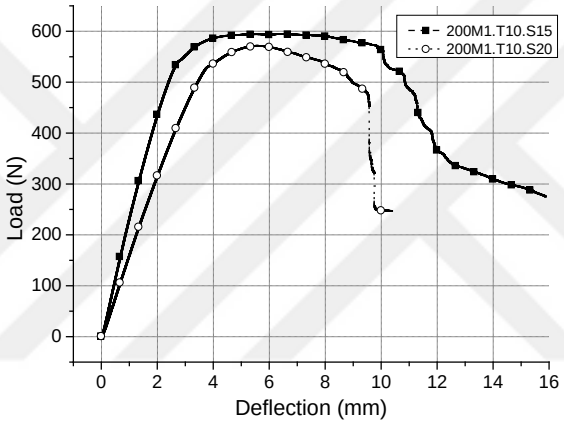


Figure 4.56. Comparison of sandwich bending load capacities tested under 150 mm and 200 mm span length

The results of load-deflection curves of sandwich panels tested under the span length of both 150 mm and 200 mm are rearranged according to core thickness and are given in Figures from 4.57 to 4.59 according to core thickness values of 10 mm, 20 mm and 30 mm, respectively. This allows a relative comparison for the selected configurations.



(a) WM **(b)** 100M1

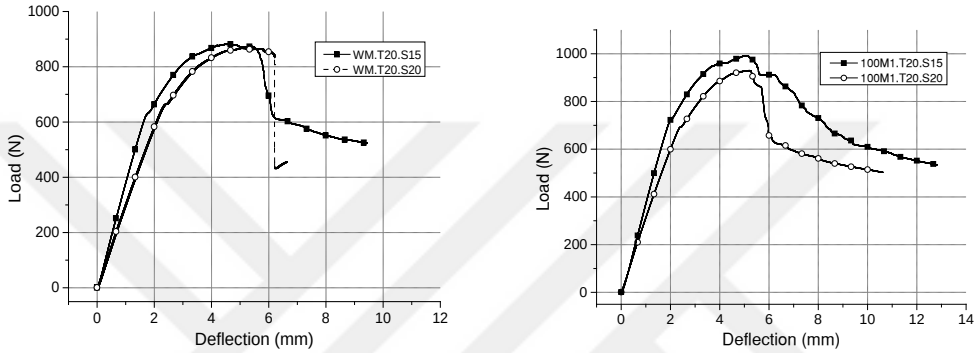


(c)200M1

Figure 4.57. Load-deflection curves of short and long-span sandwiches having 10 mm core thickness; a) WM, b) 100M1, c) 200M1

In the case of using a 10 mm thick core, the sandwich panels without any wire mesh sheets exhibited the same bending behavior except linear initial slope under both 150 mm and 200 mm span lengths. The sudden drop in bending force occurred at a mid-span deflection of approximately 10 mm for both of the span lengths. Similarly, the 200M1.T10.S20 sandwich panel showed a sudden drop in the force contrary to 200M1.T10.S15. After the facing fracture of 200M1.T10.S20 sandwich panel, the force decreased to 250 N. However, 200M1.T10.S15 sandwich carried 570 N bending loads at the same deflection value, and the load-deflection curve of the beam is changed to a decreasing slope instead of a sudden drop. In the

case of 100M1 configuration, the bending load was carried constantly for a particular amount of deflection. Then, the force decreased with a decreasing slope. After a distinct deflection point, approximately at 10 – 11 mm interval, the long-span sandwich panel failed whereas the short-span sandwich continued to carry bending load with a decreasing slope up to about MS deflection of 14 mm.



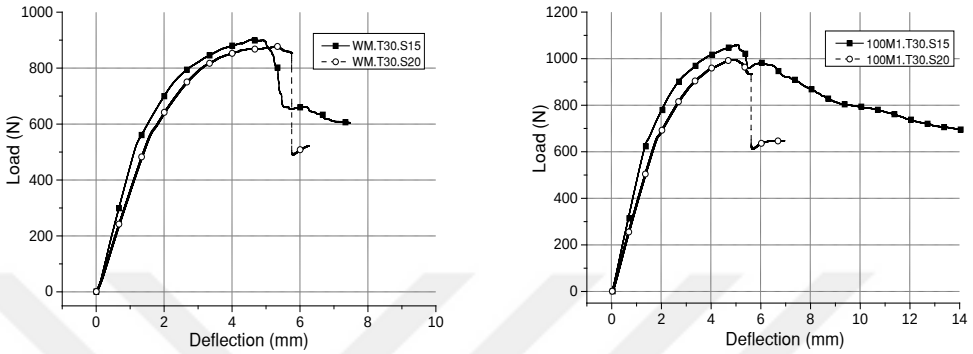
(a) (b)

Figure 4.58 Load-deflection curves of short and long-span beam sandwiches having 20 mm core thickness; a) WM, b) 100M1

The face sheets failures were clearly seen in Figure 4.58 for 20 mm thick core sandwich panels. The WM configuration of the long-span sandwich panel showed a sudden drop after the maximum bending force is reached. But, the short-span sandwich having a span length of 150 mm relatively shows a slightly decreasing slope after the point where the bending force reaches the maximum. It is evident from Figure 4.58 that 100M1 configuration with a span length of 150 mm is superior to the long-span beam sandwich panel.

30 mm thick core sandwich panels certainly underwent to face sheet compressive failure due to indentation when the specimens were subjected to bending loading at 200 mm span length. When the sandwich panel of 100M1.T30.S20 failed with a sudden drop in force at a deflection of 5,6 mm, its bending force decreased to 614 N as seen in Figure 4.59. However, 100M1.T30.S15 carried the bending load of 972 N, and a slightly decreasing slope

is observed in its load-deflection curve. Therefore, the 100M1 configuration has a significant effect in the case of short-span beams as seen in Figure 4.59.



(a) (b)

Figure 4.59. Load-deflection curves of short and long-span beam sandwiches having 30 mm core thickness; a) WM, b) 100M1

4.7. Evaluation of Flexural Characteristics

4.7.1. Load Carrying Capacity of the Sandwich Panels

The maximum bending load-carrying capacities of the sandwich panels were determined and provided in the previous sections. According to core thickness, support span length, and facing configurations of the sandwich panels, the bending load capacities are changed. Figure 4.60 shows the load-carrying capacities of 10 mm, 20 mm, and 30 mm thick foam core sandwich panels having WM and 100M1 configurations which were tested under 150 mm and 200 mm support span length.

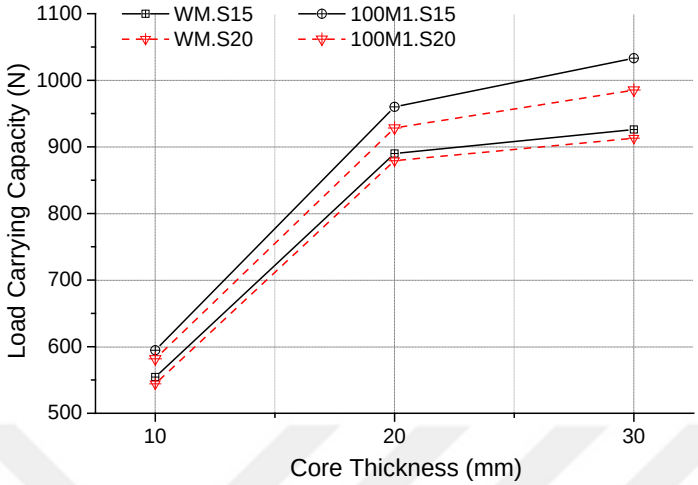


Figure 4.60. Load-carrying capacities of sandwiches based on different configurations, span length, and core thickness

As seen in Figure 4.60, the bending load-carrying capacity of the sandwich panels increases nonlinearly. When the core thickness of 20 mm was used, the load-carrying capacity increased by 60,55% compared to a 10 mm thick core sandwich panel in which the bending tests were performed under a 150 mm span length. But, 30 mm thick core contributed only 4,04% with respect to (wrt) 20 mm thick core specimens. This value increases to 7,61% in the case of using a 100M1 configuration. In addition, 100M1 configuration in short-span sandwich panels increased the bending load capacity by 7,25%, 4,8%, and 13,29% for 10 mm, 20 mm, and 30 mm core thicknesses, respectively when compared to that of WM sandwiches. The effect of span length on the load-carrying capacity of the sandwich is about less than 2% for WM sandwiches whereas a 100-mesh wire sheet (100M1) had a slight influence between the span lengths of 150 mm and 200 mm when compared to WM specimens. In the case of long-span sandwich panels, 100M1 configuration has provided better improvements on the maximum bending force. The improvement was by 6,93%, 5,59%, and 7,93% for 10 mm, 20 mm, and 30 mm core thicknesses, respectively when compared to WM. Baştürk and Tanoğlu (2013) investigated the core thickness effect of Al facing and Al foam

core sandwich panels and obtained a 14,75% increase in the load in the case of using a 20 mm thick core instead of 8 mm. Also, they stated that this value reached 32,8% for the increase of core thickness from 20 mm to 30 mm.

As discussed in the previous sections, wire mesh sheets have significantly affected the failure behavior of sandwiches under three-point bending tests. While WM sandwiches failed due to a sudden drop in bending force, 100M1 sandwiches failed with a decreasing slope in the force. Therefore, when WM specimens fail with a sudden drop in bending load, 100M1 configurations still resisted to a very large amount of bending forces as shown in Figure 4.61. For instance, 100M1 configuration in short-span sandwich panels increased the bending load by 71,99%, 44,18% and 45,32% for 10 mm, 20 mm and 30 mm core thicknesses, respectively when compared to WM specimens whereas the increments were obtained as 157,20%, 45,04% and 24,74%, respectively for long-span 100M1 sandwich panels compared to WM specimens.

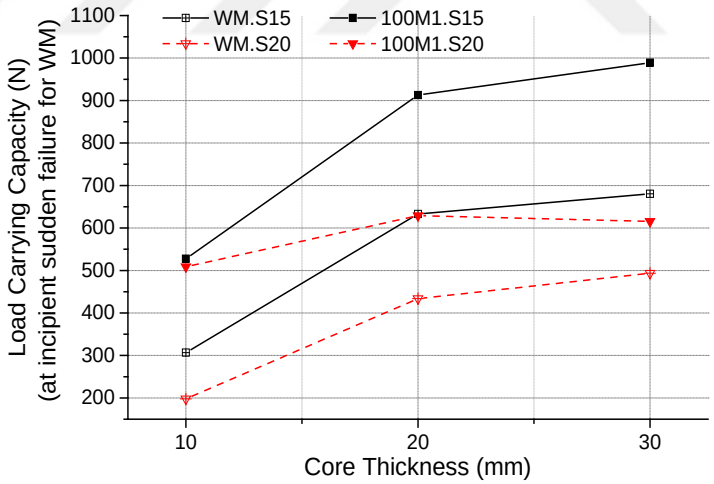


Figure 4.61. Load-carrying capacities at initiation point of sudden failure for WM sandwiches based on different configurations, span length, and core thickness

In both Figures of 4.60 and 4.61, and according to the maximum bending load capacities of the sandwiches the increase in bending force based on the increment of core thickness values are nonlinear for each of the configurations. This is because when the core thickness increases, transferring of the shear stresses between the facings became weaker. And, face sheet strength of the sandwich panels also decreases as the facing thickness remained the same while the core thickness was increased. Therefore, the increase in load-carrying capacity occurs nonlinearly between 20 mm and 30 mm core thickness. Thus, failures of the sandwich panels were due to indentation mode. The results agree with the findings of the literature. Styles et al. (2007) researched the core thickness effect on Al foam core glass fiber sandwich and reported that increasing core thickness led to core indentation.

According to the results given in the previous sections, as the core thickness increases, the failure point of mid-span deflection is getting smaller due to decreased facing stress. And shear stress between the facings reduces. Chen et al. (2001) also concluded a similar result for Al foam core Al facing sandwiches.

4.7.2. Core Shear Ultimate Stress and Face Sheet Ultimate Stress

Flexural characteristics of the sandwich panels were calculated based on both experimental ASTM standards and analytical methods. According to the equations given in Chapter 3 (Material and Method), core shear ultimate stress and face sheet ultimate stress values were determined based on both ASTM approaches (experimental) and analytical as presented in Table 4.15. In the table, the results are very close to each other. Thus, both Experimental and analytical approaches are in good agreement with each other when the core shear ultimate stress and face sheet ultimate stress values are evaluated. The calculations were carried out based on the maximum bending load of the sandwich specimens. Although there is a slight

difference between experimental and analytical results for core shear modulus, the facing stress almost yielded the same results.

The results of top face sheets were considered throughout the calculations. This is because; carbon fiber facings sandwich panels are commonly weaker under compressive forces than that of tensile force. Therefore, compressive failure has been more likely than tensile failure, and top facing has become more critical (Daniel and Gdoutos, 2009).

In order to identify the failure mode of the sandwich structures, the stresses in the core and facings have to be determined. In addition to this, designing a sandwich panel in terms of its geometrical sizes depends upon the critical stress values. The ratio of facing to core thickness (t/c) or facing to span length (t/l) can determine the core shear and/or facings stresses as well as the failure mode. For instance, Equation 13, given in the Material and Method section, provides to obtain a distinct span length for the transition of failure mode from core shear to face sheet. Therefore, the results of long-span beam sandwiches were also discussed.

As seen from Table 4.15, the core shear and face sheet ultimate-stress values of the sandwich panels decrease with the core thickness increment. Because, the increase of the core thickness reduces facing to core thickness ratio (t/c), and the face sheets become weaker. Thus, the structure fails due to face sheet compressive failure after the indentation of both core and facing material. As given in Table 3.2 in the previous chapter, shear strength of 48 kg/m^3 density PVC foam core is 0,55 MPa. If the calculated core shear stress is above 0,55 MPa, then it is expected that sandwich panels will fail based on core shear failure mode. And according to ASTM C393 Standard, short-span beam sandwiches are expected to fail due to core shear whereas long-span beam structures should fail due to face sheet failure according to ASTM D 7249. Daniel and Gdoutos (2009) also stated that short-span specimens were mainly exposed to shear, and the core shear failure was obtained as a primary failure mode since the maximum shear stress reached the shear strength of the core material, which is the critical value. When the core

shear stress values are compared to shear strength properties of PVC C70.48 foam core material (0,55 MPa), the sandwiches having 20 mm and 30 mm core thickness cannot reach the critical value of the shear strength because of the lower face sheet strength. Therefore, 10 mm thick core sandwich structures are more likely to fail based on the core shear failure. Due to reduced face sheet strength with the increase of the core thickness, the failure of sandwiches has occurred as face compression and/or indentation. This situation also matches with the load-deflection curves of the sandwich panels. It was also indicated by Styles et al. (2007) that occurrence of core failure according to increased core thickness might be a reason for the reduction of facing stress.

When the data in Table 4.15 are evaluated, it can be seen that core shear stress has a higher slope in between the core thickness of 20 mm and 30 mm than that of from 10 mm to 20 mm. In the first part, from 10 mm to 20 mm core thickness, core shear stress of WM sandwich panels decreased 16,45% whereas the reduction was 33,85% between 20 mm and 30 mm core thickness from. The higher reduction is related to the failure of the sandwich specimen.

On the other hand, the wire mesh sheets provided expected core shear failure mode according to ASTM C393 Standard for the short-span beam sandwich structures. The use of the wire mesh sheets for laminations of facings in sandwich structures increased the core shear stress and provided the ability of the interphase to transfer shear stress between the facings, and thus helped to stabilize the facings with the core material. With the aid of the wire mesh sheets, core shear becomes a dominant failure mode for 10 mm thick core sandwich panels. Especially, 100-mesh, located under the first carbon fiber fabric in the face sheet (M1), provided better results for each of the core thicknesses. When compared to WM sandwiches, 100M1 configuration increased the core shear stress by 6,28%, 4,42%, and 12,71% for 10 mm, 20 mm, and 30 mm core thickness, respectively. In addition, 200-mesh located similar to 100-mesh size also increased core shear stress by 6,28%, especially for 10 mm core thickness.

The results of long-span sandwich panels were found closer to that of short-span sandwiches for core shear stress. However, the facing stresses were found higher for long-span sandwiches. Figure 4.62 presents the core shear and facing stresses of both short and long beam WM sandwiches comparatively. The results, which are provided in Figure 4.62, are calculated based on the ASTM approach.

Table 4.15. Core shear and facings ultimate stress values of the sandwich panels based on both experimental and analytical approaches

Sandwich code	Core shear ult. stress (MPa)		Top facing ult. strength (MPa)		Lower facing ult. strength (MPa)	
	Exp.	Analyt.	Exp.	Analyt.	Exp.	Analyt.
WM.T10.S15	0,541	0,584	49,18	49,13	50,40	50,46
100M1.T10.S15	0,575	0,626	47,87	47,64	53,86	54,12
100M2.T10.S15	0,571	0,624	47,66	47,48	52,31	52,51
100M3.T10.S15	0,600	0,656	43,16	42,67	56,11	56,76
200M1.T10.S15	0,575	0,623	50,60	50,48	53,77	53,89
200M2.T10.S15	0,557	0,604	49,63	49,53	52,11	52,21
200M3.T10.S15	0,595	0,651	44,13	43,69	55,72	56,29
WM.T20.S15	0,452	0,470	41,24	41,24	41,24	41,24
100M1.T20.S15	0,472	0,492	38,02	37,90	44,20	44,34
100M2.T20.S15	0,460	0,481	34,13	33,97	42,04	42,24
100M3.T20.S15	0,467	0,491	30,77	30,52	43,30	43,65
200M1.T20.S15	0,451	0,472	38,56	38,50	41,38	41,44
200M2.T20.S15	0,410	0,430	35,93	35,88	38,63	38,69
200M3.T20.S15	0,450	0,473	34,59	34,45	41,34	41,50
WM.T30.S15	0,299	0,307	27,30	27,29	27,98	27,99
100M1.T30.S15	0,337	0,347	27,50	27,46	30,47	30,53
100M2.T30.S15	0,318	0,327	25,65	25,61	28,74	28,79
100M3.T30.S15	0,328	0,338	23,40	23,31	30,72	30,84
200M1.T30.S15	0,322	0,331	28,45	28,43	30,23	30,26
200M2.T30.S15	0,292	0,300	24,90	24,87	27,39	27,42
200M3.T30.S15	0,327	0,336	23,75	23,66	30,58	30,70
WM.T10.S20	0,528	0,573	64,36	64,30	65,97	66,03
100M1.T10.S20	0,562	0,612	62,46	62,16	70,26	70,61
200M1.T10.S20	0,549	0,596	64,52	64,36	68,55	68,71
WM.T20.S20	0,433	0,451	52,77	52,77	52,77	52,77
100M1.T20.S20	0,456	0,476	49,02	48,86	56,99	57,17
WM.T30.S20	0,299	0,307	36,43	36,42	37,34	37,36
100M1.T30.S20	0,321	0,331	34,97	34,92	38,76	38,82

As seen from Figure 4.62, there is a very slight change between short and long-span sandwiches for evaluating the core shear stresses between them. For instance, as seen in Table 4.15, the core shear stress of the WM.T10.S15 sandwich panel is just 2,40% higher than the WM.T10.S20 sandwich panel. However, the increase of facing stress of WM sandwiches in the case of testing under long-span was 30,87%, 27,96%, and 33,44% for the core thickness of 10 mm, 20 mm, and 30 mm, respectively. As reported in the literature (Carlsson and Kardomateas, 2011) larger span length is required to obtain a transition from core shear to face yield and/or face compressive failures. Therefore, it was found that the increase of support span length for sandwich structures has resulted in higher facing stresses than the short-span specimens.

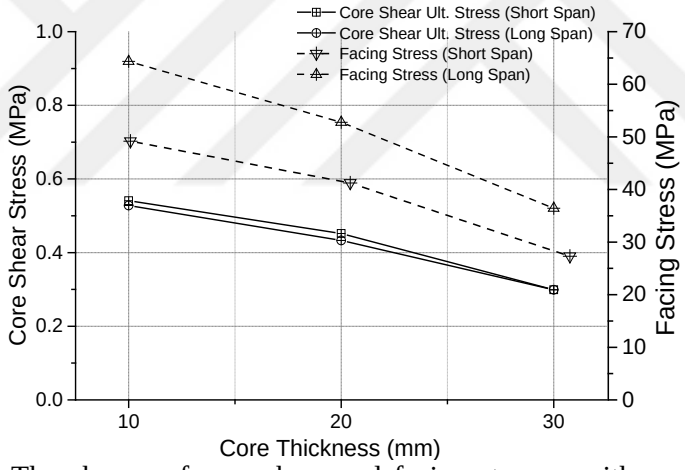


Figure 4.62. The change of core shear and facing stresses with respect to (wrt) core thickness of WM sandwich panels

4.7.3. Bending Strength of the Core and Maximum Stress in the Sandwich Facings Based on Analytical Approach

The bending strength of the core and maximum facing stress is the function of the core and facing modulus, the maximum bending moment of the structure, bending rigidity, and core and facing thickness. These are determined to evaluate

both core and facing flexural properties. The analytical approaches provided in Chapter 3 were used to calculate (M_{max}, σ_{max} and $\sigma_{f,max}$). Table 4.16 illustrates the maximum bending moment (M_{max}), core bending strength (σ_{max}), and facing maximum stress ($\sigma_{f,max}$) of the sandwich panels which are calculated based on analytical approaches. The maximum bending moment carrying capacity increases due to an increase in the core thickness, which also increases the load-carrying capacity. But the results indicated that the bending moment increases drastically from 10 mm to 20 mm thick core whereas the increment from 20 mm to 30 mm is carried out slightly as shown in Figure 4.63. For example, the maximum bending moment was obtained 65,26% higher in 20 mm thick core WM sandwiches when compared that of 10 mm thick core. However, there is almost no change between 20 mm and 30 mm thick core sandwich panels. On the other hand, 100M1.T20.S15 sandwich panels have 61,49% higher bending moment than 100M1.T10.S15 sandwiches whereas 100M1.T30.S15 sandwich panels have only 7,61% higher bending moment than 100M1.T20.S15 sandwich specimens. In general, all wire mesh sheet configurations have contributed bending moment when compared to WM sandwiches. 100M1 configuration exhibited the most significant features because it contributed to the maximum bending moment of the sandwich panels by 7,25%, 4,80%, and 13,29% for 10 mm, 20 mm, and 30 mm thick core sandwiches, respectively.

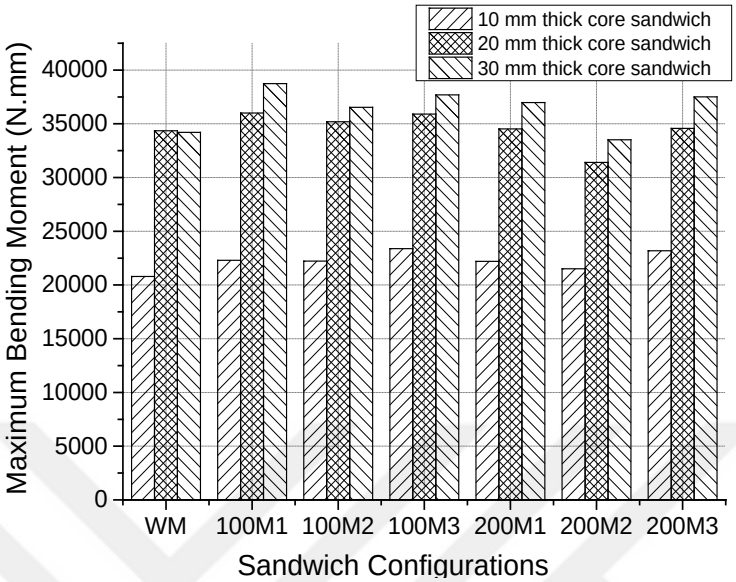


Figure 4.63. Maximum bending moment of the sandwiches wrt core thickness

In addition, long-span beam sandwiches were also yielded higher bending moment although the maximum bending load capacity of the specimens was decreased compared to the short-span length specimens. This is due to increased support span length under three-point bending tests. For instance, when the Table 4.16 is scrutinized, it can be seen that the increase in bending moment of WM sandwiches was 28,69% (for 10 mm), 26,29% (for 20 mm) and 33,47% (for 30 mm) in long-span beam sandwiches compared to short-span specimens. The same effect was also obtained inversely for both the core bending strength and sandwich facing stress. As the maximum bending moment increases according to core thicknesses, core bending strength, and laminate facing stress decreases. The relationship between them is presented in Figure 4.65 for 100M1 short-span sandwich specimens as an example.

Figure 4.64 shows the effect of both 100M1 configuration and core thickness on the maximum bending moment of the sandwich panels according to the span length. As it is seen, the sandwich specimens show similar trends for all core thicknesses for both WM and 100M1 configurations. The increased span

length resulted in a higher bending moment. In addition to this, when the Table 4.16 is examined, it can be realized that both core bending strength (σ_{max}) and maximum facing stress ($\sigma_{f,max}$) of the sandwiches have trend similarity to that of the maximum bending moment (M_{max}).

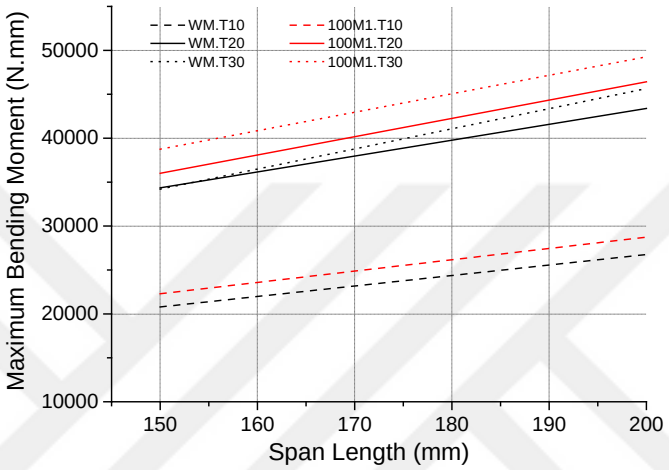


Figure 4.64. Maximum bending moment (analyt.) wrt span length of sandwich panels

Table 4.16. Maximum bending moment, core bending strength and maximum facing stress of the sandwich panels according to analytical calculations

Sandwich panels	M_{max} (N.mm)	σ_{max} (MPa)	$(\sigma_f)_{max}$ (MPa)
WM.T10.S15	20788,50	0,0311	52,86
100M1.T10.S15	22296,00	0,0292	51,58
100M2.T10.S15	22219,5	0,0323	50,83
100M3.T10.S15	23385,38	0,0313	45,78
200M1.T10.S15	22205,25	0,0320	53,17
200M2.T10.S15	21510,00	0,0297	50,33
200M3.T10.S15	23190,75	0,0324	47,70
WM.T20.S15	34355,63	0,0133	42,77
100M1.T20.S15	36004,88	0,0123	40,83
100M2.T20.S15	35188,50	0,0133	39,46
100M3.T20.S15	35907,38	0,0127	34,54
200M1.T20.S15	34526,25	0,0126	39,62
200M2.T20.S15	31412,63	0,0113	36,02
200M3.T20.S15	34573,50	0,0127	34,91
WM.T30.S15	34199,63	0,0058	27,90
100M1.T30.S15	38744,63	0,0058	28,81
100M2.T30.S15	36535,88	0,0061	26,86
100M3.T30.S15	37688,25	0,0059	23,78
200M1.T30.S15	36973,5	0,0061	28,43
200M2.T30.S15	33511,13	0,0053	25,19
200M3.T30.S15	37511,63	0,0061	24,84
WM.T10.S20	26753,50	0,0400	68,03
100M1.T10.S20	28744,00	0,0376	66,50
200M1.T10.S20	28310,00	0,0407	67,79
WM.T20.S20	43386,50	0,0167	54,01
100M1.T20.S20	46420,00	0,0158	52,65
WM.T30.S20	45647,50	0,0078	37,24
100M1.T30.S20	49267,00	0,0074	36,63

As seen from Figure 4.65, the maximum bending moment nonlinearly increases. Because when the core thickness increases at the constant facing

thickness, the sandwich structure highly resists bending and fails due to indentation. Therefore, it cannot carry higher loads because of the weaker face sheet. On the other hand, maximum facing stress linearly decreases whereas the bending strength of foam core nonlinearly decreases with respect to the core thickness. Similar trends have also been obtained in the case of testing the specimens under long-span length.

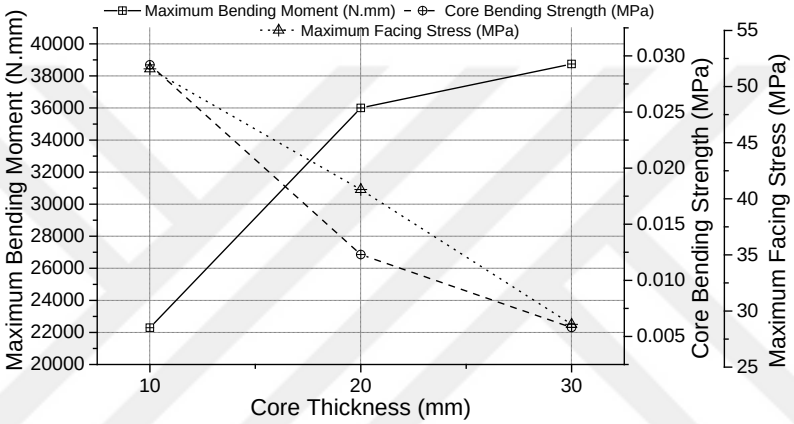


Figure 4.65. The change of maximum bending moment, core bending strength and maximum sandwich facing stress (analyt.) of the short-span 100M1 sandwich panels wrt core thickness

4.7.4. Evaluation of Flexural Stiffness, Transverse Shear Rigidity, and Core Shear Modulus based on ASTM D7250 Standard

ASTM D7250 Standard provides equations to calculate the flexural stiffness, transverse shear rigidity, and core shear modulus as discussed in Material and Method sections. According to Equations 3.9, 3.10, and 3.11, the target properties (flexural stiffness, transverse shear rigidity, and core shear modulus) can be calculated. ASTM D7250 Standard suggests how to calculate these bending characteristics based on the applied bending force and corresponding mid-span deflection values obtained from two different span length configurations. To achieve these, the force and mid-span deflection values have to be determined

appropriately such as selecting the values at the yield points since the stiffness properties can be obtained from the linear elastic region of the material. The application of the approach based on two different loading conditions has been encountered in the recent literature (Sadeghian et al., 2018; Chtourou et al., 2018; McCracken and Sadeghian, 2018).

According to the ASTM approach, provided in Chapter 3, the flexural stiffness (D), the transverse shear rigidity (U), and the core shear modulus (G) were calculated and given in Table 4.17. The standard deviations are written in parenthesis below the corresponding value. The application of the ASTM approach by using Equations 3.9, 3.10, and 3.11 are given below.

In equation 3.9, D is flexural stiffness, $P1/\Delta_1$ and $P2/\Delta_2$ are the initial stiffness of three-point bending results of sandwich panels according to the support span length of 150 mm and 200 mm, respectively. S1 and S2 are the span lengths. For instance, evaluation of 10 mm thick core WM sandwich panels, a certain point from a straight line of linear elastic range of the sandwich specimens was taken for both span lengths by using the load-deflection curves as presented in Figure 4.16 and in Figure 4.46. As an example, an approximate bending load of 120 N was selected. It was 120,084 N for 150 mm span length, and 120,004 for 200 mm span length. And the corresponding deflections were 0,547 mm and 0,750 mm, respectively. By substituting the values into Equation 3.9;

$$D = \frac{120{,}084.150^3(1-200^2/150^2)}{48.0{,}547.(1-120{,}084.150.0{,}750/120{,}084\ .200.0{,}750)} = 119{,}55\ N.m^2$$

Flexural stiffness, D, is found as 119,55 N.m^2.

By using the same data, transverse shear rigidity (U) can also be calculated according to Equation (3.10), and it was found as 10528,12 N.

$$U = \frac{120{,}084.150\,.\,(150^2/200^2 - 1)}{4.0{,}547.\left((120{,}084\,.\,150^3.\,0{,}75/120{,}084.\,200^3.\,0{,}547) - 1\right)} = 10{,}5\ kN$$

The core shear modulus, G, can be found from Equation (3.11) as follow;

$$G = \frac{10528{,}12.\,(10{,}31 - 2.0{,}82)}{(10{,}31 - 0{,}82)^2.\,50} = 19{,}02\ MPa$$

Where G is obtained as 19,02 MPa.

Table 4.17. Flexural stiffness, transverse shear rigidity and core shear modulus of the sandwich panels based on ASTM approach

Sandwich Panel	Flexural Stiffness (N.m^2)	Transverse Shear Rigidity (N)	Core Shear Modulus (MPa)
WM.T10	119,79 (2,32)	10482,90 (61,74)	18,94 (0,11)
100M1.T10	135,81 (4,06)	10519,22 (65,17)	18,69 (0,09)
200M1.T10	122,80 (4,50)	10858,86 (66,21)	19,43 (0,11)
WM.T20	436,35 (14,43)	14199,63 (38,69)	13,41 (0,03)
100M1.T20	508,79 (14,21)	14506,15 (55,75)	13,67 (0,05)
WM.T30	1033,80 (47,83)	18589,17 (40,83)	11,87 (0,03)
100M1.T30	1171,98 (83,81)	19541,92 (97,39)	12,40 (0,06)

As seen in Table 4.17, flexural stiffness strongly depends on the sandwich core thickness. When comparing the WM sandwiches, the increase in core thickness from 10 mm to 20 mm yielded 264,26% higher flexural stiffness. From 20 mm to 30 mm core, the increment in bending rigidity was obtained as 136,92%. In other words, compared to 10 mm thick core sandwiches, a 20 mm thick core sandwich panel contributed 3,64 times higher flexural stiffness whereas 30 mm thick core sandwiches contributed 8,63 times higher flexural stiffness. On the other hand, 100-mesh wire sheets stacked under the first carbon fiber layer of top facing (100M1 configuration) improved the bending rigidity of sandwich panels by 13,37%, 16,60% and 13,37% for 10 mm, 20 mm and 30 mm thick core sandwiches compared to that of each WM configuration. The configuration of 200M1

contributed to bending rigidity by 2,51% compared to 10 mm thick core WM sandwich panels. Overall, the increase of core thickness from 10 mm to 20 mm (two times) provided 3,64 times higher bending rigidity. The above findings match with the findings of the literature. In the literature, glass fiber skins with honeycomb core sandwich panel provided 3,65 times higher stiffness in the case of using a 25 mm honeycomb instead of 12 mm (Sadeghian, 2018). Bezazi et al. (2007) investigated the mechanical characteristics of glass/epoxy facing and PVC foam core (80 kg/m^3) sandwich panel. While a 25 mm thick core sandwich resulted in an initial stiffness of 185,01 N/mm, a 15 mm thick core sandwich resulted in an initial stiffness of 193,05 N/mm where the difference is only 4,35%. The skin thickness effect was investigated by Kumar and Soragaon (2014). There were two different configurations. These are 1 mm glass fiber skins with 16 mm polyurethane (PU) core and 2 mm glass fiber skins with 18 mm PU core. Increasing skin thickness with similar core material resulted in two times higher bending stiffness. Therefore, it can be concluded that increasing core thickness is more effective than that of the face sheet for further improvement of flexural stiffness. In addition to this, increasing the core thickness instead of the face sheet provides less weight penalties.

The transverse shear rigidity was obtained as 10,48 kN, 14,12 kN, and 18,59 kN for 10 mm, 20 mm, and 30 mm thick core WM sandwich panels, respectively. While the increase is 34,69% from the core thickness of 10 mm to 20 mm, it is found as 31,66% from the core thickness of 20 mm to 30 mm. Contrarily to both flexural stiffness and transverse shear rigidity, core shear modulus was decreased according to core thickness. For the case of WM sandwiches, the reduction was 29,20%, and 11,48% for the core thickness values from 10 mm to 20 mm and 20 mm to 30 mm, respectively. However, the wire mesh sheets did not contribute much to the transverse shear rigidity and to the core shear modulus as much as the flexural stiffness. For instance, the configuration of the 100M1 sandwich panel increased the transverse shear rigidity by 5,13% and the core shear

modulus by 4,67% for 30 mm thick core sandwich panel whereas it was 2,74% and 1,94% for 20 mm thick core sandwiches.

Figures 4.66 to 4.68 present flexural stiffness, transverse shear rigidity, and core shear modulus comparatively according to the core thickness of WM sandwich panels.

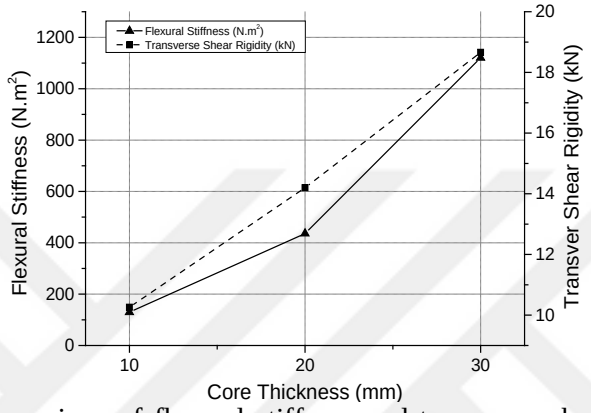


Figure 4.66. Comparison of flexural stiffness and transverse shear rigidity based on core thickness according to ASTM approach

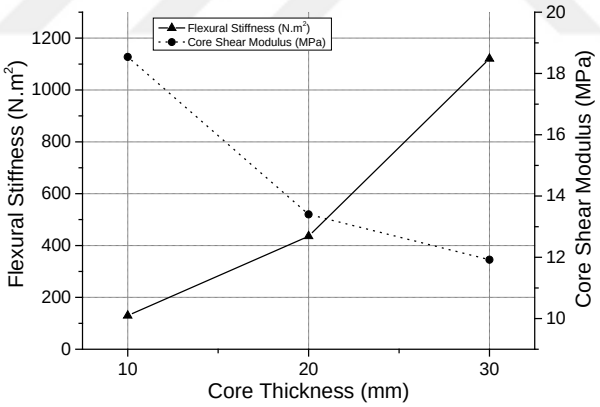


Figure 4.67. Comparison of flexural stiffness and core shear modulus based on core thickness (ASTM approach)

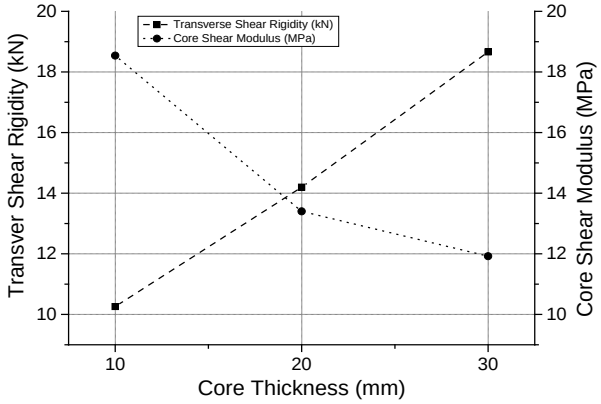


Figure 4.68. Comparison of transverse shear rigidity and core shear modulus based on core thickness (ASTM approach)

As seen from Figures 4.66 to 4.68 flexural stiffness nonlinearly increases with core thickness whereas transverse shear rigidity shows approximately linear increment according to core thickness. This is due to the effects of geometrical parameters presented in Chapter 3. On the other hand, core shear modulus decreases with respect to the core thickness. The nonlinear decrease occurs with a higher slope between the core thickness of 10 mm and 20 mm than that of 20 mm and 30 mm.

Besides the ASTM approach for evaluating the flexural characteristics of the sandwich structures, the analytical approach was also applied to predict the flexural stiffness of the specimens. In Equation (4.1) below, $(EI)_b$ is the equivalent bending rigidity and corresponds to "D" in the ASTM approach.

$$(EI)_b = D = E_f \frac{bt^3}{6} + 2bE_f t\left(\frac{c+t}{2}\right)^2 + E_c \frac{bc^3}{12} = 2D_f + D_o + D_c \quad (4.1)$$

E_f and E_c are Young's modulus of the facings and the core, respectively, b is the width, t and c are the facing and core thicknesses, respectively. $2D_f$ is the rigidity of the facings from the neutral axis, D_o is the contribution to bending stiffness of the facings from the neutral axis of the symmetrical sandwich in the core, and D_c is the core bending stiffness from its neutral axis, respectively. If the total sandwich

thickness is highly greater than the facing thickness, then the first and last terms can be neglected (Chemami et al., 2012). Li and Wang (2017) explained the reason for neglecting these terms by making optimal geometric design.

According to the equation above, the flexural stiffness of the sandwiches was calculated and given in Table 4.18. The sandwiches' facing modulus data, provided in the section of tensile test results, were used whereas core Young's modulus was obtained from the manufacturer technical data sheet (TDS, Airex C70).

Table 4.18. The flexural stiffness of the sandwich beams based on the analytical approach

Sandwich Facing Configuration	Flexural Stiffness (N.m^2)		
	10 mm thick core	20 mm thick core	30 mm thick core
WM	111,16	430,89	976,33
100M1	126,99	488,30	1103,28
100M2	114,42	439,60	993,05
100M3	124,37	470,90	1058,36
200M1	115,52	445,56	1007,83
200M2	120,51	463,89	1048,53
200M3	119,00	452,76	1019,33

As it is seen from Table 4.18 the flexural stiffness values of WM sandwiches were found as 111,16 N.m^2, 430,89 N.m^{2,} and 976,33 N.m^2. As the core thickness of sandwich specimens increases, the flexural stiffness drastically increases. Increasing the core thickness two times improves flexural stiffness 3,88 times whereas three times increase of core thickness yielded 8,78 times higher results for the flexural stiffness. However, the increment has become nonlinear and it was less for the core thickness of between 20 mm and 30 mm than that of 10 mm and 20 mm. Approximately 2,25 times higher bending rigidity was obtained in the

case of using a 30 mm thick core instead of 20 mm. Figure 4.69 shows the flexural stiffness of the produced sandwich panels according to the core thickness and wire mesh configurations.

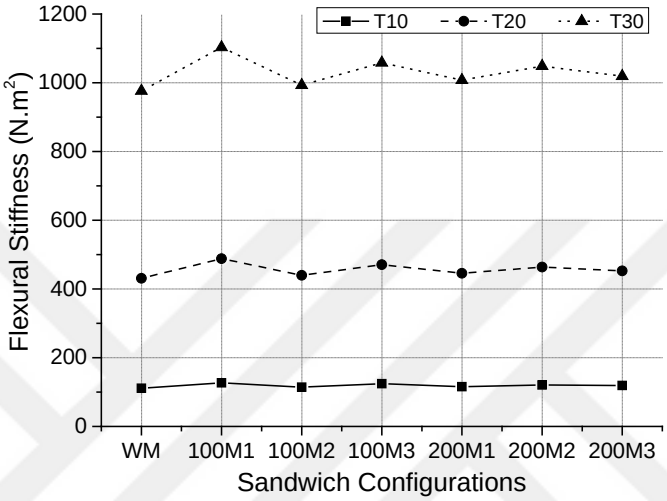


Figure 4.69. Flexural stiffness of the produced sandwich panel based on analytical approach

As presented in Figure 4.69, wire mesh sheets show different effects for each of the configurations. Except for 100M1 configuration, the results are nearly very close to each other. However, 100M1 configuration improved the flexural stiffness of the structures by 14,24%, 13,32%, and 13,00% per core thickness when compared to WM sandwiches. On the other hand, 100M1 configuration yielded 13,37%, 16,60% and 13,37% higher flexural stiffness based on experimental ASTM approach. The difference between the analytical and experimental approaches is exhibited in Figure 4.70. The experimental flexural stiffness values are in good agreement with analytically obtained results, although experimentally obtained results are slightly higher. The maximum difference between the results is 7.20% for 10 mm thick core WM sandwiches, and the rest are smaller. The percent differences between the experimental and the analytical approaches are indicated for each of the sandwich configurations in Figure 4.70. In fact, analytically

obtained results are expected to be higher than that of the experimental method since the analytical approach ignores the manufacturing errors and assumes perfect bonding in lamination. However, it might be due to the fact that the experimental approach is based on the deflection and force data selected from the initial linear region of the load-deflection curve, and ASTM D7250(D7250/D7250M-06, 2006) allows us to obtain these data with a maximum error of 10%. Therefore, this is a typical case that we expect and see in the recent literature (A. McCracken & P. Sadeghian, 2018; Sadeghian et al., 2016; R. S. Sharma & Raghupathy, 2009).

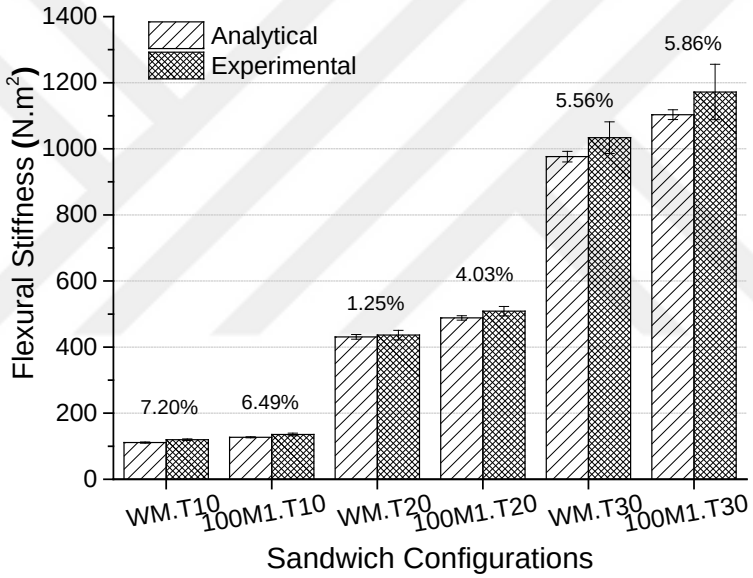


Figure 4.70. Differences of flexural stiffness values between analytical and experimental approaches

4.8. Examination of Failure Behavior of the Sandwich Panels

In this study, woven plain carbon fiber fabrics (200 g/m^2) and industrial, rigid, polyvinylchloride (PVC) having 48 kg/m^3 density were used to construct sandwich structures. Three different core thicknesses (10 mm, 20 mm, and 30 mm) were used. In order to determine the failure behavior of the panels, three-point bending tests were performed under 150 mm and 200 mm span lengths,

respectively. In addition, wire mesh sheets were used within the facings in order to examine the failure behavior of the developed sandwich panels. As also provided in the literature (Styles et al., 2007; Chemami et al., 2011; Karahan et al., 2013), sandwich panels show a linear elastic behavior from initial loading to a particular load level. This depends upon the type of constituent materials. Then it reaches to the maximum point of the load. After the peak load, a plateau is followed where the load remains approximately constant. The length of the plateau depends on the type and geometry of the core, facing thickness, and as well as the span length. At the end of the plateau, the force decreases suddenly especially for the sandwiches having fiber reinforced facing and the low-density foam core. In this study, larger plateaus were observed only for 10 mm thick core sandwich panels as presented in Figure 4.43. WM sandwiches (WM.T10.S15) suddenly failed at the end of plateau whereas the 100M1.T10.S15 still continued to carry the bending load with a decreasing slope in force. Also, other configurations such as 100M3, 200M1, and 200M3 improved the failure behavior for 10 mm thick core sandwich panels.

In the case of using thicker core such as 20 mm and/or 30 mm, there was almost no plateau and the sudden failure occurred after the load was reached to the peak. In these sandwich panels, the linear elastic range was relatively not long and a nonlinear increase was available till the maximum bending load. The nonlinear behavior depends upon the foam core properties under the effect of core shearing forces and/or indentation (Bezazi et al., 2007).

Failure of the sandwich structures may occur mainly due to the facing yield, core shear, indentation, facings debonding and facing wrinkling (Ashby et al., 2000; Daniel et al., 2002). The sandwich constituent materials' properties, geometric dimensions, and types of loading are affecting factors for the initiation and growth of the failure modes (Daniel et al., 2002). In this study, core shear and indentation were found as primary failure modes for the sandwich panels. Ashby et al. (2000) provided schematic representation of failure modes as shown in Figures 4.71 and 4.72 for core shear and indentation, respectively.

As seen in Figure 4.71, two different failure mechanisms were defined for the core shear. In Figure 4.71(a) the formation of plastic hinges occurs at mid-span under the loading roller whereas in Figure 4.71(b) the plastic hinges occur both at mid-span under loading roller and outer support rollers.

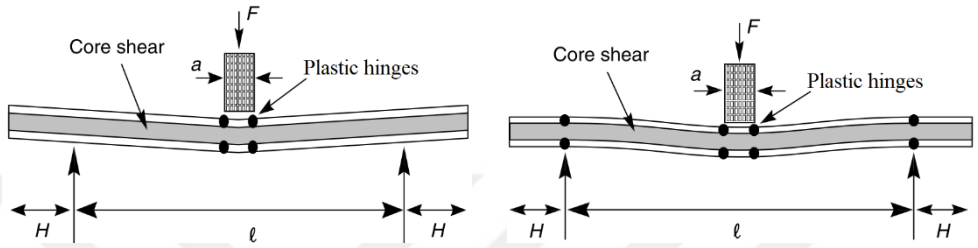


Figure 4.71. Failure mechanisms of core shear modes; a) Case I, b) Case II (Ashby et al., 2000)

The collapse force, F, was defined by Ashby et al. (2000) as the failure force by core shearing and it is calculated according to Equations (4.2) and (4.3) for the first and second cases, respectively.

$$F_I = \frac{2bt^2}{l}\sigma_y^f + 2bc\tau_y^c\left(1 + \frac{2H}{l}\right) \tag{4.2}$$

$$F_{II} = \frac{4bt^2}{l}\sigma_y^f + 2bc\tau_y^c \tag{4.3}$$

Where F_I and F_{II} are the collapse forces for case I and case II, respectively. And the notation b, t, c, and l denote the sandwich width, facing thickness, core thickness, and span length, respectively. σ_y^f and τ_y^c denote tensile yield and core shear yield strengths, respectively. τ_y^c was obtained from the manufacturer data sheet (TDS, Airex C70) whereas σ_y^f is calculated based on the following analytical equations provided by Kaw (2006);

$$\sigma_2^f = E_2.\varepsilon_2^{ult} \tag{4.4}$$

Where, σ_2^f is the transverse tensile strength of the facing material, E_2 and ε_2^{ult} are transverse modulus and transverse ultimate strain of the facing, respectively. Here, facing yield strength (σ_y^f) is taken equal to transverse tensile strength (σ_2^f) since its value is smaller than the longitudinal tensile strength as expected and taken as the critical one.

$$E_2 = \frac{E_f.E_m}{V_f.E_m + E_f.(1-V_f)} \tag{4.5}$$

$$\varepsilon_2^{ult} = \left[\frac{d}{s}.\frac{E_m}{E_f} + \left(1 - \frac{d}{s}\right).\varepsilon_m^{ult}\right] \tag{4.6}$$

Where, E_m and E_f are moduli of matrix and fiber elements, respectively, ε_m^{ult} is the ultimate strain of the matrix. d/s which is the ratio of fiber diameter to fiber spacing dependent upon V_f and it was defined by Kaw (2006) for circular cross-sectional fiber with square array orientation as follow;

$$\frac{d}{s} = \left(\frac{4V_f}{\pi}\right)^{1/2} \tag{4.7}$$

Figure 4.72 presents the schematic view of the indentation failure mode. In this kind of failure mode, the formation of plastic hinges occurs on top facing of the sandwich structures at both under the loading roller and adjacent to it. In this figure, a denotes loading roller diameter, λ is the wavelength. The collapse load, F, for indentation failure was defined by Equation (4.8) (Ashby et al., 2000).

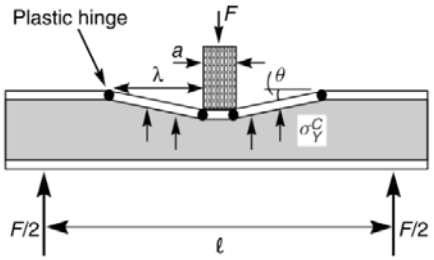


Figure 4.72. Indentation failure mode (Ashby et al., 2000)

$$F = (2\lambda + a)b\sigma_y^c + \frac{4.M_P}{\lambda} \quad (4.8)$$

$$M_P = (b.t_f)/4 \quad (4.9)$$

In order to decide the failure modes of the sandwiches, images of the bending behavior of the specimens were captured periodically by a camera during three-point bending tests. For instance, the bending behavior of WM sandwiches having a 10 mm thick core under 150 mm support span length was obtained very similar to the core shear mode of case II as shown in Figure 4.71. The images in Figure 4.73 show the time-dependent behavior of sandwiches under bending loading progressively.

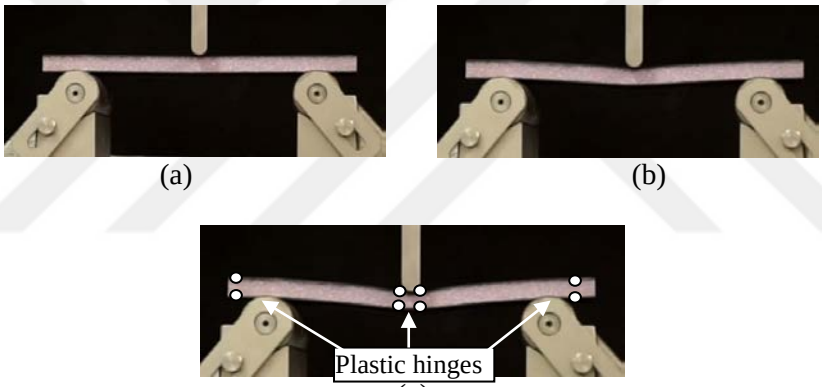


Figure 4.73. Progressive representation of bending behavior of WM.T10.S15 sandwich panel

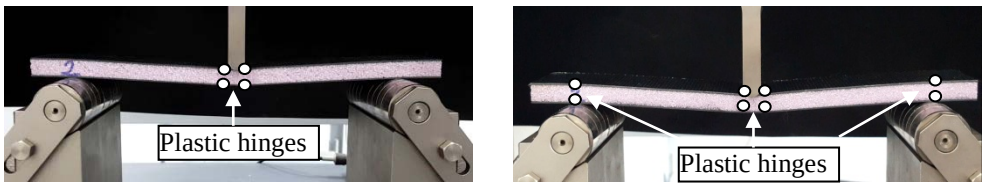
As seen in Figure 4.73, the WM.T10.S15 sandwich panel was being exposed to core shear such as in case II of Figure 4.73. The collapse force, F_{II} is calculated according to (4.3). The yield strength of the facing material was determined from the analytical equations provided above and found as 46,63 MPa for the facings of the WM.T10.S15 sandwich. Shear strength of the core material was taken as 0,55 MPa (TDS, Airex C70).

$$F_{II} = \frac{4.50.0{,}82^2}{150}.46{,}63 + 2.50.9{,}5.0{,}55 = 41{,}81 + 522{,}5 = 564{,}31\ N$$

The calculated force, 564,31 N is the failure load of the sandwich due to the core shear. In the previous sections, the average of the maximum bending load was found as 554,36 N for WM.T10.S15. This means that these two results are in good agreement, and the failure load has been predicted analytically based on the core shearing. As mentioned before, 10 mm thick core sandwich panels have large plateaus over a long displacement distance after the maximum load was reached. While the WM.T10.S15 sandwich panel showed a decreasing slope throughout the displacement distance till the sudden drop, wire mesh sandwiches provided both constant load in that region and prevented sudden drop.

The bending failure behavior of long-span beam sandwich panels is found to resemble more likely to core shear mode of the case I as given in Figure 4.71 especially for WM.T10.S20 sandwich panel. However, for 100M1.T10.S20, and 200M1.T10.S20 panels, the actual conditions were core shear mode of case II. As shown from Figure 4.74, while the plastic hinges just formed below the upper loading roller for WM.T10.S20, additional plastic hinges were formed at outer supports for 100M1.T10.S20, and 200M1.T10.S20 sandwich panels.

The collapse forces were calculated for 10 mm thick sandwich panels and given in Table 4.19 together with their maximum loads.



(a) (b)

Figure 4.74. Bending behavior of sandwich panel; a) WM.T10.S20, b) 100M1.T10.S20

Most portion of the collapse force was carried by the core material as the sandwich specimens were exposed to transverse shear forces, and the failure was developed due to core shear as discussed in the literature (Ashby et al., 2000).

A collapse mechanism map was prepared by Ashby et al. (2000) that specifies the boundaries of failure modes. According to the failure map given in Figure 4.75, 10 mm thick core sandwiches failed in core shear region, 20 mm thick core sandwiches under 150 mm span length sandwiches failed at the boundary of core shear and indentation intersect, but 200 mm span length sandwich panels failed in core shear region of the map. Lastly, 30 mm thick core sandwiches failed in the indentation region of the map. In that figure, t/c and c/l are facing to core thickness ratio and core thickness to span length ratio, respectively.

Table 4.19. Maximum bending load and collapse force by shear failure for 10 mm thick sandwich panels

Sandwich panel code	Max. Bending Load P_{max} (N) (Exp.)	Collapse Force, F (N) (Analyt.)
WM.T10.S15	554,36	564,31
100M1.T10.S15	594,56	573,40
100M2.T10.S15	592,52	573,62
100M3.T10.S15	623,61	593,74
200M1.T10.S15	592,14	569,78
200M2.T10.S15	573,6	571,80
200M3.T10.S15	618,42	588,04
WM.T10.S20	535,07	564,31
100M1.T10.S20	574,88	573,40
200M1.T10.S20	566,20	569,78

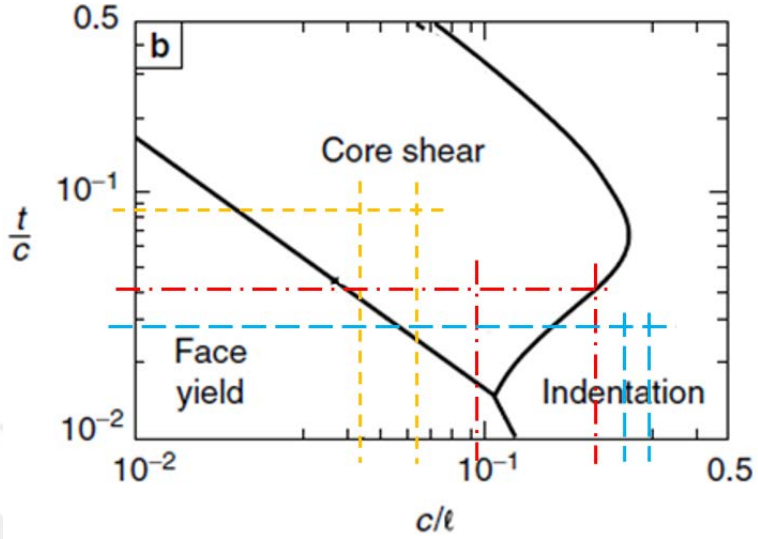


Figure 4.75. Failure mechanism map of the sandwich beams (Ashby et al., 2000) (yellow: 10 mm thick core sandwiches, red: 20 mm thick core sandwiches, blue: 30 mm thick core sandwiches; right-hand lines short-span specimens, left-hand lines: long-span specimens)

The failure modes of both the core shear and the indentation models were applied for 20 mm thick core sandwich panels as they were laid to the boundary of both core shear and indentation regions on the map given above. In order to predict the core shear collapse force, the core shear mode of case II was applied (4.3). However, the analytical model for the indentation provided by Ashby et al. (2000) did not consider the span length during finding the collapse failure force of the sandwich panels. Therefore, a different model provided by Steeves and Fleck (2004) was also used (Equation 4.10) for evaluation of the indentation failure load, P_i. The model given by Steeves and Fleck (2004) also considers the span length.

$$P_i = bt_f \left(\frac{\pi^2 \sigma_c^2 E_f d}{3L}\right)^{1/3} \tag{4.10}$$

For instance, when the Equation (4.10) is solved for WM.T20.S15, the indentation load was found as;

$$P_i = bt_f\left(\frac{\pi^2\sigma_c^2 E_f d}{3l}\right)^{1/3} = 50.0{,}82.\left(\frac{\pi^2.0{,}6^2.50750.20{,}32}{3.150}\right)^{1/3} = 824{,}83N$$

According to Ashby's model from Equation (), the indentation load was found as 955,67 N and is closer to maximum bending load of WM.T20.S15 sandwich panel that was 916,15 N. On the other hand, core shear collapse force was calculated as 1114,96 N according to case II of the core shear failure mechanism. Based on the bending behavior of WM.T20.S15, its bending behavior looks like core shear followed by the indentation. Figure 4.76 shows the bending behavior of WM.T20.S15. The analytical collapse failure force (both core shear and indentation modes) and the experimental maximum bending load were given in Table 4.20 for 20 mm thick core sandwich panels.

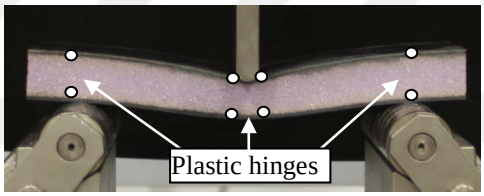


Figure 4.76. Bending behavior of WM.T20.S15

Table 4.20. Maximum bending load and collapse force by shear and indentation failures for 20 mm thick sandwich panels

Sandwich panel code	Experimental Approach	Analytical Approaches		
	Max. Bending Load P_{max} (N)	Collapse Force, F (N) (core shear mode II)	Collapse Force, F (N) (indentation) (Ashby)	Collapse Force, F (N) (indentation) (Steeve and Fleck)
WM.T20.S15	916,15	1114,96	955,67	824,83
100M1.T20.S15	960,13	1123,10	1015,75	913,88
100M2.T20.S15	938,36	1124,67	1026,79	888,73
100M3.T20.S15	957,53	1142,45	1141,56	1004,23
200M1.T20.S15	920,70	1118,72	984,10	866,96
200M2.T20.S15	837,67	1123,00	1015,09	891,83
200M3.T20.S15	921,96	1136,60	1105,63	960,52
WM.T20.S20	867,73	1104,34	955,67	749,41
100M1.T20.S20	928,4	1110,45	1015,75	830,31

In order to predict the failure load of 30 mm thick core sandwich panels, the bending behavior was observed as presented in Figure 4.77. Indentation failure mode was observed for both short and long-span sandwich specimens. The predicted failure loads were calculated based on the Equations (4.8 and 4.10) and given in Table 4.21 together with the experimental maximum bending load. As seen from the table, the experimental results are verified since they were matched well to the analytical models. However, although the specimens failed due to indentation, wire mesh sheets have favorably affected the bending behavior by preventing the sudden drop in force.

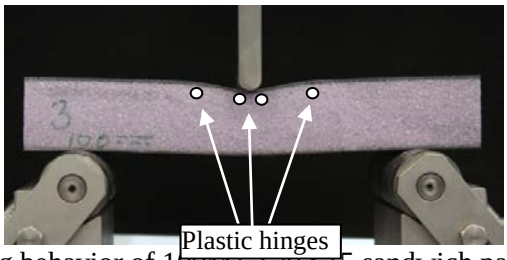


Figure 4.77. Bending behavior of 100M1.T30.S15 sandwich panel

Table 4.21. Maximum bending load and collapse force by shear and indentation failures for 30 mm thick sandwich panels

Sandwich panel code	Max. Bending Load P_{max} (N)	Collapse Force, F (N) (indentation) (Ashby)	Collapse Force, F (N) (indentation) (Steeve and Fleck)
WM.T30.S15	911,99	952,78	945,13
100M1.T30.S15	1033,19	1022,45	1046,70
100M2.T30.S15	974,29	1018,59	1017,84
100M3.T30.S15	1005,02	1143,81	1149,18
200M1.T30.S15	985,96	997,78	993,12
200M2.T30.S15	893,63	1005,53	1021,50
200M3.T30.S15	1000,31	1107,34	1099,46
WM.T30.20	912,95	952,76	858,71
100M1.T30.S20	985,34	1022,45	950,99

Indentation failure mode can be occurred due to concentrated loads on a sandwich panel which is a serious problem for sandwich design. This type of failure was explained by Daniel et al. (2002) that it results in a local compressive failure of the core and followed by local facing bending. Fortunately, using wire mesh sheets stacked in facings can control the failure of the sandwich panel and prevent catastrophic sudden drops in bending force.

4.9. Investigation of the Sandwich Parameters with ANOVA

Sandwich parameters affecting the flexural characteristics were evaluated by using a two-way analysis of variance (ANOVA). The parameters that are core thickness, wire mesh size, and span length have been explained with their levels in Chapter 3. Response Surface Methodology (RSM) was used for mathematical modeling and statistical analysis. Central composite design (CCD) was performed to investigate both the individual effects and interactions of independent variable parameters. The analyses were carried out for the responses of sandwich weight, load carrying capacity, core shear stress, facing stress, and flexural stiffness. In addition, based on the results of the ASTM approach, transverse shear stress and core shear modulus values were also evaluated.

Tables 4.22 to 4.27 illustrate ANOVA results for the responses of sandwich weight, load carrying capacity, core shear stress, facing stress, flexural stiffness, respectively. According to the suggestion of ANOVA for the best fit of the experimental data, the reduced cubic models were constructed for sandwich weight, facing stress, flexural stiffness whereas quadratic models were constructed for load-carrying capacity, load capacity that obtained after the initiation of sudden failure of WM sandwiches, and core shear stress. As seen from the tables, when the affecting parameters were investigated, the analysis results based on the constructed models are statistically significant in the 95% confidence interval since p values are obtained lower than 0,05. As it is also seen that three models have an insignificant lack of fit which is the desired situation as suggested by Montgomery (2012). However, the quadratic models, which were constructed for load-carrying capacities, core shear stress, and load-carrying capacities after WM sandwiches underwent sudden failure, resulted in a significant lack of fit.

When Tables 4.22 to 4.27 are scrutinized, it can be noticed that the most effective parameter is the sandwich core thickness as expected. However, after WM sandwiches reached the initiation point of sudden failure, the wire mesh sheets have a considerable positive effect on the load-carrying capacities of the sandwich panels since the F-value was obtained 297,85 which is the biggest F value among all responses. Other F-values of wire mesh sheet parameters are obtained as 71,33, 13,92, 15,14, 13,48, 4,67 for rest of the responses such as sandwich weight, load carrying capacity, core shear stress, facing stress, flexural stiffness, respectively.

Since p-values for individual effects of the parameters were found lower than 0,05, each parameter has a significant effect on the bending characteristics of the sandwich panels.

The models yielded *predicted correlation coefficients* (Pred. R^2) of 0,9937 for sandwich weight, 0,9721 for load-carrying capacity, 0,9681 for load capacity at which WM sandwiches underwent sudden failure, 0,9830 for core shear stress,

0,9856 for facing stress, and 0,9971 for flexural stiffness, respectively. The *adjusted* R^2 values are in good agreement with predicted ones as shown in Table 4.28.

ANOVA results with high values of R^2 confirmed that the constructed models strongly explain the significant changes in flexural characteristics based on the design parameters. In order to predict the value of the responses, mathematical expressions were developed by regression analysis based on the constructed models. The equations are given in Table 4.29.

Table 4.22. ANOVA results for sandwich weights

Source	Sum of Squares	df	Mean Square	F-value	p-value	
Model	1080.32	7	154.33	1240.39	< 0.0001	significant
A-Core Thickness	310.64	1	310.64	2496.64	< 0.0001	
B-Wire Mesh Size	8.88	1	8.88	71.33	< 0.0001	
AB	0.5276	1	0.5276	4.24	0.0466	
A^2	2.04	1	2.04	16.36	0.0003	
B^2	221.24	1	221.24	1778.17	< 0.0001	
A^2B	6.47	1	6.47	52.01	< 0.0001	
AB^2	3.89	1	3.89	31.24	< 0.0001	
Residual	4.60	37	0.1244			
Lack of Fit	0.3486	1	0.3486	2.95	0.0945	not significant
Pure Error	4.26	36	0.1182			
Cor Total	1084.93	44				

Table 4.23. ANOVA results for load carrying capacities

Source	Sum of Squares	df	Mean Square	F-value	p-value	
Model	1.453E+06	5	2.907E+05	358.55	< 0.0001	significant
A-Core Thickness	1.180E+06	1	1.180E+06	1455.91	< 0.0001	
B-Wire Mesh Size	11282.83	1	11282.83	13.92	0.0006	
AB	1636.47	1	1636.47	2.02	0.1633	
A^2	2.361E+05	1	2.361E+05	291.21	< 0.0001	
B^2	24074.56	1	24074.56	29.70	< 0.0001	
Residual	31616.12	39	810.67			
Lack of Fit	11250.92	3	3750.31	6.63	0.0011	significant
Pure Error	20365.20	36	565.70			
Cor Total	1.485E+06	44				

Table 4.24. ANOVA results for load capacities after WM sandwiches underwent sudden failure

Source	Sum of Squares	df	Mean Square	F-value	p-value	
Model	1.931E+06	5	3.862E+05	314.74	< 0.0001	significant
A-Core Thickness	1.185E+06	1	1.185E+06	965.42	< 0.0001	
B-Wire Mesh Size	3.655E+05	1	3.655E+05	297.85	< 0.0001	
AB	459.36	1	459.36	0.3744	0.5442	
A^2	1.251E+05	1	1.251E+05	101.92	< 0.0001	
B^2	2.554E+05	1	2.554E+05	208.16	< 0.0001	
Residual	47854.46	39	1227.04			
Lack of Fit	40569.49	3	13523.16	66.83	< 0.0001	significant
Pure Error	7284.96	36	202.36			
Cor Total	1.979E+06	44				

Table 4.25. ANOVA results for core shear stress values

Source	Sum of Squares	df	Mean Square	F-value	p-value	
Model	0.4532	5	0.0906	595.05	< 0.0001	significant
A-Core Thickness	0.4429	1	0.4429	2907.41	< 0.0001	
B-Wire Mesh Size	0.0023	1	0.0023	15.14	0.0004	
AB	0.0001	1	0.0001	0.4021	0.5297	
A^2	0.0030	1	0.0030	19.65	< 0.0001	
B^2	0.0050	1	0.0050	32.65	< 0.0001	
Residual	0.0059	39	0.0002			
Lack of Fit	0.0014	3	0.0005	3.78	0.0186	significant
Pure Error	0.0045	36	0.0001			
Cor Total	0.4591	44				

Table 4.26. ANOVA results for facing stress values

Source	Sum of Squares	df	Mean Square	F-value	p-value	
Model	3350.08	7	478.58	524.67	< 0.0001	significant
A-Core Thickness	973.30	1	973.30	1067.03	< 0.0001	
B-Wire Mesh Size	12.30	1	12.30	13.48	0.0008	
AB	0.4712	1	0.4712	0.5166	0.4768	
A^2	26.52	1	26.52	29.07	< 0.0001	
B^2	2.57	1	2.57	2.82	0.1017	
A^2B	9.66	1	9.66	10.59	0.0024	
AB^2	5.88	1	5.88	6.44	0.0155	
Residual	33.75	37	0.9122			
Lack of Fit	0.4623	1	0.4623	0.5000	0.4841	not significant
Pure Error	33.29	36	0.9247			
Cor Total	3383.83	44				

Table 4.27. ANOVA results for flexural stiffness

Source	Sum of Squares	df	Mean Square	F-value	p-value	
Model	6.424E+06	7	9.177E+05	2731.18	< 0.0001	significant
A-Core Thickness	2.393E+06	1	2.393E+06	7121.91	< 0.0001	
B-Wire Mesh Size	1570.26	1	1570.26	4.67	0.0372	
AB	933.47	1	933.47	2.78	0.1040	
A^2	1.342E+05	1	1.342E+05	399.27	< 0.0001	
B^2	33104.83	1	33104.83	98.52	< 0.0001	
A^2B	95.47	1	95.47	0.2841	0.5972	
AB^2	16594.35	1	16594.35	49.39	< 0.0001	
Residual	12432.31	37	336.01			
Lack of Fit	729.03	1	729.03	2.24	0.1430	not significant
Pure Error	11703.28	36	325.09			
Cor Total	6.436E+06	44				

Table 4.28. Illustration of both adjusted and predicted correlation coefficients (R^2)

Response	Adjusted R^2	Predicted R^2
Sandwich weight (g)	0,9950	0,9937
Load carrying capacity (N)	0,9760	0,9721
Load capacity at which WM sandwiches were failed suddenly (N)	0,9727	0,9681
Core shear stress (MPa)	0,9854	0,9830
Facing stress (MPa)	0,9881	0,9856
Flexural Stiffness ($N.m^2$)	0,9977	0,9971

Table 4.29 The developed mathematical expressions to predict the responses (CT: core thickness, MS: wire mesh size)

Response		Mathematical Expressions
Weight	=	+23,116+0,678.(CT)+0,109.(MS)-0,002.(CT).(MS)-(0,005.CT^2)-0,0003.$(MS)^2$+0,0001.$(CT)^2$.(MS)-7,635E-06.CT.$(MS)^2$
Load carrying capacity	=	80,389.(CT)+0,994(MS)+0,009.(CT.MS)-1,536.$(CT)^2$-0,005.$(MS)^2$-96,597
Load capacity after failure of WM sandwiches	=	65,035.(CT)+4,396.(MS)-0,005.(CT).(MS)-1,118.$(CT)^2$-0,016.$(MS)^2$-239,917
Core shear stress	=	0,612-0,005.(CT)+0,0006.(MS)-1,75E-06.(CT.MS)-0,0002.$(CT)^2$-2,23E-06.$(MS)^2$
Facing stress	=	51,723+0,037.(CT)-0,014.(MS)-0,003.(CT).(MS)-0,028.$(CT)^2$+0,0002.$(MS)^2$+0,0001.$(CT)^2$.(MS)
Transverse shear rigidity	=	5975,493+419,992.(CT)-4,776.(MS)+0,471.(CT.MS)
Core shear modulus	=	27,148-1,039.(CT)-0,005.(MS)+0,0004.(CT).(MS)+0,018.$(CT)^2$

The sandwich panels' weight increases with the size of wire mesh sheets. However, due to the larger wire diameter of 100-mesh size, its weight is greater than 200-mesh size although 200-mesh sheets have two times more holes in a unit

area. Figure 4.78 shows the changes in sandwich weight with respect to both core thickness and wire mesh size.

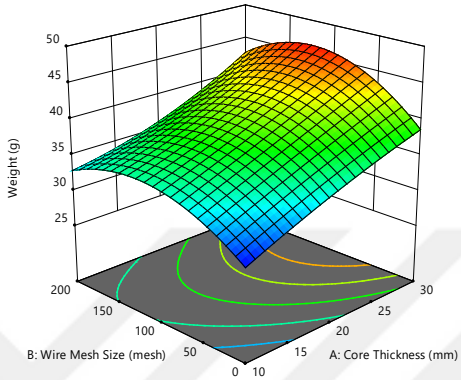
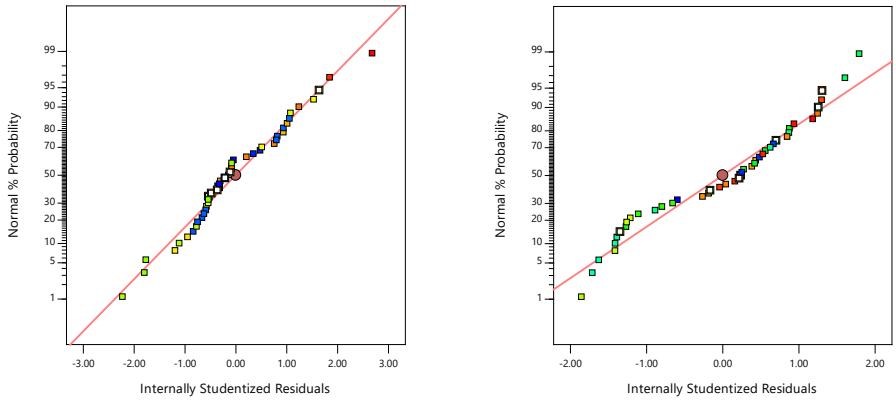


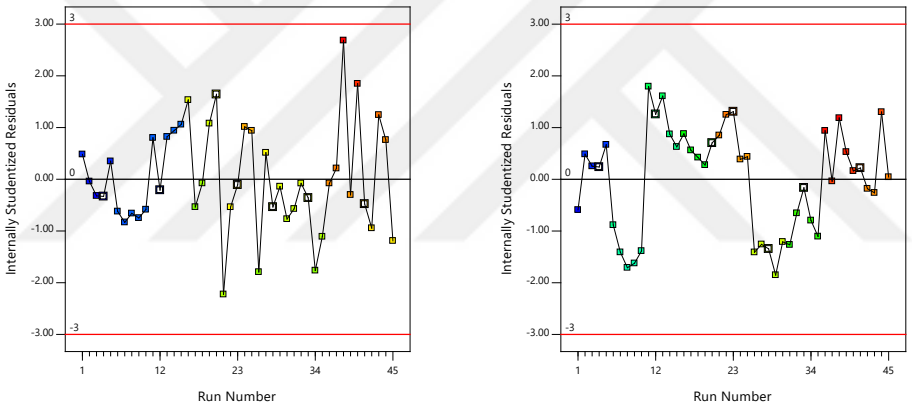
Figure 4.78. The change of sandwich panels' weight wrt core thickness and wire mesh size

The value of maximum load-carrying capacity and the load at which WM sandwiches underwent to sudden failure of the sandwich panels are normally distributed to a straight line, which means the experimental data has fitted well and normality assumption was validated as seen in Figure 4.79. That means analysis of variance is robust to the normality assumption (Montgomery, 2012). In addition, Figure 4.80 presents residual vs. run chart which confirmed the independence assumption since experimental results also distributed randomly within the plus and minus three-sigma limits. It was reported that obtaining independence can be achieved with proper randomization of the experiments (Montgomery, 2012).



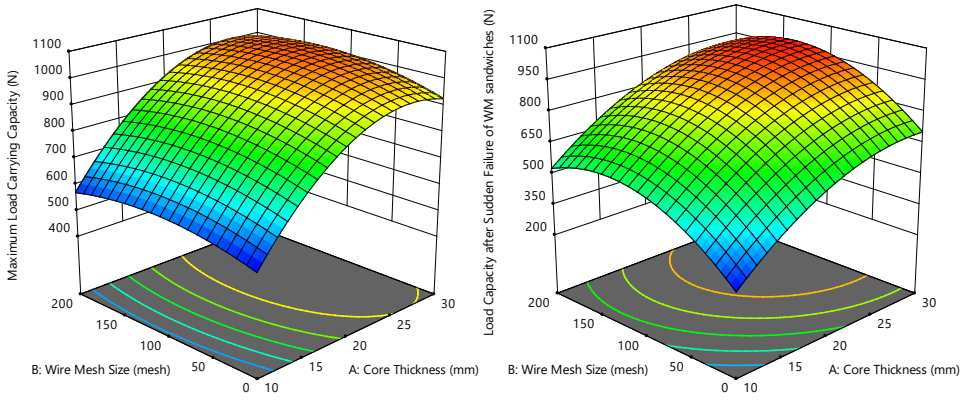
(a) (b)

Figure 4.79. Normal plot of residuals for; a) maximum load-carrying capacity, b) load capacity at which WM sandwiches underwent to sudden failure



(a) (b)

Figure 4.80. Residual vs. run charts for; a) maximum load carrying capacity, b) load capacity at which WM sandwiches underwent to sudden failure



(a) (b)

Figure 4.81. Effect of design parameters to; a) maximum load carrying capacity, b) load capacity at which WM sandwiches underwent to sudden failure

As it is seen from Figure 4.81, wire mesh sheets increase the load-carrying capacity of the sandwich panels. Although WM sandwiches underwent sudden failure at a certain deflection, the sandwiches having wire mesh sheets are able to carry a larger amount of bending loads at the same deflection values of WM specimens. In Figure 4.81(b), the favorable effect of wire mesh sheets has clearly been demonstrated. The effects of parameters on core shear stress, facing stress and flexural stiffness are presented in Figure 4.82. The changes in design parameters were found as statistically significant with the experimental results. Wire mesh sheets contributed to the results by reducing the facing stress, and by increasing both the core shear stress and the flexural stiffness. Especially, a 100-mesh wire sheet is the most effective level of the design parameter.

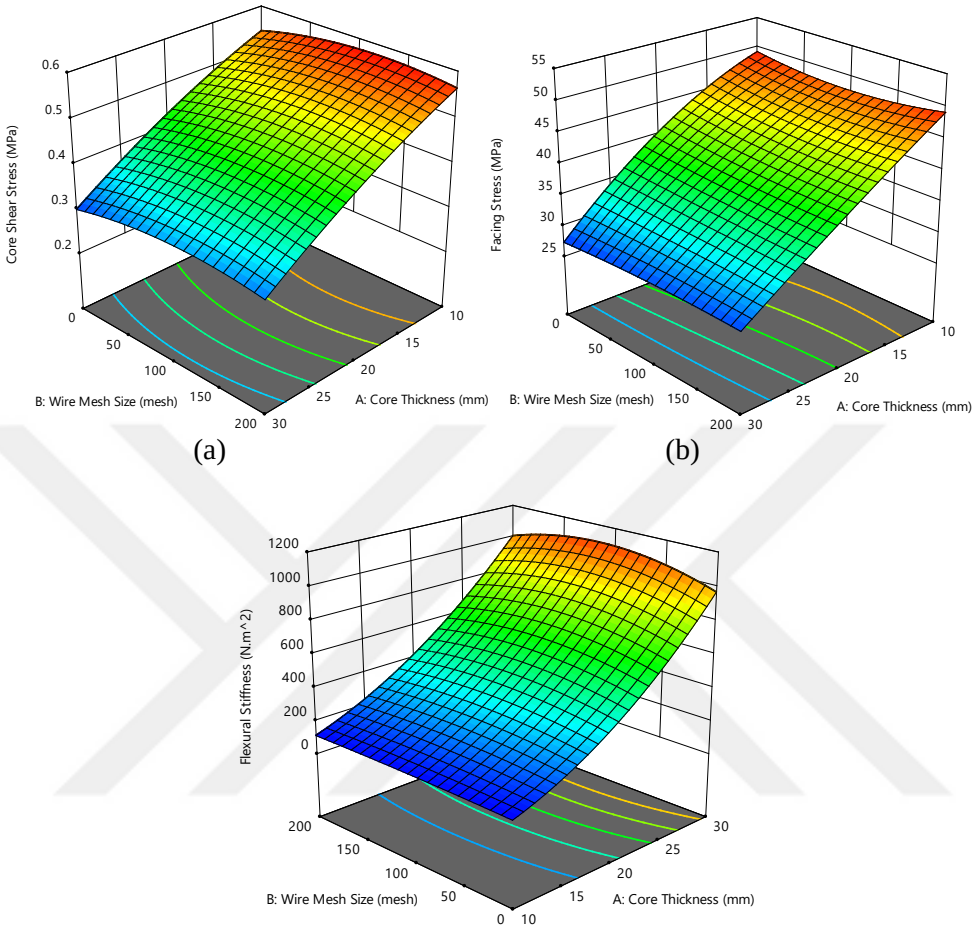


Figure 4.82. Effects of parameters on; a) core shear stress (MPa), b) facing stress (MPa), c) flexural stiffness ($N.m^2$)

Transverse shear rigidity and core shear modulus were examined based on the effects of both core thickness and wire mesh size (0 and 100-mesh). Tables 4.30 and 4.31 show ANOVA results. For evaluating transverse shear rigidity, ANOVA suggested two-factor interaction (2FI) model whereas the reduced quadratic model was used for core shear modulus.

Table 4.30. ANOVA results for transverse shear rigidity

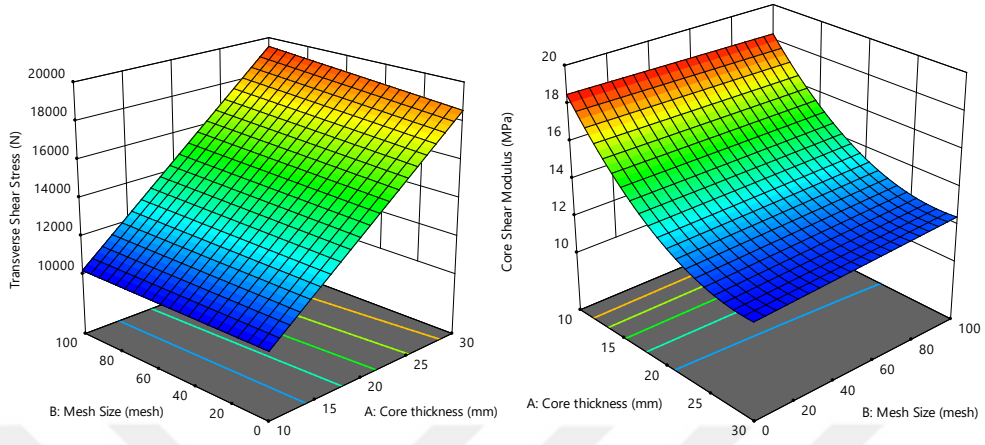
Source	Sum of Squares	df	Mean Square	F-value	p-value	
Model	3.961E+08	3	1.320E+08	3322.70	< 0.0001	significant
A-Core thickness	3.934E+08	1	3.934E+08	9899.66	< 0.0001	
B-Mesh Size	1.612E+06	1	1.612E+06	40.57	< 0.0001	
AB	1.108E+06	1	1.108E+06	27.87	< 0.0001	
Residual	1.033E+06	26	39741.48			
Lack of Fit	9.755E+05	2	4.878E+05	202.63	< 0.0001	significant
Pure Error	57770.96	24	2407.12			
Cor Total	3.972E+08	29				

Table 4.31. ANOVA results for core shear modulus

Source	Sum of Squares	df	Mean Square	F-value	p-value	
Model	217.28	4	54.32	9800.98	< 0.0001	significant
A-Core thickness	195.38	1	195.38	35251.95	< 0.0001	
B-Mesh Size	0.3353	1	0.3353	60.49	< 0.0001	
AB	0.6891	1	0.6891	124.33	< 0.0001	
A^2	20.88	1	20.88	3767.14	< 0.0001	
Residual	0.1386	25	0.0055			
Lack of Fit	0.0156	1	0.0156	3.05	0.0937	not significant
Pure Error	0.1230	24	0.0051			
Cor Total	217.42	29				

As it is seen from ANOVA tables, design parameters and their interactions are statistically significant with the constructed models. Adjusted R^2 values were found as 0,9971 and 0,9993 for transverse shear rigidity and core shear modulus, respectively. Predicted R^2 values that are 0,9967 and 0,9991 were also in a good agreement with Adjusted R^2.

The changes of transverse shear rigidity and core shear modulus according to both core thickness and wire mesh size were presented in Figure 4.83.



(a) (b)

Figure 4.83. Changes of transverse shear rigidity and core shear modulus wrt core thickness and wire mesh size

5. CONCLUSION

In this study, woven carbon fiber/epoxy and polyvinylchloride (PVC) foam core having 48 kg/m^3 density were sandwiched with a vacuum bagging method. The facing materials were hybridized with very fine wire mesh sheets in two different sizes (100-mesh and 200-mesh) and three different stacking sequence configurations (M1, M2, and M3). In addition, three different core thickness values (10 mm, 20 mm, and 30 mm) were tested under two different span lengths (150 mm and 200 mm). Based on the sandwich design parameters a systematic production process was conducted. The following conclusions were found out;

- The produced lightweight, stiff, and strong sandwich panels contributed to the materials universe by filling the holes as seen in Figure 5.1. There is a trajectory line from carbon/epoxy composite to PVC foam used in this study. The developed WM sandwiches, shown in Figure 4, are labeled as 1, 2, and 3. These structural members stand out with their lower-density and higher modulus data than their developing counterparts. Developments of sandwich structures were accepted as an alternative solution to expand the material space (Finnegan et al., 2007).

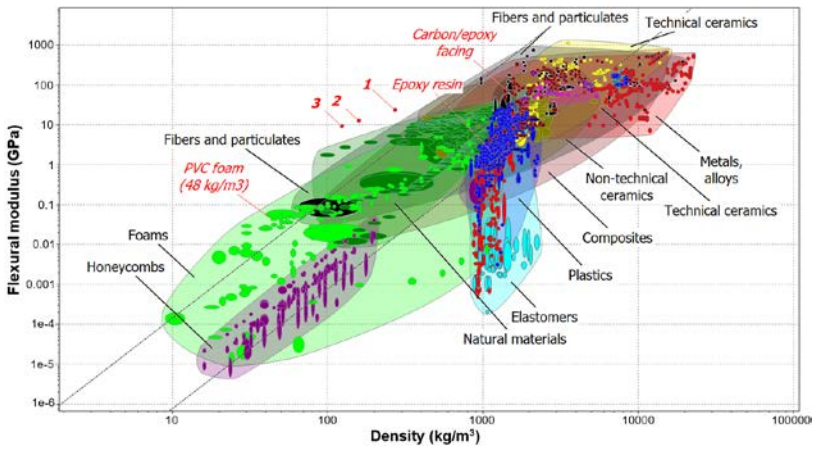


Figure 5.1. Flexural modulus vs density chart

- Multi-functional sandwich panels were developed by enhancing the failure behavior of the structures besides their high flexural stiffness to weight ratio and bending load capacity. Although carbon/epoxy/PVC foam core sandwiches were failed suddenly after the bending force was reached to the maximum, the specimens having wire mesh sheets in facings prevented the catastrophic sudden failure of the structure. Therefore, the drawbacks of carbon/epoxy/PVC core sandwiches can be eliminated by hybridization of facing with a very fine size of wire mesh sheets, which is also a substantially cost-effective manufacturing process by combining fibers and metals. In addition, contrary to the costly honeycomb and 3D printed cores, the sandwiches consist of wire mesh/carbon fiber/epoxy hybrid facings do not require special manufacturing processes and made of commercially available constituents.
- Wire mesh sheets favorably affected tensile load capacities of CFRP composites. Especially 100M1 configuration provided the highest results for tensile properties. But, tensile strength and modulus of 100M2, 100M3, 200M2, and 200M3 configurations were obtained lower than WM sandwiches. This is due to the increased thickness and strain values of the materials. The bridging effect depended upon the stacking configurations has a significant influence on the strength and failure behavior.
- Effects of wire mesh sheets on flexural characteristics of carbon fiber/epoxy/PVC foam core sandwich panels were revealed in terms of load-carrying capacity, maximum bending moment, flexural stiffness, core shear stress, facing stress, transverse shear rigidity, and core shear modulus.
- Bending load capacities of without wire mesh (WM) sandwiches, decreased by 44,67% for 10 mm, 30,91% for 20 mm, and 25,37% for 30 mm, respectively during failure. In the case of 100M1 configuration the reductions were 11,27%, 4,94% and 4,28%, respectively. 200M1

configuration provided better bending performance, and the reduction on the bending load capacities was only 3,78% for 10 mm thick core sandwich panels. Therefore, when WM sandwiches lose their load capacity after the failure, the sandwiches having wire mesh sheets still continued to carry a larger amount of bending loads at the same deflections.

- Core shear stress and sandwich facing stress values were determined for both short and long-span length sandwiches. The bending properties for both short and long-span length sandwiches are decreasing with the increase of the core thickness. This is also matching with the literature findings (Styles et al., 2007; Prakash et al., 2012). However, while facing stress of long-beam specimens were obtained higher than short-beam specimens, core shear stress was lower for long-beam specimens. Actually, the use of long or short span lengths provides a transition for failure modes between core shear to face sheet yielding. Therefore, the results are in good agreement with the literature (Carlsson and Kardomateas, 2011). Wire mesh sheets also favorably affected the results by increasing the core shear stress and decreasing the facing stress and allowed to obtain desired values.
- Flexural stiffness values of the sandwich specimens were evaluated based on both analytical classical sandwich beam theory and experimental ASTM D7250 Standard. Increasing the core thickness drastically increased the flexural stiffness. On the other hand, according to the ASTM approach, 100M1 configuration, which is the best one among the work, improved the results by 13.37%, 16.60%, and 13.37% for 10 mm, 20 mm and 30 mm thick core sandwiches, respectively.
- Transverse shear rigidity and core shear modulus were calculated based on the experimental ASTM approach. When the core thickness is increased, there is almost a linear increase in transverse shear stress whereas a nonlinear decrease is seen on core shear modulus. However, wire mesh

sheets could not improve these mechanical properties as much as the other features. As a result, it only exhibited a small percentage improvements.

- Primary failure modes were determined as core shearing for 10 mm thick core sandwiches and as indentation for 30 mm thick core sandwiches. But failure mode of 20 mm thick core sandwiches was found at a boundary of both core shear and indentation. Due to indentation failure, the increase of bending properties was obtained nonlinearly with the increase of the core thickness. For instance, 60,55% load capacity increase was obtained from 10 mm to 20 mm thick core WM sandwiches but the increment was only 4,04% from 20 mm to 30 mm thick core WM sandwiches. However, the load capacity of 100M1 configuration was increased to 7,61%. The failures of sandwiches with wire mesh sheets were carried out by a decreasing slope instead of a sudden drop which is the case for WM sandwiches.
- The failure mode analysis was carried out based on analytical collapse mechanisms and the collapse forces verified the experimentally obtained loads.
- In order to analyze the sandwich design parameters considered in this work two-way ANOVA was applied by using Response Surface Methodology (RSM). The effects of both constructed models and individual parameters are found statistically significant in the 95% confidence interval. Strong correlation coefficient (R^2) values were obtained and according to the regression analysis, the flexural characteristics can be predicted approximately.
- The results of the study indicated that hybridization of wire mesh sheets with carbon/epoxy composites could provide a strong bond capability, and increase lap shear strength between the layers.
- Hybridization of wire mesh sheets with carbon/epoxy composites can be a good alternative for fiber metal laminates (FMLs) as they are in perforated

form, which improves integration of the mesh steel to carbon fiber with complete penetration of the epoxy matrix. Because metals and FRP composites generally bonded to each other by using rivets and/or hole drilling, consequently the structure can weaken. Therefore, wire mesh sheets provide reinforcement and stabilization of the fiber structure with strong bond capability and can eliminate the additional surface treatments of metal sheets in FML applications. Polymer matrix surrounding also eliminates additional measures for corrosion protection (Sakthivel and Vijayakumar, 2017; Hasselbruch et al., 2015).

- Elimination of the disadvantage of carbon/epoxy composites by hybridization with wire mesh sheets is a substantially cost-effective process.

Briefly, due to their reasonable cost, ease of manufacturing, high E/ρ ratios and preventing catastrophic failure, they are good candidates for the applications in aviation, satellites, boat and yacht building, interior and exterior parts of the vehicles (e.g. corridor base, luggage compartments), etc (Uzay and Geren, 2020).

The followings are to be considered for future studies;

- Effects of hybrid composite laminates based on wire mesh sheets and carbon fibers on tensile and flexural properties under both static and fatigue loadings should be investigated considering different mesh sizes and stacking sequences during laminations.
- In sandwich panel applications, size effects of wire mesh sheets on different core densities should be investigated. This may also provide to obtain desired failure modes with the aid of metallic wire mesh sheets.
- Numerical studies (e.g. FEA) can be carried out by subjecting the 3D model of sandwiches to structural analysis to predict and verify the experimental results.
- Based on the experimental parameters the fuzzy predictions can be performed.

REFERENCES

Al-Shamary, A.K.J., Karakuzu, R., and Ozdemir, O., 2016. Low Velocity Impact Response of Sandwich Composites with Different Foam Core Configurations. Journal of Sandwich Structures and Materials, 18(6): 754–768.

Allan, J.R., 2000. A Protocol for Bird Strike Risk Assessment at Airports. Proceedings of the 25th International Bird Strike Committee, Amsterdam, 29-46.

Allen H.G., 1969. Analysis and Design of Structural Sandwich Panels. Oxford: Pergamon Press, 1st Edition, UK, 300.

Arbaoui, J., Schmitt, Y., Pierrot, J.L., and Royer, F.X., 2015. Comparison Study and Mechanical Characterisation of a Several Composite Sandwich Structures. International Journal of Composite Materials, 5(1): 1-8.

Ashby, M.F., 2011. Materials Selection in Mechanical Design. Elsevier Ltd, 4th Edition, The Netherlands, 640.

Ashby, M.F., Evans, A.G., Fleck, N.A., Gibson, L.J., Hutchinson, J.W., and Wadley, H.N.G., 2000. Metal Foams: a Design Guide. London: Butterworth, Heinemann, 251.

ASTM C393/C393M-11, 2011. Standard Test Method for Core Shear Properties of Sandwich Constructions by Beam Flexure. Annual Book of ASTM Standards, ASTM International, West Conshohocken, USA, 8.

ASTM D7249/D7249M-12, 2012. Standard Test Method for Facing Properties of Sandwich Constructions by Long Beam Flexure. Annual Book of ASTM Standards, ASTM International, West Conshohocken, USA, 9.

ASTM D7250/D7250M-06, 2006. Standard Test Method for Facing Properties of Sandwich Constructions by Long Beam Flexure. Annual Book of ASTM Standards, ASTM International, West Conshohocken, USA, 8.

ASTM D3039/D3039M-00, 2000. Standard Test Method for Tensile Properties of Polymer Matrix Composite Materials. Annual Book of ASTM Standards, ASTM International, West Conshohocken, USA, 13.

Atas, C., and Potoğlu, U., 2016. The Effect of Face-Sheet Thickness on Low-Velocity Impact Response of Sandwich Composites with Foam Cores. Journal of Sandwich Structures and Materials, 18(2): 215–228.

Atas, C., and Sevim, C., 2010. On the Impact Response of Sandwich Composites with Cores of Balsa Wood and PVC Foam. Composite Structures, 93: 40-48.

Baker, A., Dutton, S., and Kelly, D., 2004. Composite Materials for Aircraft Structures. American Institute of Aeronautics and Astronautics, 2nd Edition, USA, 599.

Balasubramanian, M., 2014. Composite Materials and Processing. CRC Press, 1st Edition, USA, 648.

Baştürk, S.B., and Tanoğlu, M., 2011. Mechanical and Energy Absorption Behaviors of Metal/Polymer Layered Sandwich Structures. Journal of Reinforced Plastics and Composites, 30(18): 1539-1547.

Baştürk, S.B., and Tanoğlu, M., 2013. Development and Mechanical Behavior of FML/Aluminium Foam Sandwiches. Appl Compos Mater, 20: 789–802.

Bezazi, A., Mahi, A., Berthelot, J. M., and Bezzazi, B., 2007. Experimental Analysis of Behavior and Damage of Sandwich Composite Materials in Three-Point Bending. Part 1. Static Tests and Stiffness Degradation at Failure Studies. Strength of Materials, 39(2): 170–77.

Black, S., 2003. Getting to the Core of Composite Laminates. Retrieved 2018 from http://www.compositesworld.com/articles/getting-to-the-core-of-composite-laminates

Borsellino, C., Calabrese, L., and Valenza, A., 2004. Experimental and Numerical Evaluation of Sandwich Composite Structures. Composites Science and Technology, 64: 1709–1715.

Burman, M., and Zenkert, D., 1997. Fatigue of foam Core Sandwich Beams-2: Effect of Initial Damage. Int. J. Fatigue, 19(7): 563–578.

Carlsson, L.A., and Kardomateas, G.A., 2011. Structural and Failure Mechanics of Sandwich Composites, Springer, USA, 386.

Chai, G.B., and Manikandan, P., 2014. Low Velocity Impact Response of Fibre-Metal Laminates – A Review. Composite Structures, 107: 363–381.

Chemami, A., Bey, K., Gilgert, J., and Azari, Z., 2012. Behaviour of Composite Sandwich Foam-Laminated Glass/Epoxy under Solicitation Static and Fatigue. Composites: Part B, 43: 1178–1184.

Chen, C., Harte, A.M., and Fleck, N.A., 2001. The Plastic Collapse of Sandwich Beams with a Metallic Foam Core. International Journal of Mechanical Sciences, 43(6): 1483–1506.

Chtourou, H., Martel, J.P.M., Gurnagul, N., and Ricard, M., 2018. Paper Twines in the Pultrusion Process –Pilot Production and Flexural Characterization of Sandwich Rods. Journal of Composite Materials, 0(0): 1–15.

Crosky, A., Grant, C., Kelly, D., Legrand, X., and Pearce, G., 2015. Fibre Placement Processes For Composites Manufacture. Edited by Boisse, P., Advances in Composites Manufacturing and Process Design, Elsevier, UK, 79-92.

Daniel, I.M., Gdoutos, E.E., Wang, K.A., and Abot, J.L., 2002. Failure Modes of Composite Sandwich Beams. International Journal of Damage Mechanics, 11: 309-334.

Daniel, I.M., Gdoutos, E.E., and Rajapakse, Y.D.S., 2009. Major Accomplishments in Composite Materials and Sandwich Structures. Springer, USA, 818.

DIAB Group, 2012. DIAB Guide to Core and Sandwich. Diab Core Guide Rev 1, Sweden, 32.

Dixit, A., Mali, H.S., and Misra, R.K., 2014. A Micromechanical Unit Cell Model of 2x2 Twill Woven Fabric Textile Composite for Multi Scale Analysis. J. Inst. Eng. India Ser. E, 95(1): 1-9.

Elmarakbi, A., 2013. Advanced Composite Materials for Automotive Applications Structural Integrity and Crashworthiness. Automotive Series, UK, 470.

Fan, H.L., Zeng, T., Fang, D.N., and Yang, W., 2010. Mechanics of Advanced Fiber Reinforced Lattice Composites. Acta Mech Sin, 26: 825–835.

Finnegan, K., Kooistra, G., Wadley, H.N.G., and Deshpande, V.S., 2007. The Compressive Response of Carbon Fiber Composite Pyramidal Truss Sandwich Cores. International Journal of Materials Research, 98: 1264–1272.

Fontens, O.H.P.M., Bastian, F.L., and Castrodeza, E.M., 2015. Crack Growth Resistance Curves of GLARE 3 5/4 0.3 Fiber–Metal Laminates at Low Temperature. Fatigue Fract Engng Mater Struct, 38: 268–275.

Garay, A.C., Souza, J.A., and Amico, S.C., 2016. Evaluation of Mechanical Properties of Sandwich Structures with Polyethylene Terephthalate and Polyvinyl Chloride Core. Journal of Sandwich Structures and Materials, 18(2): 229–241.

Gay, D., 2015. Composite materials design and Applications. CRC Press, 3rd Edition, USA, 635.

Gibson, L.J., 2000. Mechanical Behaviour of Metallic Foams. Ann Rev Mater Sci, 30: 191–227.

Gibson, R.F., 2012. Principles of Composite Material Mechanics, CRC Press 3rd Edition, USA, 683.

Gueuning, D., and Mathieu, F., 2016. Evolution in Composite Injection Moulding Processes for Wing Control Surfaces. Sampe (Society for the Advancement of Material and Process Engineering) Journal, 52(1): 7-12.

Gupta N, Zeltmann SE, Luong DD, and Doddamani, M., 2019. Core materials for marine sandwich structures (Chapter 7). Marine Composites, pp.187-224.

Harte, A., Fleck, N.A., and Ashby, M.F., 2000. Sandwich Panel Design Using Aluminum Alloy Foam. Advanced Engineering Materials, 2(4): 219-222.

Hasselbruch, H., von Hehl, A. and Zoch, H.W., 2015. Properties and failure behavior of hybrid wire mesh/carbon fiber reinforced thermoplastic composites under quasi-static tensile load. Mater Design, 66: 429-436.

Hedayati, R., and Sadighi, M., 2016. Effect of Using an Inner Plate between Two Faces of a Sandwich Structure in Resistance to Bird-Strike Impact. Journal of Aerospace Engineering, 29(1): 1-11.

Herbeck, L., Kleineberg, M., Schöppinger, C., 2002. Foam Cores in RTM Structures, Manufacturing Aid of High-Performance Sandwich? 23rd International SAMPE Europe Conference and Tutorials/JEC, France, 1-11.

Herranen, H., Pabut, O., Eerme, M., Majak, J., Pohlak, M., Kers, J., Saarna, M., Allikas, G., and Aruniit, A., 2012. Design and Testing of Sandwich Structures with Different Core Materials, Materials Science (Medžiagotyra) 18(1): 45-50.

Hinz, S., Omoori, T., Hojo, M., and Schulte, K., 2009. Damage Characterisation of Fibre Metal Laminates Under Interlaminar Shear Load. Composites: Part A, 40: 925–931.

Imielinska, K., Guillaumat, L., Wojtyra, R., and Castaings, M., 2008. Effects of Manufacturing and Face/Core Bonding on Impact Damage in Glass/Polyester–PVC Foam Core Sandwich Panels. Composites: Part B, 39: 1034–1041.

Jiang, B., Li, Z., and Lu, F., 2015. Failure Mechanism of Sandwich Beams Subjected to Three-Point Bending. Composite Structures, 133: 739-745.

Joseph, J. D.R., Prabakar, J., and Alagusundaramoorthy, P., 2017. Precast Concrete Sandwich One-Way Slabs Under flexural Loading. Engineering Structures, 138: 447–457.

Kar, K.K., 2017. Composite Materials Processing, Applications, Characterizations. Springer, Germany, 686.

Karahan, M., Gul, H., Karahan, N., and Ivens, J., 2013. Static Behavior of Three-Dimensional Integrated Core Sandwich Composites Subjected To Three-Point Bending. Journal of Reinforced Plastics and Composites, 32(9): 664–678.

Karlsson, K.F., and TomasAström, B., 1997. Manufacturing and Applications of Structural Sandwich Components. Composites Part A: Applied Science and Manufacturing, 28(2): 97-111.

Kabir, K., Vodenitcharova, T., and Hoffman, M., 2014. Response of Aluminium Foam-Cored Sandwich Panels to Bending Load. Composites Part B: Engineering, 64:24–32.

Kaw, A.K., 2006. Mechanics of composite materials, CRC Press, 2nd Edition, USA, 457.

Kazak, F., Schleuß, L., Ossenbrink, R., Michailov, V., and Weiß, S., 2016. Particularities of Testing Structured Sheet Metals in 3-Point Bending Tests. Materials Testing, 58: 495-500.

Kulkarni, N., Mahfuz, H., Melanie, S., and Carlson, L.A., 2004. Fatigue Failure Mechanism and Crack Growth in Foam Core Sandwich Composites under Flexural Loading. Journal of Reinforced Plastics & Composites, 23(1): 83–94.

Kumar, M.V., and Soragaon, B., 2014. Fabrication and Evaluation of Multilayered Polyurethane Foam Core Sandwich Panels for Static Flexural Stiffness. Procedia Engineering 97: 1227 – 1236.

Kurian, R., Balaji, C., and Venkateshan, S.P., 2016. Experimental Investigation of Convective Heat Transfer in a Vertical Channel with Brass Wire Mesh Blocks. International Journal of Thermal Sciences, 99: 170-179.

Kurian, R., Balaji, C., and Venkateshan, S.P., 2017. An Experimental Study on Hydrodynamic and Thermal Performance of Stainless Steel Wire Mesh Blocks In A Vertical Channel. Experimental Thermal and Fluid Science, 86: 248–256.

Li, T, and Wang, L., (2017). Bending Behavior of Sandwich Composite Structures with Tunable 3D-Printed Core Materials. Composite Structures, 175: 46-57.

Lim, T.S., Lee, C.S. and Lee, D.G., (2004). Failure Modes of Foam Core Sandwich Beams under Static and Impact Loads. Journal of Composite Materials, 38(18): 1639–1662.

Liu, C., Zhang, Y.X., and Heslehurst, R., 2014. Impact Resistance and Bonding Capability of Sandwich Panels with Fibre–Metal Laminate Skins and Aluminium Foam Core. Journal of Adhesion Science and Technology, 28(24): 2378–2392.

Liu, J., Li, Y., Gao, X., Liu, P. and Kong, L., 2015. Dynamic Response of Bird Strike on Aluminium Foam-Based Sandwich Panels. International Journal of Crashworthiness, 20(4): 325-336.

Mallick, P.K., 2007. Fiber-Reinforced Composites: Materials, Manufacturing, and Design. CRC Press, 3rd Edition, USA, 638.

Matalkah, F., Bharadwaj, H., Soroushian, P., Wu, W., Almalkawi, A., Balachandra, A.M., and Peyvandi, A., 2017. Development of Sandwich Composites for Building Construction with Locally Available Materials. Construction and Building Materials, 147: 380–387.

McCracken, A., and Sadeghian, P., 2018. Partial-Composite Behavior of Sandwich Beams Composed of Fiberglass Face Sheets and Woven Fabric Core. Thin-Walled Structures, 131: 805–815.

McDonough, W.G., Dunkers, J.P., Flynn, K.M., and Hunston, D.L., 2004. A Test Method to Determine the Fiber and Void Contents of Carbon/Glass Hybrid Composites. Journal of ASTM International, 1(3): 1-15.

McIlhagger, A., Archer, E., and McIlhagger, R., 2015. Manufacturing Processes for Composite Materials and Components for Aerospace Applications. Edited by Irving, P.E., and Soutis, C., Polymer Composites in the Aerospace Industry, Woodhead Publishing Series in Composites Science and Engineering: Number 50, Elsevier, UK, 53-75.

Mileiko, S.T., 1997. Metal and Ceramic Based Composites. Composite Materials Series, 12, Elsevier, 1st Edition, The Netherlands, 691.

Montgomery, D.C., 2012. Design and Analysis of Experiments, Wiley, 8th Edition, USA, 752.

Mostafa, A., Shankar, K., and Morozov, E.V., 2014. Experimental, Theoretical and Numerical Investigation of the Flexural Behaviour of the Composite Sandwich Panels with PVC Foam Core. Appl Compos Mater, 21: 661–675.

Ozdemir, O., Karakuzu, R., and Al-Shamary, A.K.J., 2015. Core-Thickness Effect on the Impact Response of Sandwich Composites with Poly (Vinyl Chloride) and Poly (Ethylene Terephthalate) Foam Cores. Journal of Composite Materials, 49(11): 1315–1329.

Peters, S.T., 1998. Handbook of composites. Chapman & Hall Publishing, 2nd Edition, England, 1118.

Prakash, M.D.A.A., Guptha, V.L.J., Sharma, R.S., and Mohan, B., 2012. Influence of Cell Size on the Core Shear Properties of FRP Honeycomb Sandwich Panels. Materials and Manufacturing Processes, 27(2): 169-176.

Priyanka, P., Dixit, A. and Mali, H.S., 2017. High-Strength Hybrid Textile Composites with Carbon, Kevlar, and E-Glass Fibers for Impact-Resistant Structures. A Review. Mechanics of Composite Materials, 53(5): 685-704.

Sadeghian, P., Hristozovand, D., and Wroblewski, L., 2018. Experimental and Analytical Behavior of Sandwich Composite Beams: Comparison of Natural and Synthetic Materials. Journal of Sandwich Structures and Materials, 20(3): 287–307.

Sadighi, M., Alderliesten, R.C., and Benedictus R., 2012. Impact resistance of fiber-metal laminates: A review. International Journal of Impact Engineering, 49: 77-90.

SAE International, 2013. Composite Materials Handbook, Volume 6. Structural Sandwich Composites Published by SAE International, USA.

Sakthivel, M and Vijayakumar, S., 2017. Influence of Stainless-Steel Wire Mesh on the Mechanical Behaviour in a Glass-Fibre-Reinforced Epoxy Composite. Mater Tehnol, 51: 455-461.

Santhanakrishnana, R., Kavithaa, N., Sundarama, M., and Venkatanarayanana, P.S., 2018. Effect of Pile Orientation on the Shear Strength of Stitched Foam Sandwich Panel, Materials Research, 21(6): 1-6.

Sayyad, A.S., and Ghugal, Y.M., 2017. Bending, buckling And Free Vibration of Laminated Composite and Sandwich Beams: A Critical Review of Literature. Composite Structures, 171: 486–504.

Shao, R., Wu, C., Liu, Z., Su, Y., Liu, J., Chen, G., Xu, S., 2018. Penetration Resistance of Ultra-High-Strength Concrete Protected with Layers Of High-Toughness And Lightweight Energy Absorption Materials. Composite Structures, 185: 807–820.

Sharma, N., Gibson, R.F., and Ayorinde, E.O., 2006. Fatigue of Foam and Honeycomb Core Composite Sandwich Structures: A Tutorial. Journal of Sandwich Structures and Materials, 8(4): 263-319.

Sharma, R. S., and Raghupathy, V. P., 2009. Influence of Rigid Inserts on Shear Modulus and Strength of Sandwich Beams with Polyurethane Foam as Core. Journal of Reinforced Plastics and Composites, 28(24): 3037-3047.

Sinmazçelik, T., Avcu, E., Bora, M.Ö., and Çoban, O., 2011. A review: Fibre Metal Laminates, Background, Bonding Types and Applied Test Methods. Materials and Design, 32: 3671–3685.

Steeves, C.A., and Fleck, N.A., 2004. Collapse Mechanisms of Sandwich Beams with Composite Faces and a Foam Core, Loaded in Three-Point Bending. Part I: Analytical Models and Minimum Weight Design. International Journal of Mechanical Sciences, 46: 561–583.

Steeves, C.A., and Fleck, N.A., 2004. Collapse Mechanisms of Sandwich Beams with Composite Faces and a Foam Core, Loaded in Three-Point Bending. Part II: Experimental Investigation and Numerical Modelling. International Journal of Mechanical Sciences 2004, 46(4): 585-608.

Styles, M., Compston, P., and Kalyanasundaram, S., 2007. The Effect of Core Thickness on the Flexural Behaviour of Aluminium Foam Sandwich Structures. Composite Structures, 80: 532–538.

Swift, K.G., and Booker, J.D., 2013. Manufacturing Process Selection Handbook, Chapter 5: Plastics and Composites Processing. Elsevier, 1st Edition, UK, 141-174.

Taghizadeh, S.A., Farrokhabadi, A., Liaghat, G., Pedram, E., Malekinejad, H., Mohammadi, S.F., and Ahmadi, H. 2019. Characterization of Compressive Behavior of PVC Foam Infilled Composite Sandwich Panels with Different Corrugated Core Shapes. Thin-Walled Structures, 135: 160–172.

Technical Data Sheet, Dost Kimya Inc., 2014. Carbon Fabric – 200gr/sqm 3K Plain. Rev.2.2, Turkey, 1.

Technical Data Sheet, 2011. Universal Structural Foam: Airex C70. 3A Composites.

Technical Data Sheet, 2009. Laminating Resin MGSTM L160 and Hardener H160, Hexion, The Netherlands, 10.

Technical Data Sheet, 2013. Araldite 2015. Huntsman Corporation, Switzerland, 6.

Tiantian, L., and Wang, L., 2017. Bending Behavior of Sandwich Composite Structures with Tunable 3D-Printed Core Materials. Composite Structures, 175:46–57.

Tortoç, A., 2009. Numerical study On the Fracture Toughness of Balsa/PVC Sandwich Composite Materials. Master of Science Thesis, Dokuz Eylul University, Institute of Natural and Applied Sciences, Turkey, 55.

Truxel, A., Aviles, F., Carlsson, L.A., Grenestedt, J.L., and Millay, K., 2006. Influence of Face/Core Interface on Debond Toughness of Foam and Balsa Cored Sandwich. Journal of Sandwich Structures and Materials, 8: 237-258.

Turgut, T., 2007. Manufacturing and Structural Analysis of A Lightweight Sandwich Composite Uav Wing. Master of Science Thesis. The Graduate School of Natural and Applied Sciences of Middle East Technical University, Turkey, 110.

Uzay, Ç., Acer, D., and Geren, N., 2019. Impact Strength of Interply and Intraply Hybrid Laminates Based on Carbon-Aramid/Epoxy Composites. European Mechanical Science, 3(1): 1-5.

Uzay, Ç., and Geren, N., 2020. Effect of Stainless-Steel Wire Mesh Embedded into Fibre-Reinforced Polymer Facings on Flexural Characteristics of Sandwich Structures. Journal of Reinforced Plastics and Composites, First Published Online: May 5, 2020.

Uzay, C., Geren, N., Boztepe, M.H. and Bayramoglu, M., 2019. Bending Behavior of Sandwich Structures with Different Fiber Facing Types and Extremely Low-Density Foam Cores. Materials Testing, 61(3): 220-230.

Vasiliev, V.V., and Morozov, E., 2007. Advanced Mechanics of Composite Materials. Elsevier, 2nd Edition, UK, 504.

Venugopal, M.M., Maharana, S.K., and Badarinarayan, K.S., 2013. Finite Element Evaluation of Composite Sandwich Panel under Static Four Point Bending Load. JEST-M, 2(1): 1-6.

Vinson, J.R., 1999. The Behavior of Sandwich Structures of Isotropic and Composite Materials. Technomic Publishing Company, USA, 378.

Vinson, J.R., 2001. Sandwich Structures. Appl Mech Rev, 54(3): 201-214

Vogelesang, L.B., and Vlot, A., 2000. Development of Fibre Metal Laminates for Advanced Aerospace Structures. Journal of Materials Processing Technology, 103: 1-5.

Wang, J., Chen, B., Wang, H., and Waas, A.M., 2015. Experimental Study on the Compression after- Impact Behavior of Foam-Core Sandwich Panels. Journal of Sandwich Structures and Materials, 17(4): 446–465.

Website, 2013. https://www.flickr.com/photos/bcomposite/8938412979/in/photostream/ . Accessed: 15/03/2019.

Website, 2010. https://www.compositesworld.com/articles/sqrtm-enables-net-shape-parts. Accessed: 10/07/2019.

Website, 2019. http://www.radiuseng.com/net_shape_composites. Accessed: 10/07/2019.

Wu, G., and Yang, J.M., 2005. The Mechanical Behavior of GLARE Laminates for Aircraft Structures. Overview Failure in Structural Materials, JOM, 57: 72-79.

Xu, J., Liu, J., Gu, W., Wang, Z., Liu, X., and Cao, T., 2018. Effect of Cell Size on the Energy Absorption of Closed-Cell Aluminum Foam. Materials Testing, 60: 583-590.

Yalkin, H.E., Icten, B.M., and Alpyildiz, T., 2015. Enhanced Mechanical Performance of Foam Core Sandwich Composites with Through the Thickness Reinforced Core. Composites Part B, 79: 383-391.

Yalkin, H.E., Icten, B.M., and Alpyildiz, T., 2017. Tensile and Compressive Performances of Foam Core Sandwich Composites with Various Core Modifications. Journal of Sandwich Structures and Materials, 19(1): 49–65.

Yan, L.L., Han, B., Yu, B., Chen, C.Q., Zhang, Q.C., and Lu, T.J., 2014. Three-Point Bending of Sandwich Beams with Aluminum Foam-Filled Corrugated Cores. Materials and Design, 60: 510–519.

Yan, S., Zeng, T., Fang, D.N., et al., 2010. Shear Behavior of Carbon/Epoxy Pyramidal Truss Sandwich Panels. The 1st International Conference on Advanced Polymer and Polymer Composites, China.

Yin, C., Zheng, Q., Zeng, J., Yang, J., and Xiao, J., 2015. Composite Sandwich Panel with Multifunction of Load Bearing, Heat Insulation, and Thermal Protection. Journal of Composite Materials, 49(25): 3077–3087.

Zhou, J., Hassan, M.Z., Guan, Z., and Cantwell, W.J., 2012. The Low Velocity Impact Response of Foam-Based Sandwich Panels. Composites Science and Technology, 72: 1781-1790.

CURRICULUM VITAE

Çağrı UZAY was born in 14.08.1989 in Kahramanmaraş. He graduated from Seyhan Rotary Anatolian High School in 2007 and enrolled at the Mechanical Engineering Department of Çukurova University in the same year. He graduated with his Bachelor of Science degree in Mechanical Engineering Department with the 1st ranked degree in 2012. He also completed the undergraduate program of Automotive Engineering with a double major in the same year. He started his Master of Science education in Mechanical Engineering Department of Çukurova University in 2012 and graduated in 2014. Then, he started his Doctor of Philosophy education in the same department in 2014. He had worked as an R&D Engineer in TEMSA GLOBAL A.Ş. for about two years. He has been working as a Research Assistant at Çukurova University, Department of Mechanical Engineering since 2014.